Title
Mechanisms of basolateral polarity determination by the Scrib module

Author
Khoury, Mark John

Publication Date
2022

Peer reviewed|Thesis/dissertation

Mechanisms of basolateral polarity determination by the Scrib module

By

Mark John Khoury

A dissertation submitted in partial satisfaction of the

requirements for the degree of

Doctor of Philosophy

in

Molecular and Cell Biology

in the

Graduate Division

of the

University of California, Berkeley

Committee in charge:

Professor David Bilder, Chair
Professor Iswar K. Hariharan
Professor Gian Garriga
Professor Kathleen Ryan

Spring 2022

Mechanisms of basolateral polarity determination by the Scrib module

by

Mark John Khoury

Abstract

Mechanisms of basolateral polarity determination by the Scrib module

by

Mark John Khoury

Doctor of Philosophy in Molecular and Cell Biology

University of California, Berkeley

Professor David Bilder, Chair

Cell polarity is a fundamental process in biology whereby a single cell can partition its plasma membrane into two distinct and non-overlapping domains. All cells are polarized, and cell polarity is essential for the development and homeostasis of many tissues and organs. Epithelial cells exhibit a form of polarity called apicobasal polarity that is regulated by the activity of two conserved protein groups: the Par complex, which specifies the apical domain, and the Scrib module, which, in many contexts, is required to specify the basolateral domain. Mutual antagonism between the Par complex and the Scrib module positions the apical-basolateral boundary and primarily involves the apical kinase aPKC and its substrate and inhibitor, the basolateral protein, Lgl. While the mechanisms underlying apical polarity determination by the Par complex are well-studied, the molecular basis for basolateral polarity establishment by the Scrib module proteins, Scrib, Dlg and Lgl are unclear. In this dissertation I investigate the individual functions of Scrib, Dlg and Lgl using genetic manipulations and biochemistry in *Drosophila* and describe distinct and cooperative activities that give rise to basolateral polarity.

I identified regulatory relationships between Scrib, Dlg and Lgl that govern their localization to the cell cortex and demonstrated that these three proteins possess unique, but cooperative activities that are required but not sufficient to establish the basolateral domain. I found a specific requirement for Dlg to localize Scrib and investigated potential mechanisms, ruling out previously proposed binding interactions and posttranslational modification. I described a requirement for Scrib and Dlg to control Lgl localization by negatively regulating its phosphorylation by aPKC. We proposed a model where Scrib and Dlg 'protect' Lgl at the basolateral membrane, activating Lgl's aPKC-inhibiting potential and limiting apical domain spread.

To define the molecular mechanisms of these observations, I investigated Dlg protein function in detail. I identified a putative PP1-binding motif in the Dlg HOOK domain that was essential for Dlg function, however I did not find evidence for Dlg-PP1 physical interaction and although PP1 regulates Lgl phosphorylation, the ability of Dlg and Scrib to regulate Lgl is largely separate from PP1. However, study of Dlg PP1-binding mutants revealed the requirement of the Dlg HOOK domain in localizing Scrib to the cortex. Using this information and a panel of structure-function

constructs, I defined a minimal fragment consisting of only the SH3 and HOOK domains that was necessary and sufficient for function, including Scrib recruitment.

To investigate other mechanisms of Dlg function, I collaborated with Katherine Sharp, a postdoc in the lab, to interrogate Dlg binding partners using APEX2-based proximity proteomics. Our results revealed a large number of nuclear proteins in proximity to Dlg *in vivo*. We found that a population of endogenous Dlg resides in the nucleus near to the NURF chromatin remodeling complex. Overgrowth of *dlg* mutant tumors was dependent on NURF complex activity and may result from NURF-dependent activation of Yki target genes. We identified a putative NLS sequence in the Dlg HOOK domain and demonstrated that this motif is essential for Dlg function, but its mutation does not prevent Dlg nuclear entry, suggesting the existence of an alternate NLS.

Together, the work presented in this dissertation constitute an important advance in the understanding of the molecular functions of the Scrib module proteins, Scrib, Dlg and Lgl and provide a plausible model underlying basolateral polarity via our proposed Lgl protection mechanism. These studies set the stage for future investigation of the overarching mechanisms that polarize animal cells and will enable fuller understanding of many fundamental cell polarity-dependent biological processes.

Table of Contents

Acknowledgements

Grad school is a long and difficult endeavor. As they say, "it takes a village," and so I have many people to whom I am deeply grateful and without whose help I could not have made it through this experience. First, I would like to thank my advisor, David Bilder, and express my utmost gratitude for his steadfast mentorship and guidance during my time in the lab. Not only is David a brilliant scientist, but he is also a patient and caring teacher. I will never forget the hours he spent teaching me the basics of fly genetics when I first joined the lab, or the thoughtful and insightful feedback on every piece of writing I ever sent him, no matter how trivial. I will always be indebted to David for teaching me how to really be a scientist and helping me do the best science that I could. From writing and presentation skills to "Nature colors", David's mentorship has forever impacted my perspective and approach to science in the best possible way. Lastly, David has also been a consistently kind and caring person during all the difficult times that grad school and life bring and has always demonstrated that he truly cares about his trainees. Thank you for always being there for us, David.

I would like to thank my amazing thesis committee for their feedback, help and guidance over the last several years: Iswar Hariharan, Gian Garriga and Kathleen Ryan. Your scientific input and encouragement have been invaluable. I also want to especially thank Iswar for being a second mentor during my PhD. I will always be amazed by your encyclopedic knowledge of science, medicine, and arcane facts. I learned a lot about the importance of "big picture" questions from you, and your career and life advice are always honest and insightful, for which I am very grateful.

It would be impossible for me to not acknowledge the wonderful people in the Bilder and Hariharan labs: thank you all for making the 3rd (and then 5th) floor such a fun place to work. Thank you to Geert de Vreede for being the best baymate I could ask for and always being willing to listen to my rants or talk about the mysteries of Scribble, memes or anything else during the middle of the workday. Thank you especially to fellow grad student Jack Hsi. I will miss your infectious laughter and always being able to talk to you about the trials and tribulations of grad school. Your appreciation of dark humor and SpongeBob quotes were always a great source of shared hilarity. Thank you to Alex Houser and Cindy Liu for always keeping the lab running smoothly; we would have fallen apart without you. Similarly, special thanks to Lupe Coy, without whom the lab could not function. Thank you to Katie Sharp for teaching me basic fly work and for being a great collaborator. Thank you to Dong-Yuan Chen for teaching me about follicles, FRAP and credit card points; I'll miss your dry wit and blunt life advice. Thanks to Jung Kim for always being down for in-depth science discussion and for always asking lots of questions, Stephan Gerlach for all the fun conversations and card games, and thank you to Hui-Yu Ku, Katy Ong, Kavya Adiga, Leigh Harris, Justin Crest, and Courtney Bone for being such great colleagues and friends.

To the Hariharan lab: thank you for always sharing your expertise, workout tips and flies with us. I will miss having such great neighbors and collaborators who can also dominate at circuit training. Thank you especially to Maya Emmons-Bell for being a wonderful friend and the best co-roton ever. Thanks for always being there to talk; whether it was science, life, or anything else, you always had sage wisdom to share.

To my friends in the MCB cohort and beyond: thank you for providing the fun and sanity needed to get through grad school. Thank you to Jack, Jana, Andrea and Josh for being the best group of friends possible; I don't know what I would have done without you and our JJJAMM hangouts. Thank you to the whole MCB class of 2016. There are too many to list here, but I am

grateful to have been part of such a talented, fun group. I'm looking forward to seeing the cool things you will all do.

I wouldn't be where I am without the help and support of my previous mentors and teachers. Thank you to Steven Sowa, Lydia Contreras, Anna Vorobyeva, Eric Klann, Chiye Aoki, Kenneth Birnbaum, Lionel Christiaen, Mark Siegal, Duncan Smith and many others for helping me get my start in science and teaching me to fall in love with biology.

My parents have been the most constant role models and staunch supporters of my success. I am eternally grateful for their love, support and encouragement during the last 6 years, and on innumerable occasions throughout my entire life. Thank you for showing me the importance of hard work through your example, and for giving me the space to develop my curiosity when I was growing up. No matter what pursuit I set my mind to, you were always there for me with advice and encouragement; I would not be where I am without you. Thank you to my sister Nicole, for being my best friend, who I can talk to about anything and for being the person I have the most fun hanging out with. It's good to know there's someone else who's just as weird as I am. Thank you to the rest of my family as well for their love and support: to my aunts, uncles, cousins, and especially my grandparents, John, Grace, Hanna and Norma who were always invested in my success.

Lastly, I want to thank my best friend and partner, Maiko Kitaoka. Thank you for always being there for me and supporting me no matter what. You never cease to inspire and amaze me with your energy, creativity, enthusiasm, and kindness. I have learned so much from you about what it means to be a better scientist and a better person, and I am so glad to have had a partner-in-crime like you to share in the adventures, struggles and triumphs of grad school with. I am looking forward to our future adventures, whatever those may be.

Chapter 1:
Introduction

Cell polarity is a fundamental process

Asymmetry is crucial for life. In the biological world, one can find innumerable examples of asymmetry. For example, many animals, such as fruit flies or humans, have a head-end and a tail-end. Similarly, individual cells exhibit axes of asymmetry in a process called cell polarity. Cells exist in non-uniform environments, so integration of and reaction to spatial cues is a requirement for survival. In order to achieve this, cells must polarize, where polarity is defined as the partitioning of a single cell's plasma membrane into distinct, non-overlapping domains.

Cell polarity is distinct from simple asymmetry, and although polarity and asymmetry could conceivably accomplish the same adaptive function, polarity is the dominant mode used by cells. Polarity requires balance between two domains that exist in a state of mutual antagonism. The result is a steady state distribution that is dependent on the 'strength' of each domain's input. In contrast, a pencil is asymmetric but not polarized, because if you sharpen a pencil to increase the size of the pointed end, it has no effect on the eraser on the opposite end. In a polarized system, increasing the 'strength' of one domain necessarily does so at the expense of the second domain.

All cells are polarized in some fashion. For example, bacteria asymmetrically localize sensory receptors and cell division machinery, yeast divide by asymmetric budding, neurons extend long processes from their cell bodies that carry electrical signals to distant target cells, stem cells divide unequally to give rise to daughter cells with different fates, and migrating cells specify leading and lagging edges to direct their movement in a specific direction.

In multicellular organisms, cell polarity is also critical for the organization of tissues and organs. Tissues in our bodies all have different and precise architectures. To create these complex organizations, each cell in the tissue must know where it is in space, what direction it is facing, and what other cells or environments surround it. Polarity enables cells to achieve these things by differentiating the various sides of the cell such that, for example, all the cells in an intestinal epithelium orient their 'top' sides in the same direction, which will allow for proper intestinal function and digestive physiology.

Epithelial cells as a model for polarity

One classically studied model of polarity are epithelial cells. Epithelia are among the most evolutionarily ancient cell type in metazoa and serve as the building blocks of almost all tissues and organs through their ability to form adherent sheets of cells (Cereijido et al., 2004). Epithelial cells perform diverse biological roles, most notably by forming barriers that keep tissues intact and separate the inside and outside of organs. Epithelial cells are also responsible absorbing and secreting molecules, such as in the digestive tract. Like all other cells, epithelial cells rely on their polarization to effectively carry out their physiological functions (Rodriguez-Boulan and Macara, 2014; St Johnston and Ahringer, 2010). One type of polarity adopted by epithelial cells is called apicobasal polarity, in which the axis linking the cell's free and contacting surfaces defines separate apical and basolateral domains, respectively. For this reason, the architecture of polarized epithelia is highly conserved, and many epithelial tissues are morphologically very similar, even in very distantly related species. Underscoring this importance is the fact that mutations that lead to disrupted epithelial polarity often have severe consequences for organ function and organismal viability. The roles of epithelial polarity in tissue development and homeostasis are discussed in more detail below.

A conserved toolkit polarizes cells

Underlying the morphological manifestation of cell polarity are the activities of key molecular regulators. In animal cells, polarity is regulated by conserved protein complexes that each define a specific domain of the cell. In most cell types, the Partitioning defective (Par) complex, composed of Par-3, Par-6 and atypical protein kinase C (aPKC) defines the anterior or apical domain of the cell. In some, but not all cells the Crumbs complex, composed of Crumbs (Crb), Pals1 and Patj also contributes to apical domain identity. Conversely, Par complex antagonists define the posterior or basolateral domain of the cell. There are several groups of Par complex antagonists that function in different contexts: the Scrib module, made up of Scribble (Scrib), Discs large (Dlg) and Lethal giant larvae (Lgl); the Yrt/Cora group, composed of Yurt (Yrt), Coracle (Cora), Nrx-IV and Na^+-K^+ ATPase; and the PAR-1, PAR-2 protein group. This relatively simple, highly conserved complement of proteins enables the polarization of virtually all known metazoan cell types and thus constitutes a truly fundamental aspect of basic cell biology (Goldstein and Macara, 2007; Lang and Munro, 2017; Nakajima, 2021; St Johnston and Ahringer, 2010; Tepass, 2012).

Molecular nature of epithelial polarity

From their initial discovery in forward genetic screens investingating anterior-posterior polarity in the *C. elegans* zygote and apicobasal polarity in *Drosophila* epithelia, a large body of work has helped uncovered the intricate details of the mechanisms of function of cell polarity regulators, especially with regard to apical polarity (Rodriguez-Boulan and Macara, 2014; Tepass, 2012). The following discussion will largely focus on insights from and *Drosophila* studies. The Par and Crumbs complexes are required to specify the cell's apical domain, whereas the Scrib module defines the basolateral domain. The boundary between apical and basolateral domains arises from mutual antagonism between the Par complex and the Scrib module (Tepass, 2012). The primary axis of this antagonism is between the Par complex kinase aPKC and the Scrib module protein Lgl. Lgl is a substrate of aPKC, whose phosphorylation removes Lgl from the plasma membrane and inactivates it. Conversely, basolateral Lgl is an inhibitor of aPKC kinase activity and protein localization (Bailey and Prehoda, 2015; Betschinger et al., 2003; Dong et al., 2015; Hutterer et al., 2004; Lee et al., 2006; Plant et al., 2003; Wirtz-Peitz et al., 2008; Yamanaka et al., 2003; Yamanaka et al., 2006).

From a very basic perspective, the manifestation of polarity is dependent almost entirely on protein-protein interactions. The core polarity regulating proteins of the Par, Crb and Scrib modules are highly enriched for protein binding domains and, with the exception of aPKC, do not have other enzymatic activities (**Figure 1.1**)(Flores-Benitez and Knust, 2016). Thus, cell polarization can be thought of as a building block process, where the initially localized core polarity regulators define a given cortical domain and then, through crosstalk with core cellular machinery, such as vesicle trafficking pathways, maintains the identity of the domain by polarizing secondary effector molecules, which are not themselves regulators of polarity, but are required for its functional output.

Mechanisms of apical polarity

In most cases, epithelial polarity begins with establishment of the apical domain. The small Rho GTPase Cdc42 is a central initiator of apical identity. Apically localized Cdc42•GTP is required to recruit the Par complex and is required for subsequent apical determination (Hutterer et al., 2004; Martin-Belmonte et al., 2007; Nunes de Almeida et al., 2019; Walther and Pichaud, 2010). The Par complex protein Par-3 is the first Par complex member to be polarized in many

systems, and its early apical localization is required for the recruitment of adherens junctions to the apicolateral border (Franz and Riechmann, 2010; Harris and Peifer, 2004). Subsequently, Par-3 recruits Par-6 and aPKC to the nascent apical domain (Franz and Riechmann, 2010; Harris and Peifer, 2005). Once localized there, aPKC must become activated. In many cases, this has been proposed to involve transfer of Par-6/aPKC from Par-3 to Cdc42, which upon binding to Par-6, may relieve aPKC autoinhibition and allow kinase activation (Atwood et al., 2007; Nunes de Almeida et al., 2019; Rodriguez et al., 2017; Wang et al., 2017; Yamanaka et al., 2001). Activated aPKC then phosphorylates Par-3, which dissociates it from the rest of the Par complex and excludes it from the apical domain proper, leading to its accumulation at the adherens junctions (Morais-de-Sá et al., 2010; Walther and Pichaud, 2010). Par-6/aPKC then recruit the Crb complex to the apical domain, where Crb reinforces the apical localization of Par-6/aPKC by outcompeting Par-3 for Par-6 binding (Morais-de-Sá et al., 2010). This results in mutual dependence for localization of these proteins and stabilization of apical Par-6/aPKC (Harris and Peifer, 2005; Morais-de-Sá et al., 2010). aPKC phosphorylation of Par-3 also serves to prevent Par-3 from binding Sdt, allowing Crb and Sdt to form a complex (Krahn et al., 2010).

At the apical domain, aPKC kinase activity is the main functional output of the Par complex and is required and sufficient to maintain apical identity (Hong, 2018; Sotillos et al., 2004). Controlling aPKC activity is thus imperative to the execution of the apical polarity program. aPKC activity is regulated in several ways, and is tightly linked to aPKC's localization in order to ensure substrate phosphorylation occurs at the correct time and place (Drummond and Prehoda, 2016; Hong, 2018). By default, aPKC is in an autoinhibited state, with its N-terminal pseudosubstrate motif bound to the kinase domain (Graybill et al., 2012; Zhang et al., 2014). Historically, it was thought that Par-6 negatively regulated aPKC activity and that aPKC bound to Par-6 was maintained in its autoinhibited state. aPKC could thus only be activated once Par-6 bound to apical Cdc42, relieving autoinhibition by the pseudosubstrate domain (Atwood et al., 2007; Yamanaka et al., 2001). However, subsequent work called into question the role of Par-6 in regulating aPKC activity, with evidence that Par-6 binding actually activates aPKC by allosteric displacement of the pseudosubstrate motif in a Cdc42-independent fashion (Graybill et al., 2012). A potential explanation for this discrepancy is that prior studies using bacterially expressed aPKC and Par-6 may have been subject to artifacts due to aggregation of the purified proteins. This model is compatible with spatiotemporal regulation of aPKC activity, because aPKC and Par-6 are mutually dependent for apical localization, which would ensure that aPKC only becomes activated after reaching the apical domain (Graybill et al., 2012).

Recently, Crb has also emerged as a potential aPKC activator (Dong et al., 2020). In this model, aPKC binds to Par-6, which relieves autoinhibition and recruits the complex apically due to unmasking of a lipid binding polybasic domain. However, aPKC does not yet become active because the Par-6 C-terminus occludes its kinase domain. At the apical cortex, Par-6 binds to Crb, displacing Par-6 from aPKC's kinase domain and derepressing its activity (Dong et al., 2020).

In addition to polarity proteins, other factors have also been implicated in aPKC activity regulation, including autophosphorylation, additional kinases, including mTORC2, and the lipid diacylglycerol (DAG). However, the exact roles and physiological relevance of these regulators is not well understood (Drummond and Prehoda, 2016).

Although aPKC has many substrates, the primary target of its activity in polarity is the Scrib module protein, Lgl. aPKC phosphorylation of Lgl is required to prevent Lgl's localization at the apical cell cortex and ensure the segregation of the basolateral domain (Betschinger et al., 2003; Plant et al., 2003; Yamanaka et al., 2003). In aPKC mutants, Lgl mislocalizes uniformly to

the entire cell cortex, including the apical domain (Carvalho et al., 2015; Hutterer et al., 2004; Khoury and Bilder, 2020; Ventura et al., 2020). Interestingly however, aPKC kinase activity does not seem to be strictly necessary and there are rare cases where kinase-impaired aPKC mutants can still exclude apical Lgl (Aguilar-Aragon et al., 2018; Kim et al., 2009). While normally restricted via its polarized localization, a constitutively activated, cytosolic form of aPKC is also sufficient to displace all cortical Lgl–including from the basolateral domain–and specify an ectopic apical domain that spreads throughout the whole cell (Betschinger et al., 2003; Khoury and Bilder, 2020; Sotillos et al., 2004).

Mechanisms of basolateral polarity

In contrast to the highly detailed understanding of the Par complex proteins and their individual molecular activities, comparatively little is known about the mechanisms of action of the three Scrib module proteins. Originally described in *Drosophila* over 20 years ago, Scrib, Dlg and Lgl comprise the three members of the basolateral Scrib polarity module. All three are absolutely required for cell polarity, as inactivation of any of them results in loss of polarity and spreading of the apical domain throughout the whole cell, as well as disruption of epithelial architecture (**Figure 1.2B-C**)(Bilder et al., 2000b). Lgl and Dlg were first discovered on the basis of their potent function as neoplastic tumor suppressors in larval *Drosophila* (Gateff and Schneiderman, 1969; Gateff and Schneiderman, 1974; Stewart et al., 1972). Along with Scrib, all three were subsequently identified in a forward genetic screen for regulators of epithelial morphogenesis in *Drosophila* embryos (Bilder and Perrimon, 2000; Bilder et al., 2000b). Mutation of these genes resulted in a severe disorganization of the *Drosophila* larval cuticle, a structure that is secreted by the underlying epidermis and can be used as a readout for the integrity of this tissue. The disorganized, messy nature of the mutant cuticle is the basis for the gene name "*scribble"* (Bilder and Perrimon, 2000).

The categorization of Scrib, Dlg and Lgl into a polarity regulating 'module' comes from the fact that all three encode proteins that colocalize to the basolateral domain of epithelial cells and that the localization of each requires the function of the other two (Bilder et al., 2000b). Additionally, Scrib, Dlg and Lgl exhibit strong genetic interactions and all three are required to define the basolateral domain and restrict spread of the apical domain. It is interesting to note however, that despite the close functional relationships between Scrib, Dlg and Lgl, evidence for direct physical interaction between these three proteins is lacking (Bonello and Peifer, 2018; Stephens et al., 2018). Documented interactions involve intermediary binding partners or presence in shared complexes, and instances where direct interactions have been observed do not appear to be universally conserved (Mathew et al., 2002; Nakajima et al., 2019). For example, a direct interaction between Lgl and Dlg's GUK domain was found in mammalian cells (Zhu et al., 2014). However, the Dlg GUK domain is dispensable in many systems, and recent work suggests that Lgl is not stably complexed with Scrib or Dlg (Hough et al., 1997; Ventura et al., 2020). Thus, Scrib, Dlg and Lgl are together referred to as a functional 'module,' rather than a protein complex.

Molecular composition of the Scrib module

Scrib, Dlg and Lgl all encode large scaffolding proteins with no obvious catalytic activity (Betschinger et al., 2005; Bilder and Perrimon, 2000; Woods and Bryant, 1993). Dlg belongs to the Membrane Associated Guanylate Kinase (MAGUK) protein family, characterized by the presence of one or more PDZ domains, an SH3 domain and an enzymatically inactive guanylate kinase (GUK) domain, arranged in that order (Funke et al., 2005; Woods and Bryant, 1993; Zhu

et al., 2012). MAGUK GUK domains have evolved loss of catalytic activity due to loss of nucleotide binding capability, allowing them to acquire protein binding functionality instead (Funke et al., 2005; Johnston et al., 2011; Olsen and Bredt, 2003; Zhu et al., 2012). MAGUK proteins are thought to be involved in organization of large protein complexes at the plasma membrane because of their multiple protein-protein interaction domains, and their ability to oligomerize via association of their SH3 and GUK domains (Funke et al., 2005; McGee et al., 2001; Zhu et al., 2012). Most species have multiple Dlg homologs (Dlg1-Dlg5), some of which have evolved cell type-specific functions, such as organizing the neuronal synapse (Roberts et al., 2012). Scrib is part of the much smaller Leucine Rich Repeat (LRR) and PDZ (LAP) protein family. As the name implies, these proteins contain a LRR followed by a small LAP-specific domain (LAPSD) and often several PDZ domains. Scrib is a founding member of this family along with Erbb2 interacting protein (Erbin) and Densin-180 (Bilder et al., 2000a). Although there is only a single Scribble homolog, the related LAP proteins Erbin and Lano have been shown to act "redundantly" in polarity regulation in mammalian cells (Choi et al., 2019). Lgl is an enigmatic protein containing WD-40 repeats that are thought to form a β-propeller structure. Lgl was originally proposed to be a cytoskeletal protein on the basis of its interaction with myosin and its ability to fractionate with the actin cytoskeleton (Betschinger et al., 2005; Strand et al., 1994a; Strand et al., 1994b). Additionally, Lgl may be the most evolutionarily ancient of the three Scrib module proteins, as *Saccharomyces cerevisiae*, the budding yeast, have two putative Lgl orthologs, Sro7 and Sro77, which are involved in vesicle exocytosis (Lehman et al., 1999). While invertebrates have one Lgl gene, vertebrates have evolved two Lgl homologs, Lgl1 and Lgl2, where Lgl1 has broader expression, but both genes have conserved roles in cell polarity (Klezovitch et al., 2004; Vasioukhin, 2006).

Localization of Scrib module proteins

Scrib, Dlg and Lgl all localize to the basolateral cortex and this localization is required for their function. However, there are several key differences. Scrib and Dlg both concentrate at the septate junction (SJ) in invertebrates, a structure homologous to the vertebrate tight junction (TJ), while in vertebrates, Scrib and Dlg overlap with the adherens junction (AJ) and with the TJ in some contexts (Dow et al., 2003; Ivanov et al., 2010; Laprise et al., 2004; Navarro et al., 2005). Recently, Scrib and Dlg localization to invertebrate AJs was also observed during certain stages of *Drosophila* embryogenesis (Bonello et al., 2019). Dlg localization relies on a recently discovered phospholipid binding polybasic motif within its HOOK domain that is required for its recruitment to the basolateral membrane (Hough et al., 1997; Lu et al., 2021). Refinement of Dlg localization to the SJ requires the PDZ domains, similar to Scrib (Hough et al., 1997; Lu et al., 2021). Interestingly, plasma membrane targeting by the Dlg polybasic motif is not constitutive; it is activated via allosteric regulation by a putative Scrib-dependent activity and potential phosphorylation by an unknown kinase (Lu et al., 2021). Like Dlg, Lgl also makes use of a polybasic motif for cortical localization. Phospholipid binding by Lgl's polybasic motif is negatively regulated by aPKC phosphorylation, which creates negative charge density on the polybasic motif, counteracting the electrostatic attraction between its basic amino acids and polar phospholipid head groups (Bailey and Prehoda, 2015; Dong et al., 2015; Visco et al., 2016). This electrostatic switch mechanism is a conserved feature in the regulation of aPKC substrate localization by their phosphorylation (Bailey and Prehoda, 2015). Lgl phosphorylation additionally reduces the formation of an α-helix with favorable phospholipid binding charge distribution, further increasing the effectiveness of the phosphorylation-dependent membrane

binding switch (Almagor et al., 2019). Membrane removal by aPKC ensures that Lgl localization is restricted to the basolateral domain. A similar mechanism is used by Aurora kinase during mitosis to remove Lgl from the membrane and allow correct spindle orientation (Bell et al., 2015; Carvalho et al., 2015). The molecular mechanisms of Scrib localization are less clear than that of Dlg and Lgl. Broadly, Scrib relies on its LRR and LAPSD domains for localization to the membrane, while PDZ1 and 2 may confer junctional enrichment and refine its polarization (Albertson et al., 2004; Choi et al., 2019; Legouis et al., 2003; Zeitler et al., 2004). In vertebrate cells, posttranslational S-palmitoylation also contributes to Scrib localization (Chen et al., 2016a).

Establishment of basolateral polarity

During polarization in *Drosophila* embryos, Scrib and Dlg localize to the presumptive basolateral membrane at a very early stage, with Rap1, Afadin and Par-3 dependent enrichment at Spot AJs (Bonello et al., 2019). This early localization of Scrib and Dlg is important for the organization and localization of the AJ complex (Bonello et al., 2019). *C. elegans* DLG-1 and the Scrib homolog, LET-413 are similarly required for correct localization of AJs in developing embryonic epithelia (Bossinger et al., 2001; Firestein and Rongo, 2001; Köppen et al., 2001; Legouis et al., 2000; McMahon et al., 2001). Scrib and Dlg also regulate AJs in vertebrates, with depletion of either protein leading to disrupted AJ function (Awadia et al., 2019; Laprise et al., 2004; Qin et al., 2005; Van Campenhout et al., 2011). Furthermore, there is evidence that both Scrib and Dlg physically associate with E-cadherin in vertebrates, suggesting that AJ regulation is a highly conserved feature of Scrib module function (Laprise et al., 2004; Wang et al., 2018; Yoshihara et al., 2011).

In addition to AJs, the Scrib module regulates other types of epithelial junctions, most notably, the occluding junction (TJ in vertebrates, SJ in invertebrates). Occluding junctions prevent intercellular diffusion, giving rise to the epithelial permeability barrier. As noted above, in *Drosophila* epithelia Scrib and Dlg show enriched localization to the SJ (Bilder et al., 2000b). In *scrib* or *dlg* mutants, SJs fail to form and their components are mislocalized (Bilder et al., 2003; Woods et al., 1996). However, Scrib and Dlg are not themselves core components of the SJ (Oshima and Fehon, 2011). In vertebrates, although Scrib and Dlg do not localize to TJs, they still exert a functional influence on them. Loss of function mutation results in disrupted TJ assembly and mislocalization of TJ component proteins in multiple mammalian cultured cell and tissue types (Ivanov et al., 2010; Qin et al., 2005; Stucke et al., 2007; Van Campenhout et al., 2011; Yates et al., 2013). Recently, Scrib and Dlg have also been found to play a role in a related type of junction: the tricellular junction (TCJ). The TCJ is formed by the convergence of three occluding junctions at the vertex where three epithelial cells meet. In *Drosophila*, Scrib and Dlg have been shown to regulate the localization of TCJ-specific proteins, and may even interact with them physically, thus directing TCJ assembly (Padash-Barmchi et al., 2013; Schulte et al., 2006; Sharifkhodaei et al., 2019).

Molecular mechanisms of apicobasal antagonism

At the basolateral cortex, Lgl is the business end of the Scrib module. Apicobasal polarity centers around the antagonism between Lgl and aPKC; whereas aPKC phosphorylation inactivates Lgl at the apical domain, basolateral Lgl is an inhibitor of aPKC's activity and localization (Betschinger et al., 2003; Hutterer et al., 2004; Plant et al., 2003; Wirtz-Peitz et al., 2008; Yamanaka et al., 2003; Yamanaka et al., 2006). Following formation of the apical domain, Lgl is segregated to the basolateral domain, where it is required to inhibit Par complex spread and inhibit

apical identity (Hutterer et al., 2004; Yamanaka et al., 2003; Yamanaka et al., 2006). The exact mechanisms by which Lgl inhibits aPKC are a longstanding mystery. Previous work demonstrated that Lgl could actually be part of the Par complex, in a context-dependent manner via binding to Par-6 (Plant et al., 2003; Wirtz-Peitz et al., 2008; Yamanaka et al., 2003). These studies suggested that the Lgl-containing Par complex is in an inhibited state and that exchange of Lgl for Par-3 stimulates aPKC activity (Wirtz-Peitz et al., 2008; Yamanaka et al., 2003). How might Lgl inhibit the aPKC/Par-6 complex? It has long been known that addition of Lgl to aPKC *in vitro* kinase reactions can suppress aPKC activity, however it is likely that this is due to the excess Lgl protein acting as a competitive inhibitor for the substrate being measured (Graybill et al., 2012; Holly and Prehoda, 2019). Additionally, Lgl does not stably associate with aPKC/Par-6 *in vitro*, arguing against the idea that Lgl inhibits aPKC simply by binding the Par complex (Graybill et al., 2012). These studies support the idea that Lgl might antagonize aPKC by a competitive inhibition mechanism.

While the ability of Lgl to inhibit aPKC kinase activity has been debated, Lgl's ability to restrict aPKC localization is quite clear (Grifoni et al., 2007; Holly and Prehoda, 2019; Hutterer et al., 2004; Lee et al., 2006). Interestingly, the ability of Lgl to antagonize aPKC appears to be entirely dependent on Scrib and Dlg, because in *scrib* and *dlg* mutants, polarity is lost and the Par complex mislocalizes throughout the cell cortex in a manner indistinguishable from *lgl* mutants, suggesting that Lgl requires Scrib and Dlg for its aPKC-inhibiting activity (Khoury and Bilder, 2020). Indeed, as I will discuss in Chapter 2, Scrib and Dlg appear to act as a switch in the aPKC-Lgl antagonism circuit that enables Lgl to inhibit aPKC at the basolateral domain, whereas at the apical domain, where Scrib and Dlg are not present, aPKC is able to inhibit Lgl (**Figure 1.2A**). This is reminiscent of a bistable circuit, where either of two states (in this case apical and basolateral) 'wins', a phenomenon that has been proposed to account for the behavior of other types of polarized systems (Lang and Munro, 2017). A similar type of 'protection' activity has also been described for PAR-1 in C. elegans zygote polarity, where PAR-2 shields PAR-1 from aPKC (Ramanujam et al., 2018). Interestingly, unlike PAR-1 and PAR-2, Lgl does not appear to exist in a physical complex with Scrib/Dlg, suggesting that Lgl protection utilizes indirect mechanisms (Ventura et al., 2020). Although the precise molecular nature of Scrib and Dlg's Lgl protection activity is not known, this idea gives rise to a plausible model for how balance between apical and basolateral domains could be achieved through modulation of the aPKC-Lgl relationship by Scrib/Dlg (Khoury and Bilder, 2020).

In some contexts, basolaterally localized factors other than the Scrib module antagonize Par complex funntion in apicobasal polarity. Par-1, a kinase found at the basolateral domain of some cells, phosphorylates Par-3, impairing its oligomerization ability, which then prevents Par-3 from recruiting the aPKC/Par-6 complex to the basolateral domain (Benton and St Johnston, 2003; Nam et al., 2007). More recently, additional basolateral polarity regulators have been identified in *Drosophila* studies, including Girdin and the so-called Yrt/Cora group, composed of Yrt, Cora, Nrx-IV and Na^+, K^+-ATPase (Biehler et al., 2020; Laprise et al., 2009). Similar to the Scrib module, these proteins localize to the basolateral domain and exhibit genetic interactions with apical regulators, with Yrt and Girdin negatively affecting aPKC activity (Biehler et al., 2020; Gamblin et al., 2014). However in contrast to the Scrib module, their activity is only required late in embryogenesis to maintain polarity (Laprise et al., 2009). This later acting Yrt/Cora pathway is thought to explain why Scrib module mutant embryos seem to exhibit a partial rescue of epithelial polarity at late organogenesis stages (Bilder et al., 2003; Laprise et al., 2009; Tanentzapf and

Tepass, 2003). However, the breadth of the requirement for the Yrt/Cora complex in epithelial polarity is not as wide as that of the Scrib module.

Diversity of polarity programs

Although the mechanisms of epithelial cell polarity are broadly conserved, there are context-specific differences (reviewed in (Pickett et al., 2019)). For example, in the *Drosophila* ovarian follicle epithelium, Par-3 is dispensable for Par-6/aPKC localization (Shahab et al., 2015). In *Drosophila* embryos and pupal photoreceptors, Cdc42 does not appear required for phosphorylation of aPKC substrates to occur (Hutterer et al., 2004; Walther and Pichaud, 2010). Another interesting finding is that although *C. elegans* encodes three Crb homologs, none of them have obvious mutant phenotypes and are dispensable for viability (Waaijers et al., 2015). In *C. elegans*, the Scrib and Dlg homologs, LET-413 and DLG-1 have also diverged slightly from their *Drosophila* counterparts, with DLG-1 evolving a more junction-centric role, rather than direct polarity regulation (Bossinger et al., 2001; Firestein and Rongo, 2001).

C. elegans also possesses an additional polarity regulator that is not conserved in other animals. The C. elegans zygote is polarized along its anterior-posterior axis by antagonism between anterior PARs, CDC-42, PAR-3, PAR-6 and aPKC and posterior PARs, PAR-1, PAR-2 and CHIN-1. This polarity is essential for asymmetric division of the zygote, resulting in the first lineage segregation in C. elegans development. The posterior protein, PAR-2 plays an essential role in polarization of the worm zygote, where it is a substrate for aPKC that is required to protect PAR-1 such that PAR-1 can exclude PAR-3 from the posterior (Hao et al., 2006; Ramanujam et al., 2018). Although PAR-2 is not conserved outside of nematodes, there are suggestions that its cellular function may be conserved. This idea comes from experiments showing that the *C. elegans* Lgl homolog, LGL-1 can partially compensate for PAR-2 function in *par-2* hypomorphic mutants, suggesting that LGL-1 and PAR-2 have overlapping function (Beatty et al., 2010; Hoege et al., 2010). Intriguingly, PAR-2 and Lgl both contain phosphorylation-regulated membrane binding polybasic domains with multiple aPKC phosphorylation sites (3 in Lgl, 7 in Par-2) and both proteins are required to antagonize aPKC. While suggestive, the complete functional relatedness of PAR-2 and Lgl remains to be seen, especially since Scrib and Dlg are not present in the worm zygote, indicating Lgl function in this system may not be analogous to epithelia expressing the complete Scrib module. An interesting functional test of this would be to ask whether PAR-2 can substitute for Lgl in a non-nematode polarity system.

One of the more interesting observations is that, although Scrib is indeed required for mammalian epithelial polarity, mammalian Scrib mutants were not initially seen to have overt apicobasal polarity defects (Bonello and Peifer, 2018). Instead, one of the most commonly observed phenotypes was impaired Planar Cell Polarity (PCP), leading to the belief that vertebrate Scrib did not possess an apicobasal polarity function (Montcouquiol et al., 2003; Murdoch et al., 2003; Yates et al., 2013). One potential reason for this is the existence of multiple LAP family proteins in vertebrates, which may have masked Scrib's polarity function via partial redundancy. Recent work has suggested that all three vertebrate LAP proteins–Scrib, Erbin and Lano–must be simultaneously depleted to reveal an apicobasal polarity defect in epithelial cells (Choi et al., 2019).

In some particularly dramatic cases, epithelia can polarize seemingly independently of the canonical Par and Scrib modules. For example, in the *Drosophila* midgut, polarity is established by a combination of integrin-mediated adhesion and SJ proteins. Similarly, in the sea anemone *Nematostella,* the Par complex is actively degraded in epithelializing endomesoderm and is

dispensable for polarity of this tissue (Salinas-Saavedra et al., 2018). One hypothesis for such differences in polarization mechanisms is the developmental origin of the epithelium in question (Chen et al., 2018).

Crosstalk between the Scrib module and general cellular machinery

The preceding discussion on the activities of cell polarity regulators only encompasses the first part of the manifestation of cell polarity, where the different cellular domains are defined. The end result of polarization is functional compartmentalization of the cell, and to achieve this, core cell polarity regulators must interface with the cellular machinery at large to enable the spatial regulation of these processes.

Interaction between the Scrib module and vesicle trafficking

One of the most studied examples of such a relationship is the crosstalk between cell polarity regulators and vesicle trafficking pathways. The directed movement of vesicular cargoes provides an intuitive mechanism to polarize macromolecules within the plasma membrane. Historically, exocytosis, or secretion, was thought to be the major vesicle trafficking pathway involved in polarity, and studies in yeast and cultured mammalian epithelial cells revealed important roles for polarized cargo delivery to the budding daughter cell and nascent apical domain, respectively (Fölsch et al., 2009; Shivas et al., 2010; Slaughter et al., 2009). However, more recently, the key role of endocytosis in regulating cell polarity has also come to be appreciated (Román-Fernández and Bryant, 2016; Shivas et al., 2010). Studies in *Drosophila* demonstrated the requirement of endocytic regulators from nearly every step of the internalization pathway in epithelial polarity (Lu and Bilder, 2005; Morrison et al., 2008; Windler and Bilder, 2010). The relationship between apical polarity and vesicle trafficking has been extensively reviewed elsewhere (Jewett and Prekeris, 2018; Román-Fernández and Bryant, 2016); here I will focus on the interactions between basolateral polarity regulators and vesicular transport.

Forward genetic screens in *Drosophila* to isolate polarity regulating genes uncovered a large number of mutants that shared phenotypes with Scrib module mutants, *scrib, dlg* and *lgl* (Menut et al., 2007). A large number of these mutations mapped to genes encoding proteins involved in almost every step of the endocytic pathway, including Rab5, Dynamin, Clathrin, and ESCRT proteins (Vaccari and Bilder, 2009). Similar to Scrib module mutants, these endocytic mutants exhibit loss of epithelial polarity, characterized by ectopic spread of the apical domain throughout the cell and mislocalization of junctional and polarity proteins. The similarities in these shared phenotypes led to the hypothesis that the Scrib module and endocytosis were somehow functionally linked in their regulation of cell polarity (Shivas et al., 2010).

However, the mechanisms proposed for how endocytosis controls cell polarity are markedly different than those for the Scrib module—namely, Lgl protection and aPKC antagonism. One model is that endocytosis is required to remove apical resident proteins that transiently mislocalize to the basolateral domain, so that they can be recycled back to the apical membrane (Fletcher et al., 2012). Apically localized Crb has been an appealing candidate, being the only transmembrane protein among all the polarity regulators. Initial work suggested that Crb mislocalization contributed to the polarity loss phenotypes of mutants with early endosomal dysfunction (Lu and Bilder, 2005). A model proposed that Crb is concentrated apically through positive feedback with other apical proteins, and that basolateral Lgl promotes Crb recycling back to the apical domain to prevent its mislocalization and apical spread (Fletcher et al., 2012). Although a similar role for vertebrate Lgl in promoting apical protein internalization during cell

depolarization has been demonstrated (Yamanaka et al., 2006), rigorous support for this model and a concrete molecular link between Lgl and Crb recycling awaits further investigation. Indeed, two complicating facts are that Scrib module mutants appear to have completely normal endocytic transport and that Crb is not required for apical domain expansion in endocytic mutants (de Vreede et al., 2014).

Among the three Scrib module proteins, Lgl has been the most closely implicated in vesicle trafficking. The proposed yeast homologs of Lgl, Sro7/77 interact with and regulate the exocytic machinery and this has also been demonstrated for basolateral exocytosis in mammalian MDCK cells (Lehman et al., 1999; Musch et al., 2002; Zhang et al., 2005). In *Drosophila*, Lgl has been localized to endosomes and physically associates with the V-ATPase complex to regulate endosomal acidification (Parsons et al., 2014; Portela et al., 2018). Functionally, this vesicular Lgl population negatively regulates Notch signaling by reducing vesicular acidification and preventing activation of Notch by γ-secretase (Parsons et al., 2014; Portela et al., 2015; Portela et al., 2018). Lgl plays a similar role in non-epithelial neuroblasts (*Drosophila* neural stem cells) by promoting internalization of the fate determinant Sanpodo (Roegiers et al., 2005). This Lgl function appears to be conserved in vertebrates, as Lgl has been shown to regulate Notch signaling in the retinal neuroepithelium (Clark et al., 2012), and also regulates the cell surface levels of apical junctional complexes in mouse embryonic neural stem cells (Jossin et al., 2017). In even more direct demonstrations, it was shown that Lgl regulates neuronal polarization by activating Rab10 to promote axonal trafficking (Wang et al., 2011) and more recently, that Lgl regulates oligodendrocyte differentiation by endocytosis and recycling of a specific cargo, NG2, in oligodendrocyte precursor cells (Daynac et al., 2018). Although many different connections between Lgl and vesicle trafficking pathways have been found, there are not obvious molecular themes that would unify these different connections.

There is also evidence for Scrib crosstalk with trafficking machinery. Indeed, it was observed very early on that Scrib could be seen localizing to puncta, reminiscent of endosomes (Bilder and Perrimon, 2000). More recently, LET-413, the *C. elegans* Scrib homolog was identified as a Rab10 binding partner that promotes Rab10 activation by enhancing the GEF activity of DENN-4 and mediating the GTPase cascade from Rab5 to Rab10 during endosome maturation (Liu et al., 2017). Interestingly, this work also showed that LET-413/Scrib can also interact with Rab8, Rab11 and Rab35, although the functional implications of these interactions are unclear. Likewise, fellow LAP protein Erbin can bind to the early endosomal protein SARA and influence the localization of certain cargoes, such as SMADs, to Sara+ endosomes (Sflomos et al., 2011). Scrib regulates other aspects of vesicle trafficking in specialized cases, such as the recycling of NMDA receptors via the AP2 complex at neuronal synapses, and promoting the activation of the Drosophila BMP type-I receptor, Tkv, during wing patterning, via its internalization to Rab5 endosomes (Gui et al., 2016; Piguel et al., 2014).

Support for a direct role of Dlg in regulating trafficking is less abundant than for Lgl or Scrib and has mainly been studied in non-epithelial cells. In neurons, Dlg interacts with many trafficking-related proteins, including several kinesin and myosin family members and others, such as syntaxins (Reviewed in (Walch, 2013)). In epithelial cells, at least one instance of an analogous interaction has been described, where Dlg binding to the kinesin KIF13B apparently mediates Dlg transport within the cell (Asaba et al., 2003). However, the physiological relevance of this is *in vivo* is not understood and, in this case, Dlg is not itself regulating the traffic of other cargoes. Some support for a more general role of Dlg in endosomal traffic is an identified Yeast Two-Hybrid interaction between Dlg and Hrs, a component of the ESCRT-0 complex that is involved

in early endosome maturation (Chetkovich et al., 2002). The Dlg-Hrs interaction may be conserved, as Hrs was recently identified in an *in vivo* Dlg-promixity proteomics screen (Sharp et al., 2021)..

One specific vesicle trafficking pathway for which there is good evidence for Scrib module involvement is the retromer pathway. Retromer is an alternative recycling pathway that promotes the return of cargoes to the plasma membrane by an endosome to Golgi route (Gallon and Cullen, 2015; Hsu et al., 2012). Retromer was previously implicated in cell polarity because Crb was shown to be recycled to the apical membrane via this pathway (Pocha et al., 2011; Zhou et al., 2011). Retromer recycling was then functionally linked to the Scrib module because Scrib module mutants have defects in endocytic transport of Crb—a retromer cargo—but do not have any deficit in general endocytosis or recycling of generic transmembrane cargoes (de Vreede et al., 2014). Scrib, Dlg and Lgl all exhibit positive genetic interactions with retromer components, and importantly, the mislocalization of retromer cargoes (eg Crb) in Scrib module mutants was partly dependent on the Par complex, suggesting that retromer-mediated recycling is a component of the apical antagonizing activity of the Scrib module (de Vreede et al., 2014). The relationship between the Scrib module and retromer is conserved, as Scrib was shown to influence the endocytic itinerary of E-cadherin in mammalian cells by negatively regulating its transit through the retromer pathway (Lohia et al., 2012). Thus, although the mechanisms may differ between epithelial tissue types and organisms, a functional connection between the Scrib module and the retromer is likely to be a conserved feature of cell polarity.

Regulation of cellular signaling by the Scrib module

The Scrib module has complicated and abundant relationships with many signaling pathways. This has been extensively reviewed elsewhere (Bonello and Peifer, 2018; Enomoto and Igaki, 2011; Stephens et al., 2018); here I will discuss a limited number of these interactions with direct relevance for epithelial cell polarity.

One of the earliest noted phenotypes of Scrib module mutants was neoplastic transformation of epithelial tissues into malignant tumors that led to organismal lethality (Bilder, 2004; Gateff, 1978). The current dogma is that cancer subverts existing cellular pathways to fuel its own growth. Consistently, it is now known that the tumorigenic potential of *scrib, dlg* and *lgl* mutants depends on the rewiring of physiological signaling pathways. A well studied example of this is the c-Jun N-terminal Kinase (JNK) pathway (La Marca and Richardson, 2020). JNK is a member of the MAPK family. In *Drosophila*, one mechanism for JNK signaling activation begins with binding of TNFα to one of two TNF receptor (TNFR) homologs, Wgn and Grnd. This then triggers an intracellular kinase cascade, resulting in the phosphorylation of numerous substrates that alter various cellular activities, such as proliferation. Tumors derived from Scrib module mutants strongly upregulate JNK signaling, and this is required for their neoplastic overgrowth via downstream transcriptional changes mediated by Jun/Fos and the Hippo pathway effector Yki (ortholog of vertebrate YAP)(Bunker et al., 2015; Sun and Irvine, 2011). JNK and Yki often cooperatively co-regulate transcriptional targets, and a complex network of transcription factors governs neoplastic overgrowth (Atkins et al., 2016; Kulshammer et al., 2015). Yki is also regulated by aPKC, providing another mechanism for neoplastic transcriptional activation upon polarity loss (Doggett et al., 2011). Interestingly, blocking tumor-induced JNK signaling or downstream transcriptional changes rescues apicobasal polarity loss, in addition to tumorigenic overproliferation in Scrib module mutant tissues, suggesting transcriptional regulation of cell polarity (Bunker et al., 2015; Doggett et al., 2011; Sun and Irvine, 2011; Zhu et al., 2010).

However, while it is clear that the polarized state of the cell can regulate transcriptional programs, how the transcriptome can in turn regulate polarity is unclear and will be an interesting area of future study (See Rust and Wodarz, 2021 for review).

Paradoxically, the JNK pathway also has a tumor suppressive relationship with the Scrib module. In contrast to tissues that are entirely mutant for *scrib, dlg* or *lgl*, when small groups, or clones, of cells are mutant in an otherwise WT tissue, JNK signaling eliminates these mutant cells in a surveillance mechanism known as cell competition (Baker, 2020; La Marca and Richardson, 2020). In this context, activation of JNK signaling depends on the presence of WT neighbor cells and a recently described mechanism based on mislocalization of TNFR that allows activation by systemic TNF, resulting in stimulation of apoptosis in the mutant cells, resulting in their elimination from the tissue (de Vreede et al., 2022). Removal of JNK signaling allows clones of Scrib module mutant cells to overproliferate and form tumors (Brumby and Richardson, 2003; Igaki et al., 2009).

Because cancer is a complex disease often associated with accumulation of multiple driver mutations, there has been extensive work on models of human cancer involving cooperation between Scrib module mutants and other pathways, most prominently activated Ras signaling (Richardson and Portela, 2018). When combined with Ras activation or similar manipulations, Scrib module mutation results in highly malignant phenotypes including invasion into neighboring tissues and more faithfully recapitulates human cancers than either manipulation on its own. Model systems for cancer biology involving cell polarity manipulation is a substantial topic beyond the scope of this work and the reader is referred to relevant reviews on the subject (Bilder et al., 2021; Richardson and Portela, 2018; Saito et al., 2018).

The Scrib module in tissue development and physiology

In addition to their functions at the single-cell level, Scrib, Dlg and Lgl are also involved in the development and homeostasis of a number of tissues and organs. The numerous and diverse roles of Scrib module proteins in biology emphasize both the importance of cell polarity in organ function and the necessity of a deeper molecular knowledge of Scrib, Dlg and Lgl to complete our understanding of these crucial biological processes.

As mentioned above, in *Drosophila,* one of the earliest noted biological processes involving the Scrib module was control of cell proliferation and tissue growth, as Scrib module mutant tissues overgrow to form neoplastic tumors that invariably lead to organismal lethality (Bilder, 2004; Hariharan and Bilder, 2006). These tumors stimulate many physiological responses, including organismal stress responses and non-autonomous activation of a tumor-suppressive immune response (Parisi et al., 2014). When transplanted into adult flies, these tumors result in systemic wasting affecting many organ systems, and eventual death (Figueroa-Clarevega and Bilder, 2015). The many systemic effects induced by these tumors makes them a powerful model for the study of tumor-host interactions (Bilder et al., 2021).

In vertebrates, Scrib was identified early on as a regulator of neural tube morphogenesis. The *circletail* (*crc*) mouse mutant is a frameshift allele of *Scrib* and results in an extreme form of neural tube closure defect that affects almost the entire brain and spinal cord, called craniorachischisis (Murdoch et al., 2003). Consistently, mutations in *SCRIB* have been associated with craniorachischisis and spina bifida in humans, and neural tube morphogenesis in zebrafish, suggesting this is an important and conserved function (Lei et al., 2013; Robinson et al., 2012; Žigman et al., 2011). Mechanistically, Scrib regulates neural tube morphogenesis through the PCP pathway, in cooperation with the protein Vangl2 in mice and through adhesion-dependent

oriented progenitor cell division in zebrafish (Kharfallah et al., 2017; Murdoch et al., 2003; Žigman et al., 2011).

Lgl has also been shown to have a prominent role in neural/brain development, with *Lgl1* mutant mice exhibiting severe brain abnormalities due to loss of polarity and dysregulated signaling in neural stem cells (Clark et al., 2012; Jossin et al., 2017; Klezovitch et al., 2004). Interestingly, neural progenitors in *Lgl1* mutant display impaired differentiation and failed cell cycle exit, reminiscent of the brain tumor phenotype initially described in *Drosophila lgl* mutants (Gateff and Schneiderman, 1974; Lee et al., 2006). At the level of individual neurons, Scrib and Lgl have also been demonstrated to regulate neuronal polarity, directed trafficking in neurites and even axon pathfinding (Sun et al., 2016; Szczurkowska et al., 2022; Wang et al., 2011).

There is also ample evidence for the importance of the Scrib module and polarity regulators in general in cardiovascular biology (Horne-Badovinac et al., 2001; Jiménez-Amilburu and Stainier, 2019; Jiménez-Amilburu et al., 2016; Rohr et al., 2006). Lgl regulates cardiomyocyte tissue integrity and adhesion, and *lgl* mutant zebrafish have dysmorphic cardiomyocytes and abnormal cardiac morphogenesis, partially due to disrupted Yap signaling, resulting in blood flow defects (Flinn et al., 2020). Scrib regulates blood vessel development through promoting directed endothelial cell migration through integrin binding and *scrib* mutant zebrafish have impaired intersegmental vessel angiogenesis (Michaelis et al., 2013). In adult animals, Scrib is also required to maintain endothelial cell function and loss of Scrib in mice results in endothelial cell dedifferentiation and development of atherosclerosis (Schürmann et al., 2019).

Other organ systems where Scrib module involvement has been demonstrated include regulation of craniofacial, urogenital and kidney system development by Dlg (Caruana and Bernstein, 2001; Iizuka-Kogo et al., 2007; Naim et al., 2005), mammary gland and placenta branching morphogenesis by Lgl (Ma et al., 2022; Sripathy et al., 2011) and skin morphogenesis by Scrib and Lgl (Arora et al., 2020; Pearson et al., 2015; Raman et al., 2016; Sonawane et al., 2005). This is a small selection of example contexts where the Scrib, Dlg and Lgl are required in tissue-level biological processes, beyond their single-cell roles in polarity. Clearly, elucidating the molecular mechanisms underlying their activity in cell polarity will be critical for enabling full understanding of such critical aspects of development and physiology.

Summary of Dissertation

While there is certainly much known in the literature about Scrib, Dlg and Lgl in general, and their critical importance in cell biology, development and disease is clear, a cohesive picture of the precise molecular mechanisms of action for each protein has still not emerged. One way to think about this is to consider that there are a great many facts known about the Scrib module proteins --who they bind to, what processes they affect in cells and organs-- yet, no one knows how they actually work. In this dissertation, I describe my efforts to uncover these basic mechanisms of Scrib module function, and detail the contributions I have made to understanding them.

In Chapter 2 I describe experiments to characterize the regulatory relationships between Scrib, Dlg and Lgl and to specifically understand the contribution of Scrib and Dlg to apical domain antagonism. Here, I discovered a hierarchical organization for Scrib module localization where Dlg regulates Scrib localization and both Scrib and Dlg are required for Lgl localization. I found that the ability of Dlg to recruit Scrib is independent of direct binding and posttranslational palmitoylation but requires the Dlg SH3 domain. I demonstrate that all three proteins contribute distinct functions to polarity, namely that Scrib and Dlg are required to ‘protect’ Lgl by negatively

regulating its phosphorylation. In doing so, they act as a molecular switch at the basolateral membrane to enable Lgl to inhibit aPKC, whereas at the apical domain, aPKC can inhibit Lgl in the absence of Scrib and Dlg. Finally, I demonstrate that while Scrib, Dlg and Lgl are required for epithelial polarity, they are together not sufficient to establish an ectopic apical domain.

In Chapter 3 I carry out a detailed investigation of functional regions of the Dlg protein and investigate a potential mechanism of Lgl protection. I discover that while PP1, a promising candidate for Lgl regulation by Scrib and Dlg, does affect Lgl localization and activity, the mechanism of Scrib and Dlg's Lgl protection is largely independent of PP1. Furthermore, although both Scrib and Dlg both contain conserved PP1-interaction motifs, I am unable to detect a biochemical interaction between these three proteins. However, the PP1-binding motif in Dlg is essential for its polarity and Scrib localization functions. From this, I identify a small region of the Dlg HOOK domain that is essential for Dlg function and, for the first time, demonstrate that a minimal Dlg protein composed of only the SH3 and HOOK domains is necessary and sufficient for Dlg function in polarity, including Scrib localization.

In Chapter 4, in collaborative work with Katherine Sharp, we describe a novel function for Dlg in the nucleus. We found that endogenous Dlg is present in epithelial cell nuclei and that it resides in proximity to the NURF chromatin remodeling complex in the nucleus. Furthermore, NURF complex activity is required for tumorigenic overgrowth in *dlg* mutant tissue and we propose that this is due to NURF-dependent dysregulation of Yki target genes in the absence of Dlg. Finally, we identify putative NLS sequences in the Dlg protein and demonstrate that these are essential for Dlg function. However, mutation of these sequences does not prevent Dlg nuclear entry, suggesting the true NLS resides elsewhere.

In Chapter 5, I reexamine the complicated relationship between the Scrib module and endocytic trafficking pathways and their coordinated regulation of cell polarity. My findings support a lack of endocytic defects in Scrib module mutant cells and suggest that the Scrib module and endocytic traffic may regulate epithelial polarity in parallel pathways.

Overall, my work provides important advances in our understanding of the mechanistic basis of function of the three essential and widely conserved basolateral polarity regulators: Scrib, Dlg and Lgl. I have demonstrated that each of these three proteins contributes unique, but cooperative activities to the establishment and maintenance of epithelial polarity, and I have created a framework to define what the individual activities of these proteins are and how their coordination gives rise to a polarized cell.

FIGURES

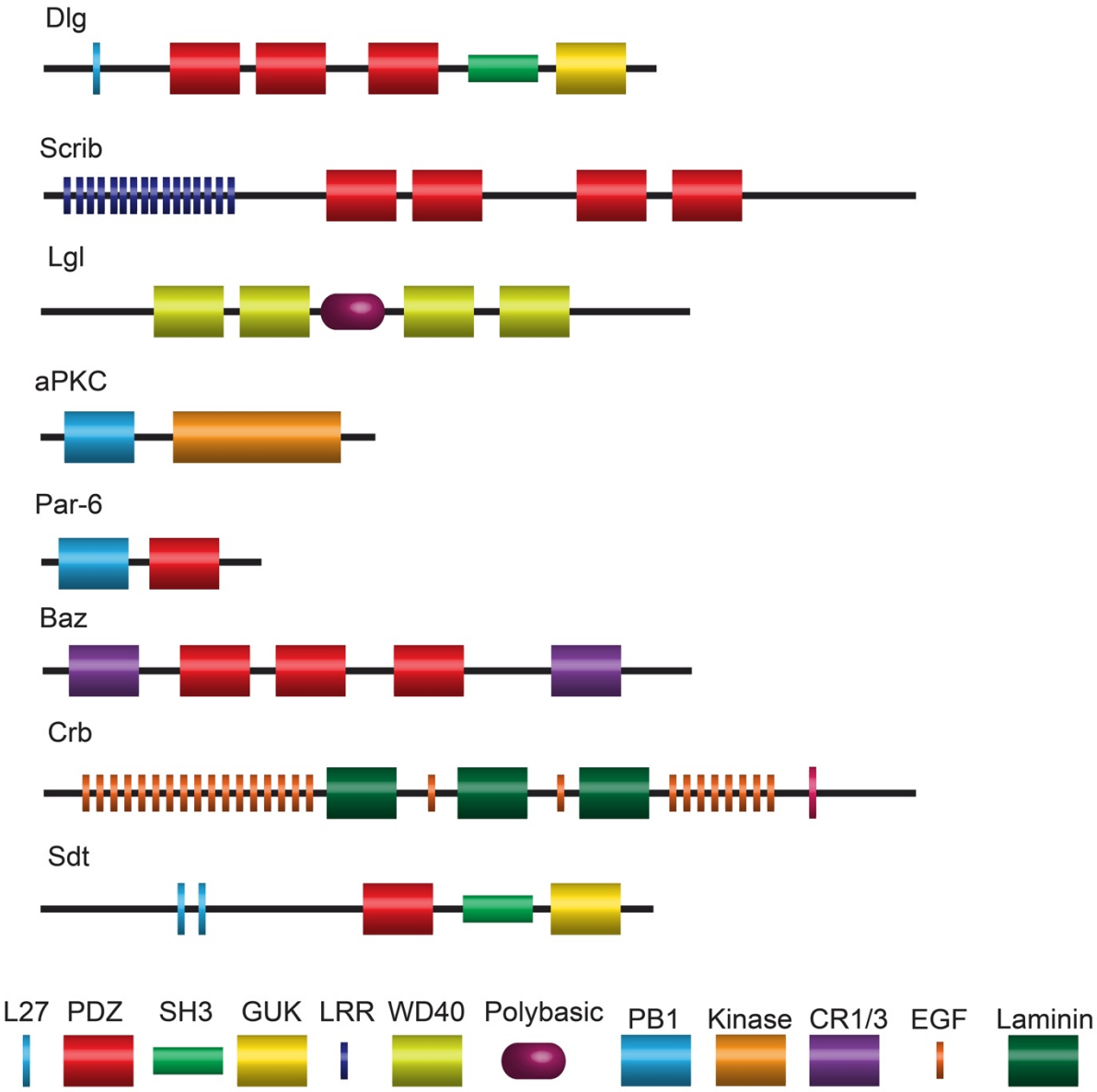

Figure 1.1 Schematic of protein domain compositions of polarity regulating proteins
Based on (Flores-Benitez and Knust, 2016). Drawings are not to scale.

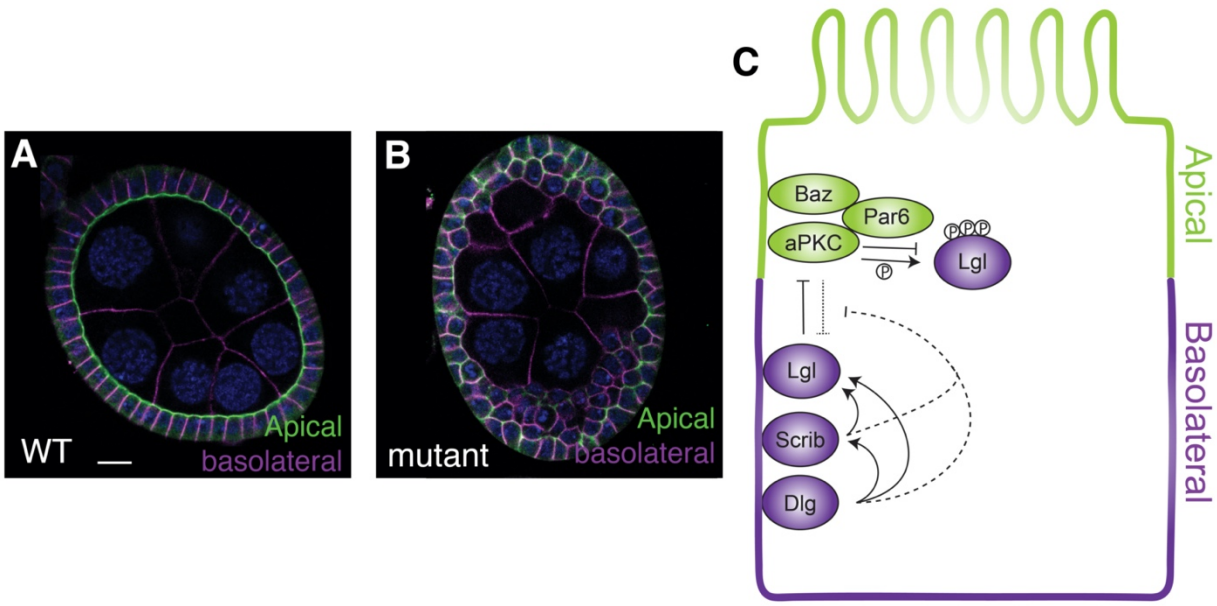

Figure 1.2 Model of polarity regulation by the Scrib module
(A) WT tissue exhibits apicobasal polarity showing separated apical and basolateral domains and monolayered tissue architecture. (B) Scrib module mutants have disrupted tissue architecture, multilayering and polarity loss characterized by mixing between apical and basolateral domains. (C) Simplified model of epithelial polarity. At the apical domain, aPKC phosphorylates Lgl and removes it from the membrane. At the basolateral domain, Scrib and Dlg are present and are able to protect Lgl from aPKC phosphorylation, maintaining its membrane localization and enabling its aPKC-inhibiting activity. Dlg is also required to localize Scrib to the basolateral membrane. Scale bar, 10μm. Adapted from (Khoury and Bilder, 2020).

Chapter 2:
Distinct activities of Scrib module proteins organize epithelial polarity

Mark J Khoury and David Bilder

Based on work originally published in *Proceedings of the National Academy of Sciences*, May 2020, 117(21), 11531-11540.

ABSTRACT
A polarized architecture is central to both epithelial structure and function. In many cells, polarity involves mutual antagonism between the Par complex and the Scrib module. While molecular mechanisms underlying Par-mediated apical determination are well-understood, how Scrib module proteins specify the basolateral domain remains unknown. Here, we demonstrate dependent and independent activities of Scrib, Dlg and Lgl using the *Drosophila* follicle epithelium. Our data support a linear hierarchy for localization, but rule out previously proposed protein-protein interactions as essential for polarization. Cortical recruitment of Scrib does not require palmitoylation or polar phospholipid binding but instead an independent cortically-stabilizing activity of Dlg. Scrib and Dlg do not directly antagonize aPKC, but may instead restrict aPKC localization by enabling the aPKC-inhibiting activity of Lgl. Importantly, while Scrib, Dlg and Lgl are each required, all three together are not sufficient to antagonize the Par complex. Our data demonstrate previously unappreciated diversity of function within the Scrib module and begin to define the elusive molecular functions of Scrib and Dlg.

INTRODUCTION

Cell polarity is defined by the coexistence of two distinct spatial identities within the confines of a single plasma membrane. This process is critical for many cell types, including stem cells, epithelial cells, migratory cells, and immune cells, to carry out their physiological functions (Campanale et al., 2017; St Johnston and Ahringer, 2010). Despite the distinct manifestations of polarity in these specialized cells, polarity in each is generated by a common pathway involving a set of conserved protein modules (Choi et al., 2019; Elsum et al., 2012; Goldstein and Macara, 2007). Foremost among these are the Par and Scrib modules, consisting of Par-3, Par-6 and atypical Protein Kinase C (aPKC) for the former and Scribble (Scrib), Discs-large (Dlg) and Lethal giant larvae (Lgl) for the latter (Elsum et al., 2012; Goldstein and Macara, 2007). These proteins play crucial roles in diverse biological processes and have also been implicated in numerous pathologies, from congenital birth defects to cancer (Elsum et al., 2012; Goldstein and Macara, 2007; Martin-Belmonte and Perez-Moreno, 2011). Thus, uncovering their molecular activities is essential to a mechanistic understanding of cell, developmental and disease biology.

A number of studies have provided important insight into the molecular function of the Par module and each of its individual components (Franz and Riechmann, 2010; Harris and Peifer, 2005; Krahn et al., 2010; Morais-de-Sá et al., 2010; Walther and Pichaud, 2010). Much of this work derives from *Drosophila* epithelial cells and neural stem cells, where the Par module regulates the apical domain and the Scrib module is required to specify the basolateral domain. The core distinction of cortical domains arises from mutual antagonism between the two modules, centering around interactions between aPKC and Lgl. In the apical domain, aPKC phosphorylates Lgl on three residues within a polybasic domain, causing it to dissociate from the plasma membrane (Bailey and Prehoda, 2015; Betschinger et al., 2003; Dong et al., 2015). Conversely, Lgl inhibits aPKC kinase activity and localization along the basolateral cortex (Hutterer et al., 2004; Lee et al., 2006; Wirtz-Peitz et al., 2008). Many details of Par protein activities and their outcomes are now understood, including specific protein-protein interactions in dynamic complexes, their structural basis, post-translational modifications and the kinetic order of events during apical polarization (Lang and Munro, 2017; Tepass, 2012).

By contrast to the wealth of mechanistic information about the Par complex, and despite the discovery of the relevant genes decades ago, the molecular mechanisms of basolateral domain specification by the Scrib module are still unknown. All three genes encode large scaffolding proteins containing multiple protein-protein interaction domains and lack obvious catalytic activity (Bilder and Perrimon, 2000; Dong et al., 2015; Jacob et al., 1987; Woods et al., 1996). Recent studies have identified novel interacting partners of Scrib module proteins, but few of these interactors have been implicated as regulators of cell polarity themselves (Bonello and Peifer, 2018; Stephens et al., 2018). Moreover, few studies have focused on the regulatory relationships within the Scrib module itself, and beyond the well-characterized aPKC-inhibiting function of Lgl, the fundamental molecular activities of Scrib and Dlg remain unknown. In this work, we identify distinct activities of Scrib, Dlg and Lgl that are required but not sufficient for basolateral polarization, shedding light on the mechanisms that restrict the Par complex to partition the epithelial cell membrane.

RESULTS

A linear hierarchy for localization but not function of basolateral polarity regulators

We used the conserved epithelial features of *Drosophila* ovarian follicle cells to study regulation of the basolateral cortical domain (Horne-Badovinac and Bilder, 2005)(**Fig. 2.1A-C**).

Cells mutant for null alleles of *scrib*, *dlg* or *lgl* encoding severely truncated or non-functional proteins, lose polarity, characterized by mixing of apical and basolateral domains and cells form multilayered masses at the poles of the egg chamber (**Fig. 2.2F-H**)(Bilder and Perrimon, 2000; Brumby et al., 2004; Woods et al., 1996). Importantly, we focused our analysis on the central follicle epithelium, where polarity-deficient cells retain relatively normal morphology that allows accurate monitoring of protein localization. We first asked whether Scrib, Dlg and Lgl have independent as well as shared functions in epithelial polarity. We generated follicle cells simultaneously mutant for one of the genes and expressing a validated RNAi transgene targeting a second gene. However, we saw no differences between single mutant cells and cells double-depleted for *scrib dlg, scrib lgl* and *lgl dlg,* and lateral aPKC spread was not enhanced in double mutants (**Fig. 2.1D-J,** quantified in **Fig. 2.1K**). These phenotypes are consistent with Scrib, Dlg and Lgl regulating polarity through a single, common pathway.

We next defined regulatory relationships between Scrib module components. Previous work in several organs has documented mutual dependence for localization, but also significant differences in their interrelationships (Albertson and Doe, 2003; Bilder et al., 2000c; Chen et al., 2018). In *dlg* mutant follicle cells, both Scrib and Lgl are mislocalized and exhibit hazy, cytoplasmic distributions (**Fig. 2.1L,M**). In *scrib* mutant follicle cells, although Lgl is mislocalized as in *dlg* mutants, Dlg maintains normal basolateral localization (**Fig. 2.1N,O**). Moreover, in *lgl* mutant follicle cells, both Scrib and Dlg maintain normally polarized cortical domains (**Fig. 2.1P,Q**). We note that for both Scrib and Lgl, mislocalization reflects a partial and somewhat variable rather than complete cortical loss, consistent with other observations (Dong et al., 2015; Dong et al., 2019; Ventura et al., 2020). We observe a similar hierarchical relationship in the embryonic epithelium, as suggested previously (**Fig. 2.2A-E**)(Bilder et al., 2000c). These results suggest a linear pathway whereby Dlg localizes independently to the cell cortex, Scrib localization requires Dlg, and Lgl localization is dependent on both other Scrib module proteins.

We then asked whether elevated levels of one protein in this pathway could compensate for loss of another, using previously validated transgenes (Carvalho et al., 2015; Koh et al., 1999; Wirtz-Peitz et al., 2008; Zeitler et al., 2004). We first tested overexpression of Lgl in *scrib* or *dlg* mutant cells and found that this did not modify the phenotype of either mutant (**Fig. 2.1R,S**). Similarly, Scrib overexpression did not modify the *dlg* mutant phenotype, and Dlg overexpression did not modify the *scrib* mutant phenotype (**Fig. 2.1T,U**). Moreover, neither Scrib nor Dlg overexpression was able to modify the *lgl* mutant phenotype (**Fig. 2.1V,W**). These data suggest that, despite the linear localization hierarchy, regulation of basolateral polarity in the follicle epithelium involves relationships that cannot be bypassed by simple overexpression of one Scrib module component.

Dlg stabilizes Scrib at the cortex

Since Dlg is required for Scrib cortical localization, we investigated the underlying mechanism. We used Fluorescence Recovery After Photobleaching (FRAP) assays to compare the stabilities of each protein at the cell cortex, using functional GFP-tagged versions expressed from endogenous loci. In WT cells, Scrib::GFP was highly stable, whereas Dlg::GFP was intermediately dynamic and Lgl::GFP was comparatively mobile (**Fig. 2.3A**). Strikingly, in *dlg*-depleted cells, Scrib::GFP exhibited an approximately fourfold increase in recovery kinetics, consistent with the loss of cortical localization also seen in fixed tissue (**Fig. 2.3B**). By contrast, although Dlg::GFP in *scrib* and *lgl* mutant cells remained localized at the cortex and mobile fractions are not changed, it also exhibited increased recovery kinetics (**Fig. 2.4A,B**), perhaps reflecting increased in-plane

mobility due to defective septate junction formation (Bilder et al., 2003; Oshima and Fehon, 2011). Importantly, however, Scrib::GFP was unchanged in *lgl* mutant cells (**Fig. 2.4C**). Additionally, we find no evidence for increased degradation of Scrib protein in *dlg* mutants (**Fig X.4D**). Thus, FRAP assays support an important role for Dlg in stabilizing Scrib on the cell cortex.

One mechanism that could localize Scrib to the cortex is a phospholipid-binding polybasic motif (PBM), as seen in other polarized proteins, including Lgl and aPKC (Bailey and Prehoda, 2015; Dong et al., 2015; Dong et al., 2019). However, an obvious PBM is not seen in the Scrib protein sequence. PBMs directly bind polar phospholipids, but mutating PI4KIIIα or expressing dominant negative PI3K (Δp60), which deplete PIP2 and PIP3, respectively, did not alter Scrib cortical localization (**Fig. 2.5A,B**)(Weinkove et al., 1999; Yan et al., 2011). Additionally, ATP depletion by Antimycin A treatment, which reduces PIP levels and is sufficient to delocalize Lgl::GFP, did not alter Scrib::GFP localization (**Fig. 2.5C-F**)(Dong et al., 2015).

An alternative mechanism by which Dlg could regulate Scrib cortical localization is via physical binding. The conserved colocalization and shared functions of Scrib module proteins has led to propositions that they function as a macromolecular complex. The Dlg GUK domain, which binds to the Dlg SH3 domain in an autoinhibitory manner, is the central mediator (McGee and Bredt, 1999; Qian and Prehoda, 2006). The GUK domain is reported to interact directly with Lgl and also indirectly with Scrib PDZ domains through the protein Gukholder (Gukh) at synapses and *in vitro*; a recent study further suggests a role for Gukh in epithelial development (Caria et al., 2018; Mathew et al., 2002; Qian and Prehoda, 2006; Zhu et al., 2014). We tested the requirement for these GUK-mediated interactions *in vivo* by analyzing a hypomorphic *dlg* deletion allele (dlg^{v59}) that removes the C-terminal two thirds of the GUK domain (**Fig. 2.3C**)(Woods et al., 1996). Apicobasal polarity and aPKC localization remained unchanged in central follicle cells mutant for this GUK-deficient allele, as did cortical localization of Lgl (**Fig. 2.3D,F,G,I**). A significant loss of cortical Scrib localization was seen, although this may be due to reduced levels of mutant Dlg (**Fig. 2.3E,H,T,V**)(Woods et al., 1996), as the additional GUK-truncating allele dlg^{1P20} and C-terminal deletion dlg^{sw} (**Fig. 2.3C**) shows unaffected Scrib as well as aPKC and Lgl localization in follicle cells (**Fig. 2.3J-M,V**). As with the GUK-deficient *dlg* alleles, no polarity defects were seen in follicle cells homozygous for a *scrib* allele that truncates the protein before the PDZ domains ($scrib^{4}$), or in maternal and zygotic (m/z) mutant embryos (**Fig. 2.3N,O**, **Fig. 2.6G-J**)(Zeitler et al., 2004). By contrast, a missense mutation in the Dlg SH3 domain (dlg^{m30}, L632P, **Fig X.3C**), which does not alter Dlg protein levels or localization, was sufficient to cause mislocalization of Scrib, as well as both Lgl and aPKC, in a manner indistinguishable from null alleles in follicle cells and m/z mutant embryos (**Fig. 2.3P,Q,R,V**, **Fig. 2.6A-F**)(Woods et al., 1996). These results reveal a role for the SH3 domain in regulating Scrib localization as well as apical domain antagonism, but show that the GUK domain is not required for epithelial polarity.

Scrib S-palmitoylation is dispensable for polarity

A third mechanism that can localize cytosolic proteins to the cortex is via post-translational attachment of lipophilic groups. To measure protein acylation, we performed Acyl-Biotin Exchange (ABE), which converts thioester-linked acyl groups to biotin that can be detected by western blot (Wan et al., 2007). To avoid the significant germline contribution of Scrib and Dlg in the ovary, we analyzed larval lysates by ABE and found that Scrib::GFP is acylated in *Drosophila* (**Fig. 2.7A**), consistent with a previous report (Strassburger et al., 2019). Recent work has shown that mammalian Scrib is S-palmitoylated on two conserved N-terminal cysteine residues, and this modification is required for Scrib cortical localization and function (**Fig. 2.7B**)(Chen et al., 2016a).

We generated a Scrib::GFP transgene in which these conserved palmitoylated cysteines are changed to alanine ($Scrib^{C4AC11A}$::GFP). Surprisingly, this protein localizes appropriately to the plasma membrane and rescues *scrib* mutant polarity phenotypes in follicle cells and imaginal epithelia (**Fig. 2.7C-E, Fig. 2.8A-D**). ABE showed that these mutations are not sufficient to abolish all acylation, suggesting that Scrib can be palmitoylated on additional non-conserved residues (**Fig. 2.7A**). We then inhibited palmitoyltransferases either pharmacologically, using 2-bromopalmitate (2-BrP) or by knocking down the *Drosophila* homolog of the Scrib-regulating palmitoyltransferase, ZDHHC7 (Flybase, CG8314), and found that both of these approaches failed to impact Scrib localization (**Fig. 2.9A-E**). Finally, we asked whether Dlg might regulate Scrib through influencing its palmitoylation. However, in *dlg* tissue no change in the acylation of Scrib::GFP could be detected by ABE (**Fig. 2.7A**). Thus, palmitoylation itself is not sufficient to localize Scrib to the cortex; instead Dlg must regulate Scrib localization by an independent mechanism.

Dlg has Scrib-independent polarity functions

To test whether cortical Scrib stabilization is the sole function of Dlg in epithelial polarity, we made use of a nanobody-based system for relocalizing GFP-tagged proteins within the cell (Harmansa et al., 2017). We tethered Scrib::GFP to the cortex via interactions with a uniformly distributed transmembrane anchor and examined apicobasal polarity in the absence of *dlg*. However, aPKC mislocalized to the lateral membrane and Lgl was displaced to the cytoplasm in these cells, as in cells depleted of *dlg* alone (**Fig. 2.7F-K**). As a complementary approach, we generated a constitutively membrane-tethered version of Scrib via attachment of an N-terminal myristoylation sequence. This myr-Scrib transgene was capable of rescuing polarity defects in *scrib* mutant follicle cells (**Fig. 2.10A-E**). However, in *dlg*-depleted cells expressing myr-Scrib, in which myr-Scrib remains cortical, neither aPKC nor Lgl mislocalization was rescued (**Fig. 2.7L,M**). The lack of rescue in these experiments suggests that Dlg has polarity functions in addition to Scrib localization and that Scrib and Dlg act in parallel to regulate apicobasal polarity.

Scrib and Dlg are not regulated by, and do not directly regulate, aPKC

We then examined the relationship between the Scrib module and aPKC. A central feature of this relationship is the exclusion of Lgl from aPKC-containing cortical domains, due to direct phosphorylation; when follicle cells are depleted of *apkc*, Lgl can reach the apical domain (**Fig. 2.11A**)(Aguilar-Aragon et al., 2018; Bell et al., 2015; Carvalho et al., 2015). We asked if Scrib and Dlg also exhibit aPKC-dependent apical exclusion, but the juxtaposition of the nurse cell membrane, which also expresses Dlg, to the apical domain of the follicle cells obscures accurate measurement. Dlg and Scrib remain localized to the basolateral cortex in *apkc*-depleted follicle cells (**Fig. 2.11B,C**), as well as in cells mutant for null alleles of the Par complex genes *par-6* and *cdc42* (**Fig. 2.12A,B**). Cells also retain basolateral Scrib and Dlg when aPKC is depleted within *lgl* mutant cells (**Fig. 2.11D,E,G,H**). Furthermore, overexpression of a constitutively active form of aPKC ($aPKC^{\Delta N}$) does not displace Scrib or Dlg from the cell cortex (**Fig. 2.11M**). Thus, localization of Scrib and Dlg depends on cues independent of aPKC activity.

The inhibitory relationship between aPKC and Lgl is well established, but it is not known whether Scrib and Dlg might also be direct inhibitors of aPKC (Betschinger et al., 2003; Lee et al., 2006; Wirtz-Peitz et al., 2008). Notably, when aPKC mislocalizes laterally in *lgl* mutant cells, it colocalizes with Scrib and Dlg, which are not displaced (**Fig. 2.11J**). This lateral aPKC is active because it can recruit Patj, whose localization is dependent on aPKC activity, to ectopic sites (**Fig.**

2.11F,I, **Fig. 2.12C,D**)(Morais-de-Sá et al., 2010; Sotillos et al., 2004). Additionally, a constitutively active, membrane targeted aPKC isoform (aPKC^{CAAX}) that is sufficient to re-specify the entire cortex as apical (shown by Patj recruitment, **Fig. 2.12C,D**), can colocalize with Scrib and Dlg at the basolateral membrane (**Fig. 2.12E**). These results rule out Scrib and Dlg as intrinsic inhibitors of aPKC, suggesting they work through Lgl to block the spread and apicalizing activity of aPKC, and that the aPKC mislocalization seen in *scrib* and *dlg* mutant cells (**Fig. 2.11K,L**) reflects a weakening of Lgl inhibitory activity in the absence of either Scrib or Dlg.

Scrib and Dlg are both required to stabilize and enable Lgl activity

If Scrib and Dlg do not directly inhibit aPKC, how do they participate in apicobasal antagonism? FRAP measurements of Lgl::GFP show that in *dlg* and *scrib*-depleted follicle cells, a clear increase in recovery kinetics and decrease of the mobile fraction compared to WT is seen (**Fig. 2.13A,B**). Whereas Lgl::GFP becomes cytoplasmic in *dlg* RNAi cells, an endogenously expressed, non-phosphorylatable Lgl fusion protein (Lgl^{S5A}::GFP) remains cortically associated in *dlg* RNAi cells (**Fig. 2.13C,D**)(Dong et al., 2015). Moreover, co-depleting aPKC in *dlg* RNAi cells restores Lgl cortical localization (**Fig. 2.13E,F**). These results are consistent with dynamic exchange of Lgl between an hypophosphorylated membrane-associated pool and an aPKC-hyperphosphorylated cytoplasmic pool, and suggest that Scrib and Dlg stabilize the former.

Cortical association of Lgl depends on interactions between polar phospholipids and charged residues within the Lgl PBM (Bailey and Prehoda, 2015; Dong et al., 2015). PIP2 and PIP3 show apicobasally polarized distributions in epithelial cells of *Drosophila* as well as vertebrates, raising the possibility that Dlg and Scrib could regulate Lgl function by altering the distribution of PIP species at the basolateral membrane (Claret et al., 2014; Krahn and Wodarz, 2012). However, using genetically encoded reporters, we did not detect differences in PIP2 distribution or levels in *dlg* or *scrib* mutants, consistent with a recent report (**Fig. 2.14A-D**)(Britton et al., 2002; Gervais et al., 2008; Ventura et al., 2020). While there was a slight increase in cortical PIP3 levels in *scrib* and *dlg* mutants (**Fig. 2.14E-H,** quantified in **Fig. 2.14I,J**), this is unlikely to have an impact on Lgl, which does not exhibit physiologically relevant differences in binding preference to different PIP species (Bailey and Prehoda, 2015).

An alternative mechanism by which Scrib and Dlg could ensure antagonism of apical identity is by simply promoting Lgl cortical localization. We therefore tested whether cortical localization of Lgl was sufficient to bypass loss of *scrib* or *dlg* function in follicle epithelia. However, in our hands although overexpression of a constitutively membrane-tethered Lgl (myr-Lgl) caused mild polarity defects in WT follicle cells, it did not alter polarity defects in *scrib*- or *dlg*-depleted follicle cells (**Fig. 2.15A-I**)(Bell et al., 2015). By contrast, a mutant Lgl protein with only the most C-terminal aPKC phosphorylation site present (Lgl^{S656A,S660A}, hereafter Lgl^{AAS}) was suggested to be a dominant inhibitor of aPKC (Carvalho et al., 2015). We confirmed that Lgl^{AAS} expression in otherwise WT follicle cells causes severe dominant phenotypes, including multilayering and loss of apical aPKC staining (**Fig. 2.13G, Fig. 2.15D**). We note that although Lgl^{AAS} localizes uniformly to the cortex including the apical domain (**Fig. 2.15K**) and can displace aPKC (**Fig. 2.13G**), it cannot establish an ectopic basolateral domain at the former apical site, as it does not recruit Scrib (**Fig. 2.13J**).

To determine whether Lgl^{AAS} is a bona fide aPKC inhibitor, we compared the phenotype of Lgl^{AAS} -expressing cells with *apkc* RNAi-expressing cells, using Bazooka (Baz, *Drosophila* Par-3) localization as a phenotypic readout (Franz and Riechmann, 2010; Harris and Peifer, 2005). Baz is an aPKC substrate, and preventing phosphorylation via *apkc* depletion or expression of non-

phosphorylatable Baz results in formation of several large aggregates in the cell, visible in maximum intensity projections of the apical surface of single follicle cells (**Fig. 5L**)(Franz and Riechmann, 2010; Krahn et al., 2010; Morais-de-Sá et al., 2010). Interestingly, Lgl^{AAS} was also capable of inducing Baz aggregates in follicle and embryonic epithelia (**Fig. 2.13M, Fig. 2.16B-E**), and co-depletion of *apkc* did not modify the follicle phenotype (**Fig. 2.13N,W, Fig. 2.16A**). Furthermore, while expression of an activated form of aPKC caused Baz to localize in a larger number of smaller, fragmented puncta, similar to the adherens junction (AJ) fragments described previously in basolateral mutants (**Fig. 2.13O,P vs. S,T**)(Bilder and Perrimon, 2000; Bonello et al., 2019), co-expression of Lgl^{AAS} resulted in aggregates indistinguishable from those caused by expression of Lgl^{AAS} alone (**Fig. 2.13Q,R,W, Fig. 2.16A**). We also directly examined the effect of Lgl^{AAS} on aPKC kinase activity by staining follicle clones with an antibody specific for S980 phosphorylated Baz (p-S980 Baz)(Morais-de-Sá et al., 2010). We observed loss of p-S980 Baz staining in 48.2% of Lgl^{AAS}-expressing clones, compared to 91.7% of *apkc* RNAi-expressing clones (**Fig. 2.16F,G**). These data are consistent with a model in which Lgl^{AAS} has enhanced aPKC-inhibiting properties compared to WT Lgl, but is not entirely equivalent to aPKC loss of function.

We then asked whether the dominant effects of Lgl^{AAS} depend on Dlg or Scrib activity. In *dlg* RNAi or *scrib* mutant cells, Lgl^{AAS} retained the ability to create several Baz aggregates, although an increased number and intermediate size suggested incomplete epistasis (**Fig. 2.13S-W, Fig. 2.16A**). Coexpression of Lgl^{AAS} also reduced the lateral expansion of aPKC seen in cells depleted of either *dlg* or *scrib* (**Fig. 2.11K,L vs. X.13G-I**). These results suggest that many apical-inhibiting effects of Lgl^{AAS} do not strictly depend on Scrib or Dlg.

The entire Scrib module is necessary but not sufficient for basolateral polarity

The fact that the activity of WT Lgl but not Lgl^{AAS} requires Scrib and Dlg suggests that Scrib and Dlg could enhance Lgl's ability to antagonize aPKC at the basolateral cortex, perhaps by protecting Lgl from aPKC phosphorylation. A model where both Scrib and Dlg are required would be consistent with the inability of either single protein to bypass loss of the other (**Fig. 1R-W**). To test if ectopic apical localization of Scrib and Dlg together would therefore allow Lgl to inhibit aPKC, we used a combination of apical domain-specific nanbody tethering and overexpression to simultaneously mislocalize one, two, or all three Scrib module proteins (Harmansa et al., 2017). However, despite robust colocalization at the apical cell surface, no effects were seen in any case on aPKC, apicobasal polarity, or epithelial architecture (**Fig. 2.17A-J**). Ectopic apical Scrib and Dlg were also unable to recruit the rest of the Scrib module to the apical domain (**Fig. 2.18A-D**). We conclude that, despite the necessity for each component in basolateral domain identity, even the entire Scrib module together is not sufficient to inhibit apical polarity determinants or establish basolateral identity.

DISCUSSION

Despite being central regulators of cell polarity in numerous tissues from nematodes to mammals, the mechanisms of Scrib module activity have remained obscure. Our work highlights previously unappreciated specificity in these activities, and begins to define the molecular functions of Scrib, Dlg and Lgl. Our data focus on the *Drosophila* follicle epithelium as well as in some cases *Drosophila* embryos, but it is important to note that tissue contexts can differ in polarity programs (Riga et al., 2020; Tepass, 2012), for instance in the adult *Drosophila* midgut epithelium, where Scrib module proteins are dispensable for epithelial organization (Chen et al., 2018). We

failed to detect phenotypic enhancement in double mutant follicle cells, compared to single mutants, which together with the complete penetrance of single mutant phenotypes suggests full codependence of function rather than functional overlap. Moreover, we were unable to bypass Scrib module mutants in any combination by overexpression of other genes in the module, consistent with unique roles for each protein. Thus, while Scrib, Dlg and Lgl act in a common "basolateral polarity" pathway, they each contribute distinct functions to give rise to the basolateral domain.

Cell polarity is particularly evident at the plasma membrane, and most polarity regulators act at the cell cortex. A key question in the field therefore has been the mechanisms that allow cortical localization of the Scrib module and Par complex proteins, which exhibit no classical membrane association domains (Flores-Benitez and Knust, 2016). We find a simple linear hierarchy for cortical localization in the follicle that places Dlg most upstream, and contrasts with that recently described in the adult midgut, where Scrib appears to be most upstream (Bilder et al., 2000c; Chen et al., 2018). Our work highlights the requirement of Dlg for Scrib localization, and provides insight into the mechanism, in part by ruling out previous models. One model involves a direct physical interaction, mediated by the Scrib PDZ domains and Dlg GUK domain (Bonello and Peifer, 2018; Mathew et al., 2002; Stephens et al., 2018). However, our *in vivo* analyses show that follicle cells mutant for alleles lacking either of these domains have normal polarity; these results are supported by data from imaginal discs (Hough et al., 1997; Woods et al., 1996; Zeitler et al., 2004). In contrast, we show that the SH3 domain is critical for Scrib cortical localization as well as polarity (Hough et al., 1997). The Dlg SH3 and GUK domains engage in an intramolecular 'autoinhibitory' interaction that negatively regulates binding of partners such as Gukh and CASK (Marcette et al., 2009; McGee et al., 2001; Newman and Prehoda, 2009; Nix et al., 2000; Qian and Prehoda, 2006; Rademacher et al., 2019; Zeng et al., 2017). The dispensability of the GUK domain provides evidence against an essential role for this mode of regulation in epithelial polarity, and highlight the value of investigating the GUK-independent function of the Dlg SH3.

We also exclude a second mechanism of Scrib cortical association. Mammalian Scrib is S-palmitoylated and this modification is required for both cortical localization and function (Chen et al., 2016a). As *Drosophila* Scrib was also recently shown to be palmitoylated, an appealing model would involve Dlg regulating this post-translational modification (Strassburger et al., 2019). However, we could detect no changes to Scrib palmitoylation in a *dlg* mutant, and chemically or genetically inhibiting *Drosophila* palmitoyltransferases also had no effect on Scrib localization, although we cannot discount the possibility that Scrib palmitoylation may be part of a multipart localization mechanism. Surprisingly, palmitoylated Scrib is incapable of reaching the cortex in *dlg* mutants. While a constitutively myristoylated Scrib can bypass this requirement for localization, it is nevertheless insufficient to support polarity in the absence of Dlg. These results indicate that Dlg regulates additional basolateral activities beyond localizing Scrib.

Lgl's role as an aPKC inhibitor is well-characterized, but how Scrib and Dlg influence this antagonism is not understood (Betschinger et al., 2003; Hutterer et al., 2004; Lee et al., 2006). Our data show that Scrib and Dlg maintain cortical Lgl by regulating its phosphorylation by aPKC, rather than by direct physical recruitment to the membrane. A contemporaneous study by Ventura et al. supports this finding, further showing that the major factor in Lgl cortical stabilization is PIP2 (Ventura et al., 2020). Our data also suggest that the basolateral-promoting activities of Scrib and Dlg are not via direct inhibition of aPKC kinase activity or intrinsic antagonism of aPKC localization. Instead, they are consistent with models in which Scrib and Dlg regulate the three specific aPKC-targeted residues in Lgl. Previous work has demonstrated that these phosphorylated

serines (656, 660, 664) are neither functionally nor kinetically equivalent, and a recent model proposes that S664 is required for basolateral polarization by mediating a phosphorylation-dependent interaction with the Dlg GUK domain (Carvalho et al., 2015; Graybill and Prehoda, 2014; Moreira and Morais-de-Sá, 2016; Zhu et al., 2014). Beyond the dispensability of the GUK domain, the enhanced ability of Lgl^{AAS} to inhibit aPKC and its ability to do so largely independently of Scrib and Dlg, argues against this model. Moreover, only Lgl^{AAS} among the phospho-mutants can dominantly affect aPKC activity, while WT Lgl can do the same only if Scrib and Dlg are present (Moreira and Morais-de-Sá, 2016). Together, these results suggest that S656 is the critical inhibitory residue whose phosphorylation must be limited to enable Lgl's activity.

The mechanism by which Lgl^{AAS} can suppress even constitutively active $aPKC^{\Delta N}$ remains unclear. aPKC substrates can act as competitive inhibitors; either an increased substrate affinity for aPKC or reduced ability to be inhibited by virtue of having fewer phosphorylation sites could make Lgl^{AAS} a more effective inhibitor than WT Lgl (Graybill and Prehoda, 2014; Holly and Prehoda, 2019; Lin et al., 2000). Supporting this idea, it was previously shown that S664, the only residue still available in Lgl^{AAS}, is phosphorylated with higher kinetic preference than S656 or S660 (Graybill and Prehoda, 2014). It is also possible that some Lgl^{AAS} phenotypes may be due to aPKC-independent effects resulting from reduced phosphorylation on S656 and S660. Nevertheless, we propose a model in which Scrib and Dlg 'protect' Lgl by limiting phosphorylation of S656, thus tipping the inhibitory balance to allow Lgl to inhibit aPKC and establish the basolateral domain.

What mechanism could underlie Scrib and Dlg protection of Lgl? One mechanism could involve generating a high phospholipid charge density at the basolateral membrane, which has been shown to desensitize Lgl to aPKC phosphorylation *in vitro* (Visco et al., 2016). However, our data do not find evidence for regulation of phosphoinositides by Scrib and Dlg. A second possibility is that Scrib and Dlg could scaffold an additional factor, such as Protein Phosphatase 1 (PP1), which counteracts aPKC phosphorylation of Lgl (Moreira et al., 2019). Alternative mechanisms include those suggested by recent work on PAR-1 and PAR-2 in *C. elegans* zygotes, a circuit with several parallels to the Scrib module (Hao et al., 2006; Motegi et al., 2011; Ramanujam et al., 2018). In this system, PAR-2 protects PAR-1 at the cortex by shielding it from aPKC phosphorylation through physical interaction-dependent and -independent mechanisms (Ramanujam et al., 2018). By analogy, binding with Scrib and/or Dlg could allosterically regulate Lgl to prevent phosphorylation, although we have ruled out the Lgl-Dlg interaction documented in the literature (Zhu et al., 2014). Scrib or Dlg might also act as a "decoy substrate" for aPKC, as PAR-2 does in PAR-1 protection (Ramanujam et al., 2018). Indeed, Scrib is phosphorylated on at least 13 residues in *Drosophila* embryos, though the functional relevance of this is not yet known (Bo Zhai et al., 2008).

Overall, our work highlights the multifaceted nature of Scrib module function. The failure to bypass Scrib module mutants by transgenic supply of any single or double combination of other module components, including several that were constitutively membrane-tethered, suggests that every member contributes a specific activity to polarity. Nevertheless, even the simultaneous ectopic localization of all three Scrib module proteins was insufficient to disrupt the apical domain. This insufficiency in basolateral specification may reflect an inability of apical Scrib and Dlg to protect Lgl from aPKC phosphorylation, perhaps due to the distinct molecular composition of the apical and basolateral domains. This supports the idea that in addition to intrinsic activity via Lgl, the Scrib module must recruit or activate additional, as yet unidentified effectors in basolateral polarity establishment. The independent as well as cooperative activities of the Scrib module

delineated here demonstrate previously unappreciated complexity in the determination of basolateral polarity and set the stage for future mechanistic studies of Scrib module function.

Acknowledgments
We thank E. Morais de Sá, D. Bergstralh, B. Thompson, V. Budnik, T. Schupbach, R. Davis, Y. Hong, F. Matsuzaki, M. Metzstein, A. Wodarz, D. St Johnston and I. Hariharan for generously providing fly stocks and reagents and C. Brownlee and K. Strassburger for providing technical expertise for the ABE experiments. We thank Laura Mathies for cloning the modified Scrib constructs. Imaging on the LSM780 was performed at the CRL Molecular Imaging Center, supported by NSF DBI-1041078. We are grateful to G. de Vreede, M. Peifer and T. Bonello, K. Prehoda, M. Kitaoka and the Bilder laboratory for helpful discussion. This work was supported by NIH grants GM068675, GM090150 and GM130388 to D.B. and AHA Predoctoral Fellowship 20PRE35120150 to M.J.K.

MATERIALS AND METHODS

Fly stocks and genetics

Drosophila stocks were raised on cornmeal molasses food at 25°C. *yw* was used as the WT control. All follicles shown are stages 5-8. Mutant alleles and transgenic lines used are listed in **Table 1**. Genotypes shown in figure panels are listed in **Table 2**. Mutant follicle cell clones were generated using either *hsFLP* or *GR1-GAL4 UAS-FLP*. Follicle cell MARCM clones were generated using *hsFLP* (Lee and Luo, 1999). For *hsFLP*-induced clones, larvae were heat shocked for 1 hour on two consecutive days starting 120 hours after egg deposition (AED). For clonal GAL4 expression using *hsFLP*, larvae were heat shocked once for 13 minutes 120 hours AED. For all clones, adult females were fed with yeast and dissected 3 days after eclosion. Because dlg^{v59} is on a chromosomal inversion, it cannot be used with FRT-based recombination, so it was analyzed in trans to dlg^{HF321}, which does not produce protein at 29°C. Pan-follicle cell expression was induced in adults using *traffic jam-GAL4 (tj-GAL4)* and temperature-sensitive *GAL80*; these were fed yeast for 2 days before shifting to 29°C for 4 days. Maternal and zygotic mutant embryos were generated from germline clones, using the dominant female technique (Chou and Perrimon, 1996) or from maternal RNAi expression with *Maternal Triple Driver-GAL4 (MTD-GAL4)*(Staller et al., 2013). Germline clones were induced by 1 hour heat shock 96 hours AED for *FRT19A* or 120 hours AED for *FRT82B*. Overexpression in embryos used *da-GAL4*. Overexpression in imaginal discs used *hh-GAL4*.

To generate *UAS-myr-Scrib::V5*, the N-terminal myristoylation signal from Src42A (ATGGGTAACTGCCTCACCACACAGAAGGGCGAACCCGACAAGCCCGCA) and C-terminal V5 tag (GGTAAGCCCATTCCAAACCCACTTCTCGGTCTGGATAGCACA) were synthesized as gBlocks with overlap to the pUASTattB backbone and Scrib CDS. The Scrib A2 CDS was amplified from pBS-ScribA2 using primers GTCCTGGGACTCAACGACAT and CGGAGTGGGTTTGGCTCTAA. These fragments were cloned into the EcoRI/XbaI linearized pUASTattB vector using a High Fidelity Gibson Assembly kit (NEB). The *UASp-*$Scrib^{C4AC11A}$*::GFP* construct was generated by mutating Scrib Cys4 and Cys11 in the pBS-ScribA2 vector using the Q5 site directed mutagenesis kit (NEB) and primers TTCAAGGGCGCCAACCGGCAGGTGGAGTTCG and GATGGGAATGGCCTTGAACATGCTCGTCTTC. Following sequence verification, mutant pBS-ScribA2 was digested with KpnI and EcoRV and this fragment was cloned into the pUASp backbone. *UAS-myr-Scrib::V5* was targeted to the attP40 landing site and *UASp-*

Scrib^{C4AC11A}*::GFP* was inserted by P element-mediated transformation through embryo injections performed by Bestgene, Inc.

Immunofluorescence and microscopy

Follicles were dissected in Schneider's medium containing 15% FBS and fixed with 4% PFA in PBS for 20 minutes. Follicles were stained in PBS containing 0.1% Triton X-100, 1% BSA and 4% NGS overnight at 4°C. Primary antibodies and dilutions are listed in **Table 1**. Following secondary antibody incubation at 1:400 for 2 hours at room temperature, tissue was mounted in glycerol-based antifade (Invitrogen). Embryos were fixed with 4% PFA for 20 minutes then devitellinized by shaking in 1:1 heptane:methanol. Following rehydration for 15 minutes in PBS 0.1% Triton X-100 and blocking for 2 hours in PBS 0.3% Triton X-100, 1% BSA 4% NGS, embryos were stained followed the same protocol described above.

Images were acquired using an inverted Zeiss LSM700 or upright LSM780 laser scanning confocal microscopes with LD C-Apochromat 40x/NA 1.1 W or Plan apochromat 63x/NA 1.4 oil objectives at 1024x1024 pixel resolution with 2 line averages. For each experiment, tissue from at least 5 females was analyzed and at least 10 ovarioles and 20 individual follicles were examined.

Fluorescence Recovery After Photobleaching (FRAP) experiments

FRAP experiments were performed as previously described (Chen et al., 2019). Briefly, follicles were dissected in media as above, supplemented with 2% human insulin (Sigma) and embedded in 0.5% low melting agarose in a glass bottom dish. Imaging was performed on an inverted Zeiss LSM700 using a LD C-Apochromat 40x/NA 1.1 W objective. Images were acquired continuously with resolution of 512 x 269 pixels and scan time of 821.67 msec. 10 pre-bleach images were acquired before an elliptical ROI covering one en face cell boundary was bleached twice with a 488nm 10mW laser at 70% power for Scrib::GFP and Dlg::GFP, or 85% power for Lgl::GFP with pixel dwell of 100.85 µsec. Intensities of the bleached region, reference region and background were manually measured using Fiji (Schindelin et al., 2012). Background and imaging-dependent photobleaching were corrected as previously described (Chen et al., 2019). Recovery curves were fitted using Graphpad Prism as previously described (Chen et al., 2019).

Acyl-Biotin Exchange (ABE)

ABE was performed according to published protocols, with modifications (Percher et al., 2017; Wan et al., 2007). Lysates were prepared from 20-24 wandering L3 larvae per genotype by homogenizing the anterior half of the carcass after removing the gut and fat body, in lysis buffer (150mM NaCl, 50mM Tris, 5mM EDTA, pH 7.4) containing 1% Triton X-100 and protease inhibitors (Thermo). Following protein concentration measurement by BCA assay (Thermo), 200µg of protein per genotype was treated with 10mM TCEP, pH 7.4 (Thermo) and 4% SDS for 30 minutes at room temperature to reduce disulfide bonds and denature proteins. Samples were then treated with 30mM N-ethylmaleimide (NEM, Thermo) for 3 hours at room temperature, to cap newly exposed cysteines. Samples were then buffer exchanged with lysis buffer 4-5 times in 10K MWCO protein concentrator columns (Millipore) to remove residual NEM. Samples were then split 50:50 and half was treated with 0.8M hydroxylamine, pH 7.4 (Sigma) to cleave S-acyl groups for 1 hour at room temperature. The other half was diluted with an equivalent amount of lysis buffer and serves as a negative control. Samples were then buffer exchanged 3 times and treated with 1µM EZ-Link BMCC Biotin (Thermo) for 1 hour at room temperature. After buffer exchanging 3 times, biotinylated protein was purified using Pierce Streptavidin Magnetic Beads

(Thermo) for 1 hour at room temperature or overnight at 4°C. Beads were washed twice and samples were eluted in 4X Laemmli sample buffer (Biorad) by boiling for 10 minutes. Biotin incorporation into proteins of interest was then analyzed by western blot. Western blotting was performed as described previously (de Vreede et al., 2018). Primary antibodies are listed in **Table 1**.

Image analysis and quantification

Image processing and quantification was performed using Fiji software (Schindelin et al., 2012). To quantify Baz particles, an approximately single-cell sized ROI of 104x104 pixels was defined. Baz particles in the ROI were then automatically segmented by creating binary masks from thresholded and smoothed images using the FeatureJ plugin. Segmented aggregates were then measured using the Analyze Particles function. To quantify aPKC localization, intensity was measured by drawing a line along the lateral and apical membranes of a single cell in medial section using the measure function in Fiji. A ratio of lateral:apical intensities was then calculated per cell and used to compute an average ratio per cell per genotype. All other cortical intensity measurements were obtained by drawing a line along the membrane of interest of single cells and calculating averages per condition. The resulting data were then analyzed using Microsoft Excel and Graphpad Prism 6. For significance in statistical tests: n.s.=$p>0.05$, *=$p<0.05$, **=$p<0.01$, ***=$p<0.001$ and ****=$p<0.0001$. The results of all statistical tests are found in **Table 3**. Figures were assembled using Adobe Illustrator.

FIGURES

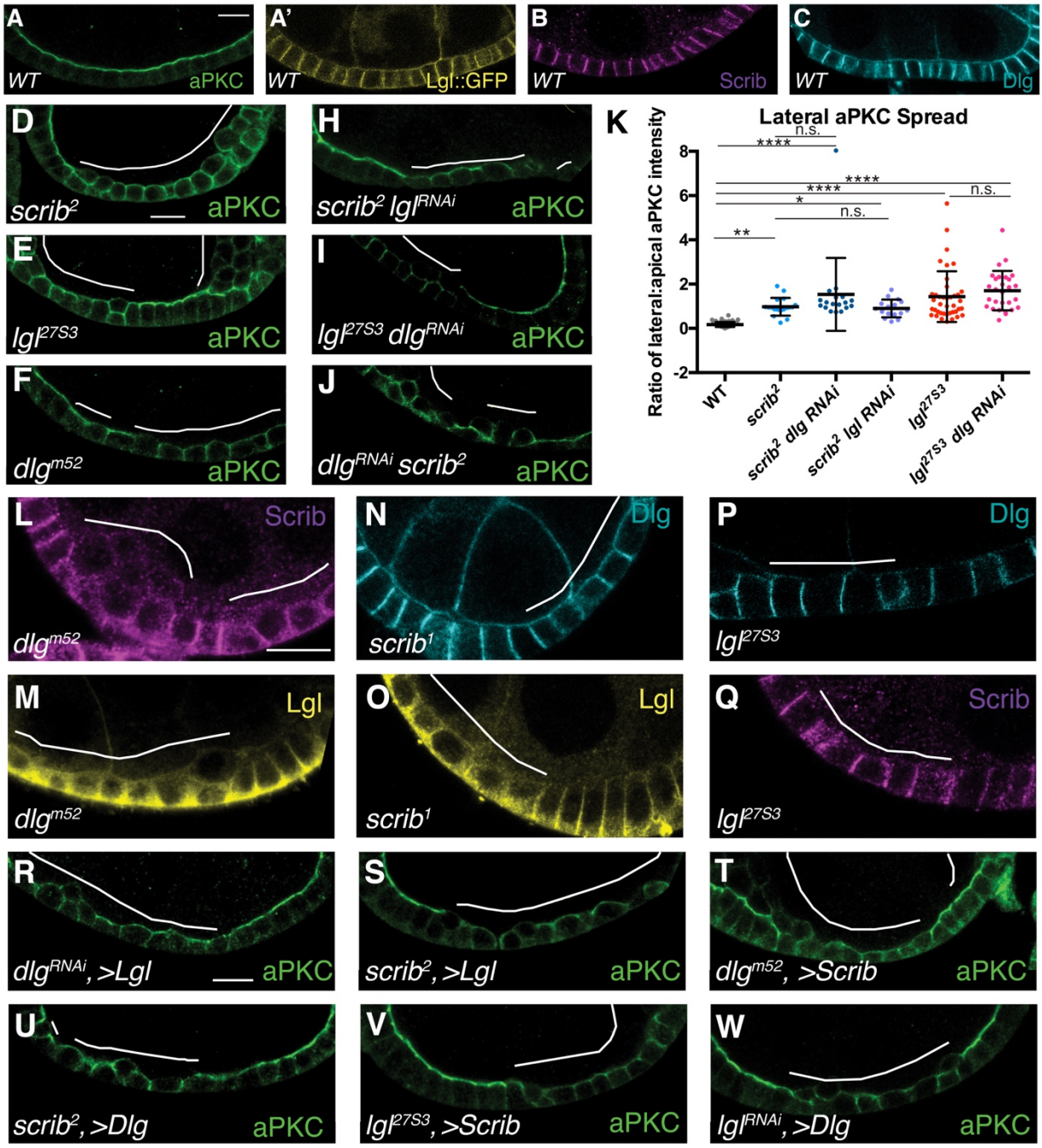

Figure 2.1. Functional relationships within the Scrib module
(A-C) Localization of polarity proteins, aPKC (A), Lgl (A'), Scrib (B) and Dlg (C) in WT follicle cells. Compared to single mutants (D-F), double depleted combinations (H-J) do not show an enhanced apical expansion phenotype. (K) Quantification of aPKC mislocalization phenotype in single and double mutants. aPKC spread represented as ratio of lateral:apical intensity in single cells. Localization of Scrib module proteins: both Scrib and Lgl show hazy, cytoplasmic mislocalization in *dlg* mutant cells (L,M). In *scrib* mutant cells, Dlg localization is normal (N), while Lgl is mislocalized (O). In *lgl* mutants, both Scrib and Dlg localizations are unchanged (P,Q).

Overexpression of Lgl does not rescue apical polarity defects in *dlg* or *scrib* mutants (R,S). Scrib overexpression cannot rescue *dlg* mutants (T) nor can Dlg overexpression rescue *scrib* mutants (U). *lgl* mutants are not rescued by Scrib or Dlg overexpression (V,W). Scale bars, 10μm. One-way ANOVA with Tukey's multiple comparisons test. Error bars represent S.D., data points are measurements from single cells. White line indicates mutant cells and/or overexpression clones in this and all subsequent figures.

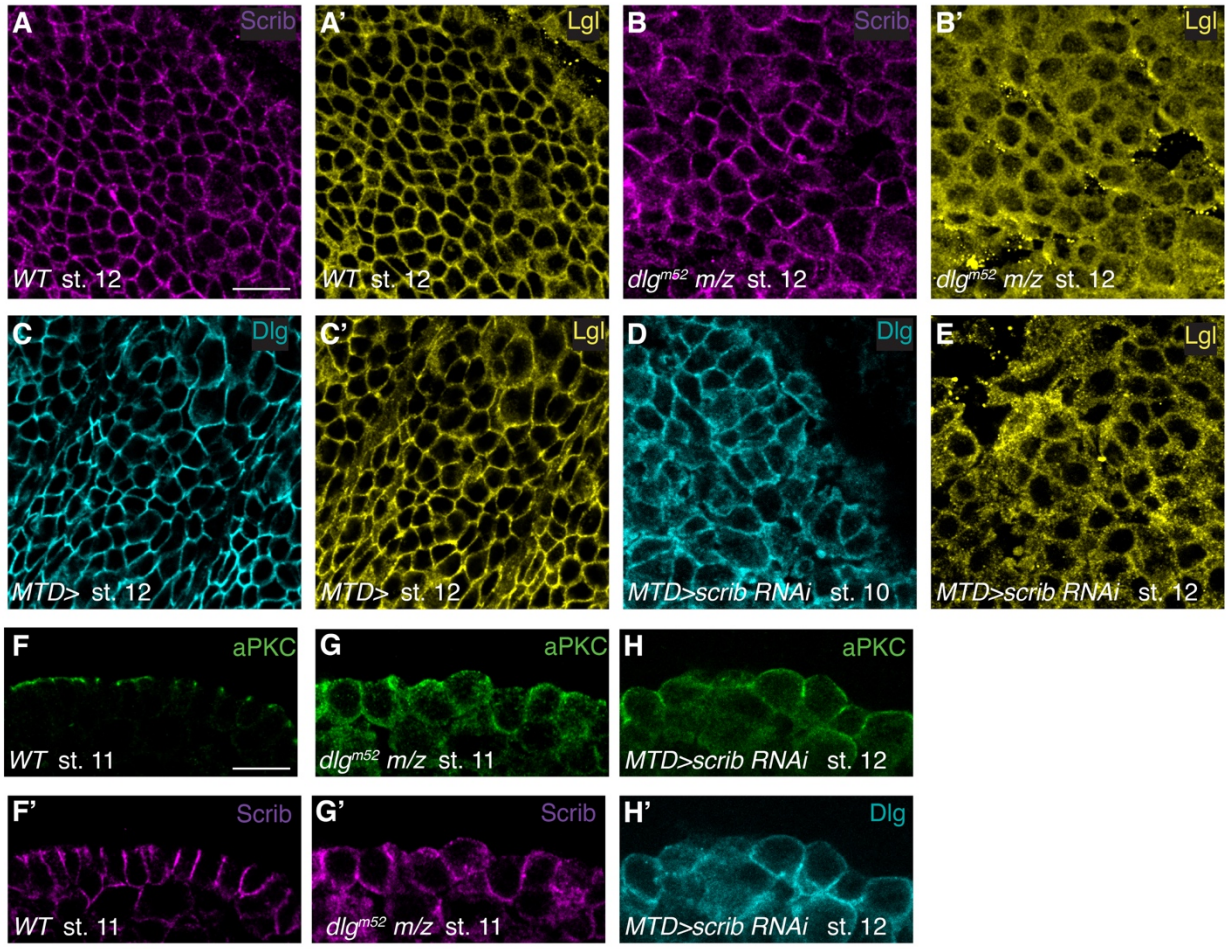

Figure 2.2. Conservation of Scrib module hierarchy in the embryonic epithelium
(A,B) Compared to paternally rescued controls (A), *dlg*^{m52} maternal/zygotic (m/z) mutant embryos mislocalize Scrib (B) and Lgl (B'). (C-E) Compared to controls (C), embryos expressing maternal *scrib* RNAi maintain cortical Dlg localization (D) but mislocalize Lgl (E). (F-H) Compared to WT (F), *dlg*^{m52} m/z mutant (G) and maternal *scrib* RNAi embryos (H) lose polarity and mislocalize aPKC laterally. Scale bars, 10µm.

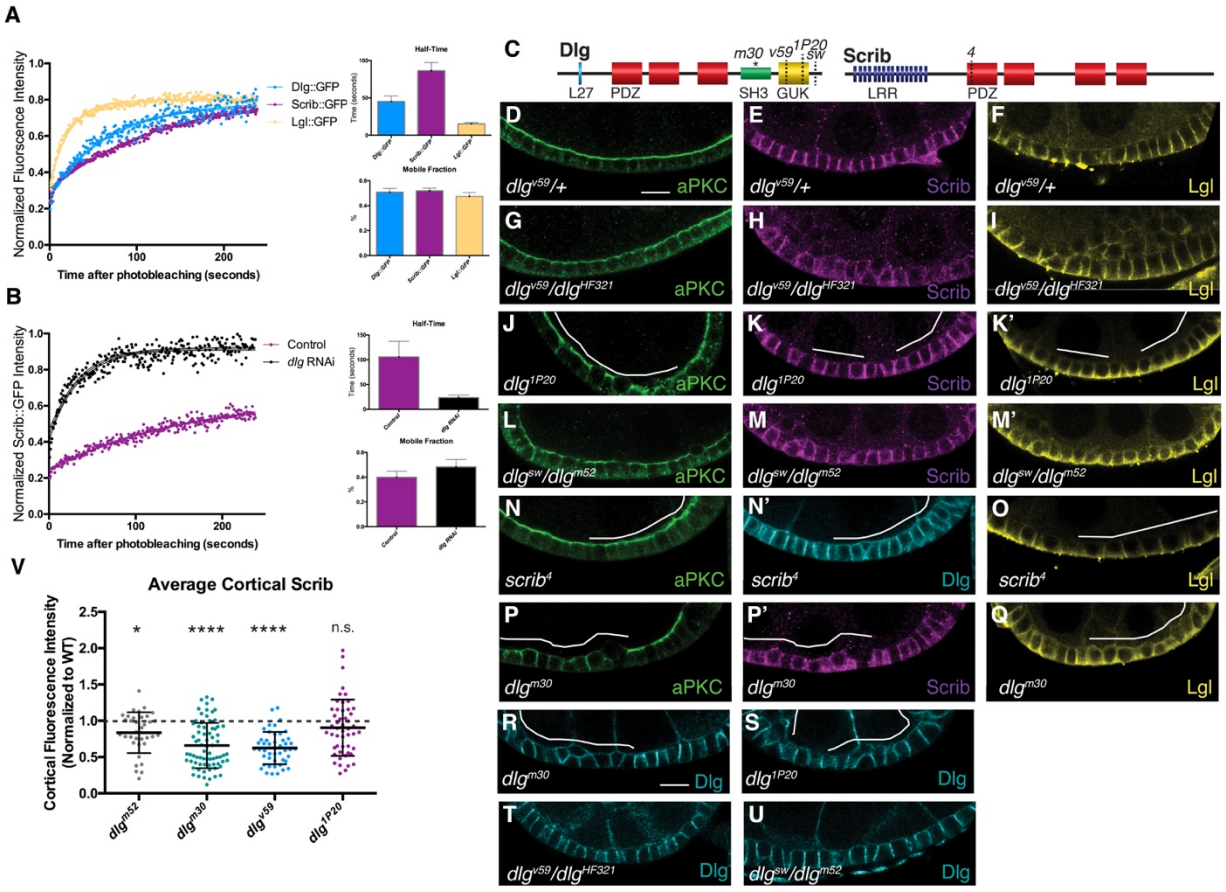

Figure 2.3. Dlg regulates cortical Scrib stability

FRAP assay (A) shows distinct mobility of Scrib, Dlg and Lgl in WT cells; Scrib is most stable and Lgl is most dynamic. (B) Scrib shows a ~4 fold increase in recovery kinetics in *dlg* RNAi cells. (C) Schematic of the mutant *dlg* alleles and *scrib* alleles used in D-U. dlg^{m30} harbors a point mutation in the SH3 domain (L632P). dlg^{v59} contains a deletion resulting in frameshift and truncation of the GUK domain. dlg^{1P20} is a nonsense mutation truncating the GUK domain. $scrib^{4}$ truncates all 4 PDZ domains. Compared to WT (D-F), aPKC (G) and Lgl (I) localizations are unaffected in cells mutant for a *dlg* GUK-deficient allele. Scrib localization (H) is partially affected, although this may be due to reduced stability of mutant Dlg. Follicle cell clones homozygous for two additional GUK mutant *dlg* alleles show normal aPKC (J,L) and Lgl (K',M') localization. (K,M) Scrib localization is also not affected. aPKC (N), Dlg (N') and Lgl (O) localizations are unaffected in cells mutant for a *scrib* allele lacking PDZ domains. (P) aPKC mislocalizes laterally in cells mutant for a *dlg* SH3 point mutant allele. Scrib (P') and Lgl (Q) also exhibit cytoplasmic mislocalization in these cells. (R-U) Dlg protein is stable and cortically localized in SH3 mutant (R) and GUK-truncated (S-U) mutant follicle cells. (T) Dlg protein levels are decreased in dlg^{v59} mutant cells, as previously described (Woods et al., 1996). (V) Quantification of cortical Scrib levels in various *dlg* mutants. Cortical Scrib is significantly decreased in cells mutant for the null allele dlg^{m52}, the SH3 point mutant dlg^{m30} and the GUK mutant dlg^{v59} compared to respective WT controls. However, Scrib levels are not significantly

decreased compared to WT in a second GUK mutant *dlg*^{1P20}. Mutants are normalized to the average of WT control from the same experiment. Gray line indicates normalized WT level. Scale bars 10µm. Error bars represent 95% confidence intervals in A,B and S.D. in V. Unpaired t-tests with Welch's correction of mutants vs. WT controls. Data points are measurements from single cells. Scale bars, 10µm.

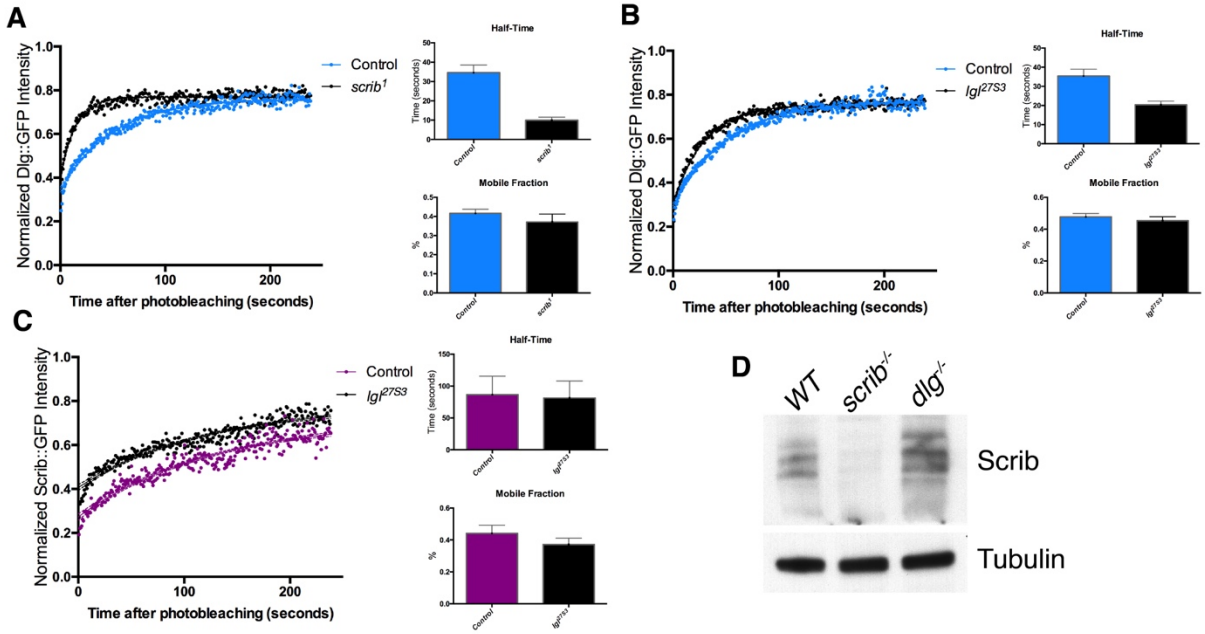

Figure 2.4. Further characterization of Scrib and Dlg dynamics
(A) Dlg::GFP shows increased FRAP recovery kinetics in *scrib* mutant follicle cells compared to controls. (B) Dlg::GFP increased FRAP kinetics are slightly increased in *lgl* mutant follicle cells. (C) Scrib::GFP does not show altered FRAP mobility in *lgl* mutant cells. (D) Scrib protein is not obviously degraded in *dlg* mutant imaginal disc tissue. Error bars represent 95% confidence intervals.

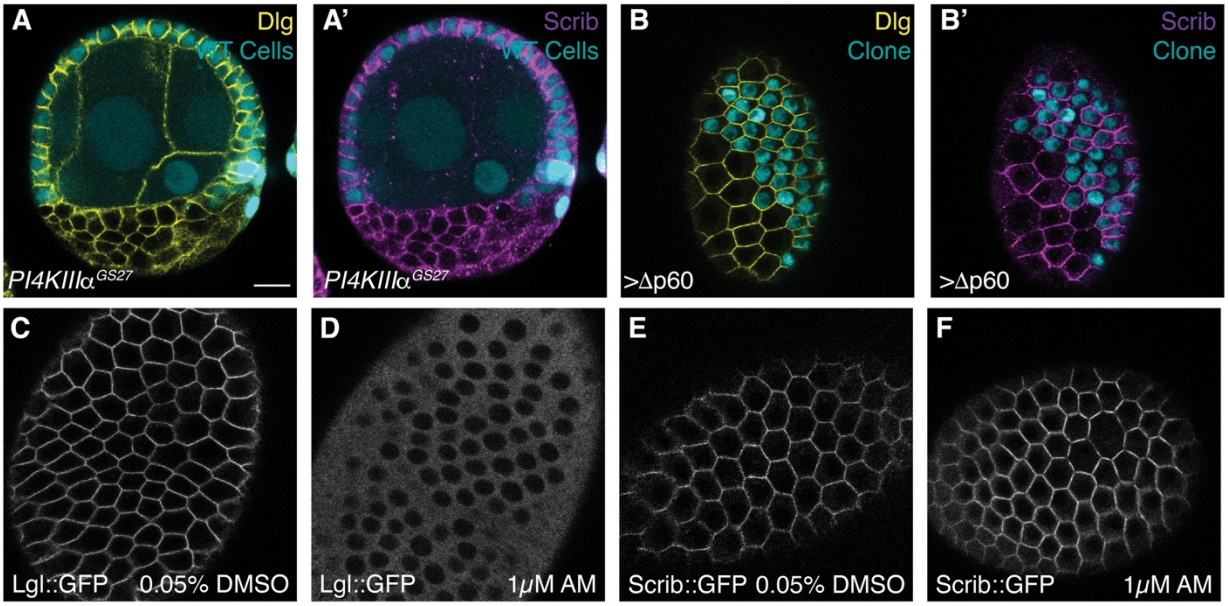

Figure 2.5. Cortical Scrib localization is independent of PIP binding

(A) PIP2 depletion by *PI4KIIIα* mutation does not displace Scrib or Dlg membrane localization. (B) PIP3 depletion by expressing dominant negative PI3K (Δp60) does not displace Scrib or Dlg membrane localization. (C,D) ATP depletion by antimycin A (AM) treatment causes Lgl::GFP to become cytoplasmic in follicle cells. (E,F) Scrib::GFP localization is not affected by AM treatment. Scale bars, 10μm.

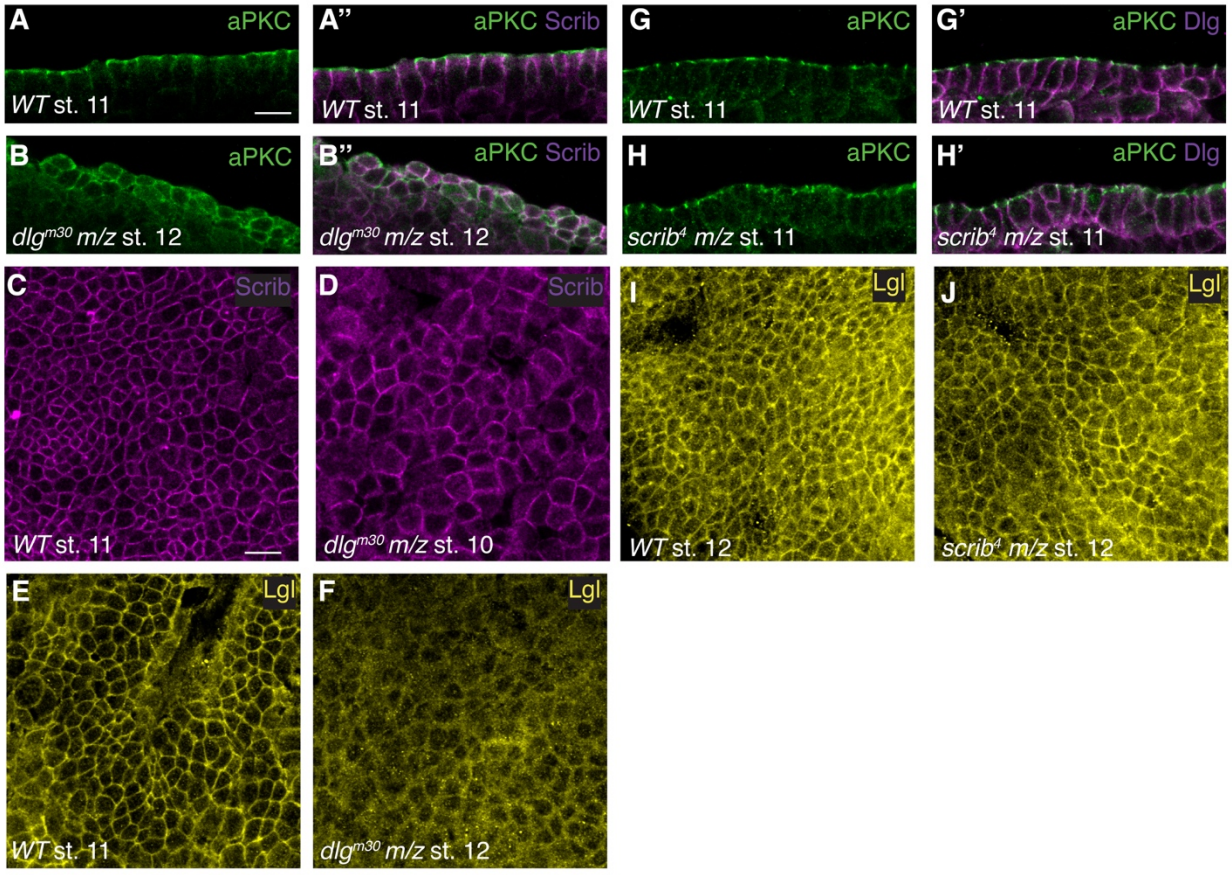

Figure 2.6. Functional assessment of Scrib and Dlg domains in embryonic epidermis
(A-F) Maternal/zygotic mutant embryos for *dlg*^{m30} lose polarity and mislocalize aPKC (A,B), Scrib (C,D) and Lgl (E,F) compared to paternally rescued WT controls. (G-J) Compared to paternally rescued controls, maternal/zygotic mutant embryos for *scrib*^{4} do not lose polarity and have normal aPKC, Dlg (G,H) and Lgl (I,J) localization. Scale bars, 10µm.

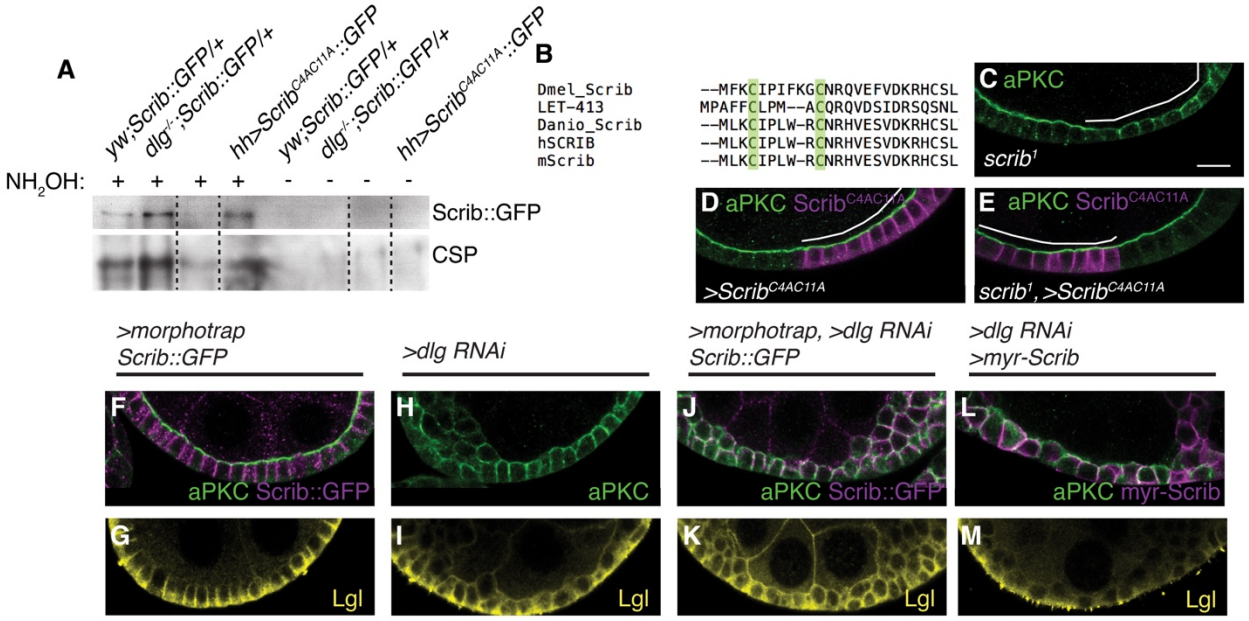

Figure 2.7. Cortical Scrib still requires Dlg for function

(A) ABE demonstrates that Scrib is palmitoylated *in vivo* in larval tissues, but this is not detectably altered in *dlg* mutant animals. Mutating two conserved cysteines ($Scrib^{C4AC11A}$) does not abolish Scrib palmitoylation. Cysteine String Protein (CSP) serves as a control palmitoylated protein. Non-NH_2OH treated lanes control for biotinylation specificity to palmitoylated residues. Dotted lines in lanes 3 and 7 indicate data excluded due to an experimental error in protein loading. (B) Alignment of Scrib protein sequences showing conservation of palmitoylated cysteine residues (green). (C-E) $Scrib^{C4AC11A}$ can fully rescue polarity loss in *scrib* mutant follicle cells, and localizes appropriately to the basolateral membrane. Compared to WT and *dlg* RNAi alone (F,G,H,I), membrane tethering Scrib by Morphotrap (J,K) or N-terminal myristoylation signal (L,M) in *dlg* RNAi cells does not rescue aPKC spread or Lgl mislocalization. Scale bars, 10µm.

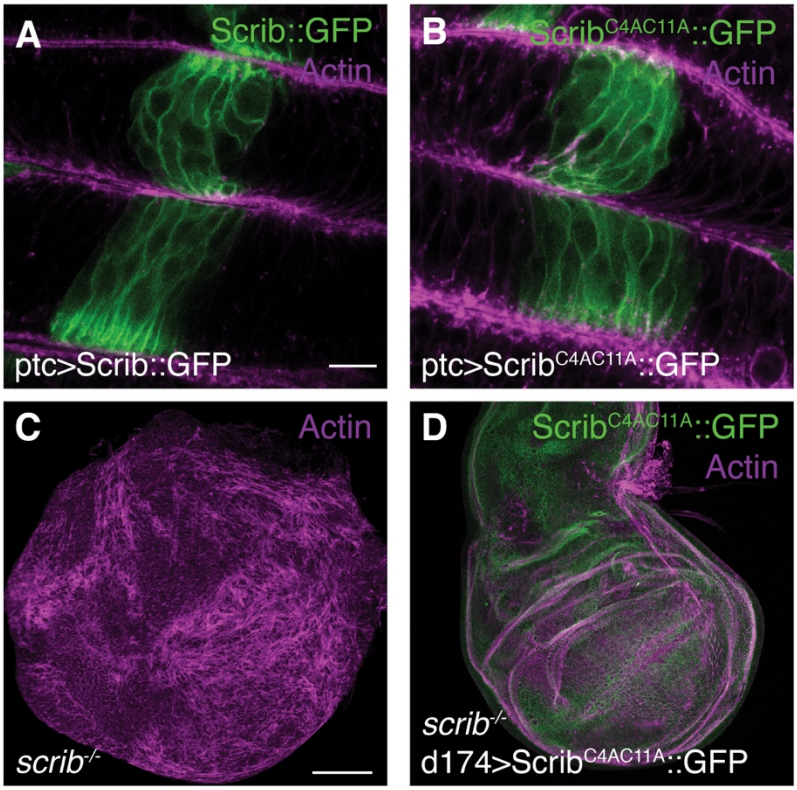

Figure 2.8. Characterization of non-palmitoylatable Scrib in the imaginal disc epithelium
(A,B) When overexpressed in the wing imaginal disc epithelium, Scrib^{C4AC11A} localizes normally to the basolateral domain and septate junction (B) similarly to WT Scrib (A). (C,D) Scrib^{C4AC11A} overexpression (D) is sufficient to rescue the overgrowth and polarity loss of *scrib* mutant imaginal disc tumors (C). Scale bars, 10μm.

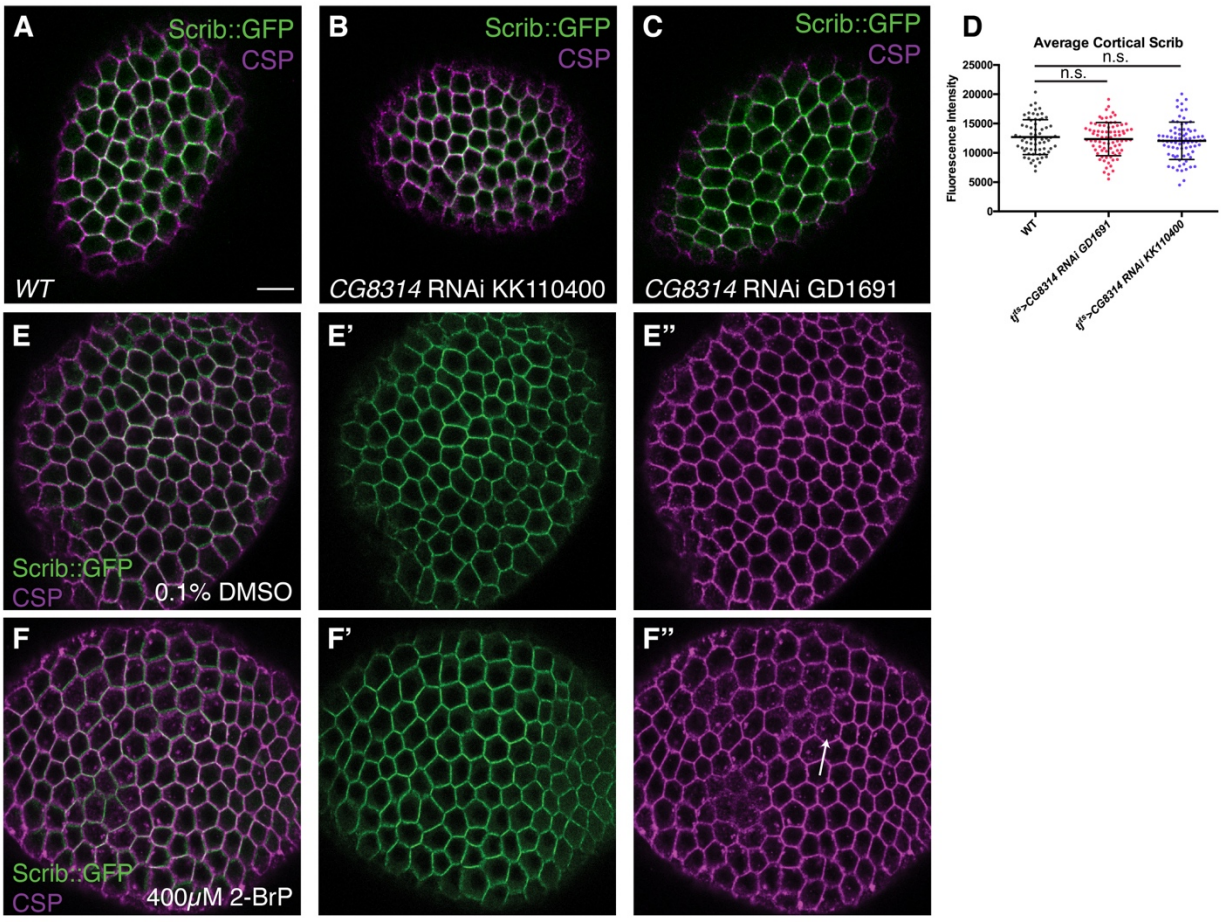

Figure 2.9. ZDHHC palmitoyltransferase activity is not required for cortical Scrib localization

(A-C) Reducing the levels of CG8314, the homolog to the human Scrib palmitoyltransferase ZDHHC7 does not affect Scrib localization in follicle cells. (D) Quantification of cortical Scrib levels in cells depleted of CG8314 compared to WT. (E,F) Chemical inhibition of ZDHHC palmitoyltransferases by 2-Bromopalmitate (2-BrP) treatment in *ex vivo* cultured follicles affects a control palmitoylated protein, CSP (E",F", arrow), but does not affect Scrib localization (E',F'). Scale bars, 10μm. One-way ANOVA with Dunnett's multiple comparisons test. Error bars represent S.D.

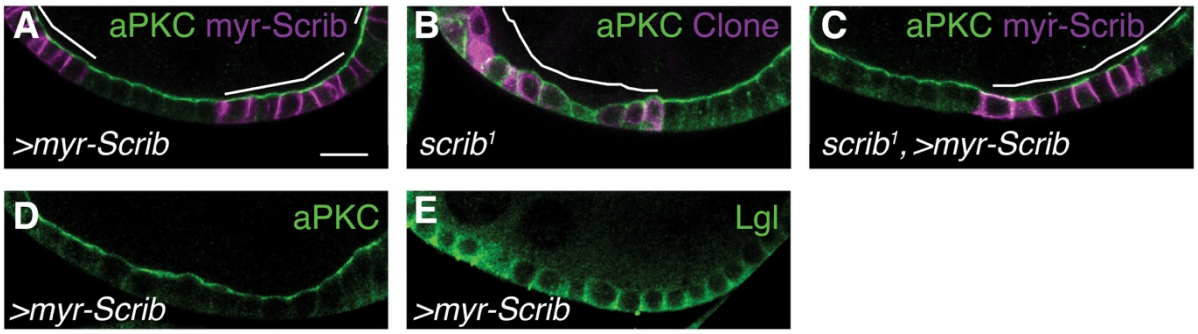

Figure 2.10. myr-Scrib rescues *scrib* loss of function

(A) Constitutively membrane-associated myr-Scrib is localized to the membrane in WT cells. (B, C) myr-Scrib rescues polarity loss in *scrib* mutant cells. (D,E) myr-Scrib expression does not disrupt aPKC (D) or Lgl (E) localization in WT cells. Scale bars, 10μm.

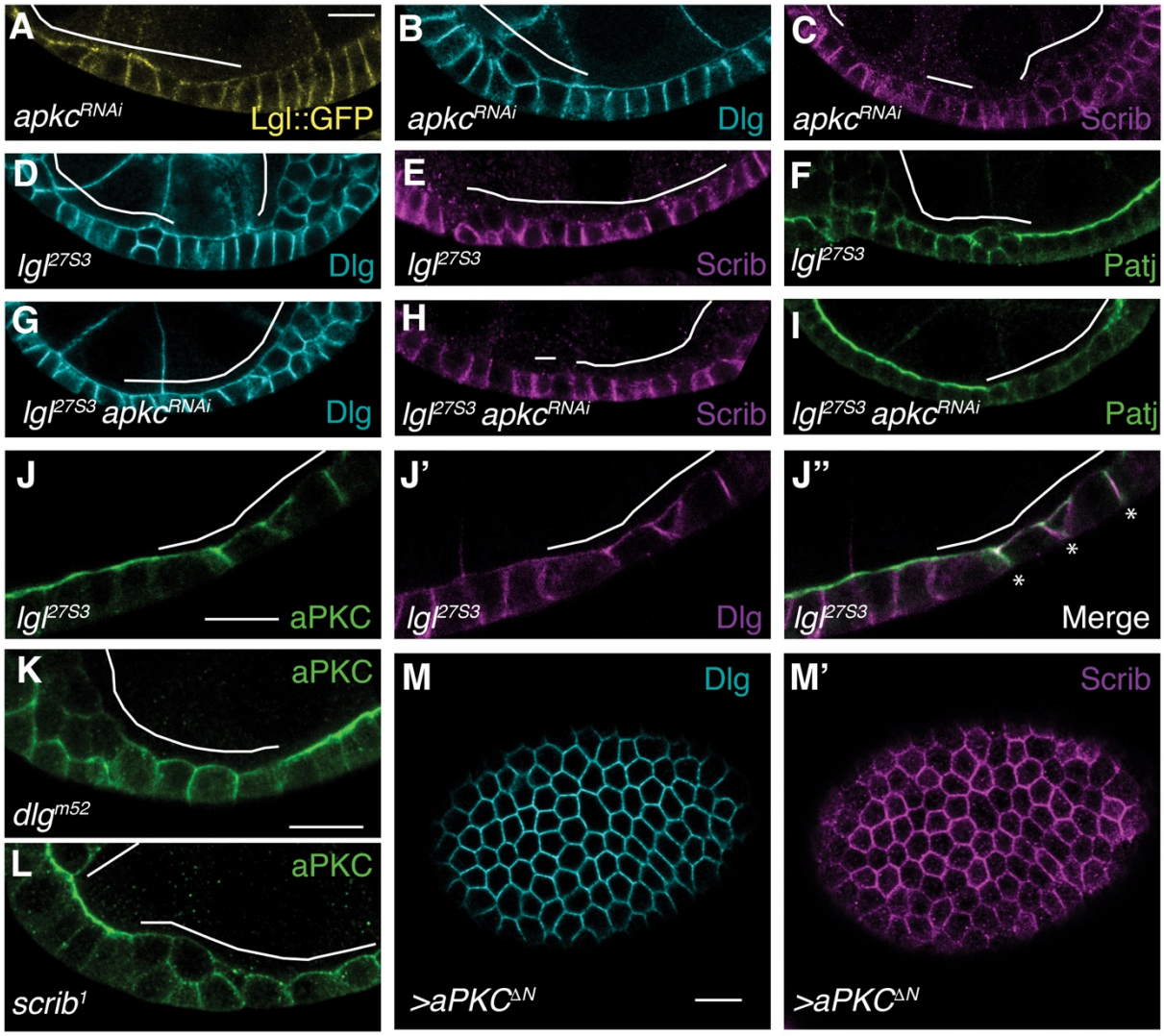

Figure 2.11. Scrib and Dlg do not directly antagonize aPKC

(A) In *apkc*-depleted follicle cells, Lgl reaches the apical membrane, but Dlg (B) and Scrib (C) remain basolaterally localized. (D,E,G,H) Scrib and Dlg localization is unaffected when apicobasal antagonism is eliminated by codepletion of *apkc* and *lgl.* Laterally mislocalized aPKC in *lgl* mutant cells (F) is active, as it recruits Patj to these sites (I). (J) aPKC spreads along the basolateral membrane in *lgl* mutant cells, where it colocalizes with Dlg (J',J''). (K,L) aPKC mislocalization is also seen in *dlg* (K) and *scrib* (L) mutant cells. (M) Expression of a constitutively active aPKC ($aPKC^{\Delta N}$) does not displace Scrib or Dlg. Scale bars, 10μm.

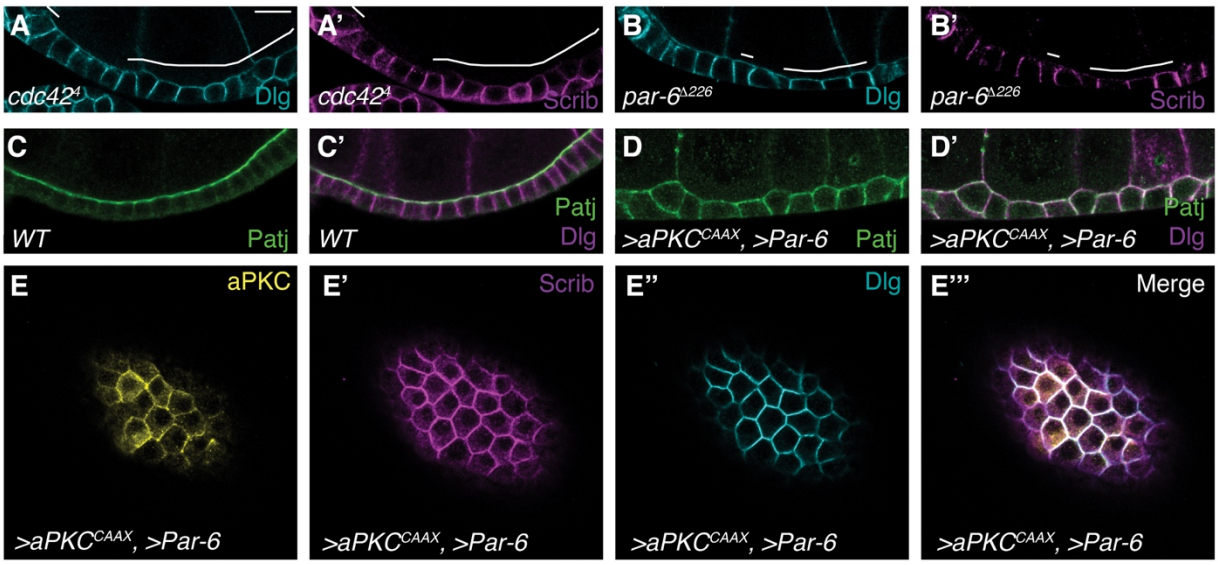

Figure 2.12. The Par Complex does not antagonize Scrib or Dlg
(A,B) Scrib and Dlg localization in null alleles of the Par complex genes, *cdc42* (A) and *par-6* (B). Scrib and Dlg retain basolateral localization in both mutants. (C,D) Expression of a gain-of-function, membrane-tethered aPKC construct ($aPKC^{CAAX}$) is sufficient to specify the entire cell cortex as an ectopic apical domain, marked by spread of Patj (D) which colocalizes with Dlg at the basolateral membrane (D'). (E) Overexpressed $aPKC^{CAAX}$ localizes uniformly to the cortex and can colocalize with Scrib and Dlg at the basolateral domain. Scale bars, 10μm.

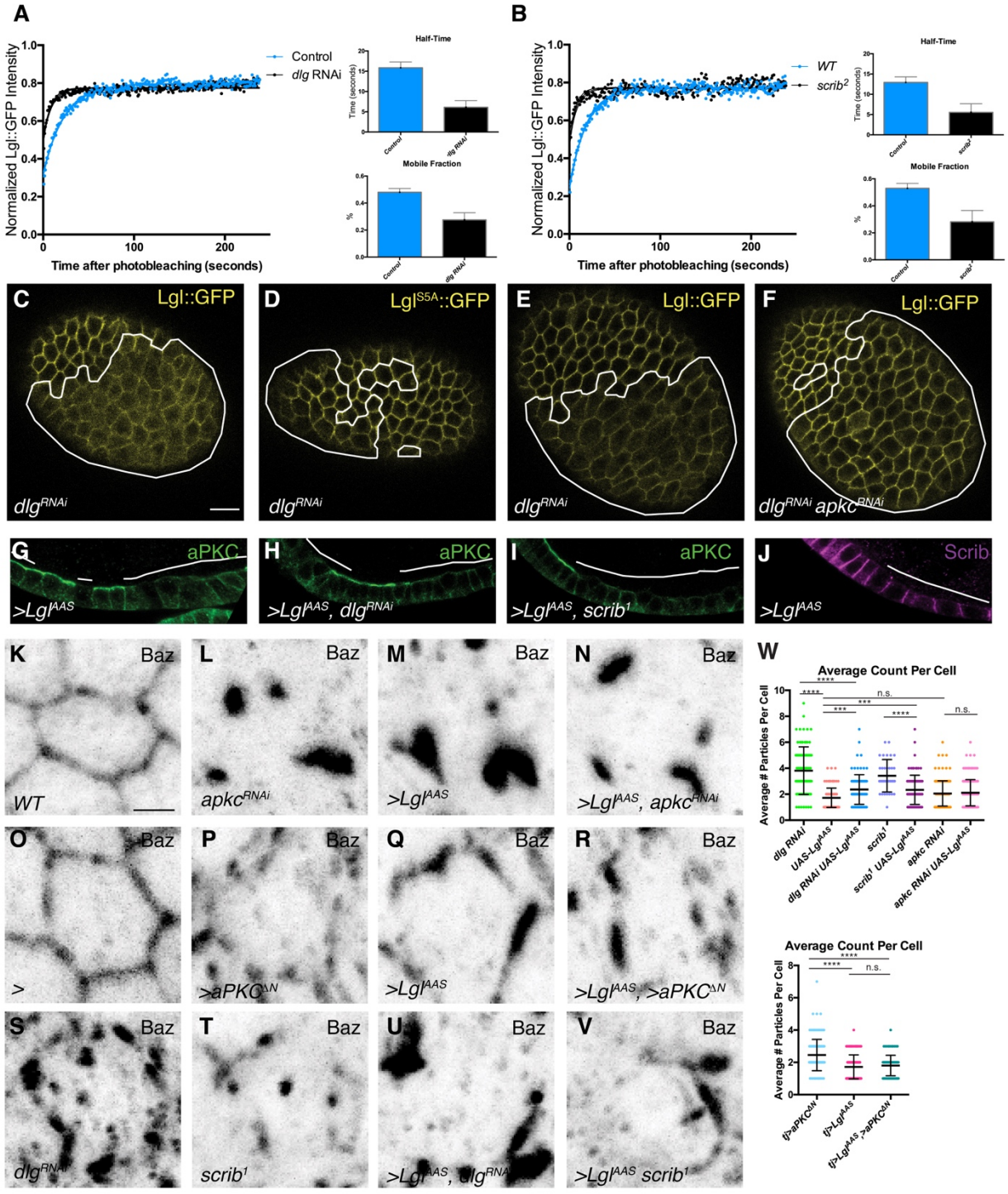

Figure 2.13. Scrib and Dlg support basolateral Lgl activity

(A,B) In both *scrib* and *dlg* mutant follicle cells, Lgl::GFP shows increased FRAP kinetics compared to WT. (C,D) In *dlg* RNAi cells, Lgl::GFP is displaced to the cytoplasm but non-phosphorylatable Lgl^{S5A}::GFP remains cortical. (E,F) Co-depletion of *apkc* rescues Lgl localization in *dlg*-depleted cell. (G) Lgl^{AAS} expression causes loss of apical aPKC. (H,I) Apical aPKC depletion by Lgl^{AAS} persists in the absence of Dlg and Scrib. (J) Lgl^{AAS} is not sufficient to

create an ectopic basolateral membrane, as it fails to recruit Scrib apically. (K-M) Baz forms several aggregates in each Lgl^{AAS}-expressing cell, similar to *apkc* depleted cells. (M,N) Depletion of *apkc* in Lgl^{AAS}-expressing cells does not modify the Baz phenotype. Compared to WT (O), expressing of a constitutively active aPKC (P) causes a Baz phenotype similar to *dlg* (S) or *scrib* loss-of-function (T). (Q,R) Co-expression of Lgl^{AAS} causes a phenotype that resembles Lgl^{AAS} alone. In *dlg*-depleted (S) or *scrib* mutant (T) cells, Baz localizes to more frequent, fragmented puncta. Expression of Lgl^{AAS} in *dlg*-depleted cells (U) or *scrib* mutant cells (V) reduces Baz particle number. (W) Quantification of Baz phenotypes in K-V. One-way ANOVA with Tukey's multiple comparisons test. K-V show maximum intensity projections centered on the nuclei of single cells. Scale bars, 10µm in C-J, 2µm in K-V. Error bars in A-B represent 95% confidence intervals, error bars in W represent S.D. Data points in W are measurements from single cells.

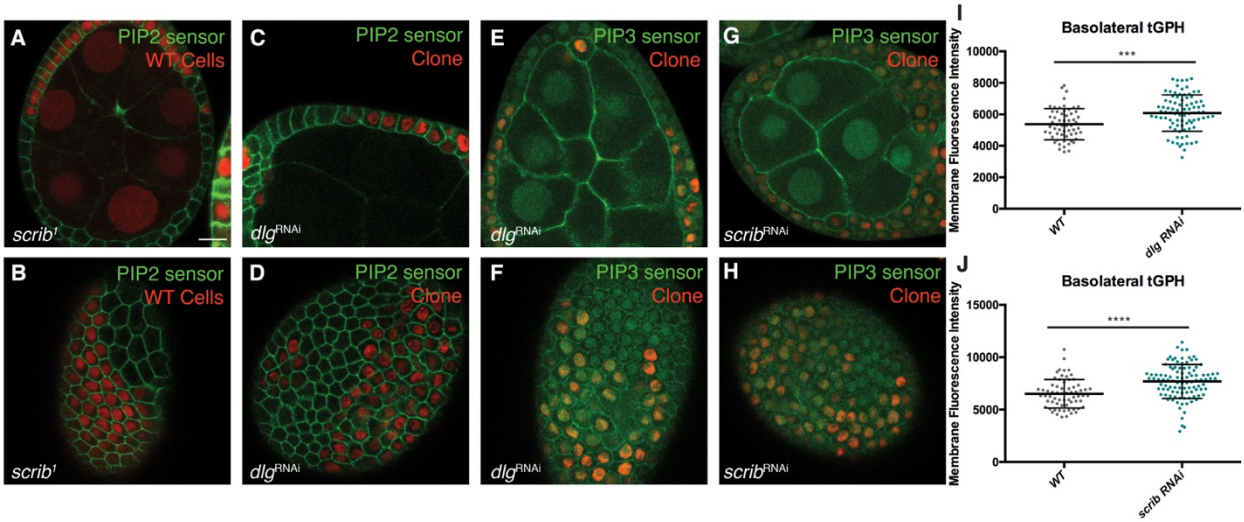

Figure 2.14. Scrib and Dlg regulation of PIP distribution
(A,B) *scrib* loss of function does not alter PIP2 levels or localization. (C,D) *dlg* loss of function also does not alter PIP2 levels or localization. (E,F) *dlg* loss of function results in a slight, but significant increase in PIP3 levels. (G,H) *scrib* loss of function results in similarly increased PIP3 levels. (I,J) Quantification of basolateral PIP3 sensor in *dlg* RNAi (I) and *scrib* RNAi (J). Scale bars, 10µm. Error bars represent S.D., data points are measurements from single cells. Unpaired t-test with Welch's correction.

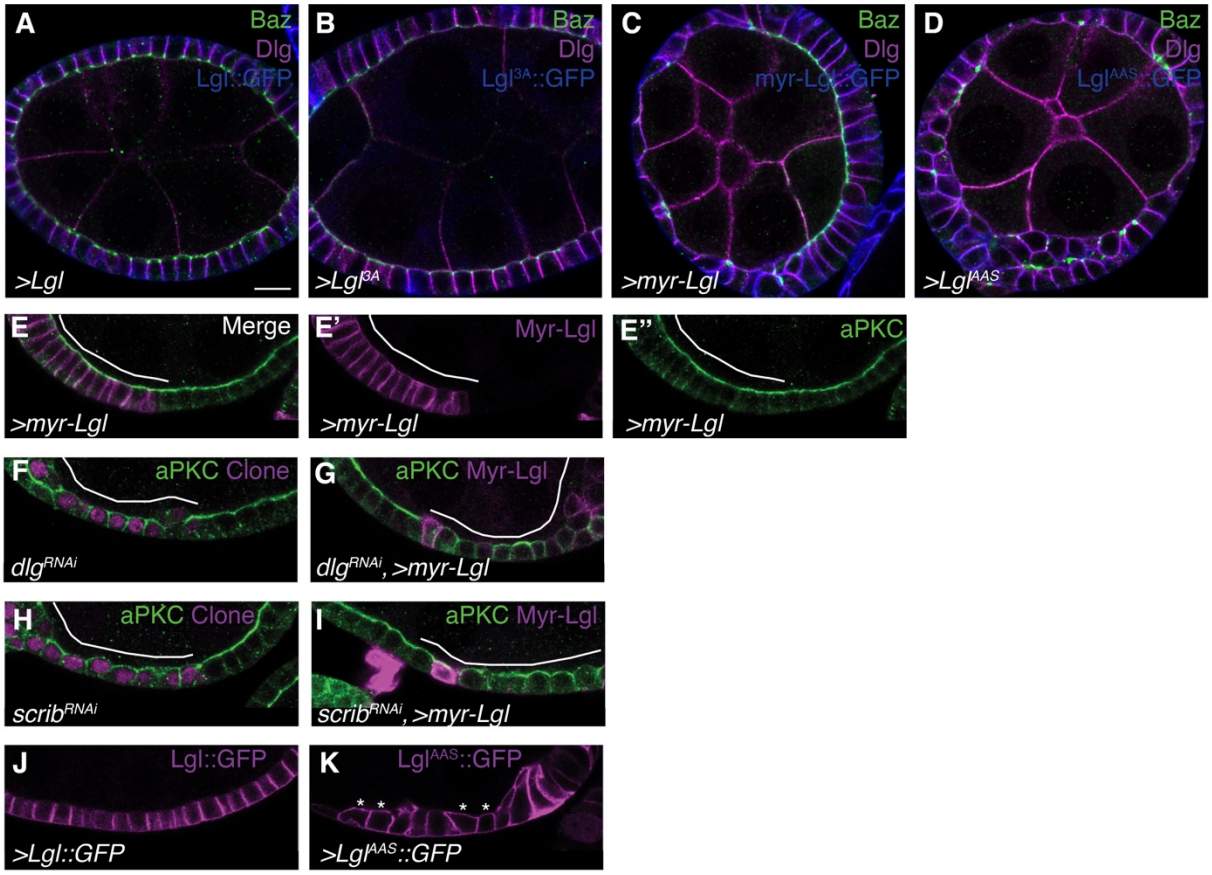

Figure 2.15. myr-Lgl cannot suppress *scrib* or *dlg* mutant phenotypes
(A-D) Phenotypes of overexpressed Lgl variants. WT Lgl (A) and non-phosphorylatable Lgl^{3A} (B) do not cause dominant phenotypes when expressed in WT cells. (C) Constitutively cortical myr-Lgl causes minor epithelial disruption and Baz aggregation in WT cells. (D) Lgl^{AAS} causes severe epithelial disruption, multilayering and Baz aggregation. (E) Clonal expression of myr-Lgl does not cause polarity defects in WT follicle cells. (F-I) myr-Lgl also does not rescue the polarity defects of *dlg* RNAi (F,G) or *scrib* RNAi (H,I) cells. (J,K) Compared to overexpressed WT Lgl (J), Lgl^{AAS} (K) localizes uniformly to the cell cortex, including the apical domain (asterisks). Scale bars, 10μm.

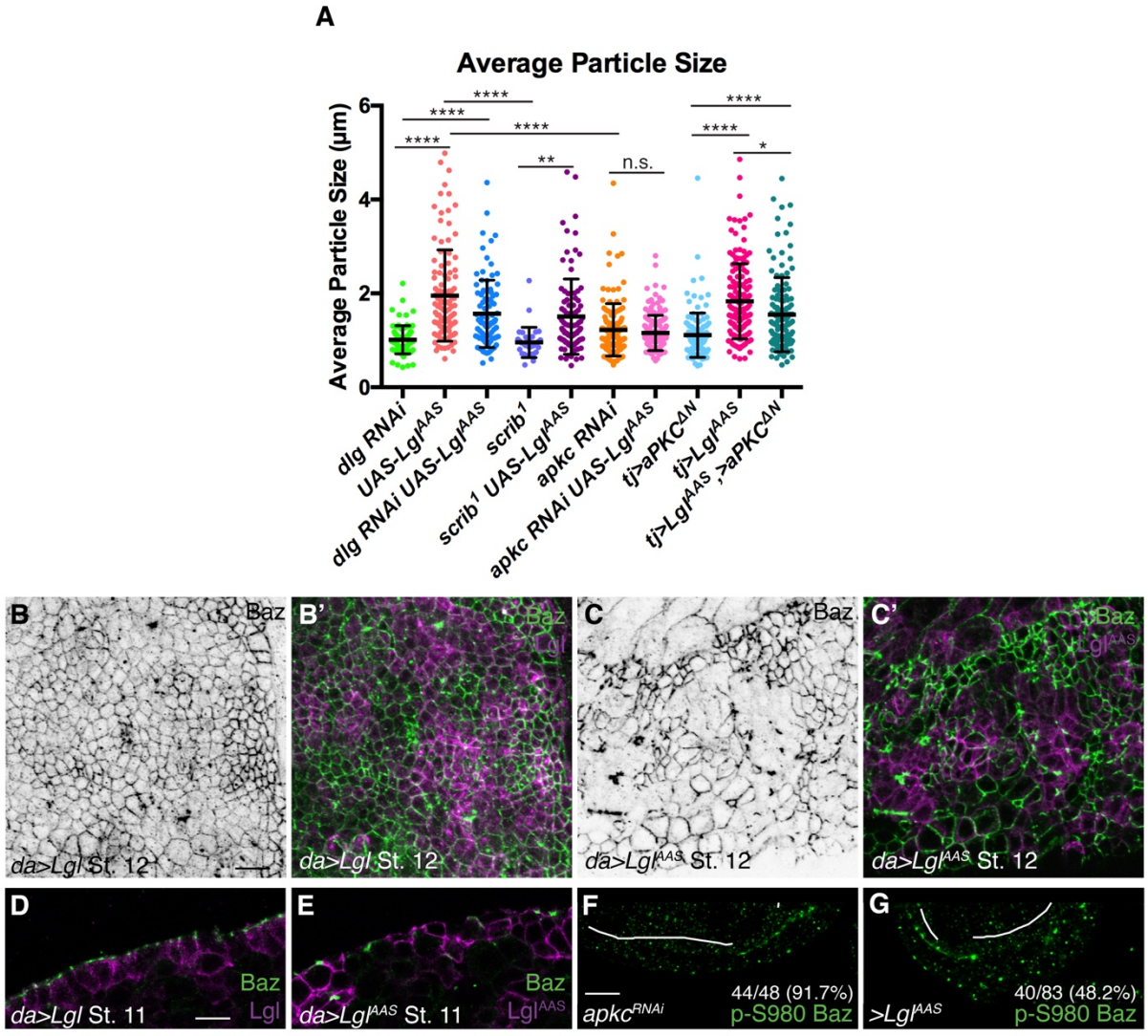

Figure 2.16. Lgl^{AAS} is a partial aPKC inhibitor

(A) Quantification of Baz aggregate size. Related to Figure 5K-V. Lgl^{AAS} induces large Baz aggregates, similar to *apkc* RNAi compared to the smaller fragments in *scrib* mutants and *dlg* RNAi. Combining Lgl^{AAS} with *scrib* mutation or *dlg* RNAi results in Baz aggregates intermediate in size compared to either genotype alone. Lgl^{AAS} shows similar interactions with constitutively active aPKC$^{\Delta N}$, which mimics basolateral loss of function. (B,C) Maximum intensity projections of embryonic epidermis show that compared to overexpressed WT Lgl (B), Lgl^{AAS} (C) can induce Baz aggregates. (D,E) Lgl^{AAS} can disrupt epithelial architecture (E) compared to WT Lgl overexpression (D). (F,G) *apkc* RNAi (F) or Lgl^{AAS} expression (G) can cause loss of Baz phosphorylation on aPKC targeted S980 (p-S980 Baz) in follicle cell clones. However, in Lgl^{AAS}-expressing cells, this phenotype is incompletely penetrant (48.2% vs. 91.7% in *apkc* RNAi). Scale bars, 10µm. One-way ANOVA with Tukey's multiple comparisons test. Error bars represent S.D., data points are measurements of single particles in single cells.

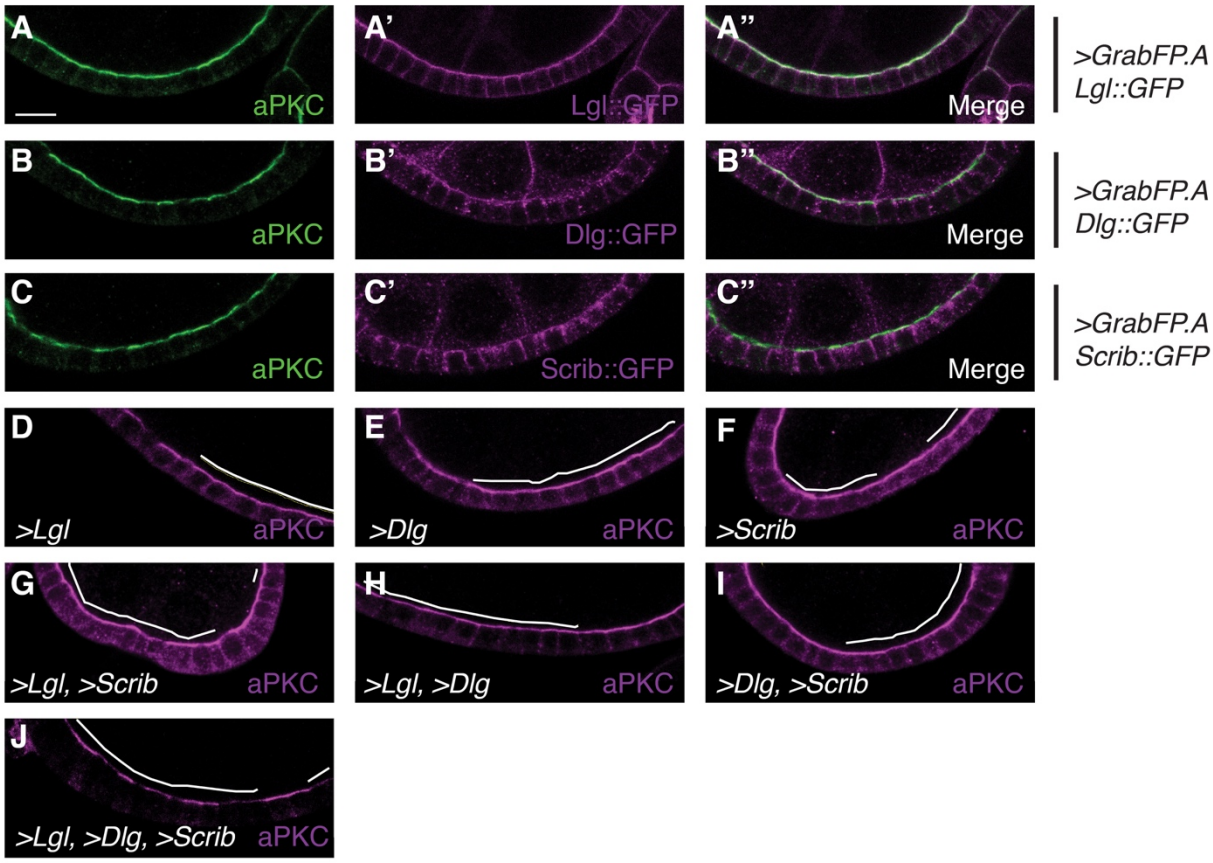

Figure 2.17. The entire Scrib module is not sufficient to establish basolateral polarity
Ectopic apical localization of Lgl (A), Dlg (B) or Scrib (C) using apical GrabFP has no effect on epithelial polarity. WT Scrib, Dlg and Lgl are not sufficient to disrupt the apical domain when overexpressed singly (D-F), in pairs (G-I), or as a holo-module (J). Scale bars, 10µm.

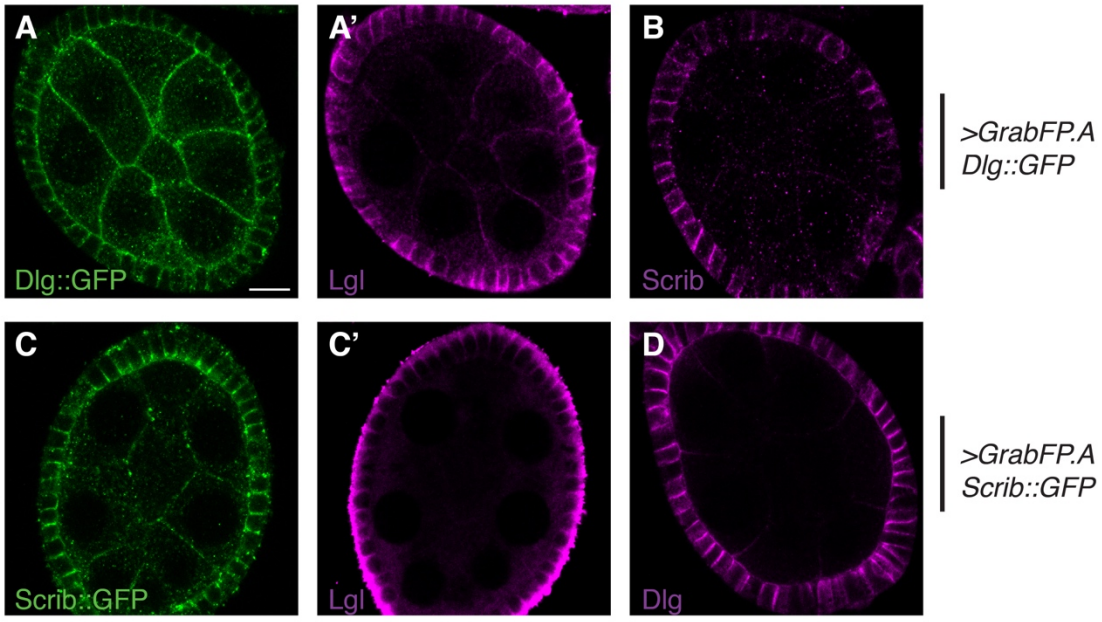

Figure 2.18. Scrib and Dlg are not sufficient to recruit endogenous Scrib module
Ectopic apically localized Dlg (A,B) or Scrib (C,D) using apical GrabFP are not able to recruit endogenous Lgl (A', C') or Scrib (B) or Dlg (D) to the apical domain. Scale bars, 10µm.

Table 1. Key resources

Reagent	Reference and Source
Fly stocks	
scrib^{1}	(Bilder and Perrimon, 2000)
scrib^{2}	(Zeitler et al., 2004)
scrib^{4}	(Zeitler et al., 2004)
dlg^{m52}	(Perrimon, 1988)
dlg$^{40.2}$	(Mendoza-Topaz et al., 2008)
dlg^{m30}	(Woods and Bryant, 1989)
dlg^{1P20}	(Perrimon, 1988), Generously provided by D. Bergstralh
dlg^{v59}	(Woods and Bryant, 1989), Generously provided by V. Budnik
dlg^{HF321}	(Perrimon, 1988)
lgl^{27S3}	(Brumby et al., 2004)
cdc42^{4}	(Fehon et al., 1997), Bloomington Drosophila Stock Center (BDSC): 9106
par-6$^{\Delta 226}$	(Petronczki and Knoblich, 2001), Generously provided by M. Metzstein
PI4KIIIα^{GS27}	(Yan et al., 2011), Generously provided by T. Schupbach
UASp-Scrib::GFP	(Zeitler et al., 2004)
UAS-EGFP::Dlg	(Koh et al., 1999)
UAS-Lgl::GFP	(Wirtz-Peitz et al., 2008)
UAS-Lgl^{AAS}*::GFP*	(Carvalho et al., 2015), Generously provided by E. Morais de Sá
UAS-myr-Scrib::V5	This study
UASp-Scrib^{C4AC11A}*::GFP*	This study
UAS-myr-Lgl::GFP	(Bell et al., 2015), Generously provided by B. Thompson

UAS-Δp60	(Weinkove et al., 1999)
UAS-aPKC$^{\Delta N}$	(Betschinger et al., 2003)
UAS-aPKC^{CAAX} UAS-Par-6	(David et al., 2010), Generously provided by Y. Hong
UAS-dlg RNAi HMS01954	BDSC: 39035
UAS-dlg RNAi GD4689	Vienna Drosophila Resource Center (VDRC): 41136
UAS-scrib RNAi HMS01993	BDSC: 39073
UAS-scrib RNAi HMS01490	BDSC: 35748
UAS-lgl RNAi HMS01905	BDSC: 38989
UAS-lgl RNAi	(de Vreede et al., 2014)
UAS-apkc RNAi JF01966	BDSC: 25946
UAS-CG8314 RNAi KK101379	VDRC: 110400
UAS-GrabFP.A.Int::mCherry	(Harmansa et al., 2017), BDSC: 68178
UAS-Morphotrap.Int::mCherry	(Harmansa et al., 2015; Harmansa et al., 2017), BDSC: 68172
Lgl::GFP	(Huang et al., 2009), Generously provided by Y. Hong
Lgl^{S5A}::GFP	(Huang et al., 2009), Generously provided by Y. Hong
Scrib::GFP CA07683	(Buszczak et al., 2007), Generously provided by R. Davis
Dlg::GFP YC0005	(Buszczak et al., 2007), BDSC: 50859
ubi-PH-PLCδ::GFP	(Gervais et al., 2008), Generously provided by T. Schupbach
tGPH	(Britton et al., 2002)
hh-GAL4	BDSC: 67046
tj-GAL4	Kyoto stock center: 104055
act>y+>GAL4 UAS-his::RFP	BDSC: 30558

tub-GAL4, UAS-CD8::GFP;tub-GAL80 FRT82B	(Lee and Luo, 1999)
tub-GAL80 FRT40A; tub-GAL4, UAS-CD8::GFP	(Lee and Luo, 1999)
tub-GAL80 FRT19A; act-GAL4 UAS-GFP	(Lee and Luo, 1999)
GR1-GAL4 UAS-FLP	(Goentoro et al., 2006)
MTD-GAL4	BDSC: 31777
da-GAL4	BDSC: 55850
$ovo^{D1\text{-}18}$ $hsFLP^{12}$ *FRT19A*	BDSC: 23880
$ovo^{D1\text{-}18}$ *FRT82B*	BDSC: 2149
Antibodies	
1:100 mouse anti-Dlg (IHC)	Developmental Studies Hybridoma Bank (DSHB): 4F3
1:500 guinea pig anti-Scrib (IHC)	(Bilder and Perrimon, 2000)
1:200 rabbit anti-Lgl (IHC)	(Ohshiro et al., 2000), Generously provided by F. Matsuzaki
1:200 rabbit anti-aPKC (IHC)	Santa Cruz Biotech: sc-216
1:500 rabbit anti-Baz (IHC)	(Wodarz et al., 2000)
1:500 rabbit anti-Patj (IHC)	(Bhat et al., 1999)
1:100 mouse anti-CSP (IHC), 1:1000 (WB)	DSHB: 6D6
1:10000 rabbit anti-GFP (WB)	Thermo Fisher: A-11122
1:100 rabbit anti-p-S980 Baz (IHC)	(Morais-de-Sá et al., 2010), Generously provided by D. St Johnston

Table 2. Genotypes

Figure	**Genotype**
Figure 1B	*ubi-nls-GFP FRT40A/iso FRT40A;GR1-GAL4 UAS-FLP/+*
Figure 1C, O, P, Figure 11L	*hsFLP[122]/+;;ubi-nls-mRFP FRT82B/scrib[1] FRT82B*
Figure 1D,M,N Figure 11K	*hsFLP[122] ubi-nls-mRFP FRT19A/dlg[m52] FRT19A*

Figure 1E,Q,R Figure 11J	*ubi-nls-GFP FRT40A/lgl[27S3] FRT40A;GR1-GAL4 UAS-FLP/+*
Figure 1F	*hsFLP/+;tub-GAL4 UAS-GFP/+;tub-GAL80 FRT82B/scrib[2] FRT82B*
Figure 1G	*hsFLP/+;tub-GAL80 FRT40A/lgl[27S3] FRT40A;tub-GAL4 UAS-GFP/+*
Figure 1H	*hsFLP tub-GAL80 FRT19A/dlg[m52] FRT19A; act5c-GAL4 UAS-GFP/+*
Figure 1I	*hsFLP/+;tub-GAL4/UAS-lgl RNAi HMS01905;tub-GAL80 FRT82B/scrib[2] FRT82B*
Figure 1J	*hsFLP/+;tub-GAL80 FRT40A/lgl[27S3] FRT40A;tub-GAL4 UAS-GFP/UAS-dlg RNAi GD4689*
Figure 1K	*hsFLP/+;tub-GAL4 UAS-GFP/UAS-dlg RNAi HMS01954;tub-GAL80 FRT82B/scrib[2] FRT82B*
Figure 1S	*hsFLP[122]/+;UAS-Lgl::GFP/UAS-dlg RNAi HMS01954;act>y+>UAS-his::RFP/+*
Figure 1T	*hsFLP/+;tub-GAL4 UAS-GFP/UAS-lgl::GFP;tub-GAL80 FRT82B/scrib[2] FRT82B*
Figure 1U	*hsFLP tub-GAL80 FRT19A/dlg[m52] FRT19A; act5c-GAL4 UAS-GFP/+;+/UAS-Scrib::GFP*
Figure 1V	*hsFLP/+;tub-GAL4 UAS-GFP/UAS-EGFP::Dlg;tub-GAL80 FRT82B/scrib[2] FRT82B*
Figure 1W	*hsFLP/+;tub-GAL80 FRT40A/lgl[27S3] FRT40A;tub-GAL4 UAS-GFP/UAS-Scrib::GFP*
Figure 1X	*hsFLP[122]/+;+/UAS-EGFP::Dlg;act>y+>UAS-his::RFP/UAS-lgl RNAi*
Figure 7A, Figure 7A, Figure 5C-F, Figure 9B,C	*Dlg::GFP/+, Scrib::GFP/+ or Lgl::GFP/+*
Figure 7B	*hsFLP[122]/+;+/UAS-dlg RNAi HMS01954;act>y+>UAS-his::RFP/Scrib::GFP*
Figure 7D,E,F	*dlg[v59]/FM7c*
Figure 7G, H, I Figure FIGURE 6C	*dlg[v59]/dlg[HF321]*
Figure 7J, K	*hsFLP[122]/+;;ubi-nls-mRFP FRT82B/scrib[4] FRT82B*
Figure 7L, M Figure 6A	*hsFLP[122] ubi-nls-mRFP FRT19A/dlg[m30] FRT19A*
Figure 7B, Figure	*hsFLP/+;tub-GAL4 UAS-GFP/+;tub-GAL80 FRT82B/scrib[1] FRT82B*

13T, Figure 10B	
Figure 7C	*hsFLP[122]/+;+/UAS-Scrib[C4AC11A]::GFP;act>y+>UAS-his::RFP/+*
Figure 7D	*hsFLP/+;tub-GAL4 UAS-GFP/UAS-Scrib[C4AC11A]::GFP;tub-GAL80 FRT82B/scrib[1] FRT82B*
Figure 7E, F	*tj-GAL4 tub-GAL80[ts]/+;UAS-Morphotrap.A::mCherry/Scrib::GFP*
Figure 7G, H	*tj-GAL4 tub-GAL80[ts]/UAS-dlg RNAi HMS01954*
Figure 7I, J	*tj-GAL4 tub-GAL80[ts]/UAS-dlg RNAi HMS01954;UAS-Morphotrap.A::mCherry/Scrib::GFP*
Figure 7K, L	*tj-GAL4 tub-GAL80[ts]/UAS-myr-Scrib::V5;+/UAS-dlg RNAi GD4689*
Figure 11A	*hsFLP[122]/+;+/Lgl::GFP;act>y+>UAS-CD8::RFP/UAS-apkc RNAi JF01966*
Figure 11B, C, Figure 13L, S9F	*hsFLP[122]/+;;act>y+>UAS-CD8::RFP/UAS-apkc RNAi JF01966*
Figure 11D, E, F	*hsFLP/+;tub-GAL80 FRT40A/lgl[27S3] FRT40A;tub-GAL4 UAS-GFP/+*
Figure 11G, H, I	*hsFLP/+;tub-GAL80 FRT40A/lgl[27S3] FRT40A;tub-GAL4 UAS-GFP/UAS-apkc RNAi JF01966*
Figure 11M, Figure 13P	*tj-GAL4 tub-GAL80[ts]/+;UAS-aPKC[ΔN]/+*
Figure 13A,C	*hsFLP[122]/+;+/Lgl::GFP;act>y+>UAS-CD8::RFP/UAS-dlg RNAi GD4689*
Figure 13B	*hsFLP[122]/+;+/Lgl::GFP;ubi-nls-mRFP FRT82B/scrib[2] FRT82B*
Figure 13D	*hsFLP[122]/+;+/Lgl[S5A]::GFP;act>y+>UAS-CD8::RFP/UAS-dlg RNAi GD4689*
Figure 13E	*hsFLP[122]/+;Lgl::GFP/ UAS-dlg RNAi HMS01954;act>y+>UAS-his::RFP/+*
Figure 13F	*hsFLP[122]/+;Lgl::GFP/ UAS-dlg RNAi HMS01954;act>y+>UAS-his::RFP/UAS-apkc RNAi JF01966*
Figure 13G, J, M, S9G	*hsFLP[122]/+;+/UAS-Lgl[AAS]::GFP;act>y+>UAS-his::RFP/+*
Figure 13H,	*hsFLP[122]/+;act>y+>UAS-his::RFP/UAS-dlg RNAi GD4689*
Figure 13I, V	*hsFLP/+;tub-GAL4 UAS-GFP/UAS-Lgl[AAS]::GFP;tub-GAL80 FRT82B/scrib[1] FRT82B*
Figure 13N	*hsFLP[122]/+;+/UAS-Lgl[AAS]::GFP;act>y+>UAS-CD8::RFP/UAS-apkc RNAi JF01966*

Figure 13Q, Figure 15L	*tj-GAL4 tub-GAL80[ts]/UAS-Lgl[AAS]::GFP*
Figure 13R	*tj-GAL4 tub-GAL80[ts]/UAS-Lgl[AAS]::GFP;+/UAS-aPKC[ΔN]*
Figure 13S, Figure 15G	*hsFLP[122]/+;+/UAS-dlg RNAi HMS01954;act>y+>UAS-his::RFP/+*
Figure 17A	*tj-GAL4 tub-GAL80[ts]/Lgl::GFP;+/UAS-GrabFP.A.Int::mCherry*
Figure 17B	*Dlg::GFP/+;tj-GAL4 tub-GAL80[ts]/+;UAS-GrabFP.A.Int::mCherry/+*
Figure 17C	*tj-GAL4 tub-GAL80[ts]/+;UAS-GrabFP.A.Int::mCherry/Scrib::GFP*
Figure 17D	*hsFLP[122]/+;+/UAS-Lgl::GFP;act>y+>UAS-his::RFP/+*
Figure 17E	*hsFLP[122]/+;+/UAS-Dlg::GFP;act>y+>UAS-his::RFP/+*
Figure 17F	*hsFLP[122]/+;;act>y+>UAS-his::RFP/UAS-Scrib::GFP*
Figure 17G	*hsFLP[122]/+;+/UAS-Lgl::GFP;act>y+>UAS-his::RFP/UAS-Scrib::GFP*
Figure 17H	*hsFLP[122]/+;UAS-Lgl::GFP/UAS-Dlg::GFP;act>y+>UAS-his::RFP/+*
Figure 17I	*hsFLP[122]/+;+/UAS-Dlg::GFP;act>y+>UAS-his::RFP/UAS-Scrib::GFP*
Figure 17J	*hsFLP[122]/+;UAS-Lgl::GFP/UAS-Dlg::GFP;act>y+>UAS-his::RFP/UAS-Scrib::GFP*
Figure 7D, I	*dlg[m52] FRT19A/ovo[D1-18] hsFLP[12] FRT19A (maternal GLC) + paternal rescue*
Figure 7E, J	*dlg[m52] FRT19A/ovo[D1-18] hsFLP[12] FRT19A (maternal GLC)*
Figure 7F	*MTD-GAL4;+*
Figure 7G, H, K	*MTD-GAL4;UAS-scrib RNAi HMS01490*
Figure 5A	*hsFLP[122] ubi-nls-mRFP FRT19A/PI4KIIIα[GS27] FRT19A*
Figure 5B	*hsFLP[122]/hsFLP;+/UAS-ΔP60;act>y+>UAS-his::RFP/+*
Figure 6B,E	*hsFLP[122] ubi-nls-mRFP FRT19A/dlg[1P20] FRT19A*
Figure 6G, I, K	*dlg[m30] FRT19A/ovo[D1-18] hsFLP[12] FRT19A (maternal GLC) + paternal rescue*
Figure 6H, J, L	*dlg[m30] FRT19A/ovo[D1-18] hsFLP[12] FRT19A (maternal GLC)*
Figure 6M, O	*hsFLP[22]/+;scrib[4] FRT82B/ovo[D1-18] FRT82B (maternal GLC) + paternal rescue*
Figure 6N, P	*hsFLP[22]/+;scrib[4] FRT82B/ovo[D1-18] FRT82B (maternal GLC)*
Figure 9A	*hsFLP[122]/+;+/UAS-CG8314 RNAi KK101379;act>y+>UAS-his::RFP/+*
Figure 10A	*hsFLP[122]/+;+/UAS-myr-Scrib::V5;act>y+>UAS-his::RFP/+*
Figure 15C	*hsFLP/+;tub-GAL4 UAS-GFP/UAS-myr-Scrib::V5;tub-GAL80 FRT82B/scrib[1] FRT82B*

Figure 15D,E	*tj-GAL4 tub-GAL80[ts]/UAS-myr-Scrib::V5*
Figure 15F	*hsFLP[122]/+;act>y+>UAS-his::RFP/UAS-myr-Lgl::GFP*
Figure 15H	*hsFLP[122]/+;+/UAS-dlg RNAi HMS01954;act>y+>UAS-his::RFP/UAS-myr-Lgl::GFP*
Figure 15I	*hsFLP[122]/+;+/UAS-scrib RNAi HMS01993;act>y+>UAS-his::RFP/+*
Figure 15J	*hsFLP[122]/+;+/UAS-scrib RNAi HMS01993;act>y+>UAS-his::RFP/UAS-myr-Lgl::GFP*
Figure 15K	*tj-GAL4 tub-GAL80[ts]/UAS-Lgl::GFP*
Figure 12A	*hsFLP[122] ubi-nls-mRFP FRT19A/cdc42[4] FRT19A*
Figure 12B	*hsFLP[122] ubi-nls-mRFP FRT19A/par-6[Δ226] FRT19A*
Figure 12D,E	*tj-GAL4 tub-GAL80[ts]/UAS-aPKC[CAAX] UAS-Par-6*
Figure 14A,B	*hsFLP[122]/+;+/ubi-PH-PLCδ::GFP;ubi-nls-mRFP FRT82B/scrib[1] FRT82B*
Figure 14C,D	*hsFLP[122]/+;UAS-dlg RNAi HMS01954/ubi-PH-PLCδ::GFP;act>y+>UAS-his::RFP/+*
Figure 14E,F	*hsFLP[122]/+;UAS-dlg RNAi HMS01954/+;act>y+>UAS-his::RFP/tGPH*
Figure 14G,H	*hsFLP[122]/+;UAS-scrib RNAi HMS01993/+;act>y+>UAS-his::RFP/tGPH*
Figure 17B,D	*UAS-Lgl::GFP/+;+/da-GAL4*
Figure 17C,E	*UAS-Lgl[AAS]::GFP/+;+/da-GAL4*

Table 3. Results of Statistical Tests

Figure	Summary	p-value
1K, aPKC spread in double mutants:		
WT vs. scrib2	**	0.0032
WT vs. scrib2 dlg RNAi	****	< 0.0001
WT vs. lgl27S3	****	< 0.0001
WT vs. lgl27S3 dlg RNAi	****	< 0.0001
WT vs. scrib2 lgl RNAi	*	0.0174
scrib2 vs. scrib2 dlg RNAi	ns	0.3184
scrib2 vs. lgl27S3	ns	0.3589
scrib2 vs. lgl27S3 dlg RNAi	*	0.0406
scrib2 vs. scrib2 lgl RNAi	ns	0.9998
scrib2 dlg RNAi vs. lgl27S3	ns	0.9981
scrib2 dlg RNAi vs. lgl27S3 dlg RNAi	ns	0.9825
scrib2 dlg RNAi vs. scrib2 lgl RNAi	ns	0.2191

lgl27S3 vs. lgl27S3 dlg RNAi	ns	0.7595
lgl27S3 vs. scrib2 lgl RNAi	ns	0.2407
lgl27S3 dlg RNAi vs. scrib2 lgl RNAi	*	0.0239
3V, Average cortical Scrib:		
WT vs. dlgm52	*	0.0395
WT vs. dlgm30	****	< 0.0001
WT vs. dlgv59	****	< 0.0001
WT vs. dlg1P20	ns	0.2838
9D, average cortical Scrib:		
WT vs. tjts>CG8314 RNAi GD1691	ns	0.7047
WT vs. tjts>CG8314 RNAi KK110400	ns	0.3328
13W, Average Baz count:		
dlg RNAi vs. UAS-LglAAS	****	< 0.0001
dlg RNAi vs. dlg RNAi UAS-LglAAS	****	< 0.0001
dlg RNAi vs. scrib1	ns	0.7148
dlg RNAi vs. scrib1 UAS-LglAAS	****	< 0.0001
dlg RNAi vs. apkc RNAi	****	< 0.0001
dlg RNAi vs. apkc RNAi UAS-LglAAS	****	< 0.0001
UAS-LglAAS vs. dlg RNAi UAS-LglAAS	***	0.0005
UAS-LglAAS vs. scrib1	****	< 0.0001
UAS-LglAAS vs. scrib1 UAS-LglAAS	***	0.0007
UAS-LglAAS vs. apkc RNAi	ns	0.2428
UAS-LglAAS vs. apkc RNAi UAS-LglAAS	ns	0.0764
dlg RNAi UAS-LglAAS vs. scrib1	****	< 0.0001
dlg RNAi UAS-LglAAS vs. scrib1 UAS-LglAAS	ns	> 0.9999
dlg RNAi UAS-LglAAS vs. apkc RNAi	ns	0.4558
dlg RNAi UAS-LglAAS vs. apkc RNAi UAS-LglAAS	ns	0.71

scrib1 vs. scrib1 UAS-LglAAS	****	< 0.0001
scrib1 vs. apkc RNAi	****	< 0.0001
scrib1 vs. apkc RNAi UAS-LglAAS	****	< 0.0001
scrib1 UAS-LglAAS vs. apkc RNAi	ns	0.5427
scrib1 UAS-LglAAS vs. apkc RNAi UAS-LglAAS	ns	0.7913
apkc RNAi vs. apkc RNAi UAS-LglAAS	ns	> 0.9999
tj>LglAAS vs. tj>aPKCÎ”N	****	< 0.0001
tj>LglAAS vs. tj>LglAAS,>aPKCÎ”N	ns	0.9994
tj>aPKCÎ”N vs. tj>LglAAS,>aPKCÎ”N	****	< 0.0001
14I,J, average cortical PIP3:		
WT vs. dlg RNAi	***	0.0002
WT vs. scrib RNAi	****	< 0.0001
16A, average Baz particle size:		
dlg RNAi vs. UAS-LglAAS	****	< 0.0001
dlg RNAi vs. dlg RNAi UAS-LglAAS	****	< 0.0001
dlg RNAi vs. scrib1	ns	> 0.9999
dlg RNAi vs. scrib1 UAS-LglAAS	****	< 0.0001
dlg RNAi vs. apkc RNAi	ns	0.4187
dlg RNAi vs. apkc RNAi UAS-LglAAS	ns	0.8503
UAS-LglAAS vs. dlg RNAi UAS-LglAAS	**	0.002
UAS-LglAAS vs. scrib1	****	< 0.0001
UAS-LglAAS vs. scrib1 UAS-LglAAS	****	< 0.0001
UAS-LglAAS vs. apkc RNAi	****	< 0.0001
UAS-LglAAS vs. apkc RNAi UAS-LglAAS	****	< 0.0001
dlg RNAi UAS-LglAAS vs. scrib1	***	0.0003
dlg RNAi UAS-LglAAS vs. scrib1 UAS-LglAAS	ns	0.9998
dlg RNAi UAS-LglAAS vs. apkc RNAi	**	0.0058

dlg RNAi UAS-LglAAS vs. apkc RNAi UAS-LglAAS	***	0.0002
scrib1 vs. scrib1 UAS-LglAAS	**	0.0018
scrib1 vs. apkc RNAi	ns	0.5437
scrib1 vs. apkc RNAi UAS-LglAAS	ns	0.8514
scrib1 UAS-LglAAS vs. apkc RNAi	*	0.0456
scrib1 UAS-LglAAS vs. apkc RNAi UAS-LglAAS	**	0.0027
apkc RNAi vs. apkc RNAi UAS-LglAAS	ns	0.9983
tj>LglAAS vs. tj>aPKCÎ”N	****	< 0.0001
tj>LglAAS vs. tj>LglAAS,>aPKCÎ”N	*	0.012
tj>aPKCÎ”N vs. tj>LglAAS,>aPKCÎ”N	****	< 0.0001

Chapter 3:
Minimal functional domains of the core polarity regulator Dlg

Mark J. Khoury and David Bilder

ABSTRACT
The compartmentalized domains of polarized epithelial cells arise from mutually antagonistic actions between the apical Par complex and the basolateral Scrib module. The Scrib module proteins Scribble and Dlg are required to limit Lgl phosphorylation at the basolateral cortex, but how Scrib and Dlg could carry out such a 'protection' activity is not clear. We tested Protein Phosphatase 1α (PP1) as a potential mediator of this activity but demonstrate that a significant component of Scrib and Dlg regulation of Lgl is PP1-independent, and no evidence for a Scrib-Dlg-PP1 protein complex was found. However, the Dlg SH3 domain plays a role in Lgl protection and, in combination with the N-terminal region of the Dlg HOOK domain, in recruitment of Scrib to the membrane. We identify a 'minimal Dlg' comprised of the SH3 and HOOK domains that is both necessary and sufficient for Scrib localization and epithelial polarity function *in vivo*.

INTRODUCTION

Cell polarity is the fundamental process by which a single cell partitions its plasma membrane into two molecularly distinct, mutually exclusive domains. The ability to polarize is crucial for the development and homeostasis of many cell types, including neurons, stem cells and epithelial cells (St Johnston and Ahringer, 2010). Epithelial cells exhibit apicobasal polarity, a feature critical for their physiological function and morphogenesis of their resident tissues (Buckley and St Johnston, 2022; Rodriguez-Boulan and Macara, 2014). Like many other polarized cells, epithelial cell polarity is often regulated by two highly conserved groups of proteins: the Par complex, composed of Par-3, Par-6 and atypical protein kinase C (aPKC) and the Scrib module, composed of Scribble (Scrib), Discs-large (Dlg) and Lethal giant larvae (Lgl) (Flores-Benitez and Knust, 2016; Goldstein and Macara, 2007). The separation of apical and basolateral domains derives from the mutual antagonism between the apical-defining Par complex and the basolateral-defining Scrib module. Apical aPKC phosphorylates Lgl, which removes it from the plasma membrane, thus excluding Lgl from the apical domain (Bailey and Prehoda, 2015; Betschinger et al., 2003; Dong et al., 2015; Plant et al., 2003). Conversely, basolateral Lgl inhibits aPKC localization to prevent apical domain spread (Hutterer et al., 2004; Wirtz-Peitz et al., 2008; Yamanaka et al., 2003).

For the Par complex, there is now detailed insight into specific functions and molecular interactions for each of its component proteins. By contrast, how the Scrib module determines basolateral polarity is poorly defined (Lang and Munro, 2017; Tepass, 2012). The major knowledge gap in Scrib module biology is the molecular mechanism of Scrib and Dlg activity. While Lgl's role as an antagonist of aPKC localization is well-known, how Scrib and Dlg act to ensure restriction of the apical domain is not understood. Addressing this question will be essential to a full understanding of cell polarity.

We previously identified several principles of Scrib module protein function, showing that Dlg is required to regulate Scrib cortical localization and providing evidence that Scrib and Dlg are both required to negatively regulate Lgl phosphorylation (Khoury and Bilder, 2020). The data led us to propose a model in which Scrib and Dlg act as molecular switches in the aPKC-Lgl relationship. At the basolateral domain, Scrib and Dlg 'protect' Lgl by limiting inhibitory aPKC phosphorylation, allowing Lgl to inhibit aPKC, whereas at the apical domain, where Scrib and Dlg are not present, Lgl is unprotected and can be inhibited by aPKC. Here, we have used a combination of *in vivo* genetics, biochemistry, and an *in vitro* polarity system to pursue potential molecular bases of this model. We fail to find evidence supporting a plausible mechanism of Lgl protection in which Scrib and Dlg recruit the phosphatase PP1, but we identify a minimal domain of Dlg that is both necessary and sufficient for Scrib recruitment and Dlg function.

RESULTS

PP1 is a candidate effector of Scrib and Dlg activity

Since Scrib and Dlg are both scaffolding proteins, it is likely that any Lgl protection activity derives from specific binding partners. To search for polarity-relevant Dlg binding partners, we have carried out APEX2-based proximity proteomics of Dlg in epithelial tissue (Sharp et al., 2021). We mined these data for potential effectors of Lgl protection and uncovered the *Drosophila* Protein Phosphatase 1α (PP1α) homolog, Pp1-87B (hereafter PP1), in the top 60 most enriched Dlg-proximity hits (log2 fold change = 4.8, p=0.001). PP1 is an appealing candidate to mediate Lgl regulation by Scrib and Dlg because PP1 was recently shown to counteract aPKC phosphorylation of Lgl in *Drosophila* epithelial cells (Moreira et al., 2019). We confirmed that *pp1* depletion

resulted in decreased cortical Lgl localization in follicle epithelial cells (**Fig. 3.6C-E**). Intriguingly, both Scrib and Dlg contain conserved protein sequences that match PP1-binding consensus motifs: Scrib contains SILK and RVxF motifs and Dlg contains an RVxF motif (**Fig. 3.1A, Fig. 3.7A**)(Hendrickx et al., 2009; Young et al., 2013). These motifs are found in proteins that bind PP1 and can act as substrate specificity factors, recruiting the general PP1 phosphatase to target proteins (Heroes et al., 2013). We therefore hypothesized that Scrib and Dlg could regulate Lgl phosphorylation by scaffolding PP1 at the basolateral cortex.

Functional tests of Scrib and Dlg PP1-binding motifs

To test the functional relevance of the putative PP1-binding motifs in Scrib and Dlg, we designed targeted mutations in these sequences. We first mutated the consensus residues of the Dlg RVxF motif to alanine (**Fig. 3.1A**). This construct (Dlg^{ASAKA}) localized to the basolateral membrane in follicle cells and was enriched at the cell cortex (PM Index > 1) (**Fig. 3.1B-C,F**). Dlg^{ASAKA} localization was slightly less cortical than overexpressed WT Dlg (**Fig. 3.1F**). However, Dlg^{ASAKA} localization was still sensitive to *scrib* depletion, suggesting that this mutation does not prevent the recently described electrostatic mechanism of Dlg membrane recruitment (**Fig. 3.1D-F**) (Lu et al., 2021). Dlg^{ASAKA} did not rescue the overproliferation or polarity defects in *dlg* mutant wing imaginal discs (**Fig. 3.1G-J**). Similarly, when expressed in *dlg* mutant follicle cell clones, Dlg^{ASAKA} had no rescuing activity and these cells were indistinguishable from *dlg* null mutants, with ectopic basolateral aPKC localization and epithelial multilayering (**Fig. 3.1K-M**). Thus, the Dlg RVxF motif is required for all tested Dlg functions.

Next, we mutated the critical residues in the Scrib SILK and RVxF motifs to alanine (**Fig. 3.7A**). As the SILK motif is located in the Scrib LRR region, a domain critical for localization and function, we also added an N-terminal myristoylation signal to negate potential complications due to LRR disruption (Zeitler et al., 2004). The resulting protein, myr-$Scrib^{TAAA/RAGA}$ localized to the basolateral membrane in the follicle epithelium and was enriched at the cell cortex (PM Index > 1), although myr-$Scrib^{TAAA/RAGA}$ localized less well to the cortex than WT myr-Scrib (**Fig. 3.7B-D**). When expressed in *scrib* mutant wing imaginal discs, myr-$Scrib^{TAAA/RAGA}$ partially rescued the epithelial architecture defects in *scrib* mutants, although growth control was not restored (**Fig. 3.7E-H**). In follicle cells, myr-$Scrib^{TAAA/RAGA}$ was able to partially rescue the polarity loss phenotype. We observed largely normal apical aPKC localization, with incomplete rescue of epithelial multilayering compared to WT myr-Scrib (**Fig. 3.7I-J**). These results suggest myr-$Scrib^{TAAA/RAGA}$ retains significant function, and thus that these PP1-interacting consensus motifs are not essential for Scrib's role in polarity.

No evidence for physical interaction between Scrib, Dlg and PP1

Given the conserved PP1-interaction motifs in both Scrib and Dlg, we tested whether a physical interaction occurs, first using *in vivo* co-immunoprecipitation (co-IP) assays with transgenic proteins overexpressed in follicle cells. In this assay, we could detect copurification of transgenic Sds22, a known PP1 binding partner (Ceulemans et al., 2002). However, Scrib or Dlg were not detected copurifying with PP1 (**Fig. 3.2A**). We were also unable to reliably detect interaction between Scrib or Dlg and PP1 when combinations of these proteins were overexpressed in cultured *Drosophila* S2 cells, even when cells were crosslinked prior to lysis to stabilize weak and transient protein-protein interactions (**Fig. 3.2B**).

Scrib and Dlg can regulate Lgl independently of PP1

As an additional functional test of the relationship between Lgl regulation by PP1 and its regulation by Scrib and Dlg, we made use of a mutant Lgl protein that cannot interact with PP1 (Lgl^{KAFA}) (Moreira et al., 2019). When expressed in the follicle epithelium, Lgl^{KAFA} exhibits an increased cytoplasmic distribution, presumably resulting from its impaired ability to be dephosphorylated and return to the membrane (**Fig. 3.2C,E,G**) (Moreira et al., 2019). When expressed in *scrib*- or *dlg*-depleted cells rather than WT cells, Lgl^{KAFA} cortical localization was even further reduced, suggesting that even in the absence of PP1 regulation, Lgl^{KAFA} is still dependent on Scrib and Dlg (**Fig. 3.2F-G**). Interestingly, there was no difference between Lgl^{KAFA} and Lgl^{WT} cortical levels in *scrib*- or *dlg*-depleted cells (**Fig. 3.2G**). Furthermore, overexpression of PP1 in *scrib*- or *dlg*-depleted cells did not rescue Lgl mislocalization (**Fig. 3.6F-H**). Together, these data suggest that Scrib and Dlg's polarity functions include a PP1-independent component.

A cell culture assay for Scrib recruitment

Although we did not find evidence to functionally implicate PP1 in Scrib/Dlg activity, mutating the Dlg RVxF motif nevertheless caused severe loss of function. We therefore tested other, PP1-independent, functions of this protein region. In addition to protecting Lgl, Dlg also stabilizes Scrib at the cell cortex (Khoury and Bilder, 2020; Ventura et al., 2020). We sought to precisely define the regions of Dlg required to recruit Scrib. To this end, we adapted a previously described induced polarity assay using cultured *Drosophila* S2 cells (Johnston, 2020; Johnston et al., 2009). In this method, transgenic expression of the homotypic cell adhesion protein Echinoid (Ed) is used to create a polarized cortical domain at the contact point between two clustered Ed-expressing cells. By fusing a protein of interest to the Ed intracellular domain, one can create polarized localization of any construct. Importantly, S2 cells do not exhibit native cell-cell adhesion or polarity, although they express a subset of polarity proteins (including Scrib and Dlg) at low to moderate levels. We reasoned that fusing Dlg to Ed would create a discrete cortical domain of polarized Dlg that could recruit endogenous Scrib (**Fig. 3.3A**). Indeed, an Ed-fused fragment of Dlg encompassing its PDZ3-SH3-HOOK-GUK domains was able to robustly recruit Scrib to the polarity site, compared to a control construct containing Ed alone (**Fig. 3.3B-C**). Because the same Dlg fragment can provide polarity function *in vivo* (Hough et al., 1997; Lu et al., 2021), the Ed assay provides a useful platform to dissect regions mediating Scrib recruitment by Dlg.

We then tested a series of Ed-Dlg constructs encompassing additional domain truncations and mutations. Consistent with *in vivo* experiments on Dlg function, we found that PDZ3 and GUK were individually dispensable for Scrib recruitment, although GUK deletion resulted in a mild impairment of Scrib recruitment compared to the full-length construct (**Fig. 3.3D**)(Hough et al., 1997; Khoury and Bilder, 2020; Lu et al., 2021). A construct mimicking the dlg^{m30} missense mutation in SH3 retained partial ability to recruit Scrib, unlike the *in vivo* situation (Khoury and Bilder, 2020), although it was significantly worse than the WT construct (**Fig. 3.3D**). We generated a second SH3 domain mutation, designed to disrupt conserved residues that would make up the PxxP binding region of a canonical SH3 domain, and found that this construct also disrupted the ability of Ed-Dlg to recruit Scrib (**Fig. 3.8A-B**).

Dlg SH3-HOOK is a minimal fragment necessary and sufficient for polarity *in vivo*

We then turned to the HOOK domain, where the RVxF motif resides. A HOOK-deleted Dlg construct fails to rescue imaginal disc polarity *in vivo*, but this protein localizes to the nucleus rather than the plasma membrane, limiting interpretation (Hough et al., 1997). In the S2 induced

polarity assay, the HOOK domain was essential, as a HOOK-deleted construct failed to recruit Scrib (**Fig. 3.3D**). Interestingly, the same failure was seen with a construct carrying the Dlg^{ASAKA} mutation (**Fig. 3.3D**). We then tested individual HOOK residues and found that even single amino acid mutations in the RVxF consensus sequence resulted in equivalent disruption of Scrib recruitment activity (**Fig. 3.8A-B**). In contrast, mutations in evolutionarily conserved residues at the opposite, C-terminal end of the HOOK domain had no effect, suggesting that the HOOK N-terminal region contains the major functional elements (**Fig. 3.8A-B**). Finally, since single amino acid changes in either the HOOK or SH3 domains disrupt Scrib recruitment, we tested the sufficiency of the domains. Neither domain displayed function alone, but strikingly a fragment composed of SH3-HOOK was sufficient to mediate Scrib clustering (**Fig. 3.3D**).

We then tested whether this Dlg construct ($Dlg^{SH3\text{-}HOOK}$) was also sufficient for function *in vivo*, comparing it to a $Dlg^{SH3\text{-}HOOK\text{-}GUK}$ construct. As expected, $Dlg^{SH3\text{-}HOOK\text{-}GUK}$ rescued polarity and epithelial architecture in *dlg*-deficient imaginal discs; growth control also appeared normal (**Fig. 3.4G**)(Lu et al., 2021). Excitingly, the smaller $Dlg^{SH3\text{-}HOOK}$ also rescued polarity, architecture and growth control in *dlg*-deficient imaginal discs (**Fig. 3.4H**). We confirmed this result by taking advantage of a validated *dlg* RNAi line that targets the PDZ2-encoding sequences, allowing us to deplete the endogenous protein but not our transgenes which lack this domain. Depletion of *dlg* in the posterior compartment of wing imaginal discs generates mispolarized tumors, but coexpression of $Dlg^{SH3\text{-}HOOK}$ efficiently rescued epithelial polarity, architecture and growth, to a degree indistinguishable from the rescue provided by $Dlg^{SH3\text{-}HOOK\text{-}GUK}$ (**Fig. 3.9**). We then tested the constructs in the follicle epithelium. Both transgenic proteins localized to the basolateral membrane, albeit at reduced levels compared to WT Dlg (**Fig. 3.4A-D**). When expressed in *dlg*-depleted follicle cells (**Fig. 3.4I**), both $Dlg^{SH3\text{-}HOOK\text{-}GUK}$ and $Dlg^{SH3\text{-}HOOK}$ reduced the basolateral expansion of aPKC to ameliorate polarity and restore monolayer organization (**Fig. 3.4J-L**), although the former was more efficient than the latter. Intriguingly, even in cases with altered epithelial architecture, $Dlg^{SH3\text{-}HOOK}$ restored Scrib recruitment to WT levels, as did $Dlg^{SH3\text{-}HOOK\text{-}GUK}$ (**Fig. 3.4M-P**). These data support the conclusion that the SH3 and HOOK domains mediate both Dlg's Lgl protection and Scrib recruitment activities and that they together constitute a minimal functional unit of the protein that can support epithelial polarity, albeit less efficiently in some tissues than others.

The Dlg SH3-HOOK unit regulates Scrib localization, and SH3 provides an additional polarity function

Finally, we investigated the relationship between Dlg's Scrib recruitment and Lgl protection activities. Nuclear localization of the previous HOOK deletion construct prevented conclusions about its role in the former process. We therefore complemented *dlg* null mutant follicle cells *in vivo* with our HOOK domain missense mutant construct and found that, as in the S2 cell assays, it fails to rescue Scrib cortical localization (**Fig. 3.5A-D**). The SH3 domain is required for Scrib recruitment *in vivo*, since dlg^{m30} homozygous cells are defective in recruiting Scrib to the cortex (Khoury and Bilder, 2020). To determine if the SH3 domain is required only for Scrib recruitment, we expressed a membrane-tethered Scrib protein (myr-Scrib) in dlg^{m30} homozygous follicle cells. Strikingly, this combination yielded a partial rescue of polarity, as assessed by degree of aPKC mislocalization, compared to myr-Scrib in *dlg* null cells (**Fig. 3.5E-I**). Whereas our previous data show that both SH3 and HOOK domains are required for Scrib localization, this experiment suggests that regions including HOOK cooperate with Scrib to provide Lgl 'protection' activity that can be further enhanced by an intact SH3.

How does SH3-HOOK regulate Scrib recruitment? In cultured mammalian cells it was recently shown that the Scrib LRR and LAPSD domains, which are both necessary and sufficient for polarity function in *Drosophila* (Albertson et al., 2004; Bonello et al., 2019; Choi et al., 2019; Khoury and Bilder, 2020; Zeitler et al., 2004), can co-IP with Dlg1 (Troyanovsky et al., 2021). We tested this Scrib fragment in the S2 induced polarity assay but could not detect recruitment of endogenous Dlg by Ed-Scrib$^{LRR+LAPSD}$ (**Fig. 3.10A-C**). The ability of Dlg to recruit Scrib in this system, but not vice versa, parallels *in vivo* data showing Scrib localization to be dependent on Dlg, but Dlg localization to be largely independent of Scrib (Khoury and Bilder, 2020; Lu et al., 2021). We were also unable to coIP transgenic Scrib$^{LRR+LAPSD}$ and Dlg$^{PDZ3\text{-}SH3\text{-}HOOK\text{-}GUK}$ from S2 cells (**Fig. 3.10D**), even with crosslinking and by increasing the starting material used by severalfold. Combined with our induced polarity and *in vivo* genetic experiments, these data support the idea that Dlg recruits Scrib via its SH3-HOOK domains, but that this recruitment may not reflect direct physical binding between the two proteins.

DISCUSSION

The molecular mechanism of Scrib module function has been a longstanding challenge in the study of cell polarity. Much work has focused on identifying binding partners of Scrib module proteins, with less attention given to the relationships that exist within the Scrib module itself. Here, we perform fine-grained functional analysis of the Dlg protein, defining its minimal required domains. These experiments identified a critical SH3-HOOK module that facilitates Scrib localization and is both necessary and sufficient for Dlg's polarity activity *in vivo*.

Our search for Scrib module effectors yielded PP1 as an appealing candidate for Lgl regulation. Such a role would be consistent with studies from mammalian cell culture, where both Scrib and Dlg have been found to bind to PP1 (Hendrickx et al., 2009; Nagasaka et al., 2013; Troyanovsky et al., 2021; Van Campenhout et al., 2011; Young et al., 2013), and have been proposed to act as targeting factors that direct PP1 to specific substrates. We failed to find evidence for a physical complex between Scrib, Dlg and PP1 in *Drosophila,* and our data mutating PP1-binding consensus sequences support alternative functions for these motifs, unrelated to PP1-binding. Although we cannot rule out that PP1-Scrib module interactions occur in Drosophila at a low affinity, we note that a direct role for such interactions in regulating mammalian cell polarity remains to be demonstrated. Moreover, our data demonstrate that Scrib and Dlg influence Lgl localization at least partially independently of PP1, which is consistent with the weak phenotype of *pp1* compared to *scrib* module mutants (**Fig. 3.6A-B**) (Moreira et al., 2019).

Our data using Lgl^{KAFA} are consistent with two possible roles of Scrib and Dlg in polarity. First, Scrib and Dlg could limit Lgl phosphorylation through partners other than PP1, since Lgl mislocalization in *dlg*-depleted cells can be restored by co-depletion of aPKC or by mutating Lgl phosphorylation sites to alanine (Khoury and Bilder, 2020; Ventura et al., 2020). Second, Scrib and Dlg's regulation of Lgl could involve a phosphorylation-independent component. Consistent with this possibility, we found that a non-phosphorylatable Lgl protein (Lgl^{S5A}) still exhibited reduced cortical localization in *scrib*- and *dlg*-depleted cells (**Fig. 3.11**). These findings draw parallels with the *C. elegans* zygote, where PAR-2 can 'protect' PAR-1 both by physical binding as well as competing for aPKC's activity to reduce PAR-1 phoshorylation (Ramanujam et al., 2018). However, evidence for physical binding of Lgl with Scrib or Dlg in *Drosophila* is currently lacking, outside of a report of binding to the polarity-dispensable GUK domain (Zhu et al., 2014). Thus, although speculative, the analogy of PAR-1 regulation to Lgl 'protection' should provide an appealing basis for future experiments. Lastly, although Scrib and Dlg do not require PP1 to

regulate Lgl, it is possible that PP1 requires Scrib and Dlg to do so, since the degree of Lgl mislocalization in *scrib*- and *dlg*-depleted cells is not enhanced by removing PP1-dependent regulation (Lgl^{KAFA}, **Fig. 3.2G**).

Dlg is required for Scrib recruitment, proximity assays reliably detect Scrib near Dlg (Nakajima et al., 2019; Sharifkhodaei et al., 2019; Sharp et al., 2021), and an optogenetic relocalization experiment showed that either Scrib or Dlg can induce relocation of the other protein (Ventura et al., 2020). However, we were unable to biochemically detect a Scrib-Dlg complex in extracts from follicles or when the proteins were overexpressed in cell culture. A recent mass spec dataset from *Drosophila* embryos also failed to detect Scrib in Dlg IP samples and vice versa (Nakajima et al., 2019). In flies, biochemical evidence for such a complex involves coIP from synapse-containing tissues such as larval muscle and adult brains (Mathew et al., 2002; Rui et al., 2017); in mammalian cells evidence for coIP comes from cultured cells (Awadia et al., 2019; Troyanovsky et al., 2021). Several of the above cases involve mutual binding partners, and require that partner for coIP, such as Gukholder at the neuronal synapse and SGEF in epithelia (Awadia et al., 2019; Mathew et al., 2002). Given the inconsistent evidence for biochemical interaction, we feel that it is prudent to continue to refer to the Scrib proteins as a 'module' rather than a complex.

Our studies identify a critical motif in the Dlg N-terminal HOOK domain that is, in combination with the SH3 domain, required for polarity and Scrib localization. In the wing imaginal disc, SH3 and HOOK are alone sufficient to support full polarity function. In follicle cells, SH3 and HOOK are also sufficient to support Scrib recruitment. Polarity activity in this tissue is less efficient, with full architectural rescue that is less penetrant than with the SH3-HOOK-GUK construct. The SH3-HOOK-rescued follicle cell clones resemble clones mutant for GUK-truncated *dlg* alleles, where polarity in cells retaining epithelial structure is largely normal (Khoury and Bilder, 2020). A follicle-specific role for the GUK domain may involve its known role in spindle orientation, which is required in this follicle but not the wing disc epithelium (Bellaïche et al., 2001; Bergstralh et al., 2013; Bergstralh et al., 2016). Overall, the data demonstrate that SH3 and HOOK domains alone are the minimal elements required for Dlg to recruit cortical Scrib and provide some polarity function.

How might the SH3 and HOOK domains operate? MAGUK-family SH3 domains are "non-canonical" in that they cannot bind the polyproline ligands bound by typical SH3 domains, because they lack key residues in the PxxP binding pocket (McGee et al., 2001). The HOOK domain is a conserved linker of variable length between the SH3 and GUK domains (Zhang et al., 2013) that is thought to create interdomain allostery, facilitating an intramolecular interaction that enables functions that the individual domains lack in isolation (McCann et al., 2012; McGee and Bredt, 1999; McGee et al., 2001; Rademacher et al., 2019; Zhang et al., 2013). One demonstrated function of HOOK domains is to negatively regulate binding of certain GUK domain ligands, presumably by influencing the SH3-GUK interaction (Golub et al., 2017; Marcette et al., 2009; Qian and Prehoda, 2006). However, the dispensability of the GUK domain for polarity *in vivo* and in the S2 induced polarity assay reveals that such regulation is not important for Scrib recruitment and polarity function. A second function of HOOK is to mediate electrostatic binding to the membrane (Lu et al., 2021), but our experiments mutating non-polar amino acids and supplying membrane tethering in S2 cells show that additional SH3-dependent functions reside in HOOK. Our single amino acid resolution mutant analysis reveals that the HOOK N-terminus is essential to this function, and an appealing model is that it works with the SH3 domain to bind an additional scaffolding factor to permit Scrib recruitment. Once Scrib has been recruited, SH3-HOOK and Scrib are together competent to protect Lgl through an unknown cooperative activity that defines

basolateral identity. In support of this model, we find that constitutively tethering Scrib to the membrane can partially bypass a *dlg* SH3 mutant allele, demonstrating that a primary function of SH3 is to recruit Scrib. To our knowledge, this is the first case where a Scrib construct can rescue a *dlg* mutant, providing further evidence for the cooperative nature of Scrib module function in basolateral polarity and pointing to the Dlg SH3-HOOK as a primary mediator of this. Exploring this model will be an important aspect of future studies.

In sum, our in-depth interrogation of the core polarity regulator Dlg defines a minimally sufficient fragment composed of the SH3-HOOK domains, as well as single amino acids in the HOOK domain, that are essential for polarity function. These domains cooperatively recruit Scrib to the cell cortex and supply an additional function that is independent of PP1 that enables Lgl to antagonize aPKC. The data advance our understanding of how basolateral polarity is established and contribute a significant step towards mechanistic understanding of the Scrib module machinery.

Acknowledgements

We thank E. Morais-de-Sá, C. Johnston and Y. Hong for fly stocks and reagents, L. Mathies for cloning the UAS-Dlg constructs and K. Prehoda, Y. Hong, M. Kitaoka and the Hariharan and Bilder labs for helpful discussions. We thank the UC Berkeley Cell Culture Facility for help with S2 cell experiments. Stocks obtained from the Bloomington Drosophila Stock Center (NIH P40OD018537) and resources from the Drosophila Genomics Resource Center (NIH 2P40OD010949) were used in this study. This work was supported by NIH grant R35 GM130388 to D.B. and AHA Predoctoral Fellowship 20PRE35120150 to M.J.K.

Competing interests

The authors declare no competing or financial interests.

MATERIALS AND METHODS

Fly stocks and genetics

Drosophila stocks were raised on cornmeal molasses food at 25°C. Mutant alleles and transgenic lines used are listed in **Table 1**. Follicle cell mutant clones were generated using the MARCM technique with hsFLP induction by 37°C heat shock for 1 hour on three consecutive days beginning at 120 hours after egg deposition (AED) for *FRT19A* stocks, and two consecutive days for *FRT82B* stocks. For clonal GAL4 expression, larvae were heat shocked once for 13 minutes at 37°C 120 hours AED to generate flip out clones. For all clonal experiments, newly eclosed females were fed with yeast and dissected three days after eclosion. Unless otherwise noted, pan-follicle cell expression used *traffic jam-GAL4* and temperature sensitive *tub-GAL80ts*. After one-two days on yeast, newly eclosed females were shifted to 29°C for three days to induce GAL4 expression before ovary dissection.

Molecular cloning

To generate *UAS-Dlg^{ASAKA}::HA,* pUASTattB was digested with EcoRI and XbaI and overlapping fragments amplified from the Dlg cDNA were assembled using Gibson assembly. For the *UAS-Dlg$^{SH3\text{-}HOOK\text{-}GUK}$::HA* and *UAS-Dlg$^{SH3\text{-}HOOK}$::HA* constructs, pUASTattB was digested with XhoI and XbaI and fragments encompassing the appropriate domains were amplified from the pUASTattB-Dlg^{WT} vector and assembled via Gibson assemnbly. *UAS-myr-Scrib$^{TAAA/RAGA}$::V5* was generated from *UAS-myr-Scrib::V5* by first using the NEBuilder Gibson Assembly kit to

insert a KpnI site 5' of the myr signal. Then, the resulting plasmid was digested with KpnI and AgeI and fragments containing the desired mutations were amplified and assembled using the NEBuilder Gibson Assembly kit. To generate the Ed-Dlg constructs for S2 cell expression, mutations of interest were introduced into the *pMT-Ed::GFP::Dlg*$^{PDZ3\text{-}SH3\text{-}HOOK\text{-}GUK}$ plasmid (Garcia et al., 2014) using the NEBaseChanger site directed mutagenesis kit as directed by the manufacturer (NEB). To generate the cytosolic *pMT-GFP:: Dlg*$^{PDZ3\text{-}SH3\text{-}HOOK\text{-}GUK}$ and *pMT-Scrib*$^{LRR+LAPSD}$*::V5 p*lasmids, the corresponding regions of the Dlg and Scrib cDNAs were amplified from the *pMT-Ed::GFP::Dlg*$^{PDZ3\text{-}SH3\text{-}HOOK\text{-}GUK}$ and *pUASTattB-myr-Scrib::V5* plasmids, respectively. Fragments were then assembled using the NEBuilder HiFi DNA assembly kit (NEB) as instructed into XhoI/EcoRI or AgeI/EcoRI linearized *pMT-His-V5* backbone, respectively. The Dlg sequence used in this study is NP_996405.1 and the Scrib sequence is NP_001036761.3. Primers used for cloning are given in **Table 1**. The deletions made with respect to the Dlg and Scrib reference protein sequences are given in **Table 2**.

S2 cell culture and induced polarity assay

S2 cells were cultured using standard methods at 25°C in Schneider's media (Invitrogen) supplemented with 10% FBS and 1% penicillin/streptomycin. Transfections were performed using the Effectene kit (Qiagen) according to manufacturer's instructions. $2x10^6$ cells per well of a 6-well plate were transfected with 500ng of DNA per plasmid. Cells were incubated in transfection complexes for 48 hours and then switched into fresh media containing 0.5mM $CuSO_4$ to induce expression of the metallothionein promoter for 48 hours before experiments. The induced polarity assay was performed essentially as described previously (Johnston, 2020). After 48 hours of induction, transfected S2 cells were resuspended in 3 mL of fresh media containing 0.5mM $CuSO_4$. The cell suspensions were agitated in an orbital shaker at 150 RPM in 6-well plates for 2 hours to induce cell clusters. 1 mL per condition of the clustered cell suspension was then allowed to settle on poly-D-lysine coated coverslips and adhere for 30 minutes. The cells were then fixed for 20 minutes in 4% PFA and processed for immunofluorescence as described below.

Immunofluorescence and microscopy

Ovaries were dissected in PBS and individual ovarioles were separated prior to fixation in 4% PFA for 20 minutes. Wing imaginal discs were dissected from wandering L3 larvae in PBS and fixed for 20 minutes in 4% PFA. Samples were blocked for 30 minutes to 1 hour in 0.1% PBS-T containing 4% NGS and 1% BSA before staining with primary antibodies overnight at 4°C in blocking buffer. Following 3 washes in PBS-T, samples were incubated in 1:400 fluorescent secondary antibodies (Invitrogen) for 2 hours at room temperature. Primary antibodies used are given in **Table 1**. Imaging was performed on either a Zeiss LSM700 inverted point scanning confocal microscope or an upright Zeiss Axio Imager 2 microscope with Apotome 2 using Plan Apochromat 20x/NA 0.8 or LD C-Apochromat 40x/NA 1.1 W objectives. Uncropped confocal images were 1024x1024 pixels with 2 line averages, and widefield images were 512x512 pixels.

Image analysis and quantification

Image processing and quantification was performed using FIJI software (Schindelin et al., 2012). To quantify Scrib, Dlg and Lgl cortical localization, a 1.17µm wide rectangular ROI spanning a single cell-cell boundary and a second identical width ROI were measured in en face sections. The ratio of membrane:cytoplasmic fluorescence intensity was computed to define the Plasma Membrane Index (PM Index)(Lu et al., 2021). To quantify aPKC localization, lines along

the apical and basolateral membranes were measured in FIJI and the ratio of basolateral:apical intensity was computed to give a measure of lateral mislocalization. To quantify enrichment at S2 cell polarity domains, a 0.39µm wide rectangular ROI spanning the contact site between two S2 cells and a second ROI on a non-contacting section of the membrane were measured and the ratio of contact:non-contact fluorescence intensity was computed to give the Enrichment Index. In all cases measurements were taken from single cells, with averages were calculated for each condition. Figures were assembled with Adobe Illustrator.

Coimmunoprecipitation and Western blotting

Ovary tissue was lysed in ice cold IP buffer (10mM Tris, 150mM NaCl, 0.5mM EDTA, 0.5% NP-40)(Nakajima et al., 2019) by homogenization. S2 cells were resuspended in ice cold IP buffer and lysed for 30 minutes at 4°C by nutation. Lysates were then cleared by centrifugation at 13,400 x g for 20 minutes at 4°C. Following protein concentration determination by BCA assay (ThermoFisher), 200µg of protein per sample was then loaded onto antibody-conjugated Protein G Dynabeads (ThermoFisher) and rotated overnight at 4°C. The following day, antibody-bead complexes were washed 3 times with lysis buffer before eluting the samples by boiling for 10 minutes in 4x loading dye (Bio-Rad) containing 10% β-mercaptoethanol. 60µg 'input' samples were also prepared in the same way by boiling in β-mercaptoethanol-containing loading dye. Antibodies used for IP are listed in **Table 1**. To induce crosslinking, cells were washed several times with ice cold sterile PBS to remove traces of culture media. The cells were then incubated in 2mM disuccinimidyl suberate (DSS, ThermoFisher) in PBS for 30 minutes at room temperature. The crosslinking reaction was then quenched by adding Tris to a final concentration of 20mM and incubating for 15 minutes at room temperature.

Western blotting was performed as previously described (de Vreede et al., 2018). Proteins were separated by SDS-PAGE on 7.5% TGX precast gels (Bio-Rad) before being blotted onto methanol-activated 0.45µm PVDF membranes (GE Healthcare) at 300mA for 1 hour. Membranes were then blocked for 1 hour with TBS-T containing 3% BSA before probing with primary antibodies overnight at 4°C. The following day, membranes were washed 3 times in TBS-T before being incubated in 1:2000 secondary antibodies in blocking buffer for 2 hours at room temperature. Following 3 more washes, blots were imaged by ECL chemiluminance (WesternBright) on HyBlot CL autoradiography film (Denville Scientific). Primary antibodies are listed in **Table 1**.

Multiple sequence alignment

Protein sequence alignments were created with Clustal Omega (Madeira et al., 2019) and visualized with SnapGene Viewer. The Uniprot sequences used for Dlg were: *H. sapiens* Q12959, *M. musculus* Q811D0, *R. norvegicus* Q62696, *D. rerio* Q5PYH6, *X. tropicalis* Q28C55 and *D. melanogaster* P31007. For Scrib, the sequences used were: *H. sapiens* Q14160, *M. musculus* Q80U72, *R. norvegicus* D3ZWS0, *D. rerio* A0A1L1QZF0, *X. tropicalis* XP_031759453.1 and *D. melanogaster* Q7KRY7.

Statistical analyses

The statistical tests used for each experiment are described in the corresponding Figure 3.legends. No data points were excluded. For each experiment ovaries from at least 5 females were examined, with at least 10 ovarioles being analyzed. All plots show individual data points for all measurements used. All experiments were repeated a minimum of two times. Definitions of

significance used are: n.s. (not significant) $P > 0.05$, *$P < 0.05$, **$P < 0.01$, ***$P < 0.001$, ****$P < 0.0001$. Data were analyzed using Microsoft Excel and GraphPad Prism 6.

Data availability

The Dlg APEX2 proteomics dataset was previously published (Sharp et al., 2021) and is available from MassIVE proteomics repository and Proteome Exchange using accession numbers MSV000087186 and PXD025378, respectively. All other reagents and data will be made available upon request.

FIGURES

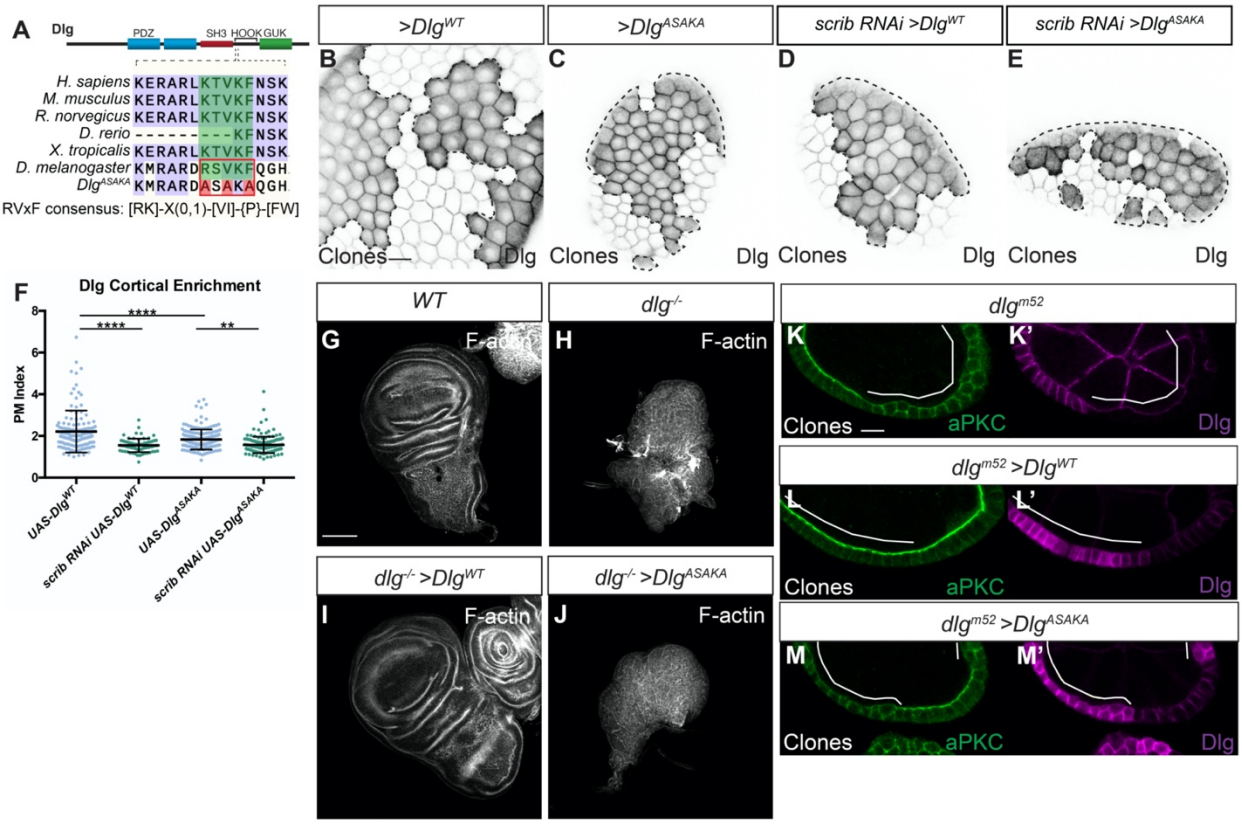

Figure 3.1. The Dlg RVxF motif is critical for function

(A) Cartoon showing location of the RVxF motif in the Dlg protein and conservation of the motif across species. The resides mutated in Dlg^{ASAKA} are highlighted in red. The RVxF consensus as defined by (Wakula et al., 2003) is shown. (B-E) Like Dlg^{WT} (B), Dlg^{ASAKA} localizes to the basolateral membrane and is enriched at the cell cortex (C). Dlg^{WT} localization (D) as well as Dlg^{ASAKA} localization (E) is sensitive to *scrib*-depletion, quantified in (F). (G-J) Compared to WT (G), *dlg* null mutant wing discs form disorganized tumors (H). Expression of Dlg^{WT} rescues this phenotype (I), while expression of Dlg^{ASAKA} does not rescue (J). (K-M) In the follicle epithelium, dlg^{m52} null mutants (K) lose polarity, characterized by lateral aPKC spread, and this is rescued by expressing Dlg^{WT} (L). In contrast, polarity loss is not rescued by Dlg^{ASAKA} expression (M). Scale bars, 10µm except in G-J, 100µm. Dotted lines in (B-E) and white lines in (K-M) indicate clones of given genotype. (F) One-way ANOVA with Tukey's multiple comparisons test. Error bars represent S.D. Data points are PM Index measurements in single cells. PM Index=cortical/cytoplasmic intensity. **P < 0.01, ****P < 0.0001.

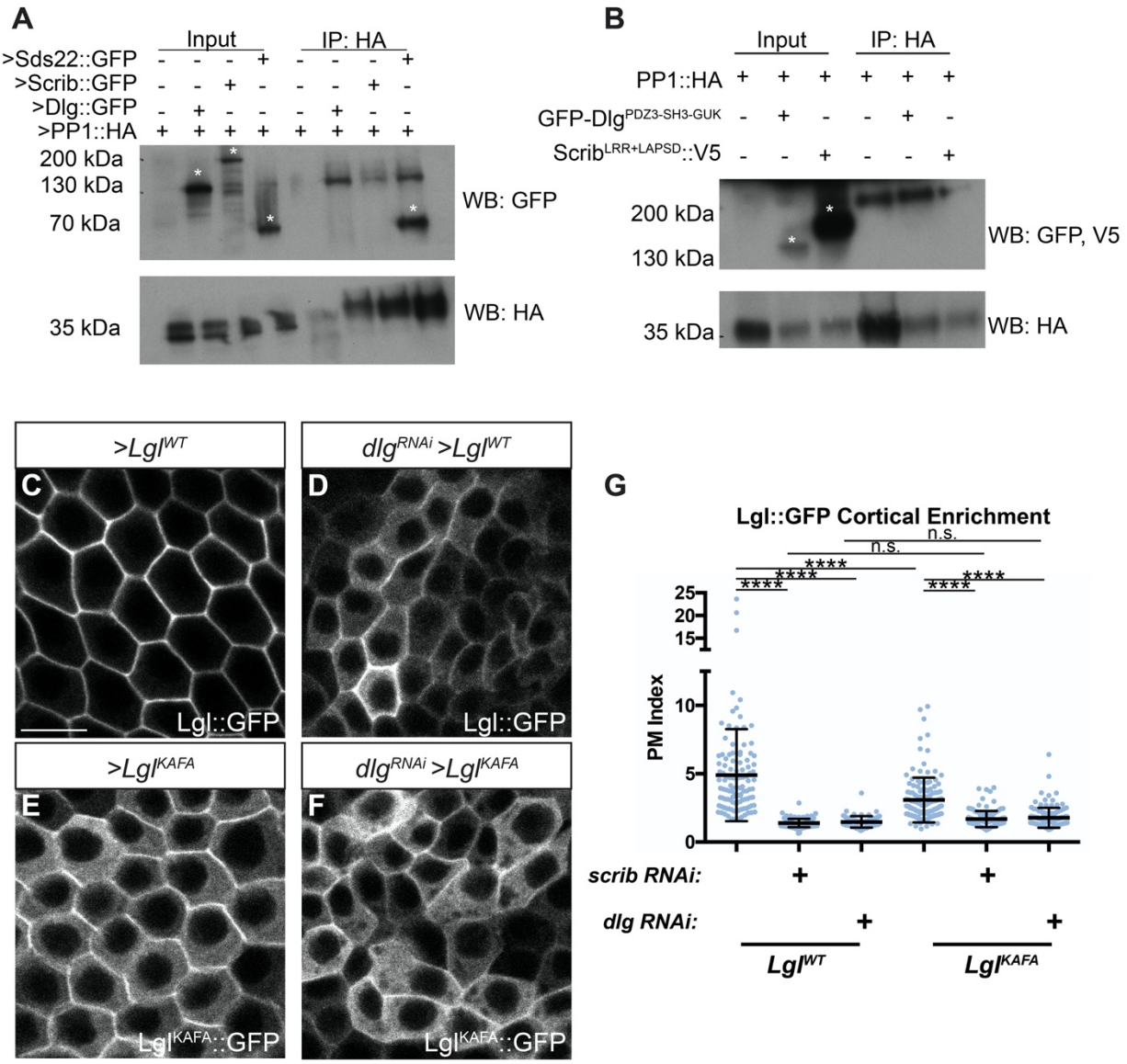

Figure 3.2. Scrib and Dlg regulate Lgl independently of PP1

(A) CoIP of transgenic Scrib or Dlg and PP1 from follicle cells fails to detect an interaction, although interaction between PP1 and Sds22 is robustly captured. (B) CoIP of overexpressed Dlg or Scrib and PP1 from S2 cells following *in situ* crosslinking also failed to reliably detect interaction between these proteins. Asterisks in (A-B) indicate relevant bands. Lgl^{WT} membrane localization (C) is severely disrupted by *dlg* RNAi (D). Lgl^{KAFA} (E) has increased cytoplasmic localization compared to Lgl^{WT} and is further decreased by *dlg* RNAi (F). (G) Quantification of Lgl membrane localization. Scale bars, 10µm. (G) One-way ANOVA with Tukey's multiple comparisons test. Error bars represent S.D. PM Index=cortical/cytoplasmic intensity. Data points are measurements from individual cells. n.s. (not significant) $P > 0.05$, ****$P < 0.0001$.

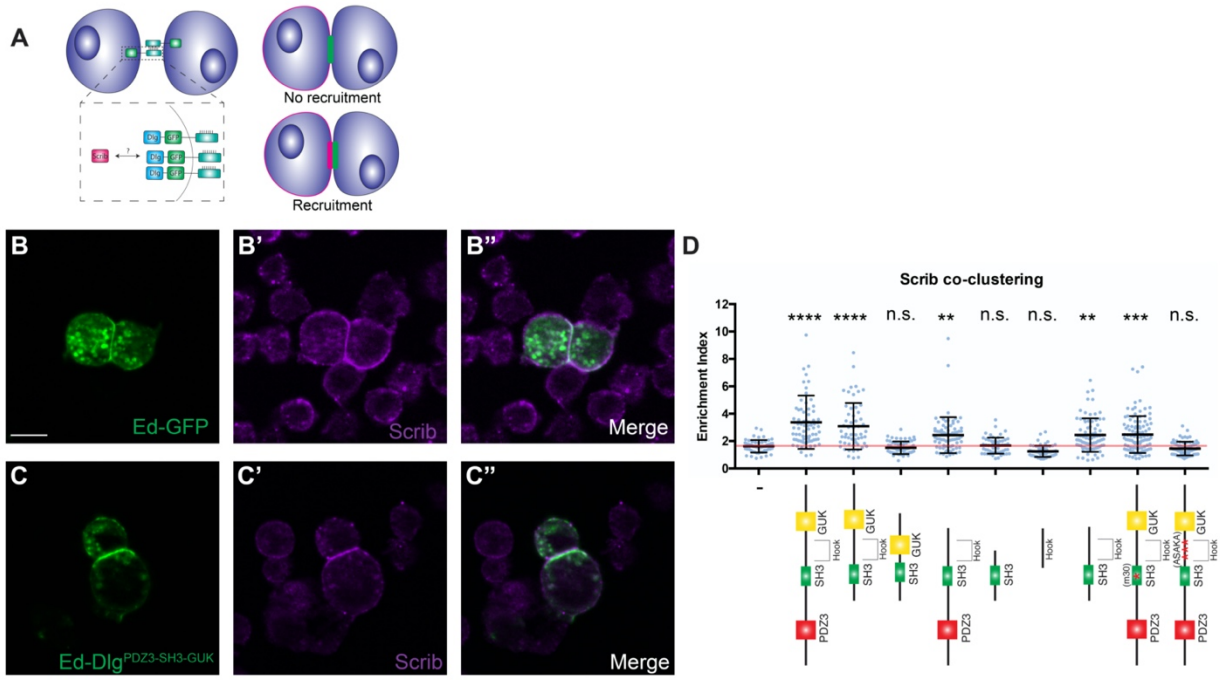

Figure 3.3. Dlg$^{SH3\text{-}HOOK}$ is sufficient for Scrib localization in an induced polarity system
(A) Cartoon of S2 induced polarity assay. Polarizing Dlg by fusion to Ed enables testing of Scrib recruitment in a minimal synthetic system. (B) S2 cells expressing Ed-GFP can be clustered by adhesion between Ed molecules, but this does not alter Scrib localization. (C) When Dlg$^{PDZ3\text{-}SH3\text{-}HOOK\text{-}GUK}$ is fused to Ed, it creates a polarity crescent at the contact site that is able to recruit Scrib. (D) Quantification of Scrib recruitment to the polarity site in various Ed-Dlg constructs schematized below. Dlg$^{PDZ3\text{-}SH3\text{-}HOOK\text{-}GUK}$ is able to enrich Scrib, while the Ed-GFP negative control cannot. The HOOK and SH3 domains are necessary and, when in combination, sufficient to recruit Scrib. Statistical tests are versus the Ed-GFP negative control construct. Red line indicates the average for the Ed-GFP negative control and indicates no Scrib contact site enrichment. Scale bar, 10µm. (D) One-way ANOVA with Tukey's multiple comparisons test. Error bars indicate S.D. Data points are individual cell clusters. Enrichment index = contact site/non-contact site intensity. n.s. (not significant) $P > 0.05$, **$P < 0.01$, ***$P < 0.001$, ****$P < 0.0001$.

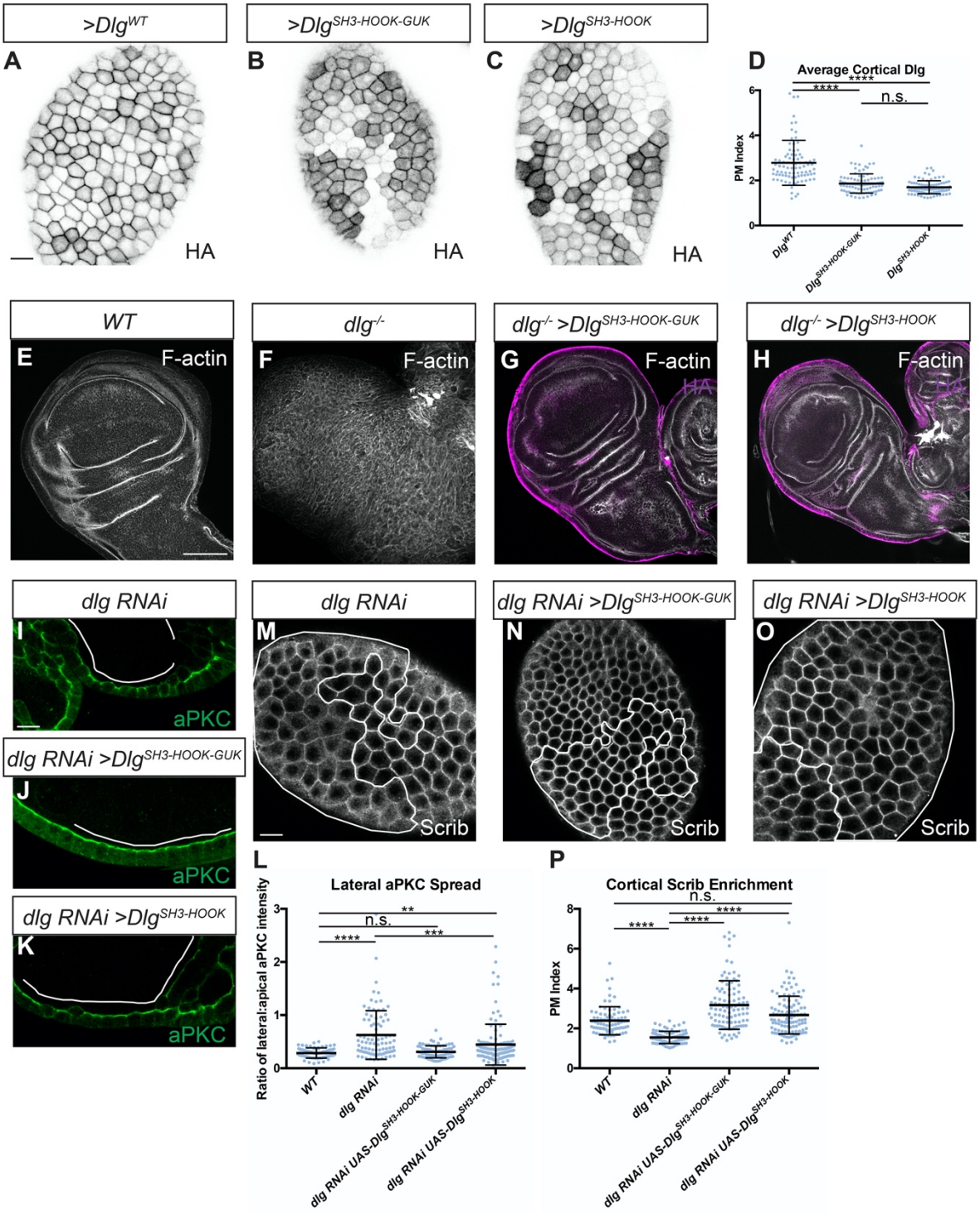

Figure 3.4. Dlg SH3 and HOOK domains are sufficient for function *in vivo*

(A-C) Like WT Dlg (A), Dlg$^{SH3\text{-}HOOK\text{-}GUK}$ (B) and Dlg$^{SH3\text{-}HOOK}$ (C) localize to the basolateral membrane in follicle cells. All constructs contain an HA epitope tag used for detection. (D) Quantification of cortical localization in (A-C). (E-H) Compared to WT (E) and *dlg* null mutants (F), Dlg$^{SH3\text{-}HOOK\text{-}GUK}$ (G) and Dlg$^{SH3\text{-}HOOK}$ (H) fully rescue polarity and epithelial architecture in wing imaginal discs. (I-K) In monolayered *dlg*-depleted follicle cells (I), both Dlg$^{SH3\text{-}HOOK\text{-}GUK}$ (J)

and $Dlg^{SH3\text{-}HOOK}$ (K) provide polarity-rescuing activity, quantitated in (L). Full restoration of monolayering is more efficient by $Dlg^{SH3\text{-}HOOK\text{-}GUK}$ than $Dlg^{SH3\text{-}HOOK}$: 89.5% (n=38) of $Dlg^{SH3\text{-}HOOK\text{-}GUK}$ show no regions of multilayering in rescued follicles, compared to 20.5% (n=39) of $Dlg^{SH3\text{-}HOOK}$ rescued follicles and 0% (n=37) of follicles with *dlg*-depleted clones. (M-O). Both $Dlg^{SH3\text{-}HOOK\text{-}GUK}$ (N) and $Dlg^{SH3\text{-}HOOK}$ (O) fully rescue loss of cortical Scrib seen in *dlg*-depleted cells (M), quantified in (P). Scale bars, 10µm except E-H, 100µm. White lines indicate clones of given genotypes. (D, L, P) One-way ANOVA with Tukey's multiple comparisons test. Error bars indicate S.D. PM Index=cortical/cytoplasmic intensity. aPKC spread is a ratio of lateral:apical fluorescence intensity. Data points are individual cell measurements. n.s. (not significant) $P > 0.05$, $^{**}P < 0.01$, $^{***}P < 0.001$, $^{****}P < 0.0001$.

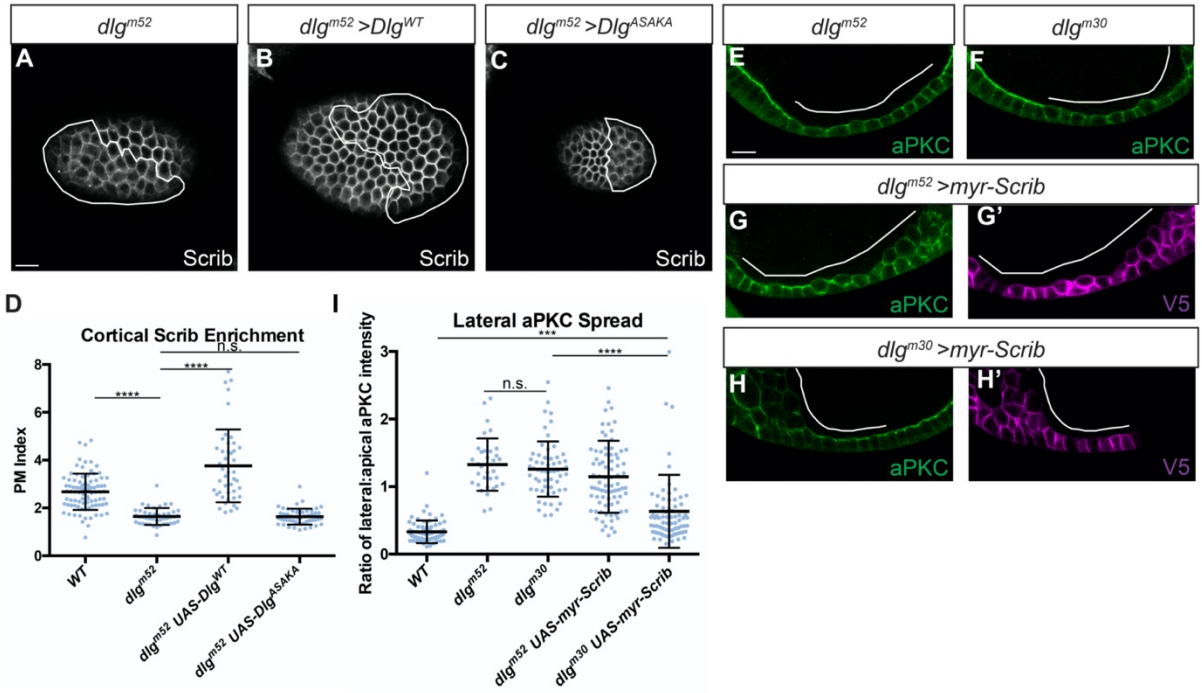

Figure 3.5. Dlg SH3-HOOK is primarily required to regulate Scrib localization

(A) *dlg*^{m52} null mutant cells show reduced cortical localization of Scrib. (B) Scrib mislocalization is rescued by expression of Dlg^{WT}. Scrib mislocalization is not rescued by expression of Dlg^{ASAKA} (C). (D) Quantification of Scrib localization in (A-C). (E-H) Both *dlg*^{m52} null mutants (E) and *dlg*^{m30} SH3 point mutant cells (F) lose polarity and mislocalize aPKC. (H) Preventing Scrib mislocalization by cortical tethering (myr-Scrib) partially suppresses the polarity loss phenotypes of *dlg*^{m30} SH3 mutant cells but not *dlg*^{m52} null mutant cells (G). (G'-H') myr-Scrib contains a V5 epitope tag used for detection. (I) Quantification of aPKC mislocalization in (E-H). Scale bars, 10μm. White lines indicate clones of given genotypes. (D,I) One-way ANOVA with Tukey's multiple comparisons test. Error bars indicate S.D. PM Index=cortical/cytoplasmic intensity. aPKC spread is a ratio of lateral:apical fluorescence intensity. Data points are individual cell measurements. n.s. (not significant) $P > 0.05$, ***$P < 0.001$, ****$P < 0.0001$.

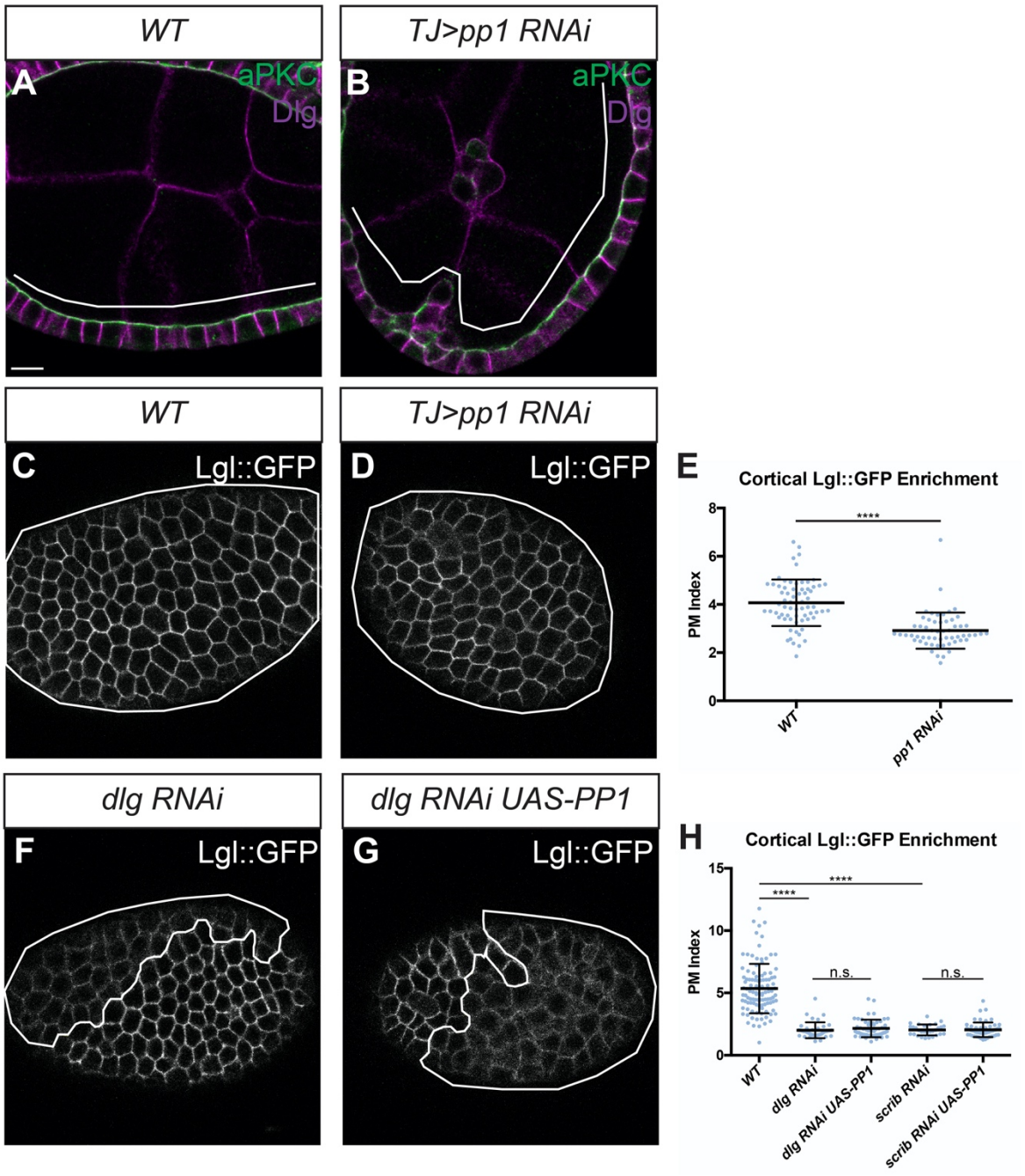

Figure 3.6. Lgl localization requires both PP1 and Scrib/Dlg

Compared to WT cells (A), *pp1*-depleted cells (B) exhibit mild polarity loss and occasional multilayering. Compared to WT cells (C), *pp1*-depleted cells display mild loss of cortical Lgl (D, also compare to *dlg*-depletion in F). (E) Quantification of Lgl localization. (F) *dlg*-depleted cells strongly mislocalize cortical Lgl and this is not rescued by overexpression of PP1 (G). (H) Quantification of Lgl localization. Scale bars, 10µm. (E) Two-tailed t-test with Welch's correction. (H) One-way ANOVA with Tukey's multiple comparisons test. Error bars indicate S.D. PM Index=cortical/cytoplasmic intensity. Data points are individual cell measurements. n.s. (not significant) $P > 0.05$, ****$P < 0.0001$.

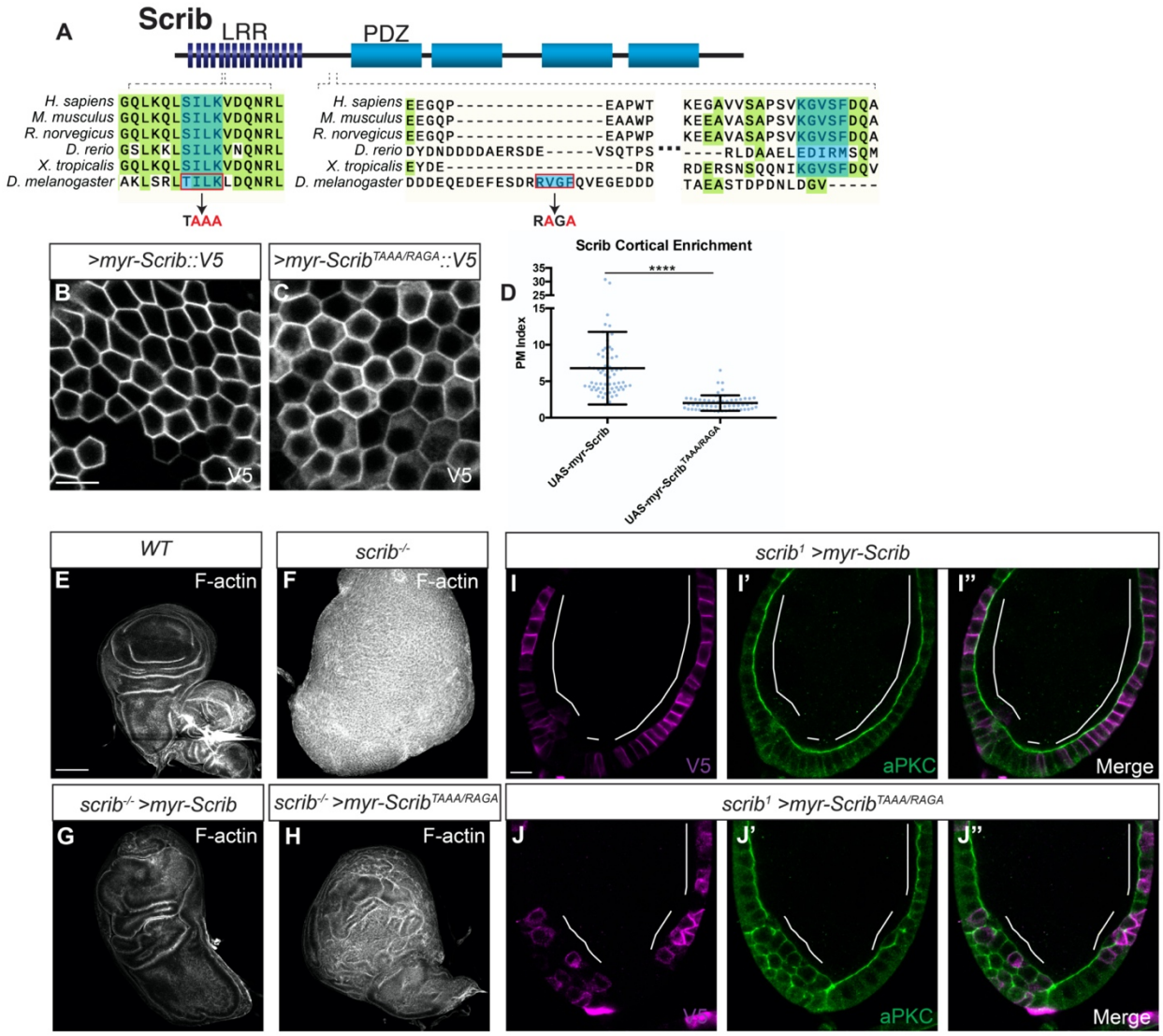

Figure 3.7. Scrib PP1-binding consensus motifs are partially required for function

(A) Cartoon showing the Scrib protein domain composition and location of the SILK and RVxF motifs. Below: alignment showing conservation of the SILK motif and RVxF motifs. Note that in vertebrates (right), the RVxF motif is located slightly C-terminal to its position in insects (left). Red boxes indicate residues mutated in myr-$^{ScribTAAA/RAGA}$ construct. Compared to WT myr-Scrib (B), myr-Scrib$^{TAAA/RAGA}$ (C) localizes less well to the cell cortex but is still enriched at the basolateral membrane, quantified in (D). Both constructs contain V5 epitope tags, used for detection. (E-H) Compared to WT wing discs (E), *scrib* mutant wing discs overgrow and form tumors (F). Overexpression of myr-Scrib largely rescues these phenotypes (G), while expression of myr-Scrib$^{TAAA/RAGA}$ only partially rescues the *scrib* mutant phenotype (H). (I-J) Compared to myr-Scrib (I), myr-Scrib$^{TAAA/RAGA}$ (J) provides less efficient rescue of *scrib* mutant: myr-Scrib shows complete restoration of the monolayered epithelium in 78.6% (n=14) of follicles, compared to rescue by myr-Scrib$^{TAAA/RAGA}$ (complete restoration in 36.8% of follicles; n=19). Scale bars, 10µm, except E-H, 100µm. (D) Two-tailed t-test with Welch's correction. Error bars indicate S.D. PM Index=cortical/cytoplasmic intensity. Data points are individual cell measurements. ****P < 0.0001.

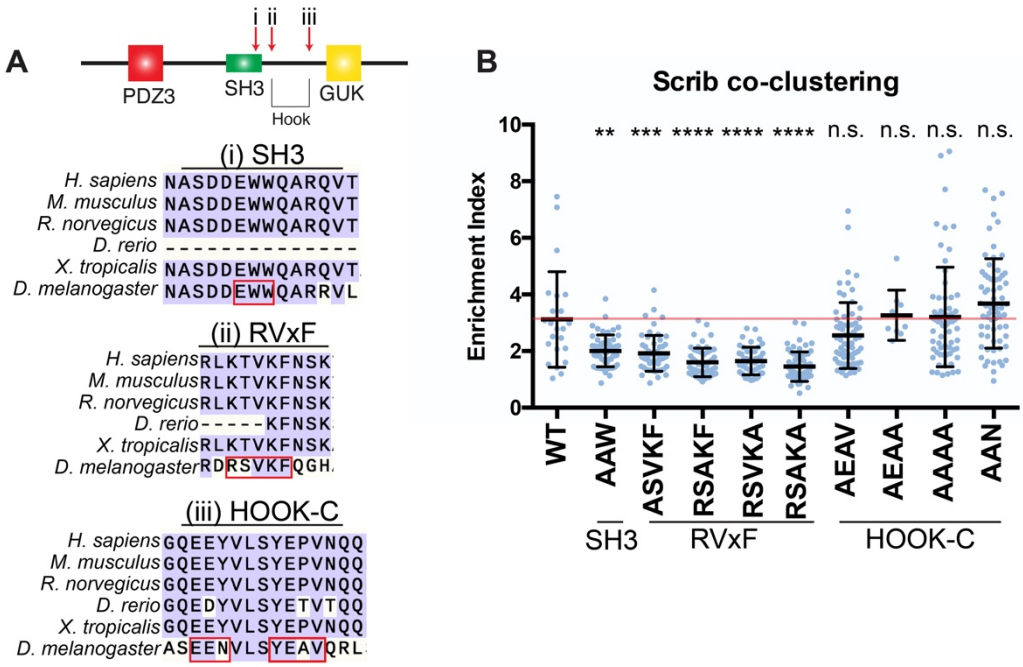

Figure 3.8. In depth examination of Dlg SH3 and HOOK domains

(A) Schematic of the Dlg domains used in the Ed-Dlg$^{PDZ3\text{-}SH3\text{-}HOOK\text{-}GUK}$ construct, with sequence alignments showing conservation of the SH3 and HOOK domain sequences chosen for study. Motifs targeted for mutation are indicated by red outlines. Arrows in cartoon indicate relative locations of targeted sequences in the protein. (B) Quantification of Scrib recruitment to the polarity site in S2 induced polarity assay. Compared to the WT Ed-Dlg$^{PDZ3\text{-}SH3\text{-}HOOK\text{-}GUK}$ construct, which does recruit Scrib, the SH3 mutant AAW construct has reduced ability to recruit Scrib. Similarly, all four constructs targeting single residues of the RVxF motif show equally impaired ability to recruit Scrib. However, the four constructs targeting conserved residues in the C-terminal HOOK domain do not impair Scrib recruitment. Red line indicates the average for the WT construct control. One-way ANOVA with Tukey's multiple comparisons test. Error bars indicate S.D. Data points are individual cell clusters. Statistical tests are comparisons to the Ed-Dlg$^{PDZ3\text{-}SH3\text{-}HOOK\text{-}GUK}$ control construct. Enrichment index = contact site/non-contact site intensity. n.s. (not significant) $P > 0.05$, **$P < 0.01$, ***$P < 0.001$, ****$P < 0.0001$.

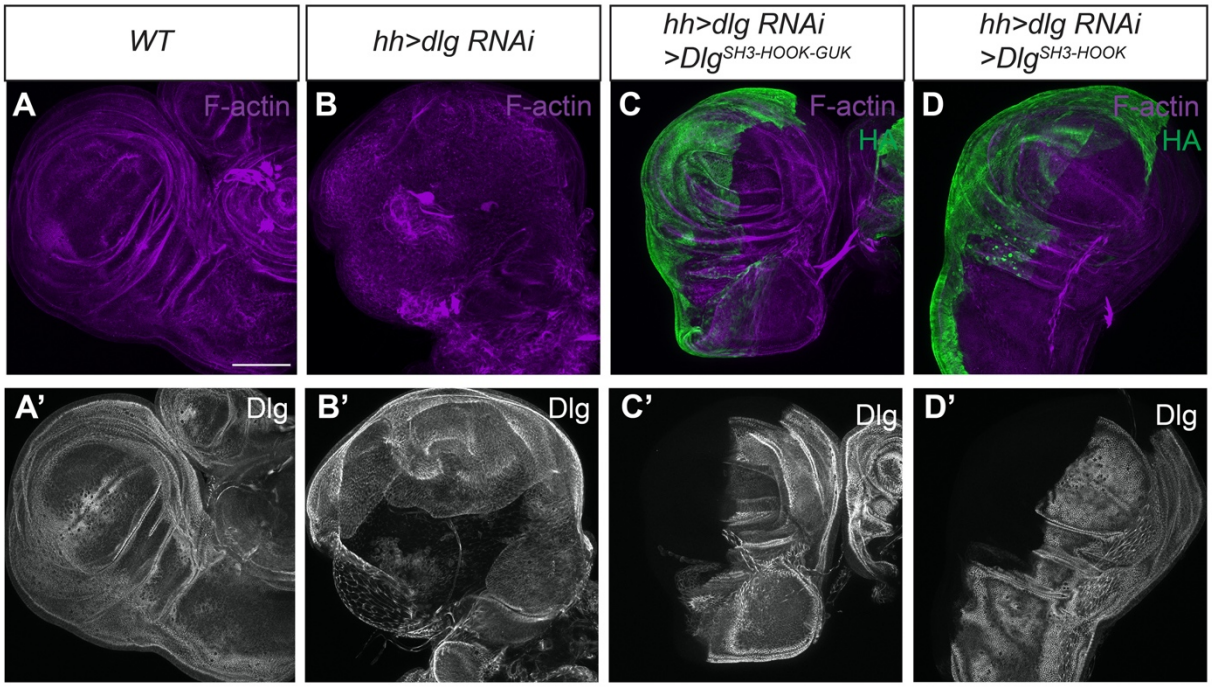

Figure 3.9. Validation of RNAi rescue approach for minimal Dlg constructs
(A-D) Knocking down *dlg* in the posterior half of the wing disc using an RNAi construct targeting PDZ2-encoding sequences (B) causes polarity loss and disrupted epithelial architecture. These phenotypes are fully rescued by co-expression of $Dlg^{SH3\text{-}HOOK\text{-}GUK}$ (C) and $Dlg^{SH3\text{-}HOOK}$ (D), and neither constructs is targeted by the RNAi reagent used to deplete endogenous Dlg (C', D'). Scale bars, 100μm.

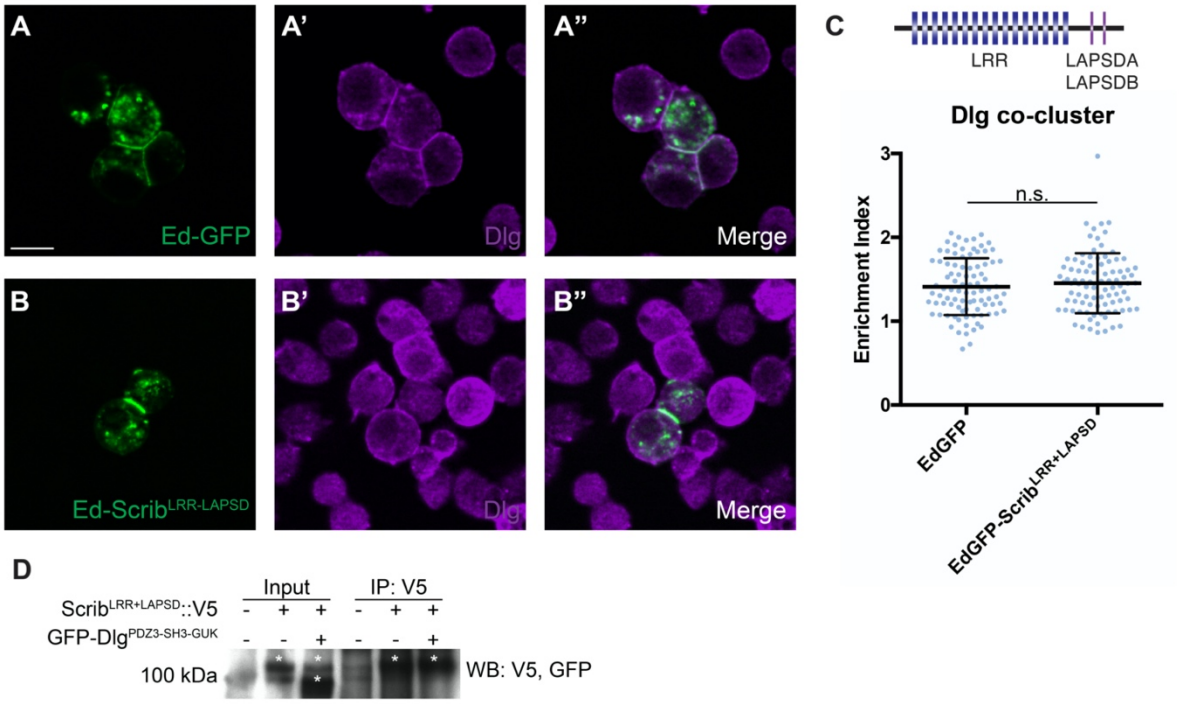

Figure 3.10. Using S2 cell induced polarity to study Scrib-Dlg interaction
(A) Ed-GFP expression in S2 cells allows induction of a polarity domain where cells adhere. (B) Fusing the Scrib LRR+LAPSD domains to Ed creates a domain of polarized Scrib. (C) Schematic of the Scrib domains used in the Ed-Scrib$^{LRR+LAPSD}$ construct. Quantification of Dlg enrichment shows that Scrib cannot recruit Dlg to the polarity site. (D) CoIP assay of Scrib$^{LRR+LAPSD}$ and Dlg$^{PDZ3-SH3-HOOK-GUK}$ from S2 cells fails to detect interaction between these proteins. Scale bars, 10µm. (C) Two-tailed t-test with Welch's correction. Error bars indicate S.D. Data points are individual cell clusters. Enrichment index = contact site/non-contact site intensity. n.s. (not significant).

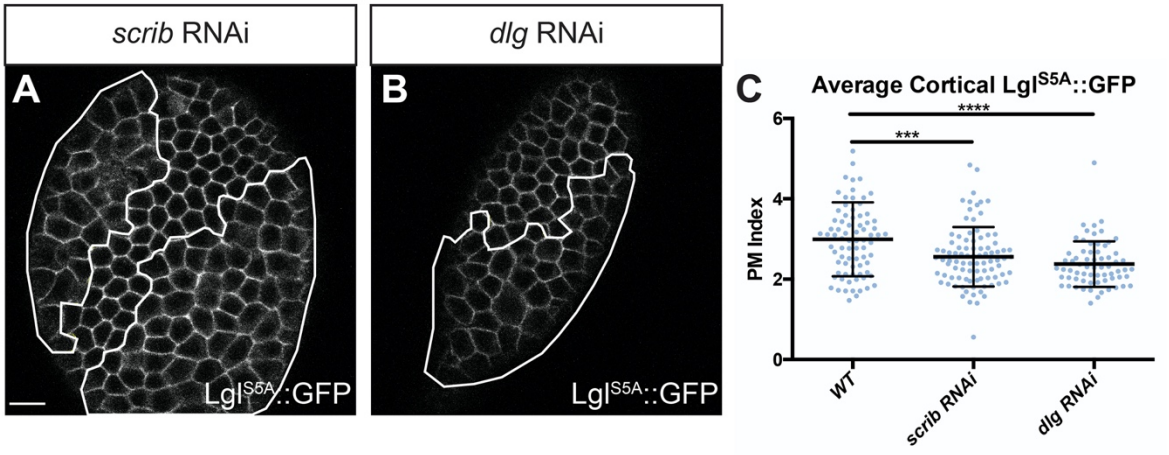

Figure 3.11. Scrib and Dlg protection of Lgl is partly independent of phosphorylation
(A-B) Compared to its localization in WT cells, non-phosphorylatable Lgl^{S5A} exhibits a slight, but significant, reduction in cortical levels in *scrib* RNAi (A) and *dlg* RNAi expressing cells (B). (C) Quantification of LglS5A::GFP levels. *scrib* or *dlg* RNAi both significantly reduce Lgl^{S5A} cortical levels compared to WT cells. Scale bars, 10µm. PM Index=cortical/cytoplasmic intensity. Data points represent individual cell measurements. Error bars represent S.D. (C) One-way ANOVA with Dunnett's multiple comparisons test. ***P < 0.001, ****P < 0.0001.

Table 1. Key Resources

Reagent	Reference and Source
***Drosophila* stocks**	
UAS-Dlg^{WT}::HA	(Sharp et al., 2021)
UAS-Dlg^{ASAKA}::HA	This study
UAS-Dlg$^{SH3\text{-}HOOK}$::HA	This study
UAS-Dlg$^{SH3\text{-}HOOK\text{-}GUK}$::HA	This study
UAS-myr-Scrib::V5	(Khoury and Bilder, 2020)
UAS-myr-Scrib$^{TAAA/RAGA}$::V5	This study
dlg^{m52}	(Perrimon, 1988)
dlg^{m30}	(Woods and Bryant, 1989)
dlg$^{40.2}$	(Mendoza-Topaz et al., 2008)
scrib^{1}	(Bilder and Perrimon, 2000)
UAS-dlg RNAi HMS01954	Bloomington Drosophila Stock Center (BDSC): 39035
UAS-scrib RNAi HMS01993	BDSC: 39073
UAS-Pp1-87B RNAi HMS00409	BDSC: 32414
UAS-Pp1-87B::HA	BSDC: 24098
UASp-Sds22::GFP	BDSC: 65851
UAS-Scrib::GFP	(Zeitler et al., 2004)
UAS-EGFP::Dlg	(Koh et al., 1999)
UAS-Lgl::GFP	(Wirtz-Peitz et al., 2008)
UAS-Lgl^{KAFA}::GFP	(Moreira et al., 2019), Generously provided by E. Morais de Sá.
Lgl::GFP	(Dong et al., 2015), Generously provided by Y. Hong.
Lgl^{S5A}::GFP	(Dong et al., 2015), Generously provided by Y. Hong
act>y+>GAL4 UAS-his::RFP	BDSC: 30558
tub-GAL80 FRT19A; act-GAL4 UAS-GFP	(Lee and Luo, 1999), BDSC: 42726, 5134
tj-GAL4	Kyoto Stock Center: 104055
hh-GAL4	(Tanimoto et al., 2000)
D174-GAL4	(Sharp et al., 2021)
Plasmids	
pMT-Ed-GFP	(Johnston et al., 2009), Generously provided by C. Johnston.
pMT-Ed-GFP-Dlg$^{PDZ3\text{-}SH3\text{-}HOOK\text{-}GUK}$	(Garcia et al., 2014), Generously provided by C. Johnston.
pMT-Ed-GFP-Dlg$^{SH3\text{-}GUK,\Delta HOOK}$	Generously provided by C. Johnston.
pMT-Ed-GFP-Dlg$^{SH3\text{-}GUK}$	This study
pMT-Ed-GFP-Dlg$^{PDZ3\text{-}SH3\text{-}HOOK}$	This study
pMT-Ed-GFP-Dlg^{SH3}	This study
pMT-Ed-GFP-Dlg^{HOOK}	This study
pMT-Ed-GFP-Dlg$^{SH3\text{-}HOOK}$	This study
pMT-Ed-GFP-Dlg$^{PDZ3\text{-}SH3\text{-}HOOK\text{-}GUK[m30]}$	This study

pMT-Ed-GFP-Dlg$^{PDZ3\text{-}SH3\text{-}HOOK\text{-}GUK[ASAKA]}$	This study
pMT-Ed-GFP-Dlg$^{PDZ3\text{-}SH3\text{-}HOOK\text{-}GUK[ASVKF]}$	This study
pMT-Ed-GFP-Dlg$^{PDZ3\text{-}SH3\text{-}HOOK\text{-}GUK[RSAKF]}$	This study
pMT-Ed-GFP-Dlg$^{PDZ3\text{-}SH3\text{-}HOOK\text{-}GUK[RSVKA]}$	This study
pMT-Ed-GFP-Dlg$^{PDZ3\text{-}SH3\text{-}HOOK\text{-}GUK[RSAKA]}$	This study
pMT-Ed-GFP-Dlg$^{PDZ3\text{-}SH3\text{-}HOOK\text{-}GUK[AEAV]}$	This study
pMT-Ed-GFP-Dlg$^{PDZ3\text{-}SH3\text{-}HOOK\text{-}GUK[AEAA]}$	This study
pMT-Ed-GFP-Dlg$^{PDZ3\text{-}SH3\text{-}HOOK\text{-}GUK[AAAA]}$	This study
pMT-Ed-GFP-Dlg$^{PDZ3\text{-}SH3\text{-}HOOK\text{-}GUK[AAN]}$	This study
pMT-Ed-GFP-Dlg$^{PDZ3\text{-}SH3\text{-}HOOK\text{-}GUK[AAW]}$	This study
pMT-Ed-GFP-Scrib$^{LRR+LAPSD}$	This study
pMT-Scrib$^{LRR+LAPSD}$::V5	This study
pMT-GFP::Dlg$^{PDZ3\text{-}SH3\text{-}HOOK\text{-}GUK}$	This study
Antibodies	
Mouse anti-Dlg (1:100 IHC)	Developmental Studies Hybridoma Bank (DSHB): 4F3
Rabbit anti-aPKC (1:200 IHC)	Santa Cruz Biotech: sc-216
Guinea pig anti-Scrib (1:500 IHC)	(Bilder and Perrimon, 2000)
Rabbit anti-HA tag C29F4 (1:500 IHC, 1:10,000 WB, 1:200 IP)	Cell Signaling Technologies (CST): #3724
Mouse anti-HA tag 6E2 (1:10,000 WB)	CST: #2367
Mouse anti-HA tag 2-2.2.14 (1:200 IP)	Invitrogen: 26183
Rabbit anti-GFP (1:5000 WB)	Origene: TP-401
Mouse anti-GFP JL-8 (1:10,000 WB)	Clontech: 632380
Mouse anti-V5 (1:500 IHC, 1:200 IP, 1:5000 WB)	Invitrogen: R960-25
Primers	
myrScrib_silk_F	tgaatagggaattggggtaccatgggtaactgcctcaccac
myrScrib_Silk_R	tctgatccaacgcggcagcagtcagtct
myrScrib_rvxf_F	tgctgccgcgttggatcagaatcgattgcagcggttgaacgatac
myrScrib_Rvxf_R	cctccacttgggcgccagcggcgcgatc
myrScrib_AgeI_F	cgctggcgcccaagtggagggcgaagatg
myrScrib_AgeI_R	ggtacgacggggagcgggcaccggttgacccgtggaactgtctatc

Nterm_Dlg_F	actctgaatagggaattggctcgagcaaaATGACAACGAGGAAAAAGAAGCGC
Nterm-Dlg-RVxF	tggGCcttaGcgctgGCgtccctagctcgcattttgcg
Dlg-RVxF-Cterm	gacGCCAGCgCtaagGCccagggacatgcggcag
Dlg_Cterm_R	ggttccttcacaaagatcctctagaatcTTAAGCGTAGTCTGGGAC
Dlg-SH3_for	Actctgaatagggaattggctcgagcaaaatgcagtaccgcccagaggag
Dlg-SH3-HOOK_rev	Ccgactgggagtagttgatggacaaacgctgtac
Dlg-Cterm_for	catcaactactcccagtcgggaccaacc
Ed-PDZ3-SH3-HOOK-GUK m30 F	TGTGCGCGCCCCGTTTGACTACG
Ed-PDZ3-SH3-HOOK-GUK m30 R	TACAGCGATCGCTTTTGCG
Ed-PDZ3-SH3-HOOK-GUK ASAKA F	TAAGGCCCAGGGACATGCGGCAGCT
Ed-PDZ3-SH3-HOOK-GUK ASAKA R	GCGCTGGCGTCCCTAGCTCGCATTTTGC
Ed-PDZ3-SH3-HOOK-GUK delPDZ3 F	GAGGAGTACAATCGCTTCG
Ed-PDZ3-SH3-HOOK-GUK delPDZ3 R	GCGCGGTTCTCTGGTTAT
Ed-PDZ3-SH3-HOOK-GUK delGUK F	TCCCAGTCGGGACCAACC
Ed-PDZ3-SH3-HOOK-GUK delGUK R	GTAGTTGATGGACAAACGCTGTAC
Ed-PDZ3-SH3-HOOK-GUK deltaSH3_F	CGAGCTAGGGACCGCAGC
Ed-PDZ3-SH3-HOOK-GUK deltaSH3_R	TTGCGTGGTGCGCAGCAG
Ed-PDZ3-SH3-HOOK-GUK ASVKF_F	TAAGTTCCAGGGACATGCGGCAGCT
Ed-PDZ3-SH3-HOOK-GUK ASVKF_R	ACGCTGGCGTCCCTAGCTCGCATTTTGC
Ed-PDZ3-SH3-HOOK-GUK RSAKF_F	TAAGTTCCAGGGACATGCGGCAGCT
Ed-PDZ3-SH3-HOOK-GUK RSAKF_R	GCGCTGCGGTCCCTAGCTCGCATTTTGC
Ed-PDZ3-SH3-HOOK-GUK RSVKA_F	TAAGGCCCAGGGACATGCGGCAGCT
Ed-PDZ3-SH3-HOOK-GUK RSVKA_R	ACGCTGCGGTCCCTAGCTCGCATTTTGC
Ed-PDZ3-SH3-HOOK-GUK RSAKA_F	TAAGGCCCAGGGACATGCGGCAGCT
Ed-PDZ3-SH3-HOOK-GUK RSAKA_R	GCGCTGCGGTCCCTAGCTCGCATTTTGC

Ed-PDZ3-SH3-HOOK-GUK AAW661/2_F	GTGGCAGGCACGACGAGTTCTC
Ed-PDZ3-SH3-HOOK-GUK AAW661/2_R	GCTGCATCGTCGGAGGCATTGGT
Ed-PDZ3-SH3-HOOK-GUK EEN768_F	GAACGTGTTGTCCTACGAGGCC
Ed-PDZ3-SH3-HOOK-GUK EEN768_R	GCCGCGGAAGCTCCTTCAGCATTG
Ed-PDZ3-SH3-HOOK-GUK AEAV_F	CGTGTTGTCCGCAGAGGCCGTACAGC
Ed-PDZ3-SH3-HOOK-GUK AEAV_R	TTCTCCTCGGAAGCTCCT
Ed-PDZ3-SH3-HOOK-GUK AEAA_F	GCCGCACAGCGTTTGTCCATCAAC
Ed-PDZ3-SH3-HOOK-GUK AEAA_R	CTCTGCGGACAACACGTTCTCCTC
Ed-PDZ3-SH3-HOOK-GUK AAAA_F	GCCGCACAGCGTTTGTCCATCAAC
Ed-PDZ3-SH3-HOOK-GUK AAAA_R	CGCTGCGGACAACACGTTCTCCTC
Ed_scrib_Gibson_F	gcatggacgagctgtacaagctatgttcaagtgcattcccatcttc
Ed_scrib_Gibson_R	ccttcgaagggccctctagagtcggtgctagcctctgc
GFP_fwd	ctactagtccagtgtggtggatggtgagcaagggcgag
GFP_rev	tgctgacagcggatctcttgtacagctcgtc
PDZ3-SH3-HOOK-GUK_fwd (for cytosolic Dlg)	caagagatccgctgtcagcaccgaggatataac
PDZ3-SH3-HOOK-GUK_rev (for cytosolic Dlg)	aatggtgatggtgatgatgatcatagagattccttggaaggtac
scrib_fwd (for cytosolic Scrib)	ctactagtccagtgtggtggatgttcaagtgcattcccatcttcaag
scrib_rev (for cytosolic Dlg)	cttcgaagggccctctagacgcgtcggtgctagcctct

Table 2. Scrib and Dlg transgenic constructs

Construct	**Description**
Dlg^{ASAKA}	RSVKF 675-679 to ASAKA
DlgSH3-HOOK	Fragment encompassing aa564-784+961-975
DlgSH3-HOOK-GUK	Fragment encompassing aa564-975
myr-$Scrib^{TAAA/RAGA}$	TILK 286-289 to TAAA and RVGF 621-624 to RAGA
pMT-Ed-GFP-$Dlg^{PDZ3\text{-}SH3\text{-}HOOK\text{-}GUK}$	Fragment encompassing aa473-975
pMT-Ed-GFP-$Dlg^{SH3\text{-}GUK,\Delta HOOK}$	Fragment encompassing aa597-678+771-975
pMT-Ed-GFP-$Dlg^{SH3\text{-}GUK}$	Fragment encompassing aa568-975
pMT-Ed-GFP-$Dlg^{PDZ3\text{-}SH3\text{-}HOOK}$	Fragment encompassing aa473-784+961-975
pMT-Ed-GFP-Dlg^{SH3}	Fragment encompassing aa597-678+766-783+961-975

pMT-Ed-GFP-Dlg^{HOOK}	Fragment encompassing aa473-485+671-784+961-975
pMT-Ed-GFP-Dlg$^{SH3\text{-}HOOK}$	Fragment encompassing aa473-485+564-784+961-975
pMT-Ed-GFP-Dlg$^{PDZ3\text{-}SH3\text{-}HOOK\text{-}GUK[m30]}$	L608→P
pMT-Ed-GFP-Dlg$^{PDZ3\text{-}SH3\text{-}HOOK\text{-}GUK[ASAKA]}$	RSVKF 675-679 to ASAKA
pMT-Ed-GFP-Dlg$^{PDZ3\text{-}SH3\text{-}HOOK\text{-}GUK[ASVKF]}$	RSVKF 675-679 to ASVKF
pMT-Ed-GFP-Dlg$^{PDZ3\text{-}SH3\text{-}HOOK\text{-}GUK[RSAKF]}$	RSVKF 675-679 to RSAKF
pMT-Ed-GFP-Dlg$^{PDZ3\text{-}SH3\text{-}HOOK\text{-}GUK[RSVKA]}$	RSVKF 675-679 to RSVKA
pMT-Ed-GFP-Dlg$^{PDZ3\text{-}SH3\text{-}HOOK\text{-}GUK[RSAKA]}$	RSVKF 675-679 to RSAKA
pMT-Ed-GFP-Dlg$^{PDZ3\text{-}SH3\text{-}HOOK\text{-}GUK[AEAV]}$	YEAV774-777 to AEAV
pMT-Ed-GFP-Dlg$^{PDZ3\text{-}SH3\text{-}HOOK\text{-}GUK[AEAA]}$	YEAV774-777 to AEAA
pMT-Ed-GFP-Dlg$^{PDZ3\text{-}SH3\text{-}HOOK\text{-}GUK[AAAA]}$	YEAV774-777 to AAAA
pMT-Ed-GFP-Dlg$^{PDZ3\text{-}SH3\text{-}HOOK\text{-}GUK[AAN]}$	EEN768-770 to AAN
pMT-Ed-GFP-Dlg$^{PDZ3\text{-}SH3\text{-}HOOK\text{-}GUK[AAW]}$	EWW641-643 to AAW
pMT-Ed-GFP-Scrib$^{LRR+LAPSD}$	Fragment encompassing aa1-715

Chapter 4:
Evidence for a Nuclear Role for *Drosophila* Dlg as a Regulator of the NURF Complex

Katherine A. Sharp[1], Mark J. Khoury [1], Frederick Wirtz-Peitz[2] and David Bilder[1]*
[1]Department of Molecular and Cell Biology, University of California-Berkeley, Berkeley CA
[2]Department of Genetics, Harvard Medical School, Boston, MA

Based on work originally published in *Molecular Biology of the Cell,* 32:ar23 (2021)

ABSTRACT
Scrib, Dlg, and Lgl are basolateral regulators of epithelial polarity and tumor suppressors whose molecular mechanisms of action remain unclear. We used proximity biotinylation to identify proteins localized near Dlg in the *Drosophila* wing imaginal disc epithelium. In addition to expected membrane- and cytoskeleton-associated protein classes, nuclear proteins were prevalent in the resulting mass spectrometry data set, including all four members of the NURF chromatin remodeling complex. Subcellular fractionation demonstrated a nuclear pool of Dlg and proximity ligation confirmed its position near the NURF complex. Genetic analysis showed that NURF activity is also required for the overgrowth of *dlg* tumors, and this growth suppression correlated with a reduction in Hippo pathway gene expression. Together, these data suggest a nuclear role for Dlg in regulating chromatin and transcription through a more direct mechanism than previously thought.

INTRODUCTION

Discs-large (Dlg), Scribble (Scrib), and Lethal giant larvae (Lgl) are evolutionarily conserved polarity-regulating proteins found at the basolateral membranes of epithelial cells, where they restrict the localization of the aPKC and Par complexes to the apical region of the cell (Campanale et al., 2017; Elsum et al., 2012; Rodriguez-Boulan and Macara, 2014). They can also regulate the formation and maintenance of cell junctions, the division axis of epithelial cells, and the asymmetric division of stem cells (Albertson and Doe, 2003; Bergstralh et al., 2013; Bilder et al., 2003; Campanale et al., 2017; Johnston et al., 2009; Nakajima et al., 2019; Rodriguez-Boulan and Macara, 2014; Tepass and Tanentzapf, 2001; Woods et al., 1996). In *Drosophila* epithelia, loss of any one of these three proteins causes not only loss of polarity but also neoplastic transformation and tumorous overgrowth (Bilder, 2004; Bilder et al., 2000c; Hariharan and Bilder, 2006; Humbert et al., 2008). Overgrowth results from an aberrant transcriptional program that is driven by Yorkie (Yki), the transcriptional activator of the Hippo pathway (Bunker et al., 2015; Doggett et al., 2011; Grzeschik et al., 2010; Hariharan and Bilder, 2006; Sun and Irvine, 2011; Zhu et al., 2010).

Dlg, Scrib, and Lgl are conserved in vertebrates where they each have multiple homologs (Elsum et al., 2012). As in flies, the vertebrate proteins have been implicated in regulation of tumor growth, with changes detected in a variety of human cancers (Halaoui and McCaffrey, 2015). They are also involved in apicobasal polarity and formation of both adherens and occluding tight junctions in epithelial cells (Choi et al., 2019; Su et al., 2012) and have a similar role in endothelial cells (Elsum et al., 2012; Lizama and Zovein, 2013; Worzfeld and Schwaninger, 2016). Further, Dlg homologs regulate the migration of epithelial cells during development. Mutations in these genes can result in cleft palate (Caruana and Bernstein, 2001), hydrocephalus (Nechiporuk et al., 2007), and defects in renal and urogenital systems (Elsum et al., 2012; Iizuka-Kogo et al., 2007; Nechiporuk et al., 2007).

Despite the importance of Scrib, Dlg, and Lgl for development, homeostasis, and disease, we still have a limited understanding of their molecular functions and the mechanisms by which they regulate cell biology and gene expression. Scrib and Dlg are multivalent "scaffolding" proteins containing a variety of protein-protein interaction domains and motifs. Scrib contains 4 PDZ domains and a leucine-rich repeat domain, while Dlg contains three PDZ domains, one SH3 domain, and a catalytically-dead guanylate kinase domain (Campanale et al., 2017; Elsum et al., 2012; Su et al., 2012; Tepass and Tanentzapf, 2001). Understanding the function of these scaffolds will require defining the proteins with which they interact as well as how those interactions change and are regulated over space and time within cells. However, PDZ and other domains are thought to facilitate weak and transient interactions, often involving plasma membrane-embedded receptors, making it difficult to define the full complement of proteins with which they interact using traditional biochemical methods (Amacher et al., 2020). Numerous prior efforts have used co-immunopreciptitation with mass spectrometry (IP-MS) to identify binding partners for Dlg, Scrib, and Lgl (Anastas et al., 2012; Audebert et al., 2004; Belotti et al., 2013; Dash et al., 2018; Drew et al., 2017; Ivarsson et al., 2014; Michaelis et al., 2013; Nagasaka et al., 2013; Nakajima et al., 2019; Portela et al., 2018; Van Campenhout et al., 2011; Waaijers et al., 2016) (reviewed in (Stephens et al., 2018)). However, such experiments have yielded largely non-overlapping lists of binding partners and relatively few mechanistic insights. The limited utility of some IP-MS approaches may additionally derive from the use of non-epithelial cell lines in which functionally important interactions may not exist.

We sought a different approach that could be carried out in intact epithelial cells and that would not rely on strong, stable interactions between proteins. We therefore turned to proximity-based biotin labeling using the APEX2 enzyme. APEX2 is an ascorbate-peroxidase derived from the pea plant that, in the presence of hydrogen peroxide, catalyzes the conversion of phenol into a phenoxyl radical. In cells supplied with biotin-phenol as a substrate, APEX2 covalently labels proteins with biotin within a 20nm radius of the enzyme (**Figure 4.1A**). By leveraging the strength and specificity of streptavidin-biotin binding, labeled proteins can then be efficiently and cleanly isolated and identified by MS (Chen et al., 2015; Hung et al., 2014; Hung et al., 2016; Lam et al., 2014; Martell et al., 2012; Rhee et al., 2013). Proximity-based biotinylation has been used in a variety of experimental systems to identify catalogs of proteins associated with a particular organelle or localized to a particular subcellular region. Importantly, this method can also capture protein-protein interactions that cannot be isolated by more conventional methods (Bagci et al., 2020; Chen et al., 2015; Gingras et al., 2019; Hung et al., 2014; Mannix et al., 2019; Rhee et al., 2013; Tan et al., 2020; Trinkle-Mulcahy, 2019; Van Itallie et al., 2013).

As an entry point into understanding Scrib module function, we used an APEX2-tagged *Drosophila* Dlg to identify nearby proteins in an epithelium *in vivo*. In addition to previously proposed Dlg binding partners and other cortical proteins, there was a surprising enrichment of nuclear proteins, including the NURF complex of chromatin regulators. We demonstrate that a nuclear pool of Dlg exists in proximity to NURF members and provide evidence that NURF facilitates the growth of *dlg* tumors by activating neoplastic transcriptional programs. Our results further demonstrate the utility of proximity-based proteomics for the elucidation of the localization and function of individual proteins, particularly for multivalent scaffolding proteins.

RESULTS

An APEX2-Dlg transgene for proteomics

To identify proteins enriched near Dlg in the cells of an intact epithelial sheet, we used APEX2-based *in vivo* proximity labeling. We drove an N-terminally tagged *UAS-3xMyc-APEX2-Dlg* (APEX2-Dlg) construct using a broadly but moderately expressed GAL4 driver (*D174-GAL4*) in a *dlg* null background. In these animals, APEX2-Dlg was the only Dlg protein present. APEX2-Dlg restored the morphology of *dlg* mutant discs (**Figure 4.1B,E,H**), and adult flies were rescued to viability and fertility (**Figure 4.1C,D,F,G,I,J**), demonstrating that this transgenic protein is fully functional. Because proximity-based proteomics labels not only direct binding partners but all proteins within a 20nm radius of the enzyme (Martell et al., 2012) (**Figure 4.1A**), it is critical that APEX2-tagged constructs localize comparably to their wild-type counterparts. Comparison to endogenously tagged Dlg::EGFP revealed that APEX2-Dlg displayed similar localization along the basolateral membranes of wing disc epithelial cells (**Figure 4.1K-L**). We tested the enzymatic function of APEX2-Dlg by treating both control and experimental discs with hydrogen peroxide and comparing the amount of biotinylation by western blot. As expected, increased biotinylation was seen in lysate from discs expressing APEX2-Dlg as compared to control (Figure 4.1M), and we successfully isolated the biotinylated proteins using streptavidin beads from both control and experimental samples (**Figure 4.1M and Figure 4.2**). Finally, we assessed whether APEX2-Dlg would biotinylate proteins known to be in close proximity to endogenous Dlg. Indeed, western blotting revealed that Scrib was present in the streptavidin-bead eluate from experimental but not control samples, verifying that APEX2-Dlg was functioning as designed (**Figure 4.1N, Figure 4.2**).

Proximity biotin labeling and mass spectrometry analysis

We next collected samples from APEX2-Dlg epithelia for mass spectrometry. Larvae were dissected to isolate the wing, haltere, and leg imaginal discs that are found together in the thorax. Samples were collected in batches, subjected to biotin labelling, and a small fraction of each post-labeling reaction lysate was reserved to verify consistent sample quality (**Figure 4.2C,D**). Batches were then pooled into three biological replicates for both the experimental and control genotype, each containing the thoracic discs of 400 larvae. Samples were tandem mass tag (TMT) labeled and then pooled for LC-MS3 (see Methods for details).

The MS results yielded a list of 485 proteins with a p-value below the statistical threshold and a log2 fold change of at least 2 between experimental and control samples (**Table 1**). This list included many translation initiation and elongation factors as well as ribosomal proteins. It is possible that these proteins were labeled because APEX2-Dlg is translated from a UAS construct that is being continually produced. We therefore excluded them from further analysis, leaving a final dataset of 413 proteins (**Table 2**).

We then performed cellular component Gene Ontology (GO) analysis on this dataset. Gratifyingly, enriched terms included "basolateral membrane" and "septate junction" (**Figure 4.3A,B**). The proteins that led to these terms included both Scrib and Lgl, which function with Dlg in a module to regulate polarity, as well as Cora, Nrg, FasIII, Vari, and Atpα which are junctional components whose localization is regulated by Dlg (Bilder et al., 2003; Izumi and Furuse, 2014; Lee et al., 2020; Oshima and Fehon, 2011; Woods et al., 1996). The dataset also included proteins previously identified as direct physical interactors of *Drosophila* Dlg (Kinesin heavy chain, Calmodulin Kinase II, 14-3-3 zeta and epsilon) (Koh et al., 1999; Nakajima et al., 2019; Siegrist and Doe, 2005). Other hits include the co-associated RNA binding proteins Caprin and Fmr1, the latter of which interacts with Lgl (Baumgartner et al., 2013; Zarnescu et al., 2005). Interestingly, "Proton-transporting V-type ATPase, V1 domain" is another enriched term in the GO analysis (**Figure 4.3A and Table 3**), and a recent study identified an indirect physical interaction between the V-ATPase proton pump and Lgl in cultured *Drosophila* cells (Portela et al., 2018). Altogether, these results support the hypothesis that proximity-based proteomics can capture a snapshot of Dlg biology in living epithelia (**Figure 4.3A and Table 3**).

Nuclear Localization of Dlg

The GO analysis also highlighted some unexpected results. Proteins annotated to the term "nucleus" were enriched in the dataset (**Figure 4.3A,B, Table 3**). This was surprising because microscopy of fixed and immunostained tissue as well as live imaging with tagged fluorescent proteins detect Dlg localization almost exclusively at the basolateral membranes of epithelial cells (**Figure 4.1 A,B**). However, proteins associated with the GO-term "nuclear pore" were also overrepresented in the dataset and included proteins found in the pore's cytoplasmic filaments, the central ring which spans the nuclear envelope, and the nuclear basket (Nup358, Nup155, and Nup50 and Tpr; **Figure 4.3A,B, Table 3**). Proximity to these components is consistent with nuclear import of Dlg isoforms, all of which have molecular masses greater than 100 kDa.

We therefore investigated whether a nuclear pool of Dlg might exist in epithelia. We performed sub-cellular fractionation of wing disc lysates to generate nuclear and cytoplasmic fractions, validated by western blotting for their canonical markers Lamin and Tubulin, respectively. Strikingly, a portion of Dlg is indeed found in the nuclear fraction (**Figure 4.3C**). It is not technically feasible to quantify the exact proportion of Dlg in the nucleus because of sample loss inherent to the fractionation protocol; however, taking into account the proportion of each

fraction analyzed by western blot (**Figure 4.3C**), we infer that the amount of nuclear Dlg is small compared to that found in the cytoplasm. Because Dlg, Scrib, and Lgl co-localize at the cortex and work together in many biological contexts, we asked if either Scrib or Lgl were also found in the nuclear fraction. Western blotting of fractions showed a nuclear population of Scrib (**Figure 4.3C**), but not Lgl (**Figure 4.3D**). In *dlg* null flies, this nuclear population of Scrib was lost (**Figure 4.3E**). However, in *scrib* null flies, Dlg was still found in the nuclear fraction (**Figure 4.3E**). We therefore conclude that Dlg enters the nucleus independent of Scrib and that it is required for Scrib's nuclear localization, similar to the relationship between the proteins at the cell cortex (Albertson and Doe, 2003; Bilder et al., 2000c; Khoury and Bilder, 2020; Ventura et al., 2020).

Nuclear Dlg is in close proximity to the NURF complex

Having identified the existence of a small nuclear pool of Dlg, we considered what its function could be. In addition to "nucleus" and "nuclear pore," the proteins associated with the term "chromatin remodeling complex" were also enriched in the APEX2-Dlg proteomic dataset (**Figure 4.3A,B**). While several chromatin remodeling complexes were over-represented, for only one were all members of the complex present in the proteomic dataset: the nucleosome remodeling factor (NURF) complex (**Figure 4.3A,B, Table 3**).

The NURF complex is a conserved molecular machine that catalyzes, through an ATP-dependent mechanism, the sliding of nucleosomes along DNA to regulate gene expression (Alkhatib and Landry, 2011; Badenhorst et al., 2002; Bouazoune and Brehm, 2006; Kwon et al., 2016). In *Drosophila*, NURF is made up of four proteins: Iswi, Caf1-55, and Nurf-38 and E(bx) (aka NURF301) (Alkhatib and Landry, 2011; Xiao et al., 2001). E(bx) serves as a scaffold for the other three proteins. The NURF complex does not inherently possess sequence-specific DNA binding activity. Instead, it moves particular nucleosomes on specific target genes by binding to transcriptional regulatory proteins that themselves have DNA sequence specificity (Alkhatib and Landry, 2011; Kwon et al., 2016; Xiao et al., 2001). For example, the *Drosophila* NURF complex binds the GAGA transcription factor Trithorax-like (Trl) to move nucleosomes out of promoter regions—including those of Yki target genes—thereby facilitating transcriptional activation (Alkhatib and Landry, 2011; Kwon et al., 2016; Oh et al., 2013).

The APEX2 proteomic data suggest that Dlg is found within 20nm of the NURF complex. To verify this, we turned to a proximity ligation assay (PLA) which creates a punctate fluorescent signal when two target proteins are less than 40nm apart (Söderberg et al., 2006). We performed PLA using α-Dlg and α-GFP antibodies on wing discs expressing the NURF complex member E(bx) endogenously tagged with GFP. We further expressed *dlg* RNAi in the posterior compartment of the E(bx)::GFP wing discs (**Figure 4.4A**) as an internal negative control for specificity. A positive PLA signal was detected in epithelial cells from the control side of wing discs (**Figure 4.4B**) that was significantly greater than single antibody background signal (**Figure 4.4D**) and also significantly greater than signal from the *dlg*-depleted portion of the discs (**Figure 4.4C, E**). As a final control, we performed PLA on wing discs expressing Polybromo endogenously tagged with GFP. Polybromo is a member of the PBAP complex, one of two SWI/SNF chromatin remodeling complexes in *Drosophila* (Bouazoune and Brehm, 2006). We detected other SWI/SNF complex members in our MS data (**Tables 2,3**) including Brm and Bap60 (**Figure 4.3B**), but not Polybromo. We therefore reasoned that Polybromo::GFP would be a stringent negative control. We did not detect PLA signal significantly above single antibody background between Dlg and Polybromo::GFP (**Figure 4.4F**).

An advantage of PLA in this context is its sensitivity, which allows small numbers of protein molecules to be visualized via microscopy with good spatial resolution. The PLA signal detected between Dlg and E(bx)::GFP appeared in the nuclei of epithelial cells (**Figure 4.4B**). Because Dlg has a well-established role in regulating spindle orientation during cell division (Albertson and Doe, 2003; Bergstralh et al., 2013; Johnston et al., 2009; Nakajima et al., 2019), we considered that the nuclear Dlg signal from both MS and cell fractionation could derive exclusively from dividing cells. However, the PLA signal was even across cells and not limited to those undergoing mitosis. Thus, in addition to confirming a population of Dlg near the NURF complex, this method also enabled the detection of endogenous Dlg in the nuclei of intact cells, for the first time to our knowledge. These data corroborate the evidence from MS and sub-cellular fractionation that a nuclear pool of Dlg exists and lies specifically near the NURF complex.

The NURF complex is required for overgrowth of *dlg* tumors

We next sought to determine if there was a functional connection between Dlg and the NURF complex. Depleting *dlg* with RNAi from the boundary between anterior and posterior compartments of the wing disc using a conditionally active *ptc^{ts}GAL4* (see Methods) can cause neoplastic overgrowth in the hinge regions both proximal and distal to the pouch; within the pouch *dlg*-depleted cells undergo apoptosis likely due to cell competition (**Figure 4.5D**). Depleting the NURF complex components *E(bx)* or *iswi* in otherwise WT discs using *ptc^{ts}GAL4* has no effect on hinge cells and only minor effects, inducing limited apoptosis, in the pouch (**Figure 4.5A-C**). Strikingly, co-expressing RNAi against either NURF complex component along with *dlg* RNAi rescued the overgrowth of *dlg*-depleted cells (**Figure 4.5E-F**). Examination of apoptotic cells revealed that *dlg*-depleted cells co-expressing NURF complex RNAi did not have significantly increased levels of apoptotic cells in either the hinge or pouch compared to *dlg* RNAi alone (**Figure 4.6A-G**), demonstrating that rescue of *dlg* RNAi by NURF complex depletion is not due to synthetic lethality. A similar reduction of tumor size by RNAi against NURF components was seen when *dlg* was depleted in the posterior compartment of wing discs induced using *hhGAL4* (**Figure 4.7D-F**). Again with this driver, expressing either NURF RNAi alone had little effect on tissue size although these animals showed a small developmental delay (**Figure 4.7A-C**). We noticed that NURF RNAi restores the architecture of cells depleted of *dlg* using *ptc^{ts}GAL4* but not using *hhGAL4*. The latter tumors overgrow more than the former, and previous work has shown that mitotic cells are particularly challenged by polarity remodeling (Bergstralh et al., 2013; Moreira et al., 2019; Osswald and Morais-de-Sá, 2019; Ragkousi et al., 2017); moreover, increased cell divisions may dilute the store of Dlg protein translated prior to the onset of RNAi. Finally, we also observed that heterozygosity for a null allele of E(bx), *E(bx)$^{NURF301-4}$,* partially suppressed the frequency of the pouch fold (55.2%, compared to 96.3% for *dlg* RNAi alone) and hinge overgrowth phenotypes (15.8%, compared to 55.2% for *dlg* RNAi alone) in *dlg* RNAi wing discs using the *ptc^{ts}GAL4* model (**Figure 4.8A-E**).

We tested the specificity of the requirement of NURF complex for tumor growth. Co-expression of a neutral RNAi construct targeting RFP did not rescue *dlg* RNAi phenotypes, suggesting that the suppression we observed is not due to titration of GAL4 by multiple UAS transgenes (**Figure 4.9A-C**). A constitutively-active form of Yki (S168A) induces strong hyperplastic overgrowth when expressed in the *ptc^{ts}GAL4* stripe (**Figure 4.5J**) but this growth was not rescued by *E(bx)* or *iswi* RNAi (**Figure 4.5K,L**). Even though there is also a nuclear pool of Scrib (**Figure 4.3C,E**), overgrowth in *scrib* RNAi tumors was also not rescued by RNAi against either NURF component, and we did not observe altered levels of apoptosis in the pouch of *scrib*

RNAi cells co-depleted for NURF components (**Figure 4.5G-I, Figure 4.6G,H-J**). These results suggest that the reduction of tumor size by NURF RNAi is not a general characteristic of all tumors and the rescue we observe is specific to *dlg*.

NURF complex promotes Yki target-gene expression in *dlg* tumors

Transcriptional changes that drive neoplastic tumor growth in *Drosophila* are driven by a signaling network involving JNK-mediated regulation of the Fos transcription factor and aPKC-mediated regulation of Yki (Atkins et al., 2016; Kulshammer et al., 2015). Because the NURF complex, via its interaction with Trl, participates in activation of Yki target genes (Oh et al., 2013), we asked if this might account for NURF complex role in promoting *dlg* tumor growth. NURF RNAi-mediated suppression of *dlg*-depleted tumor growth did not rescue epithelial architecture (**Figure 4.7**), but it caused significant suppression of a reporter for Yki activity, *ex-LacZ* (Hamaratoglu et al., 2006; McCartney et al., 2000). While NURF RNAi alone had no effect on expression of *ex-LacZ* in otherwise WT tissue (**Figure 4.10A-C**), *ex-LacZ* expression was reduced to normal levels in *dlg* RNAi tissue co-expressing either NURF RNAi (**Figure 4.10D-F**). However, in *scrib* RNAi tumors, where overgrowth is not suppressed, *ex-LacZ* levels are unchanged by NURF RNAi (**Figure 4.10G-I**). Thus, the ability of NURF RNAi to limit tumor overgrowth correlates with the extent to which it limits Yki target gene activation in that tumor type. The failure of NURF RNAi to reduce the overgrowth caused by Yki^{S168A} (**Figure 4.5J-L**) suggests that the NURF complex is not absolutely required for Yki to drive proliferation, and that strong, constitutive activation of Yki can overcome an unfavorable chromatin environment to drive gene expression. Altogether, these data support a model where nuclear Dlg negatively regulates the NURF complex to limit Yki driven growth.

Nuclear localization of Dlg involves sequences outside of consensus NLSs

In order to explore a function for nuclear Dlg, we investigated potential nuclear localization signals (NLSs). Prediction algorithms consistently identified two regions enriched in basic amino acids that are characteristic of recognized NLSs (**Figure 4.11A**). The first lies at the C-terminus of PDZ1, while the second is in the so-called E-F region at the N-terminus of the HOOK domain, which itself lies between the SH3 and GUK domains. Both are conserved in the human homolog hDlg1, and for the latter, experimental evidence consistent with an NLS has been demonstrated. Transgenic constructs have previously deleted either the E-F or the entire HOOK domain; each results in mutant Dlg proteins that show strongly increased nuclear localization visible by immunohistochemistry (Hough et al., 1997; Lu et al., 2021). Since these data indicate that the E-F region cannot constitute the sole NLS of Dlg, we mutated basic residues within the predicted NLSs in both the E-F region as well as PDZ1 to alanine ($Dlg^{2XNLS>A}$, **Figure 4.11A**).

When overexpressed in *dlg* mutant discs or follicle cells, $Dlg^{2XNLS>A}$ had no detectable rescuing activity compared to expression of WT Dlg (**Figure 4.11B,C, Figure 4.12H-J**). Both $Dlg^{2XNLS>A}$ and matched WT Dlg transgenic proteins exhibited membrane and cytoplasmic localization in disc and follicle cells (**Figure 4.11D-E, Figure 4.12A-D**). Quantitation of membrane localization in follicle cells showed that, while $Dlg^{2XNLS>A}$ was enriched at the membrane (PM Index >1), its localization was reduced compared to WT Dlg (**Figure 4.12A-D,G**). We considered whether this might be due to disruption of electrostatic membrane binding, since the mutated residues in NLS2 of $Dlg^{2XNLS>A}$ partially overlap with a recently described membrane binding polybasic region (**Figure 4.11A**)(Lu et al., 2021). However, localization was further reduced in *scrib*-depleted cells (**Figure 4.12E-G**), while Dlg constructs that lack electrostatic

membrane binding are insensitive to *scrib* depletion (Lu et al., 2021). Most importantly, to determine if mutation of both predicted NLS altered Dlg's ability to enter the nucleus, we carried out subcellular fractionation studies on protein extracted from imaginal discs. $Dlg^{2XNLS>A}$ protein could still be detected in the nuclear fraction, similarly to the matched overexpressed WT Dlg (**Figure 4.11F**). We conclude that nuclear entry of Dlg can involve sequences outside of the two predicted NLSs.

DISCUSSION

Here we report the use of an *in vivo* proximity-based biotin labeling approach to investigate new biological functions of the polarity-regulating tumor suppressor Dlg. Our strategy used transgenic replacement of Dlg by an APEX2-tagged version, coupled with mass spectrometry of subsequently tagged proteins; critically, we carried this out in native epithelial tissue. The resultant MS data led to the discovery of a nuclear pool of native Dlg that is not apparent by microscopy but that nevertheless lies near the NURF chromatin remodeling complex. We further found that NURF is required for the overgrowth of epithelia lacking Dlg and suggest that this may be due to the role of NURF in activating pro-proliferative *yki* target genes.

To our knowledge, our data provide the first demonstration of endogenous *Drosophila* Dlg in the nucleus. Dlg is a member of the membrane-associated guanylate kinase (MAGUK) family of proteins that are generally found at cell-cell junctions, but nuclear localization of many MAGUKs has also been observed including hDlg1 (Mantovani and Banks, 2003; Narayan et al., 2009; Roberts et al., 2007) as well as ZO-1 (González-Mariscal et al., 1999; Gottardi et al., 1996), ZO-2 (Islas et al., 2002), CASK1 (Hsueh et al., 2000), MAGI-2 (Dobrosotskaya et al., 1997), and Nagie Oko (Bit-Avragim et al., 2008). Due to their size, movement of MAGUKs into and out of the nucleus must involve active transport via NLS and nuclear export signals (NES) respectively, consistent with the presence of several importin proteins as well as the nuclear import regulator Ran in our Dlg proximity biotinylation dataset (**Tables 1,2**). The predicted NLS in the Dlg E-F/HOOK region is conserved in hDlg1. The SH3-HOOK-GUK region undergoes an intramolecular interaction that regulates exposure of sequences that can mediate several Dlg functions (Lu et al., 2021; Marcette et al., 2009; McGee et al., 2001; Newman and Prehoda, 2009; Nix et al., 2000; Qian and Prehoda, 2006; Rademacher et al., 2019; Zeng et al., 2017); the increased nuclear localization of transgenic Dlg or hDlg1 deleted for the GUK domain raises the possibility that nuclear entry could be one of these (Kohu et al., 2002; Lu et al., 2021; Thomas et al., 2000). The predicted NLS in Dlg PDZ1 is conserved not only in hDlg1 but also in the MAGUKs ZO-1, ZO-2 and their *Drosophila* homolog Polychaetoid. We were unable to predict an NES, although such sequences have been detected in vertebrate ZO-1 (Islas et al., 2002), ZO-2 (González-Mariscal et al., 2006; Islas et al., 2002; Jaramillo et al., 2004), and Nagie Oko (Bit-Avragim et al., 2008). However, various transgenically-expressed truncations of Dlg localize strongly to nuclei (Bachmann et al., 2004; Hough et al., 1997; Lu et al., 2021; Thomas et al., 2000), including one that deletes the E-F region itself. Additionally, coding exons that are alternatively spliced in a neural-specific isoform of Dlg are sufficient to drive nuclear localization; these protein sequences are conserved with hDlg1 (Bachmann et al., 2004). Clearly, MAGUKs have evolved and maintained multiple mechanisms of nuclear entry and exit; our data demonstrate that this may be true even for proteins where a nuclear pool is not visible by microscopy.

We attempted to test the nuclear function of *Drosophila* Dlg by mutating two conserved and predicted NLSs; however, this failed to abolish nuclear entry. This result agrees with a recently published Dlg transgene that deletes the three PDZ domains while also mutating 15 basic

residues in and adjacent to the predicted E-F region NLS to glutamine; nuclear localization of the mutant protein is visible, again emphasizing that an additional NLS must reside outside of the consensus sequences (Lu et al., 2021). Interestingly, $Dlg^{2XNLS>A}$ provided no rescuing activity, consistent with the deleterious effects of mutations in the HOOK domain (Hough et al., 1997; Lu et al., 2021). Previous work shows that PDZ and GUK domains are not absolutely required for Dlg function, while the SH3 and HOOK domains are (Hough et al., 1997; Khoury and Bilder, 2020; Lu et al., 2021; Thomas et al., 2000). Our results hint at a critical role for the 8 basic amino acids in the E-F region within HOOK that is independent of electrostatic membrane binding; these can be the subject of future experiments.

Nakajima and Gibson recently used coimmunoprecipitation to isolate Dlg-associated proteins from embryos. Their dataset identified several proteins involved in nuclear pore traffic (Ran, CRM1, NUP358) but not NURF components (Nakajima et al., 2019). Similarly, we were unable to co-immunoprecipitate (Co-IP) Dlg and NURF complex member E(bx) (data not shown). It is possible that Dlg and E(bx) associate through an interaction that is not stable enough to pull down or that Dlg may interact with another member of the NURF complex (for which reagents for co-IP were not available) or through an intermediary protein. Any of these possibilities would highlight the utility of APEX2 fusion proteins to facilitate the *in vivo* detection of weak and/or transient interactions that are hard to discover by other methods. In the case of the Scrib module, they could provide a path forward to identifying relevant interactors, which has been a major obstacle in understanding the biology of these key polarity-regulating tumor suppressors.

It has long been observed that Scrib, Dlg, and Lgl are required to maintain the proper transcriptional state of epithelial tissues (Bunker et al., 2015; Doggett et al., 2011; Grzeschik et al., 2010; Hariharan and Bilder, 2006; Sun and Irvine, 2011; Zhu et al., 2010). Our observations that Dlg is near the NURF complex in the nucleus and that the NURF complex is required for Yki-driven overgrowth of *dlg* tumors suggest that Dlg may regulate transcription through a much more direct mechanism than previously thought. Several other MAGUKs physically interact with transcription factors, including ZO-2 with Jun, Fos, C/EBP (Betanzos et al., 2004), Myc (Huerta et al., 2007), YAP (Oka et al., 2010) (the vertebrate homolog of Yki), and TEAD (Gallego-Gutiérrez et al., 2021), while CASK1 can form a trimeric complex in the nucleus with the T-box transcription factor Tbr-1 and CINAP, a nucleosome assembly protein that facilitates chromatin remodeling (Hsueh et al., 2000; Wang et al., 2004).

While we found a functional role for the NURF complex in tumor overgrowth in *dlg* mutants, the same assays did not produce evidence for a functional connection between the NURF complex and Scrib. This is intriguing, given the close relationship between Scrib and Dlg in epithelial polarity and our evidence here that Scrib is also detectable in the nucleus. However, it is clear that Scrib and Dlg do not have overlapping functions (Elsum et al., 2012; Stephens et al., 2018); recent work has demonstrated distinct roles for the two proteins, in part by showing that they cannot substitute for one another in epithelial polarity (Khoury and Bilder, 2020; Ventura et al., 2020). Independent roles have also been documented for the *C. elegans* Scrib and Dlg homologs (Firestein and Rongo, 2001; Legouis et al., 2000; McMahon et al., 2001) and recent proteomic studies in *C. elegans* as well as *Drosophila* uncover only modestly overlapping sets of Scrib- and Dlg-interacting proteins (Nakajima et al., 2019; Waaijers et al., 2016)(Reviewed in Stephens *et al.*, 2018). Of particular relevance here, transcriptome profiling of *scrib* and *dlg* mutant wing disc tumors also found only partially overlapping changes in gene expression (Bunker et al., 2015). It is therefore plausible that while Dlg may regulate transcription via the NURF

complex, Scrib's effects on gene expression may be exerted in a distinct manner. Whether these effects require nuclear entry of Scrib will await further study.

The association between nuclear *Drosophila* Dlg and the NURF complex extends data about other nuclear MAGUKs and supports the importance of this understudied aspect of these highly conserved proteins. Still, as we were unable to separately test the functions of cytoplasmic and nuclear Dlg pools, we cannot definitively conclude that the latter drives the observed growth phenotypes. We also do not know how Dlg proteins move through the pore; whether the nuclear population is a small, stable pool or a transient, dynamic one; or the signals or cellular states that cause their nuclear localization. Nonetheless, our data indicate that a comprehensive understanding of this critical protein may have to include its function not just at the plasma membrane but also in the nucleus.

Methods

Drosophila stocks and Genetics

Drosophila melanogaster stocks were raised on cornmeal molasses food. Experimental crosses were raised at 25°C unless otherwise noted. Fly lines used are listed in **Table 4**. *ptc^{ts}GAL4* denotes the use of *ptcGAL4* in combination with temperature sensitive GAL80 (GAL80ts), to allow conditional GAL4 expression upon temperature shift. For experiments using *ptc^{ts}GAL4*, crosses were started at 25°C. Adults were removed after 48 hours then after another 24 hours, vials were shifted to 29°C to induce Gal4 expression. Wing discs were dissected from wandering third instar larvae starting 72 hours after temperature shift and continuing every 24 hours thereafter for 1-3 additional days to track tumor development. For clonal GAL4 expression in follicle cells, larvae were heat shocked for 13 minutes at 37ºC 120 hours after egg deposition (AED). For follicle cell MARCM experiments, larvae were heat shocked for 1 hour on 3 consecutive days starting at 120 hours AED. Ovaries were dissected from adult females fed on yeast for 3 days after eclosion. *UAS-3xMyc-APEX2-Dlg* contains the *dlgA* coding sequence with the *dlg S97*-specific exon using a cDNA provided by Ulrich Thomas; it was cloned into a Gateway N-terminal *3xMyc-APEX2* destination vector. *UAS-Dlg-3xHA* was cloned into the *pUAST-attB* vector and contains a C-terminal flexible linker followed by a 3xHA tag. *UAS-Dlg$^{2XNLS>A}$-3xHA* was cloned from *UAS-Dlg-3xHA* using Gibson assembly (NEB). All transgenes were inserted into the *attP40* site.

Immunofluorescence and Microscopy

Wandering third-instar larval imaginal discs were dissected in PBS and fixed for 20 minutes in 4% PFA. Samples were rinsed in PBS. Follicles were dissected in Schneider's medium containing 15% FBS and fixed for 20 minutes in 4% PFA. Primary and secondary antibodies were diluted in PBST (0.1% Triton X-100) with 4% NGS (Gibco) and 1% BSA (Gibco). Primary antibodies (**Table 4**) were incubated with samples overnight at 4°C. Secondary fluorophore-conjugated antibodies (Molecular Probes) were diluted 1:400 and incubated for 2 hours at room temperature. Phalloidin and DAPI incubated with samples for 20 minutes in PBS. Images were captured on a Zeiss LSM700 scanning confocal microscope or a Zeiss Axio Imager M2 with Apotome 2 with Plan Apochromat 20x/NA 0.8, LD C-Apochromat 40x/NA 1.1 W and Plan Apochromat 63x/NA 1.4 oil objectives at 1024x1024 pixels with 2 line averages.

For all imaginal disc experiments, at least 15 discs were examined per condition, except in Fig. S3H-I, where 7 discs were analyzed per genotype. For follicle cell experiments, tissue from at least 5 females was analyzed and at least 10 ovarioles and at least 2 egg chambers per ovariole

were examined. Images are representative of at least 2 independent biological replicates. Reported phenotypes were observed with at least 80% penetrance in all cases unless otherwise noted.

Dlg cortical enrichment was quantified as described in (Lu et al., 2021). For single cells in en face confocal sections, the fluorescent signal intensity of at the membrane and in the cytoplasm were quantified in Fiji (Schindelin et al., 2012) using rectangular ROIs of fixed 1.17µm width, approximately the thickness of the cell cortex. The ratio of membrane:cytoplasmic intensity was calculated to give the "plasma membrane index" (PM index). Average PM indices were calculated for all cells per genotype.

Dcp-1 enrichment was quantified by taking the mean fluorescence intensity in maximum intensity projected images of a 63.77µm-wide rectangular ROI spanning the *ptc^{ts}GAL4*-expressing stripe and an adjacent, equivalently sized control ROI outside the GAL4 domain and calculating the ratio of these two values per disc. Ratios were calculated separately for the wing pouch and the hinge.

Western Blots

Protein concentrations in samples were measured by BCA protein assay (Pierce). Proteins were electrophoresed at 150V for one hour through 7.5% or 4-20% mini-PROTEAN TGX gels (Bio-Rad) and blotted at 300 mA for one hour onto PVDF membranes. Membranes were blocked in 3% BSA in TBS-T for one hour. All antibodies were incubated with membrane in blocking solution. Primary antibodies were incubated overnight at 4°C. Streptavidin-HRP and HRP-conjugated secondary antibodies were incubated with the membrane for two hours at room temperature. Blots were developed with standard ECL reagents (Advansta).

Sample preparation and biotin labeling for Mass Spectrometry

Larvae were reared at room temperature (21-23°C). Thoracic discs were dissected in chilled labeling media: Schneider's medium (Gibco) containing 1% Pen/Strep (Caisson Labs), 10% FBS (Gibco), 500µM biotin-phenol (aka biotinyl tyramide, AdipoGen Life Sciences), and 2mM probenecid (Thermo). Samples were incubated at room temperature with nutation for 30 minutes. Labeling media was removed. Samples were incubated in 1mM hydrogen peroxide for 1 minute. Samples were then washed three times in quenching buffer [5mM Trolox (Sigma), 10mM sodium azide (Sigma), and 10mM sodium ascorbate (Sigma) in PBS] and three times in PBS. Samples were lysed in RIPA buffer [50mM Tris-HCl, pH8.0, 150mM NaCl, 1% NP-40, 0.5% sodium deoxycholate, 0.1% SDS and protease inhibitors (Pierce mini-tablets)] using a pellet pestle motor and a polypropylene pestle. All solutions were pre-chilled on ice. Lysates were spun at 14,000 rpm in a table-top microfuge for 10 minutes at 4°C to remove debris, and supernatants were saved as final sample lysate. A 5µL lysate sample was reserved for western blot analysis. Remainder was incubated with streptavidin-conjugated magnetic beads (Pierce) for one hour at room temperature. Beads were washed twice in TBS with 0.1% Tween20, then three times with RIPA buffer. For western blot analysis of pull-down of biotinylated proteins, beads were boiled for 5 minutes in 60µL SDS-PAGE sample buffer: NuPAGE LDS buffer (Thermo) with 20mM DTT (Sigma) and 2mM biotin (Thermo). Supernatant was saved as eluate 1 (E1). Beads were then boiled for 5 minutes in 40µL sample buffer and supernatant was saved as eluate 2 (E2). For mass spectrometry, labeled lysates were prepared in batches and stored at -80°C until all samples had been collected. Samples were then thawed, pooled into three replicates from 400 larvae each, and biotinylated proteins were isolated as described above. Protein-bound beads were kept in PBS at 4°C. Mass

spectrometry, including remaining sample prep, was performed by the UC Davis Mass Spectrometry Facilities.

Proteins on beads were received and the buffer was exchanged with 4 washes of 50mM TEAB (Tri Ethyl Ammonium Bicarbonate). The proteins were then digested off the beads overnight with trypsin at room temperature. The following day, the supernatant was removed, and the beads were washed with 50mM TEAB and pooled with the supernatant. The peptides in all six sample were quantified using Pierce Fluorescent Peptide assay (Thermo Scientific).

TMT Labeling

Based on the Fluorescent Peptide assay, the volume for 20 µg of the most concentrated sample was determined, and equal volumes of each sample were diluted with 50mM TEAB to 25 µl per replicate. Each sample was labeled with TMT 6 Plex Mass Tag Labeling Kit (Thermo Scientific). Briefly, 20 µl of each TMT label (126-131) was added to each digested peptide sample and incubated for an hour. The reaction was quenched with 1µl of 5% Hydroxylamine and incubated for 15 minutes. All labeled samples were then mixed together and lyophilized to almost dryness. The TMT labeled sample was reconstituted in 2% Acetonitrile 0 .1% TFA and desalted with a zip tip.

LC-MS3

LC separation was done on a Dionex nano Ultimate 3000 (Thermo Scientific) with a Thermo Easy-Spray source. The digested peptides were reconstituted in 2% acetonitrile /0.1% trifluoroacetic acid, and 5µl of each sample was loaded onto a PepMap 100Å 3U 75 um x 20 mm reverse phase trap where they were desalted online before being separated on a 100 Å 2U 50 micron x 150 mm PepMap EasySpray reverse phase column. Peptides were eluted using a 90-minute gradient of 0.1% formic acid (A) and 80% acetonitrile (B) with a flow rate of 200nL/min. The separation gradient was run with 2% to 5% B over 1 minute, 5% to 10% B over 9 minutes, 10% to 20% B over 27 minutes, 20% to 35% B over 10 minutes, 35% to 99%B over 10 minutes, a 2 minute hold at 99%B, and finally 99% to 2%B held at 2% B for 5 minutes.

MS3 Synchronous Precursor Selection Workflow

Mass spectra were collected on a Fusion Lumos mass spectrometer (Thermo Fisher Scientific) in a data-dependent MS3 synchronous precursor selection (SPS) method. MS1 spectra were acquired in the Orbitrap, 120K resolution, 50ms max inject time, 5 x 105 max inject time. MS2 spectra were acquired in the linear ion trap with a 0.7Da isolation window, CID fragmentation energy of 35%, turbo scan speed, 50 ms max inject time, 1 x 104 AGC and maximum parallelizable time turned on. MS2 ions were isolated in the ion trap and fragmented with an HCD energy of 65%. MS3 spectra were acquired in the orbitrap with a resolution of 50K and a scan range of 100-500 Da, 105 ms max inject time and 1 x 105 AGC.

MS3 SPS Workflow

Database searching: Tandem mass spectra were extracted by Proteome Discoverer 2.2. Charge state deconvolution and deisotoping were not performed. All MS/MS samples were analyzed using SequestHT (XCorr Only) (Thermo Fisher Scientific, San Jose, CA, USA) in Proteome Discoverer 2.2.0.388). Sequest (XCorr Only) was set up to search uniprot-proteome-3AUP000000803.fasta (unknown version, 21134 entries) and an equal number of decoy sequences, assuming the digestion enzyme trypsin. Sequest (XCorr Only) was searched with a fragment ion mass tolerance of 0.60

Da and a parent ion tolerance of 10.0 PPM. Carbamidomethyl of cysteine and TMT6plex of lysine were specified in Sequest (XCorr Only) as fixed modifications. Deamidated of asparagine, oxidation of methionine and acetyl of the n-terminus were specified in Sequest (XCorr Only) as variable modifications.

Criteria for protein identification: Scaffold (version Scaffold_4.8.4, Proteome Software Inc., Portland, OR) was used to validate MS/MS based peptide and protein identifications. Peptide identifications were accepted if they could be established at greater than 74.0% probability to achieve an FDR less than 1.0% by the Scaffold Local FDR algorithm. Protein identifications were accepted if they could be established at greater than 35.0% probability to achieve an FDR less than 1.0% and contained at least 2 identified peptides. This resulted in a peptide decoy FDR of 0.31% and a Protein Decoy FDR of 0.8%. Protein probabilities were assigned by the Protein Prophet algorithm (Nesvizhskii, Al et al Anal. Chem. 2003;75(17):4646-58). Proteins that contained similar peptides and could not be differentiated based on MS/MS analysis alone were grouped to satisfy the principles of parsimony. Proteins sharing significant peptide evidence were grouped into clusters.

Quantitative data analysis: Scaffold Q+ (version Scaffold_4.8.4, Proteome Software Inc., Portland, OR) was used to quantitate Label Based Quantitation (TMT) peptide and protein identifications. Peptide identifications were accepted if they could be established at greater than 74.0% probability to achieve an FDR less than 1.0% by the Scaffold Local FDR algorithm. Protein identifications were accepted if they could be established at greater than 35.0% probability to achieve an FDR less than 1.0% and contained at least 2 identified peptides. Protein probabilities were assigned by the Protein Prophet algorithm (Nesvizhskii, Al et al Anal. Chem. 2003;75(17):4646-58). Proteins that contained similar peptides and could not be differentiated based on MS/MS analysis alone were grouped to satisfy the principles of parsimony. Proteins sharing significant peptide evidence were grouped into clusters. Channels were corrected by correction factors supplied by the manufacturer in all samples according to the algorithm described in i-Tracker (Shadforth, I et al BMC Genomics 2005;6 145-151). Normalization was performed iteratively (across spectra) on intensities, as described in Statistical Analysis of Relative Labeled Mass Spectrometry Data from Complex Samples Using ANOVA (Oberg, Ann L. et al., Journal of proteome research 7.1 (2008): 225–233). Medians were used for averaging. Spectra data were log-transformed, pruned of those matched to multiple proteins, and weighted by an adaptive intensity weighting algorithm. Of 3635 spectra in the experiment at the given thresholds, 3247 (89%) were included in quantitation. Differentially expressed proteins were determined by applying Permutation Test with unadjusted significance level $p < 0.05$ corrected by Benjamini-Hochberg.

Data Availability

Raw data, mzML and Scaffold results are available from the MassIVE proteomics repository (MSV000087186) and Proteome Exchange (PXD025378).

GO analysis

Cellular component Gene Ontology analysis was performed using the BiNGO plug-in for Cytoscape using all genes in the *Drosophila melanogaster* genome as a reference set. User selected settings were as follows: hypergeometric statistical test; Benjamini-Hochberg false discovery rate (FDR) used to correct P-values; significance level set to 0.05.

Multiple Sequence Alignment
Multiple sequence alignment of Dlg NLS sequences was made with Clustal Omega (Madeira et al., 2019). Aligned sequences were visualized using SnapGene Viewer. The following protein sequences were used: *H. sapiens*: UniProt Q12959, *M. musculus*: UniProt Q811D0, *R. norvegicus*: UniProt Q62696, *D. rerio*: UniProt E7FAT1, *X. tropicalis*: UniProt Q28C55, *D. melanogaster*: UniProt P31007.

Subcellular Fractionation
60-70 wandering third instar larvae were dissected in PBS. Cells were lysed using 5 strokes with the small pestle in a Dounce homogenizer in: 10mM HEPES, pH7.6, 10mM KCl, 1.5mM $MgCl_2$, .5 mM DTT, and 0.05% NP-40. After homogenization, samples were incubated on ice for 10 minutes and then spun at 3000 rpm for 10 minutes in a tabletop microfuge. Supernatant was spun at 14,000 x g for 10 minutes and supernatant was cytoplasmic fraction. Pellet from first spin was rinsed in PBS. Pellet was then resuspended in: 5mM HEPES, pH7.6, 1.5mM $MgCl_2$, 300mM NaCl, 0.2mM EDTA, and 26% glycerol. Nuclei in resuspended pellet were lysed by 20 strokes with the large pestle of a Dounce homogenizer. Sample was incubated on ice for 30 minutes and then spun at 24,000 x g for 20 minutes. Supernatant was nuclear fraction. All buffers were pre-chilled on ice and contained protease inhibitors (Pierce). All spins were conducted at 4°C.

PLA
Proximity ligation assay was performed using a Duolink In Situ Orange Mouse/Rabbit Kit (Sigma) according to the manufacturer's instructions with the following modifications. Samples were dissected and fixed as for immunofluorescence. Tissue was permeabilized in PBST then washed 3x in PBS before proceeding. All subsequent steps were performed in recommended volumes in tubes with mounting of samples onto slides as the final step. Confocal images were taken on a Zeiss LSM 700 scanning microscope. For quantification, the total number of PLA puncta were counted in a maximum projection of a 101.61 x 101.61 x 24 µm volume from two regions of each disc: control and *dlg* RNAi. Presented images are a maximum projection of 5µm depth. Images were processed and analyzed in Fiji. Statistics were done in Prism.

Statistical Methods
Statistical significance was determined using two tailed t-test or one-way ANOVA with Tukey's multiple comparisons test. Analysis of mass spec data is described above in "MS3 SPS Workflow" and used Permutation Test with unadjusted significance level $p < 0.05$ corrected by Benjamini-Hochberg. GO analysis is described above and used hypergeometric test with Benjamini-Hochberg false discovery rate (FDR) to correct P-values; significance level set to 0.05. In figures, n.s. is $P>0.05$, * is $p<0.05$, ** is $p<0.01$, *** is $p<0.001$ and **** is $p<0.0001$.

Acknowledgements
We thank Laura Mathies for cloning $Dlg^{2XNLS>A}$, Norbert Perrimon for key reagents, the UC Davis Core Proteomics facility for assistance and the Bilder lab for helpful discussions. LC-MS was supported by a NIH shared instrumentation grant S10OD021801. This work was supported by NIH grants R01 GM090150 and R35 GM130388 to D.B., American Heart Association (AHA) Postdoctoral Fellowship 17POST33660155 to K.A.S. and AHA Predoctoral Fellowship 20PRE35120150 to M.J.K.

FIGURES

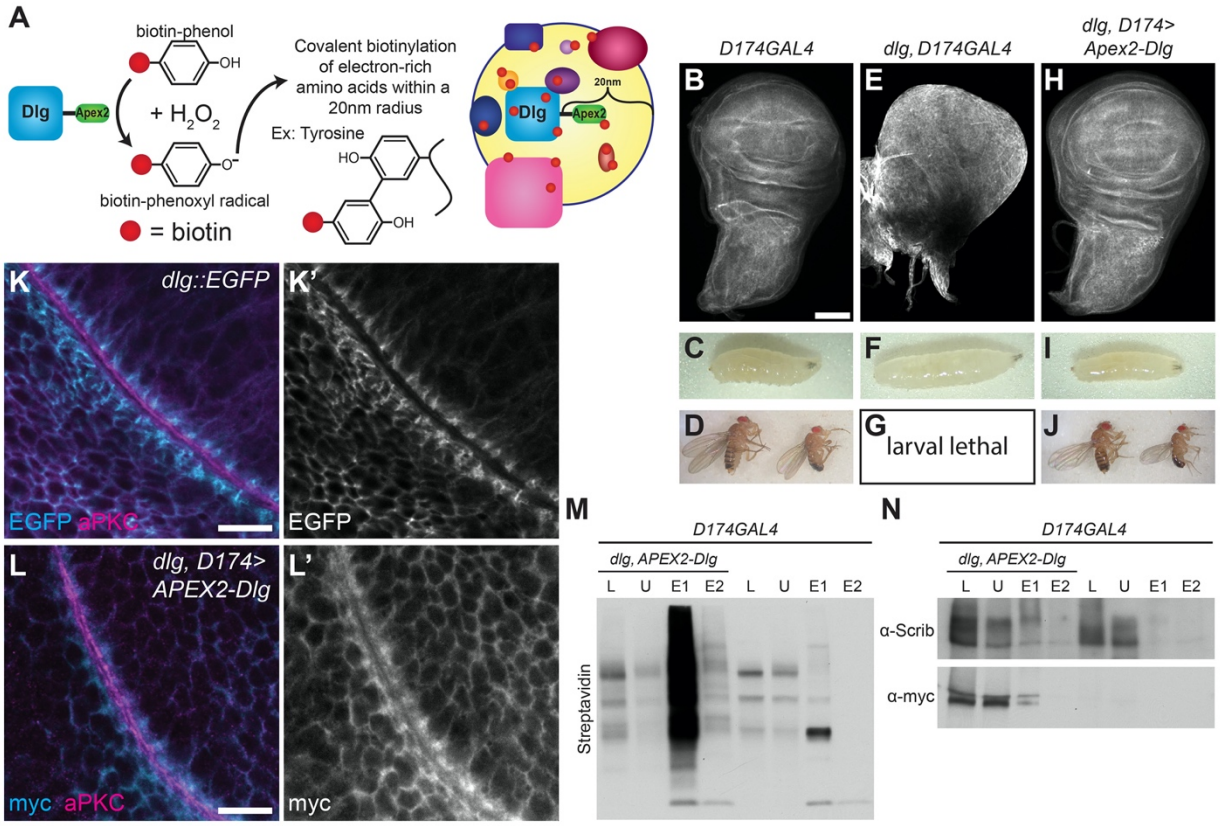

Figure 4.1: A fully functional APEX2-Dlg efficiently labels proteins with biotin
A. In the presence of H_2O_2, APEX2 catalyzes the conversion of biotin-phenol into a phenoxyl radical that can then covalently label proteins with biotin within a 20nm radius of the enzyme.
B-D: Control *D174GAL4* 3rd instar larval wing disc (B), larva (C), and adult (D) fly with normal size and morphology. Scale bar = 100µM.
E-G: *dlg*, *D174GAL4* wing discs (E) form neoplastic tumors. Larvae (F) are overgrown and no adult flies eclose (G) because animals die as giant larvae. Scale bar = 100µM.
H-J: *dlg* mutant phenotypes were rescued by *UAS-3xMyc-APEX2-Dlg* (*APEX2-Dlg*). Wing discs (H) have normal size and morphology, larvae are normal in size (I), and adult viability (J) and fertility are restored. Scale bar = 100µM.
K. Endogenously tagged Dlg::EGFP reflects Dlg localization along the epithelial basolateral membrane of wing disc cells. Localization is excluded from the apical domain labeled by α-aPKC staining. Scale bar = 10µM.
L. APEX2-Dlg (α-myc) localization recapitulated normal Dlg localization along the basolateral domain of wing disc cells and is excluded from the apical domain. Scale bar = 10µM.
M. APEX2-Dlg efficiently labeled cellular proteins with biotin as seen by increased Streptavidin-HRP signal in experimental disc lysate (L, lane 1) compared to lysate from control discs (L, lane 5). Some biotinylated protein remained unbound to beads (U, lanes 2 and 6), but most was serially eluted off streptavidin-conjugated beads (eluate (E) 1 and 2, lanes 3, 4, 7, and 8). Biotinylation catalyzed by APEX2 was particularly apparent in these eluates.

N. Both experimental (lane 1) and control (lane 5) lysates (L) contained Scrib, but only experimental lysate contained APEX2-Dlg (α-myc). While some Scrib and APEX2-Dlg remained unbound (and possibly unlabeled) (U, lanes 2 and 5), both were detected in the experimental but not control streptavidin-bead eluate (E1, E2, lanes 3-4 and 7-8) showing that both proteins were labeled with biotin only in the presence of the APEX2 tag.

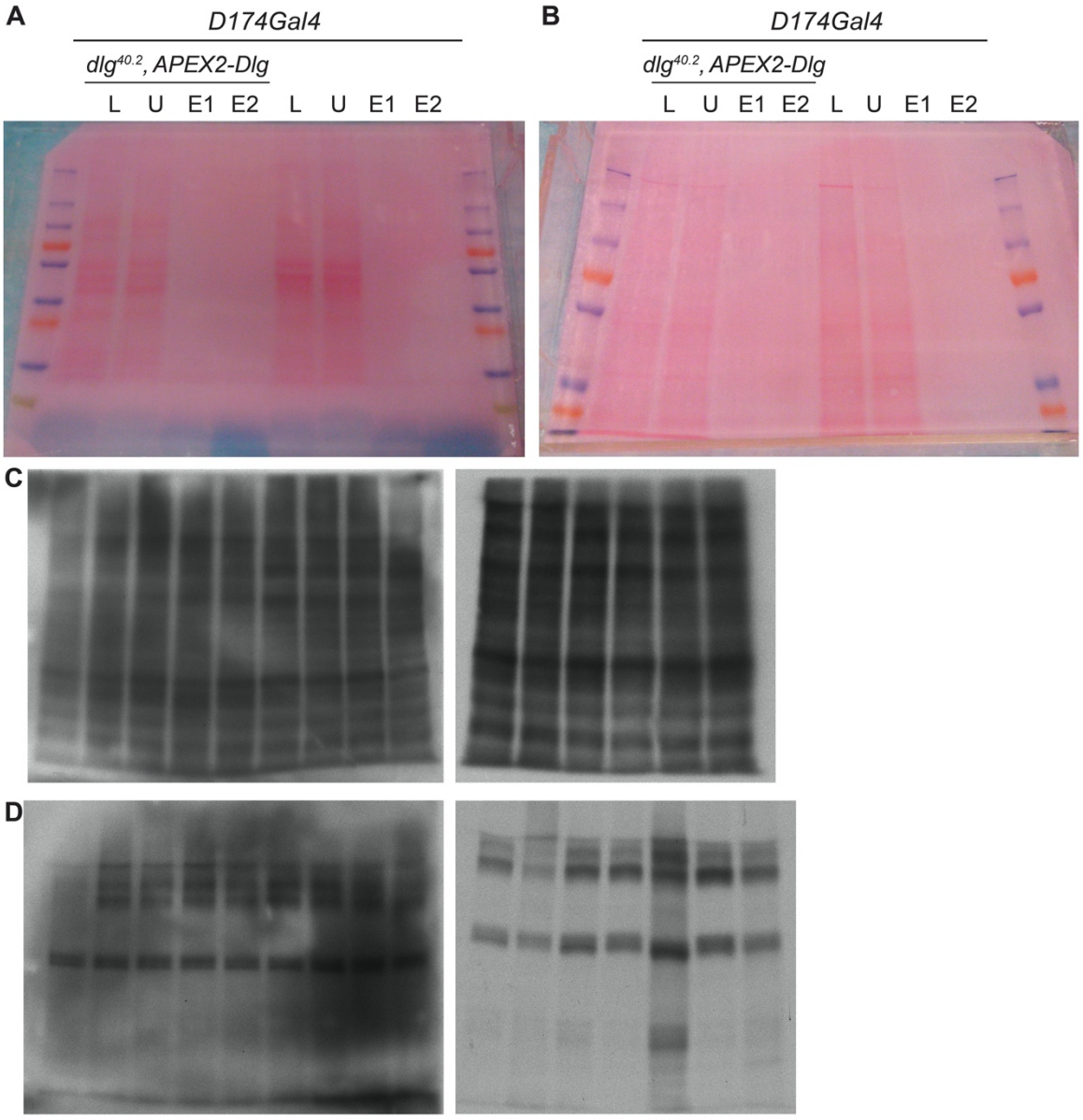

Figure 4.2: Loading and labeling controls

A-B. Ponceau-S staining as a protein loading control for Western blots in Figures 1G-H, showing equal amount of protein loaded in the lysate (L) and unbound (U) lanes for both experimental and control samples. Protein loading of eluates was below detection level of PonceauS staining, but efficient isolation of biotinylated proteins and subsequent elution from streptavidin beads was seen (Figures 1G-H).

C-D. Streptavidin-HRP signal from MS sample lysate batches after labeling reaction but before pull-down with streptavidin beads. Each experimental (**C**) and control (**D**) batch showed clear bands without signs of protein degradation. Experimental batches showed consistent biotin labeling catalyzed by APEX2.

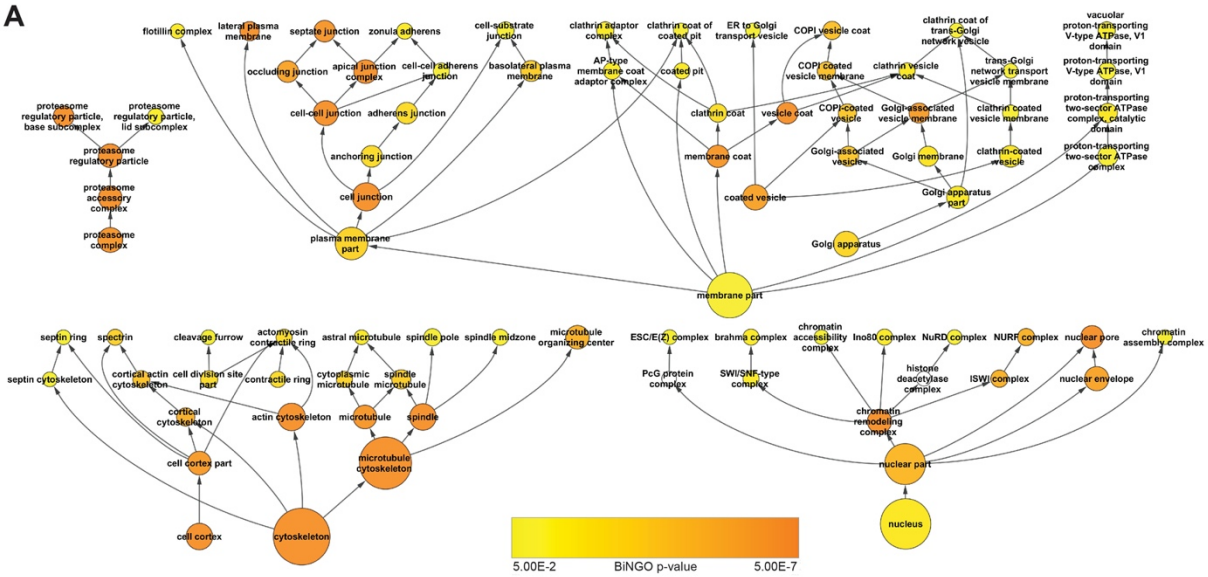

B

GO Terms- Cellular Component	P-value	Example genes
basolateral plasma membrane (GO:0016323)	1.91E-04	*dlg, alpha-Cat, Fas3, scrib, lgl, rhea, Zasp52, Actn*
septate junction (GO:0005918)	7.34E-07	*dlg, cora, Nrg, Fas3, scrib, lgl, vlc, Atpalpha, vari*
nuclear pore (GO:0005643)	1.82E-07	*Nup358, Nup154, Nup50, Mtor*
chromatin remodeling complex (GO:0016585)	2.89E-09	*pont, HDAC1, E(bx), brm, Iswi, Bap60, Caf1-55, Mi-2, Nurf-38*
NURF complex (GO:0016589)	1.56E-05	*E(bx), Iswi, Caf1-55, Nurf-38*

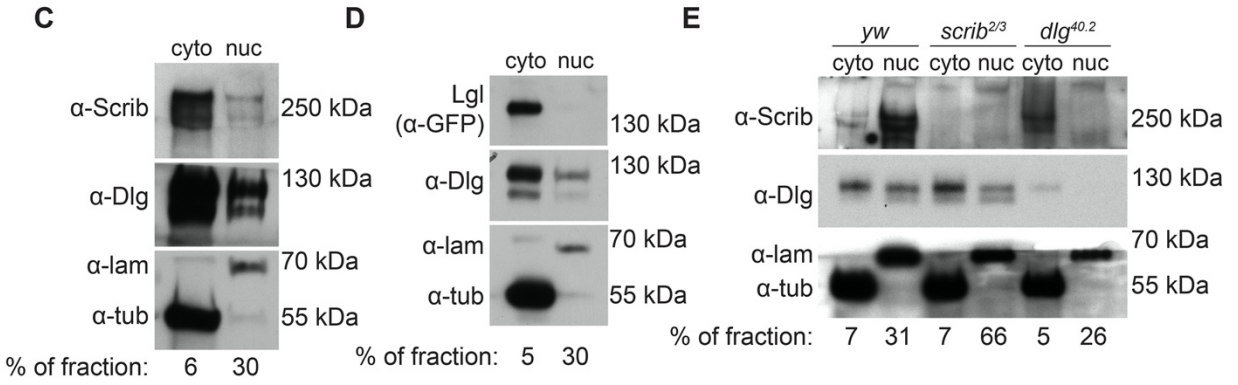

Figure 4.3: Existence of a nuclear pool of Dlg

A. Hierarchical map of selected enriched cellular component GO terms from APEX2-Dlg proximity biotinylation. Size of circles indicates the number of genes associated with a given term. Color of the circle indicates the p-value of enrichment for that term as indicated by the provided scale. Enriched terms include the proteasome; membrane-associated terms including regions of the cell, types of membrane associated proteins, and types of vesicles; cytoskeleton-related terms including actin and microtubule cytoskeletons; and nuclear terms. Map was pruned for viewability. Full list of enriched terms and their associated p-values is found in Supplementary Table 3.

B. Selected enriched GO terms with their associated FDR-corrected p-values, and examples of genes from the dataset associated with each term. “Basolateral plasma membrane” and “septate junction” were expected terms, while “nuclear pore,” “chromatin remodeling complex,” and “NURF complex” were unexpected.
C-E: Western blots of fractionated disc extracts, probed with Tubulin (α-tub) to mark the cytoplasmic fraction and Lamin (α-lam) to mark the nuclear fraction. Percentage of fraction loaded into each lane is given below; higher percent of less concentrated nuclear fractions were loaded to equalize total protein per lane. Native Scrib and Dlg are found in both cytoplasmic and nuclear fractions of disc cells (C), but endogenously GFP-tagged Lgl is detected only in cytoplasmic and not nuclear fraction (D). Dlg is still found in both the nuclear and cytoplasmic fractions of *scrib* null samples, but in *dlg* null samples, Scrib is detected only in the cytoplasmic fraction (E). We note that in different experimental replicates, the relative cytoplasmic:nuclear ratio of Scrib protein is variable.

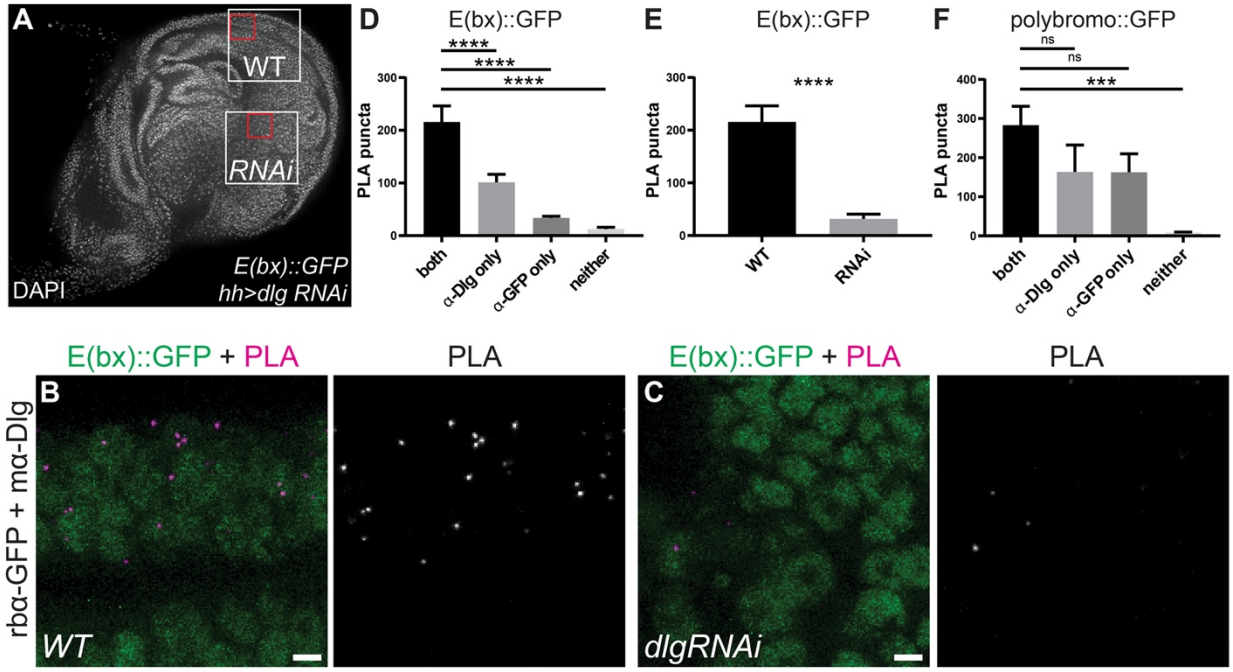

Figure 4.4: Nuclear Dlg can be detected *in vivo* in proximity to E(bx)

A. *E(bx)::GFP* wing disc nuclei expressing *UAS-dlg-RNAi* in the posterior compartment under control of *hhGAL4,* used for PLA. Yellow boxes indicate wild-type and *dlg* knockdown areas where signal in D, E was quantified. Red boxes indicate regions shown in B,C.

B. PLA from wild-type region; note that nearly all signal is within nuclei marked by E(bx)::GFP. Scale bar = 10μM.

C. PLA from *dlg* RNAi region shows nearly no signal. Scale bar = 10μM.

D. PLA signal is significantly increased between E(bx)::GFP and Dlg in WT tissue with both antibodies compared to samples with a single antibody or neither antibody. Graph displays mean with error bars of SEM. Ordinary one-way ANOVA. For ****, $p<0.0001$. For both, n= 14 wing discs; α-Dlg only, n= 15 wing discs; α-GFP only, n= 15 wing discs; neither, n= 12 wing discs.

E. PLA signal is significantly increased between E(bx)::GFP and Dlg in wild-type tissue compared to *dlg* RNAi tissue. Graph displays mean with error bars of SEM. Paired, two-tailed t-test. For ****, $p<0.0001$. n=14 wing discs.

F. There is no significant PLA signal between Polybromo::GFP and Dlg compared to single antibody background. Graph displays mean with error bars of SEM. Ordinary one-way ANOVA. For ns, $p>0.05$. For ***, $p=0.0001$. For both, n= 16 wing discs; α-Dlg only, n= 13 wing discs; α-GFP only, n= 13 wing discs; neither, n= 16 wing discs.

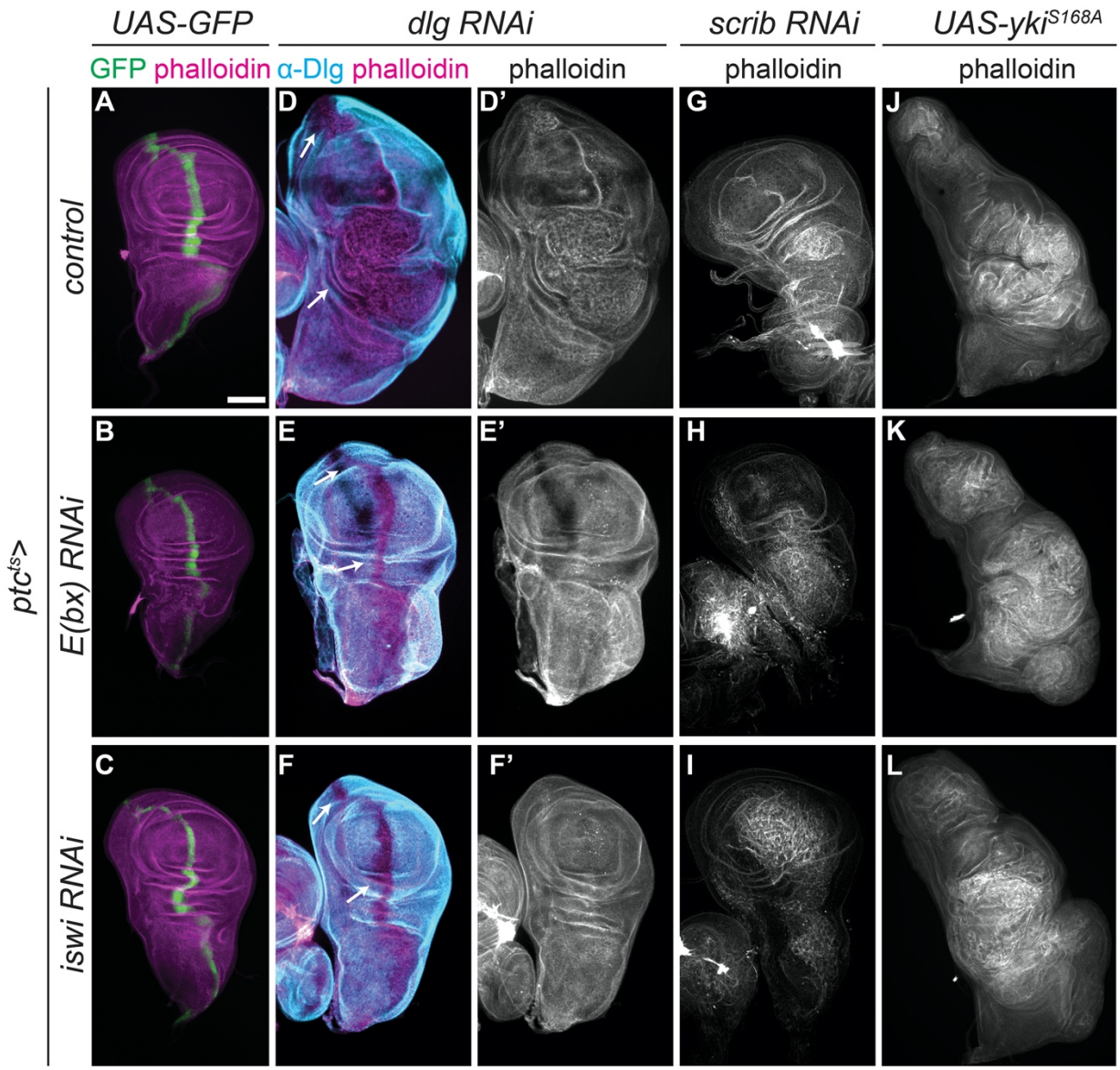

Figure 4.5: Overgrowth of *dlg*-depleted epithelia requires NURF complex

A-C. *ptc^{ts}GAL4* drives expression of GFP along the AP compartment boundary (A). Discs expressing RNAi against NURF complex members *E(bx)* (B) or *iswi* (C) in the Ptc stripe have normal size and morphology.

D-F. Depleting *dlg* in the Ptc stripe caused neoplastic overgrowth in both proximal and distal hinge regions (D, arrows). Overgrowth was rescued by either *E(bx)* RNAi (E) or *iswi* RNAi (F).

G-I. Depleting *scrib* with RNAi in the Ptc stripe also caused neoplastic tumors (G), but tumor formation and growth were unaffected by co-expression of either *E(bx)* (H) or *iswi* (I) RNAi.

J-L. Expressing the constitutively active YkiS168A mutant in the Ptc stripe caused hyperplastic overgrowth of wing discs (J). Yki-driven overgrowth was unaffected by co-expression of either *E(bx)* (K) or *iswi* (L) RNAi. Scale bar = 100µM.

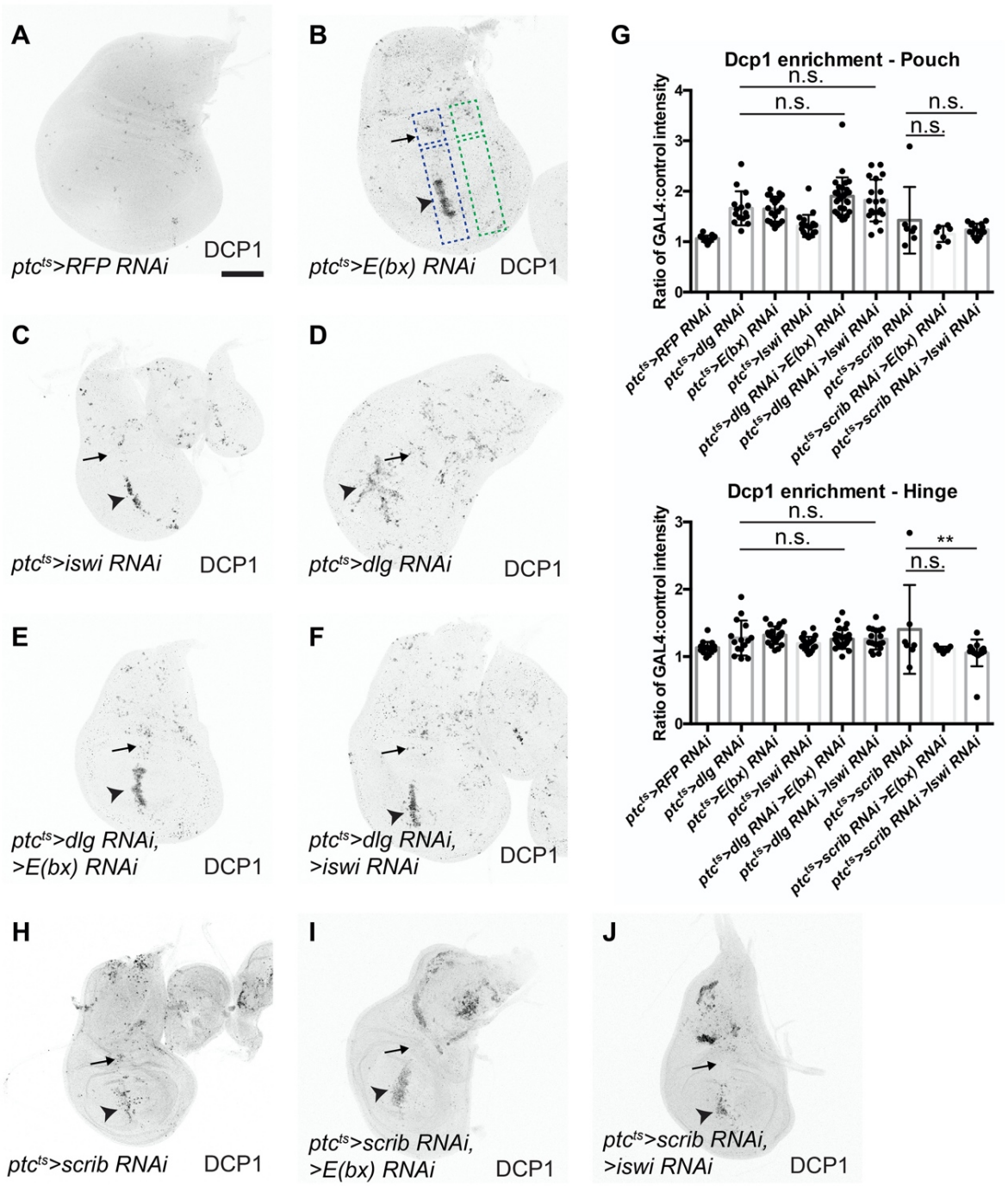

Figure 4.6: Rescue of *dlg* RNAi tumors by NURF RNAi is not due to synthetic lethality
A-F. Compared to control wing discs (**A**), knockdown of *E(bx)* (**B**) or *iswi* (**C**) or *dlg* (**D**) increases cell death (Dcp-1 staining) in the wing pouch region (arrowheads) but not the hinge. Combining *E(bx)* RNAi (**E**) or *iswi* RNAi (**F**) with *dlg* RNAi does not induce cell death in the hinge (arrow), nor increase pouch cell death compared to single RNAi, quantified in (**G**).
H-J. Compared to *scrib* RNAi (**H**) alone, co-expressing *E(bx)* (**I**) or *Iswi* RNAi (**J**) with *scrib* RNAi does not result in increased cell death in the wing pouch or the hinge, quantified in (**G**). One-way ANOVA with Tukey's multiple comparisons test. Dcp-1 enrichment is represented as

the ratio of fluorescence intensity in the *ptc^{ts}GAL4* expressing domain (blue box) and a control ROI adjacent to the GAL4 domain (green box). Scale bars, 100μm. **P<0.01, n.s. P>0.05.

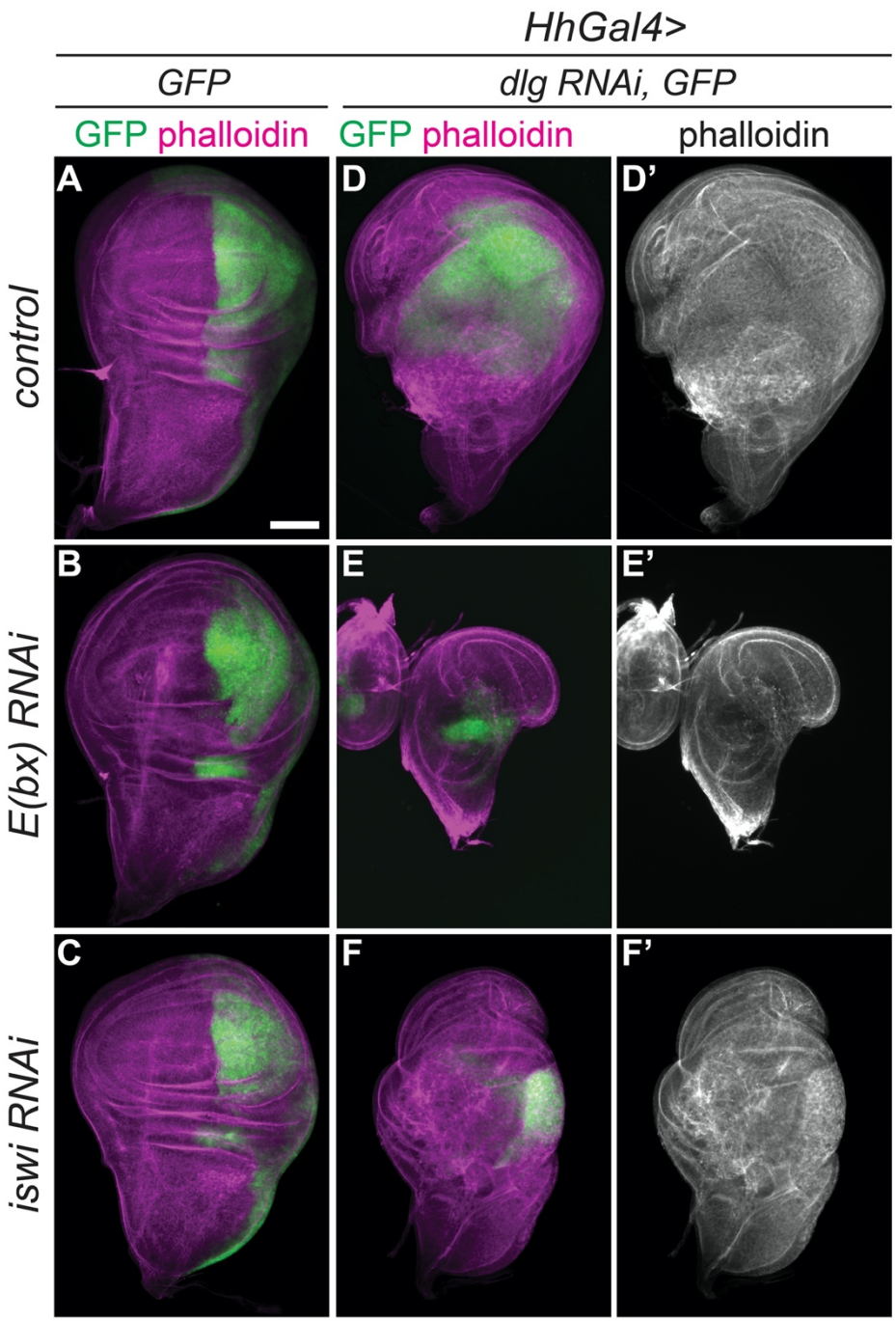

Figure 4.7: NURF RNAi reduces overgrowth in other *dlg* RNAi tumor systems
A-C. *hhGAL4* drives expression of *UAS-GFP* in the posterior compartment of wing discs (**A**). This expression domain and disc morphology were unaffected by either *E(bx)* (**B**) or *iswi* (**C**) RNAi. **D-F**. Expressing *dlg* RNAi under *hhGAL4* control causes overgrown, neoplastic tumors (**D**). Co-expression of *E(bx)* (**E**) or *iswi* (**F**) RNAi reduced the size of these tumors but did not rescue tissue architecture. Scale bars, 100µm.

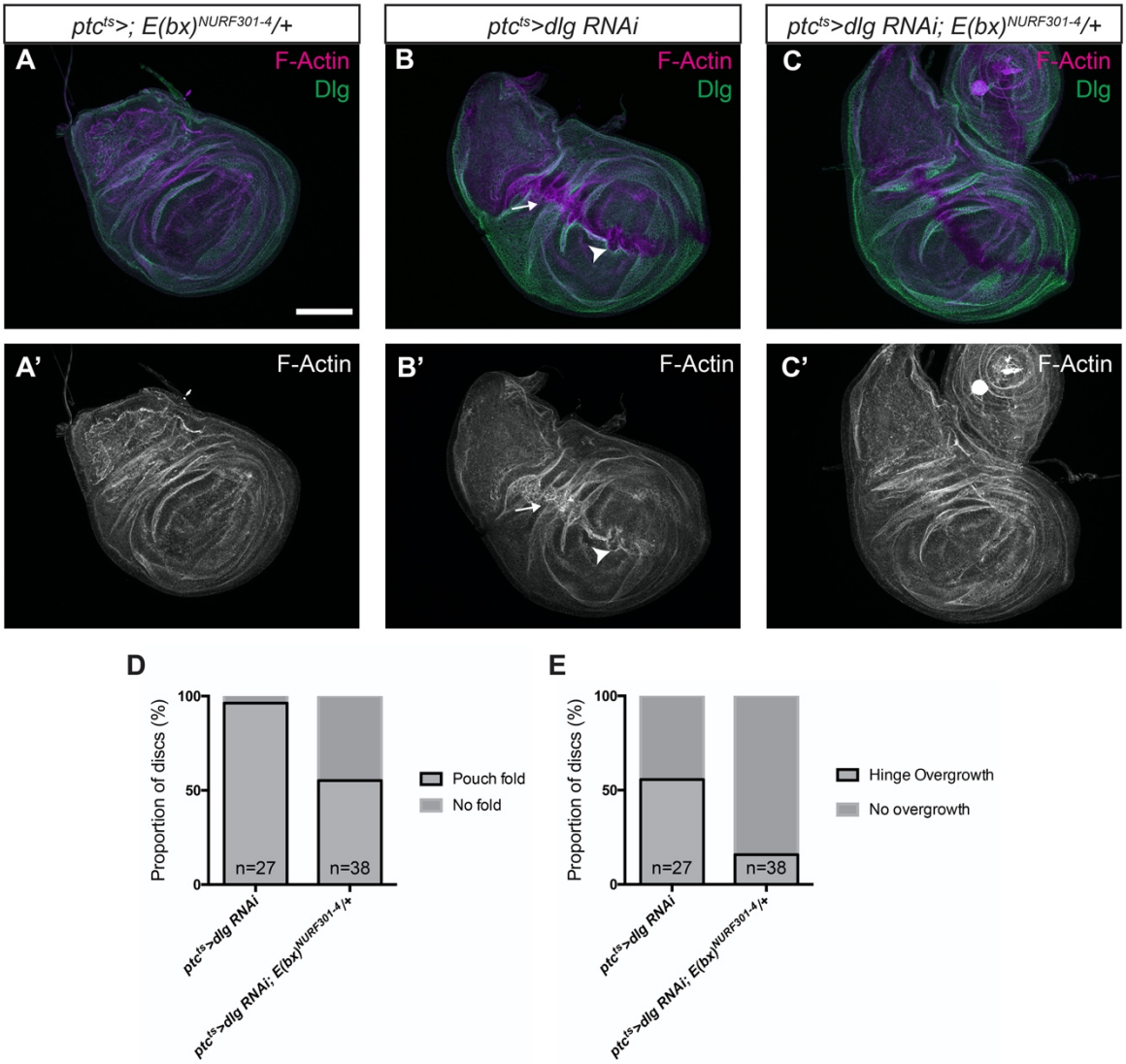

Figure 4.8: Genetic interactions between *dlg* and *E(bx)*

A-C. Heterozygosity for a loss of function *E(bx)* allele (**C**) partially suppressed the frequency of *dlg* RNAi phenotypes (**B**) reducing pouch folding (arrowhead) from 96.3% (26/27) of discs in *dlg* RNAi alone, to 55.2% (21/38) (**D**) and hinge overgrowth (arrow) from 55.6% (15/27) to 15.8% (6/38) of discs (**E**). Scale bars, 100µm.

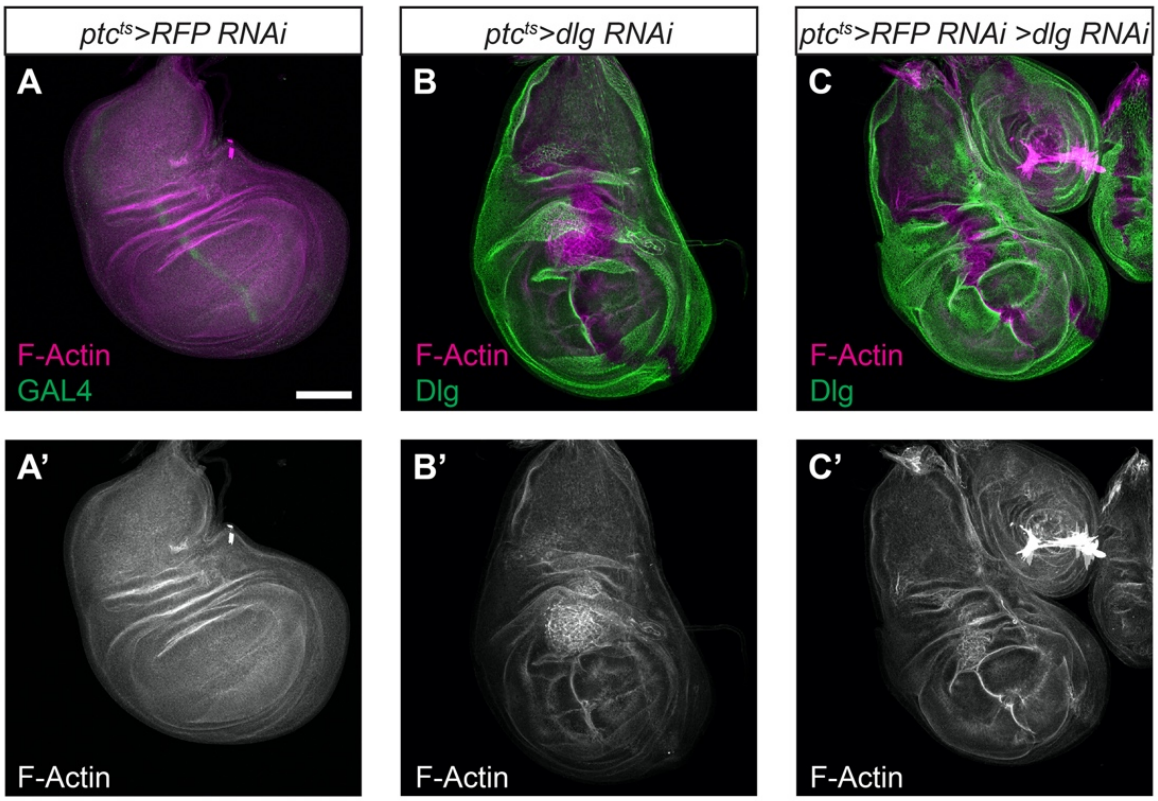

Figure 4.9: GAL4 titration controls for *dlg* RNAi
A-C. Co-expression of a control RFP RNAi construct with *dlg* RNAi (**C**) does not rescue the phenotypes seen when *dlg* RNAi is expressed alone (**B**). Scale bars, 100µm.

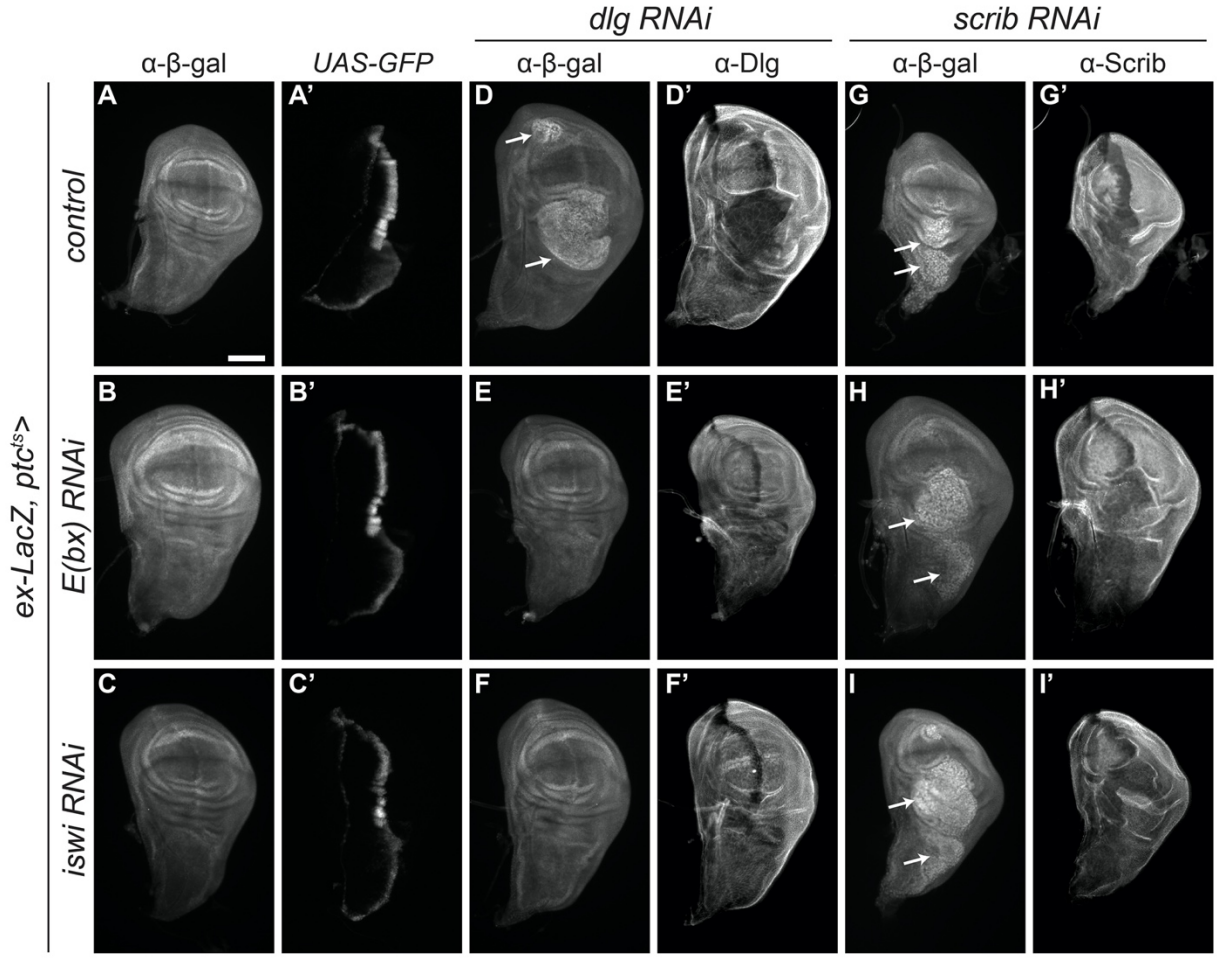

Figure 4.10: NURF RNAi rescues Yki target gene expression in *dlg* tumors
A-C. *ex-LacZ* expression (α-β-gal) in control wing discs (A) was unaffected by either *E(bx)* (B) or *iswi* (C) RNAi.
D-F. *ex-LacZ* levels were elevated in neoplastically overgrown regions of *dlg* RNAi discs. (D, arrows). *E(bx)* (E) or *iswi* (F) RNAi coexpression rescued both overgrowth and *ex-LacZ* levels.
G-I. *ex-LacZ* levels were also elevated in neoplastically overgrown areas of *scrib* RNAi discs (G). Neither overgrowth nor *ex-LacZ* levels were rescued with co-expression of *E(bx)* (H) or *iswi* (I) RNAi. The phenotype here was made less severe than in Figure 4G-I by reducing *ptc^{ts}GAL4* activity time, to facilitate comparison of normal to tumorous tissue. Scale bar = 100μM.

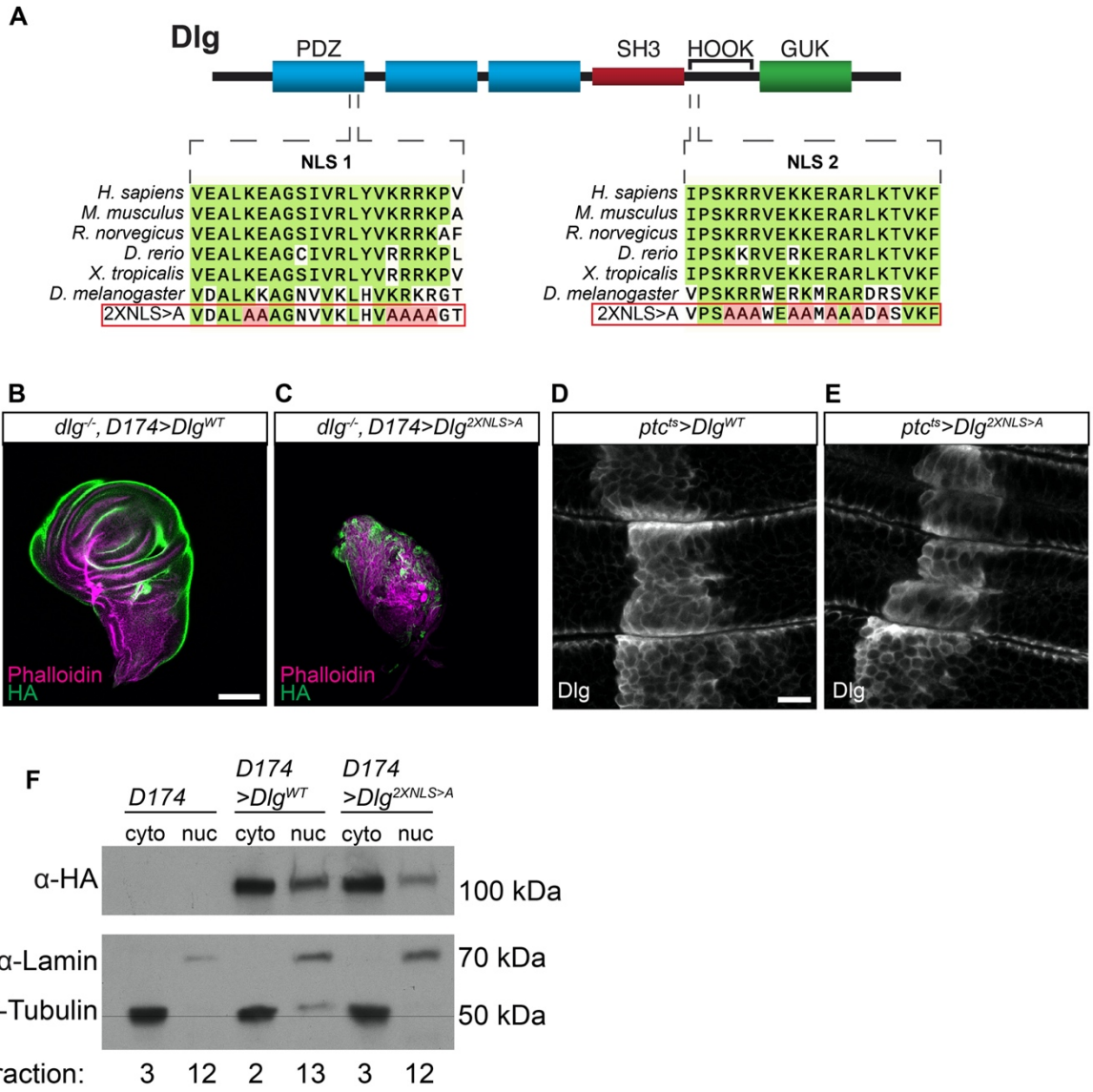

Figure 4.11: Dlg nuclear localization involves sequences outside of predicted NLSs

A. Diagram of Dlg protein, with predicted nuclear localization signals (NLSs) shown in relation to conserved domains. Conservation of NLSs is shown in alignment of Dlg homologs. Mutations in $Dlg^{2XNLS>A}$ are shown in red.

B, C. *dlg* null mutant wing discs are rescued by expression of Dlg^{WT} (B) but not $Dlg^{2XNLS>A}$ (C)

D, E. Localization of Dlg^{WT} (D) under *ptc-GAL4* is comparable to $Dlg^{2XNLS>A}$ (E), although the latter shows more cytoplasmic staining. Transgenes are detected by anti-Dlg staining: compare to endogenous protein localization neighboring the stripe.

F. Western blots of fractionated disc extracts expressing transgenic Dlg proteins, detected by α-HA. Blots are also probed with Tubulin (α-tub) to mark the cytoplasmic fraction and Lamin (α-lam) to mark the nuclear fraction. Dlg^{WT} and $Dlg^{2XNLS>A}$ are both found in the nuclear as well as the cytoplasmic fraction. Scale bars in B,C=100μm, in D-E=10μm.

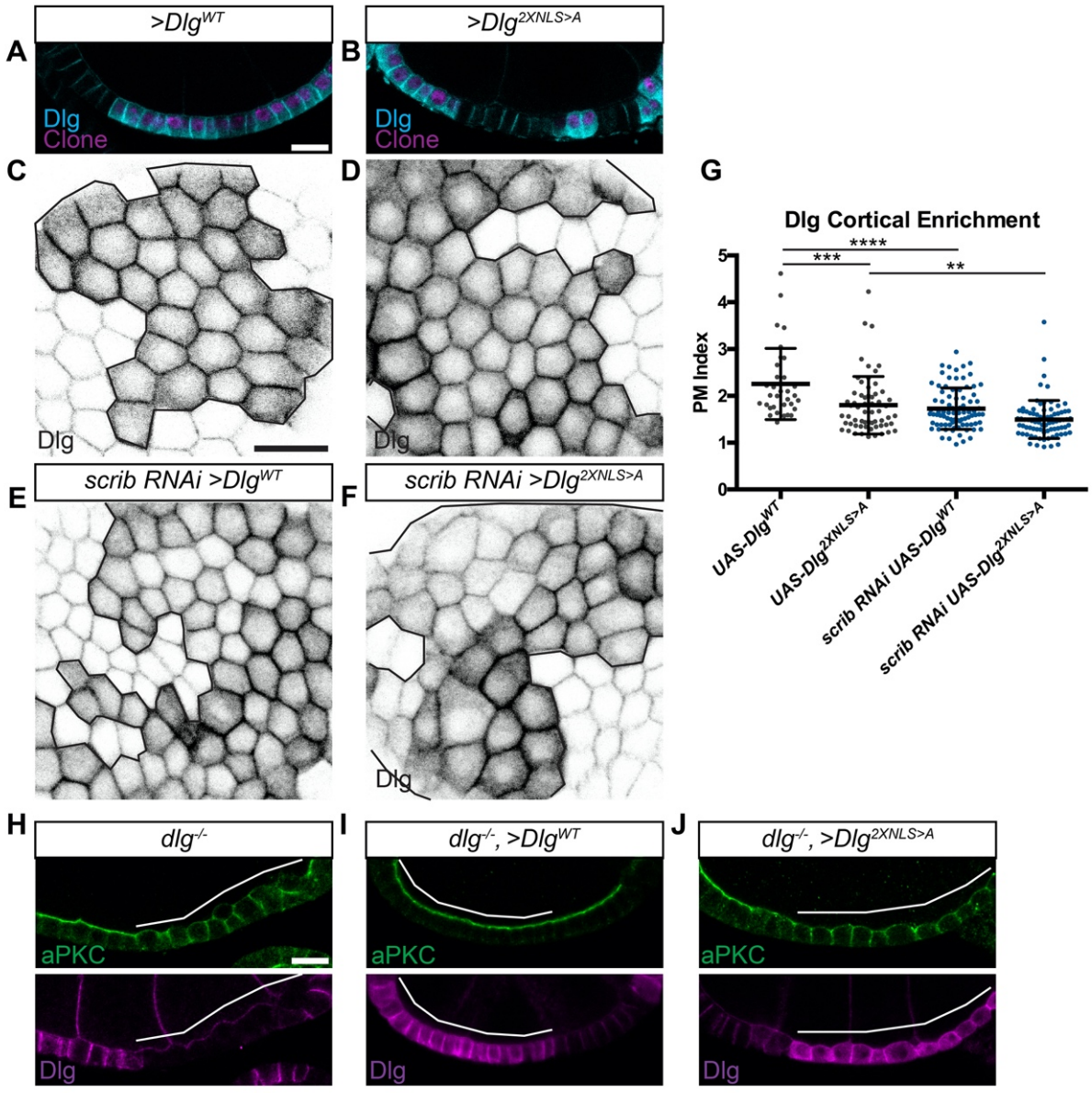

Figure 4.12: Transgenic Dlg localization in follicle epithelium

A-E. Clones overexpressing Dlg^{WT} (**A, C**) compared to $Dlg^{2XNLS>A}$ (**B,D**) in cross-section (**A, B**) or en face (**C,D**) views. White/black lines indicate clone boundaries. Localization is similar, although $Dlg^{2XNLS>A}$ shows 20% lower cortical enrichment, quantified in (**G**).

E-F. When expressed in a *scrib*-depleted background, both Dlg^{WT} (**E**) and $Dlg^{2XNLS>A}$ (**F**) show reduced cortical enrichment than when expressed in a WT background, quantified in (**G**)

H-J. *dlg* null mutant follicle cell clones (**H**) are rescued by expression of Dlg^{WT} (**I**) but not $Dlg^{2XNLS>A}$ (**J**). One-way ANOVA with Tukey's multiple comparisons test. Error bars represent S.D., data points represent measurements from single cells. **P<0.01, ***P<0.001, ****P<0.0001. Scale bars, 10μm.

Table 1. Complete Dlg-APEX2 proteomics hit list

Accession Number	Permutation Test (p-value) Benjamini-Hochberg (p< 0.04787)	Log2 Fold Change by Category (APEX / Reference)	gene name	FlyBase ID
DLG1_DROME	< 0.0001	11.34	dlg1	FBgn0001624
Q8SX89_DROME	0.001	10.05	kuk	FBgn0038476
Q7KUX7_DROME (+3)	0.001	9.81	eIF4H1	FBgn0262734
ZW10_DROME	0.001	9.79	Zw10	FBgn0004643
Y1505_DROME	0.001	8.9	CG11505	FBgn0035424
A0A0B4K7N9_DROME (+4)	0.001	8.88	cnn	FBgn0013765
Q9VDF4_DROME	< 0.0001	8.2	Cortactin	FBgn0025865
A0A0B4LGI9_DROME (+1)	< 0.0001	7.98	CG3760	FBgn0022343
A0A0B4LEY1_DROME (+3)	< 0.0001	7.35	Sec31	FBgn0033339
GGYF1_DROME	0.001	7.27	Gyf	FBgn0039936
A0A0B4K618_DROME (+1)	< 0.0001	7.21	Fmr1	FBgn0028734
Q9VFT4_DROME	< 0.0001	7.2	rin	FBgn0015778
E4NKG1_DROME	< 0.0001	7.18	Capr	FBgn0042134
CADE_DROME	< 0.0001	7.15	shg	FBgn0003391
Q960D3_DROME (+1)	< 0.0001	7.01	vig2	FBgn0046214
C8VV14_DROME	< 0.0001	6.98	Ald	FBgn0000064
D5AEK7_DROME (+1)	0.001	6.61	CG4729	FBgn0036623
Q9XTL2_DROME	< 0.0001	6.31	Stam	FBgn0027363
Q7JZD3_DROME (+1)	< 0.0001	6.28	Eb1	FBgn0027066
X2JC16_DROME	0.017	6.28	CG8184	FBgn0030674
Q9V426_DROME	0.003	6.26	vig	FBgn0024183
41_DROME [2]	< 0.0001	6.25	cora	FBgn0010434
E1JJF9_DROME (+2)	< 0.0001	5.98	Nrg	FBgn0264975
CTNA_DROME	< 0.0001	5.95	alpha-Cat	FBgn0010215
Q9W2I5_DROME-DECOY	0.016	5.85	CG10505	FBgn0034612
Q7KTL4_DROME (+2)	< 0.0001	5.81	sip2	FBgn0031878
EF1D_DROME	0.001	5.77	eEF1delta	FBgn0032198
A0A0B4K7U5_DROME (+2)	< 0.0001	5.71	lig	FBgn0020279
CAZ_DROME	0.001	5.65	caz	FBgn0285954
LVA_DROME	< 0.0001	5.61	lva	FBgn0029688
A1Z968_DROME	< 0.0001	5.6	NAT1	FBgn0010488

B7Z0Z0_DROME (+2)	0.001	5.58	Dsp1	FBgn0278608
A0A0B4LF26_DROME	0.001	5.52	eIF3j	FBgn0027619
M9NEA1_DROME (+3)	< 0.0001	5.49	stai	FBgn0266521
M9PBD9_DROME (+1)	< 0.0001	5.48	RanGAP	FBgn0003346
EIF3I_DROME	< 0.0001	5.47	eIF3i	FBgn0015834
B7Z120_DROME [7]	0.001	5.43	Tlk	FBgn0283657
A0A126BEE6_DROME	0.001	5.39	CG8223	FBgn0037624
PNUT_DROME	< 0.0001	5.38	pnut	FBgn0013726
EF1B_DROME	< 0.0001	5.35	eEF1beta	FBgn0028737
FAS3_DROME [3]	< 0.0001	5.34	Fas3	FBgn0000636
A1Z6I7_DROME	< 0.0001	5.32	BubR1	FBgn0263855
Q9VPF3_DROME	0.00082	5.27	CG11796	FBgn0036992
M9PFE5_DROME (+2)	0.001	5.25	cmb	FBgn0036365
Q7K5M6_DROME	< 0.0001	5.21	CG10939	FBgn0010620
PRDX1_DROME	< 0.0001	5.04	Jafrac1	FBgn0040309
Q9VFV9_DROME	< 0.0001	5.02	Droj2	FBgn0038145
RUVB1_DROME	< 0.0001	4.98	pont	FBgn0040078
A4V4F2_DROME (+1)	< 0.0001	4.97	Flo2	FBgn0264078

Top 50 identified proteins from the complete APEX dataset. The full table can be found at: https://www.molbiolcell.org/doi/suppl/10.1091/mbc.E21-04-0187/suppl_file/mc-e21-04-0187-s02.xlsx

Table 2. Curated Dlg-APEX2 proteomics hit list

Accession Number	Permutation Test (p-value) Benjamini-Hochberg (p< 0.04787)	Log2 Fold Change by Category (APEX / Reference)	gene name	FlyBase ID
DLG1_DROME	< 0.0001	11.34	dlg1	FBgn0001624
Q8SX89_DROME	0.001	10.05	kuk	FBgn0038476
ZW10_DROME	0.001	9.79	Zw10	FBgn0004643
Y1505_DROME	0.001	8.9	CG11505	FBgn0035424
A0A0B4K7N9_DROME (+4)	0.001	8.88	cnn	FBgn0013765
Q9VDF4_DROME	< 0.0001	8.2	Cortactin	FBgn0025865
A0A0B4LGI9_DROME (+1)	< 0.0001	7.98	CG3760	FBgn0022343
A0A0B4LEY1_DROME (+3)	< 0.0001	7.35	Sec31	FBgn0033339
GGYF1_DROME	0.001	7.27	Gyf	FBgn0039936
A0A0B4K618_DROME (+1)	< 0.0001	7.21	Fmr1	FBgn0028734
Q9VFT4_DROME	< 0.0001	7.2	rin	FBgn0015778

E4NKG1_DROME	< 0.0001	7.18	Capr	FBgn0042134
CADE_DROME	< 0.0001	7.15	shg	FBgn0003391
Q960D3_DROME (+1)	< 0.0001	7.01	vig2	FBgn0046214
C8VV14_DROME	< 0.0001	6.98	Ald	FBgn0000064
D5AEK7_DROME (+1)	0.001	6.61	CG4729	FBgn0036623
Q9XTL2_DROME	< 0.0001	6.31	Stam	FBgn0027363
X2JC16_DROME	0.017	6.28	CG8184	FBgn0030674
Q7JZD3_DROME (+1)	< 0.0001	6.28	Eb1	FBgn0027066
Q9V426_DROME	0.003	6.26	vig	FBgn0024183
41_DROME [2]	< 0.0001	6.25	cora	FBgn0010434
E1JJF9_DROME (+2)	< 0.0001	5.98	Nrg	FBgn0264975
CTNA_DROME	< 0.0001	5.95	alpha-Cat	FBgn0010215
Q9W2I5_DROME-DECOY	0.016	5.85	CG10505	FBgn0034612
Q7KTL4_DROME (+2)	< 0.0001	5.81	sip2	FBgn0031878
A0A0B4K7U5_DROME (+2)	< 0.0001	5.71	lig	FBgn0020279
CAZ_DROME	0.001	5.65	caz	FBgn0285954
LVA_DROME	< 0.0001	5.61	lva	FBgn0029688
A1Z968_DROME	< 0.0001	5.6	NAT1	FBgn0010488
B7Z0Z0_DROME (+2)	0.001	5.58	Dsp1	FBgn0278608
M9NEA1_DROME (+3)	< 0.0001	5.49	stai	FBgn0266521
M9PBD9_DROME (+1)	< 0.0001	5.48	RanGAP	FBgn0003346
B7Z120_DROME [7]	0.001	5.43	Tlk	FBgn0283657
A0A126BEE6_DROME	0.001	5.39	CG8223	FBgn0037624
PNUT_DROME	< 0.0001	5.38	pnut	FBgn0013726
FAS3_DROME [3]	< 0.0001	5.34	Fas3	FBgn0000636
A1Z6I7_DROME	< 0.0001	5.32	BubR1	FBgn0263855
Q9VPF3_DROME	0.00082	5.27	CG11796	FBgn0036992
M9PFE5_DROME (+2)	0.001	5.25	cmb	FBgn0036365
Q7K5M6_DROME	< 0.0001	5.21	CG10939	FBgn0010620
PRDX1_DROME	< 0.0001	5.04	Jafrac1	FBgn0040309
Q9VFV9_DROME	< 0.0001	5.02	Droj2	FBgn0038145
RUVB1_DROME	< 0.0001	4.98	pont	FBgn0040078
A4V4F2_DROME (+1)	< 0.0001	4.97	Flo2	FBgn0264078
PFD6_DROME	0.001	4.95	Pfdn6	FBgn0036918
M9NFR5_DROME (+1)	0.001	4.95	yps	FBgn0022959
1433E_DROME	< 0.0001	4.94	14-3-3epsilon	FBgn0020238
Q9VWH9_DROME-DECOY	0.001	4.9	CG12204	FBgn0031022
Q86BM5_DROME (+1)	< 0.0001	4.87	Akap200	FBgn0027932

A list of the top 50 hits from the curated list. The full table can be found at: https://www.molbiolcell.org/doi/suppl/10.1091/mbc.E21-04-0187/suppl_file/mc-e21-04-0187-s03.xlsx

Table 3. Dlg-APEX2 proteomics GO analysis
The full table can be found at: https://www.molbiolcell.org/doi/suppl/10.1091/mbc.E21-04-0187/suppl_file/mc-e21-04-0187-s04.xlsx

Table 4. Key Resources

fly line	source	identifier
dlg::EGFP	Bloomington Drosophila Stock Center	Flybase ID: FBst0059417
D174Gal4	Chen et al., 2008	Flybase ID: N/A
UAS-3xMyc::APEX2::Dlg	Norbert Perrimon	Flybase ID: N/A
$dlg^{40.2}$	Mendoza-Topaz et al., 2008	Flybase ID: FBal0240608
dlg^{m52}	Perrimon, 1988	Flybase ID: FBal0002683
yw	Bloomington Drosophila Stock Center	Flybase ID: FBst0001495
lgl::GFP-C	Huang et al., 2009	Flybase ID: FBal0247905
$scrib^{2}$	Bilder and Perrimon, 2000	Flybase ID: FBal0103576
$scrib^{3}$	Wu et al., 2001	Flybase ID: FBal0127890
E(bx)::GFP	Bloomington Drosophila Stock Center	FlybaseID: FBst0068180
polybromo::GFP	Bloomington Drosophila Stock Center	FlybaseID: FBst0055823
HhGal4	Bloomington Drosophila Stock Center	Flybase ID: FBal0121962
UAS-dlg-RNAi 41136	Vienna Drosophila RNAi Center	FlybaseID: FBst0463952
ptc-Gal4, tubGal80ts (aka ptc^{ts}*Gal4)*	Bloomington Drosophila Stock Center	FlybaseID: FBti0002124

tub-GAL80ts	Bloomington Drosophila Stock Center	FlybaseID: FBti0027799
UAS-NLS-GFP	Bloomington Drosophila Stock Center	FlybaseID: FBti0012492
UAS-E(bx)-RNAi	Bloomington Drosophila Stock Center	FlybaseID: FBst0033658
UAS-iswi-RNAi	Bloomington Drosophila Stock Center	FlybaseID: FBst0032845
UAS-scrib-RNAi 39073	Bloomington Drosophila Stock Center	FlybaseID: FBst0039073
UAS-scrib-RNAi 35748	Bloomington Drosophila Stock Center	FlybaseID: FBti0145013
UAS-yki^{S168A}	Zhang et al., 2009??	FlybaseID: FBal0265568
UAS-dlg-RNAi 39035	Bloomington Drosophila Stock Center	Flybase ID: FBst0039035
UAS-GFP	Bloomington Drosophila Stock Center	FlybaseID: FBti0013988
ex-LacZ	Bloomington Drosophila Stock Center	FlybaseID: FBal0031223
act>y+>GAL4 UAS-his::RFP	Bloomington Drosophila Stock Center	FlybaseID: FBst0030558
hsFLP[122]	Struhl and Basler, 1993	FlybaseID: FBtp0001101
hsFLP[1] tub-GAL80 FRT19A	Lee and Luo, 1999	FlybaseID: FBst0005134
act-GAL4 UAS-GFP	Lee and Luo, 1999	FlybaseID: FBst0042726
UAS-Dlg-HA	This study	Flybase ID: N/A
UAS-Dlg$^{2XNLS>A}$-HA	This study	Flybase ID: N/A
UAS-RFP-RNAi-67852	Bloomington Drosophila Stock Center	Flybase ID: FBst0067852

E(bx)[NURF301-4]	Bloomington Drosophila Stock Center	Flybase ID: FBst0009904
antibody	**source**	**identifier**
Rabbit anti-aPKC 1:500 (IF)	Santa Cruz Biotech	SC-937; RRID:AB_632229
Mouse anti-myc 1:500 (IF) 1:2000 (Western)	Sigma-Aldrich	M4439; RRID:AB_439694
Streptavidin-HRP 1:50,000 (Western)	Invitrogen	Cat. No: 19534-050
GP anti-Scrib 1:500 (IF) 1:2000 (Western)	Bilder Lab	
Mouse anti-Dlg 1:1000 (IF) 1:5000 (Western) 1:2400 (PLA) 1:100 (IF)	DSHB	4F3 RRID; AB_528203
Mouse anti-Lamin 1:1000 (Western)	DSHB	adl67.10; RRID:AB_528336
Mouse anti-Tubulin 1:5000 (Western)	DSHB	E7; RRID:AB_528499
Rabbit anti-GFP 1:6000 (PLA) 1:45,000 (Western)	Torrey Pines	TP401; RRID:AB_10013661
Rabbit anti-β-gal 1:1000 (IF)	Abcam	AB616; RRID:AB_305327
Rabbit anti-HA tag 1:500 (IF)	Cell Signaling Technologies	3724; RRID: AB_1549585
Mouse anti-HA tag 1:10,000 (WB)	Cell Signaling Technologies	2367; RRID:AB_10691311
Rabbit anti-cleaved Drosophila Dcp-1 1:500 (IF)	Cell Signaling Technologies	9578; RRID:AB_2721060
Mouse anti-GAL4 (RK5C1) 1:1000 (IF)	Santa Cruz Biotech	SC-510; RRID:AB_627655
chemical	**source**	**identifier**
PonceauS		
Phalloidin-TRITC 1:500	Sigma-Aldrich	P1951; RRID:AB_2315148
DAPI	Thermo	D1306, RRID:AB_2629482
software	source	identifier
Fiji	ImageJ	http://fiji.sc/

Illustrator	Adobe	www.adobe.com/uk/products/photoshop.html
Excel	Microsoft	https://products.office.com/en-us/excel
Prism	Graphpad	www.graphpad.com/scientificsoftware/prism/
Zen	Zeiss	
Scaffold	Proteome Software	http://www.proteomesoftware.com/products/scaffold/
Cytoscape	Cytoscape Consortium	https://cytoscape.org/
Clustal Omega	EMBL-EBI	https://www.ebi.ac.uk/Tools/msa/clustalo/
SnapGene Viewer	SnapGene	https://www.snapgene.com/

Chapter 5:
Parallel regulation of epithelial polarity by endocytic traffic and the Scrib module

Mark J Khoury and David Bilder

ABSTRACT
Intracellular vesicle trafficking is crucial for many developmental and homeostatic processes. Delivery of specific cargo proteins to the appropriate subcellular compartment or membrane domain allows cells to carry out their physiological functions and the resulting asymmetry is a defining feature of cell polarity. Vertebrate cell culture assays have long provided evidence for exocytic traffic in control of cell polarity. For the *in vivo Drosophila* system, evidence has been less clear and more focused on endocytosis. Due to the phenotypic similarities between mutants in Scrib module genes and those encoding endocytic regulators, we investigated the relationship between the Scrib module and the endocytic trafficking pathway using the *Drosophila* follicle and imaginal disc epithelia. We find that despite the highly similar mutant phenotypes, endocytosis and the Scrib module regulate epithelial polarity in independent pathways. Scrib and Dlg localize to the basolateral membrane normally in the absence of endocytosis and aPKC-Lgl antagonism is incompletely disrupted in endocytic mutants. Furthermore, genetic interactions reveal additive phenotypes in Scrib module-endocytic double mutants. Although acting in parallel, apicobasal antagonism does contribute to cargo sorting by the retromer complex and reciprocally, apical endocytosis may provide negative feedback to limit apical domain spread. Finally, we rule out mis-sorting of the *Drosophila* TNF receptor Grindelwald (Grnd) as contributing to the neoplastic tumor phenotype in Scrib module mutants and show that Grnd can signal from the plasma membrane in the absence of endocytosis. Our data provide insight into the functional relationship between core cell polarity complexes and the intracellular trafficking machinery and highlight the complexity of the cell polarity network.

INTRODUCTION

Intracellular vesicle trafficking is an essential process by which cells can deliver macromolecular cargoes to specific locations. In addition to internal membrane-bound compartments, vesicle trafficking is used to sort proteins at the plasma membrane (Rodriguez-Boulan et al., 2005; Román-Fernández and Bryant, 2016; Stoops and Caplan, 2014). Localization of specific molecules to different parts of the cell cortex is the defining feature of cell polarity (Goldstein and Macara, 2007; Johnston, 2018; St Johnston and Ahringer, 2010). Many cell types, notably epithelial cells, depend on polarity for their development, physiology and homeostasis (Rodriguez-Boulan and Macara, 2014; St Johnston and Ahringer, 2010). Thus, it is intuitive that directed vesicle trafficking and cell polarity must be functionally linked. Indeed, directed traffic is crucial in a number of polarized cell types. Migrating cells use endocytosis to modulate the activity of signaling receptors at the leading edge, shape chemokine gradients and remodel adhesion sites (Jékely et al., 2005; Kriebel et al., 2008; Nishimura and Kaibuchi, 2007). Neurons use both endocytosis and directed cargo sorting to selectively localize proteins to either axons or dendrites (Al-Bassam et al., 2012; Farías et al., 2012; Lee et al., 2012; Sampo et al., 2003). In more specialized cases, cells undergoing complex morphogenetic movements during embryogenesis rely on endocytosis and other trafficking pathways to give rise to cell shape change, junctional rearrangement and organ assembly (Lanahan et al., 2010; Lee and Harland, 2010; Pelissier et al., 2003; Riggs et al., 2003; Roeth et al., 2009; Sokac and Wieschaus, 2008; Song et al., 2013).

In epithelial cells in particular, polarized transport has been heavily implicated in the establishment and maintenance of cell polarity (reviewed in (Jewett and Prekeris, 2018; Mostov et al., 2003; Román-Fernández and Bryant, 2016)). *In vitro* studies using epithelial cell lines has demonstrated roles of endocytosis, recycling and secretion pathways in apical membrane establishment and lumen formation by delivery of apical cargoes such as Crumbs3 and podocalyxin; in the latter case by removing it from the basal surface and redirecting it to the apical membrane initiation site (AMIS) (Bryant et al., 2010; Bryant et al., 2014; Schlüter et al., 2009). Interestingly, work on polarized trafficking in epithelia in vertebrates has mostly focused on exocytosis and recycling; biosynthetic traffic was proposed to be the major delivery route to the basolateral membrane and most apical traffic was thought to be a combination of secretion and transcytosis from the basolateral side (Bartles et al., 1987; Bryant et al., 2014; Deborde et al., 2008; Hunziker and Fumey, 1994; Mostov et al., 2003). Specific sorting signals for apical versus basolateral sorting have also been identified (Stoops and Caplan, 2014; Weisz and Rodriguez-Boulan, 2009). Despite these advances, mechanistic links between trafficking and polarity proteins have remained understudied and applicability of these findings to *in vivo* epithelia has been mixed (Shivas et al., 2010).

A series of studies in *Drosophila* sparked renewed interest in crosstalk between trafficking and polarity when it was found that cells mutant for genes encoding endocytic pathway components exhibit loss of epithelial cell polarity and neoplastic overgrowth, strikingly phenocopying mutants in the basolateral polarity regulating Scrib module (Lu and Bilder, 2005; Menut et al., 2007; Moberg et al., 2005; Morrison et al., 2008; Robinson and Moberg, 2011; Vaccari and Bilder, 2005; Windler and Bilder, 2010). Several intriguing models have been proposed to account for how disrupted endocytosis could lead to polarity loss (Fletcher et al., 2012; Shivas et al., 2010), but general mechanistic principles to link endocytosis and the Scrib module in epithelia have been difficult to identify, although a few functional interactions have been reported (de Vreede et al., 2014; Liu et al., 2017; Parsons et al., 2014).

In this work, we sought to rigorously test the functional relationship between endocytosis and the Scrib module. We demonstrate that both the Scrib module and endocytosis act to limit apical domain spread in separate, parallel pathways and that endocytic dysfunction is insufficient to account for Scrib module mutant phenotypes. Our work highlights the complexity inherent in the cell polarity circuit and suggests that crosstalk between polarity and trafficking is likely multilayered and indirect.

RESULTS

Scrib module localization is independent of endocytic trafficking

Epithelial cells mutant for genes in various steps of the endocytic trafficking pathway lose apicobasal polarity and tissue architecture and form neoplastic tumors (Vaccari and Bilder, 2009). Due to the similarity of these phenotypes and mutants of the Scrib module genes *scrib, dlg* and *lgl,* we wondered if the defects in endocytic mutants reflected impaired function of Scrib module proteins (Vaccari and Bilder, 2009). Because localization of polarity proteins to the plasma membrane is crucial to their function (Johnston, 2018; Martin-Belmonte and Mostov, 2008; Rodriguez-Boulan and Macara, 2014; St Johnston and Ahringer, 2010), we began by examining the localization of Scrib, Dlg and Lgl in cell clones mutant for the endocytic adaptor gene, *ap2σ* (*ap2σ*^{KG0245})(Windler and Bilder, 2010). We restricted our analysis to the follicle epithelium of the ovary because the simple monolayered epithelial architecture allows facile evaluation of polarity. However, we did not detect defects in localization of Scrib, Dlg nor Lgl in *ap2σ*^{KG0245} mutant cells and all three proteins localized normally in the mutant clones compared to WT twin spots (**Fig. 5.1A,B,** quantified in **1C**). As a second method of altering endocytic function, we increased endocytic flux by overexpressing the early endosome regulator Rab5 along with a constitutively active form of Rab11 (Rab11^{CA}), a regulator of recycling endosomes. Scrib and Dlg localization was also normal in follicle cells co-overexpressing Rab5 and Rab11^{CA} (**Fig. 5.1D**). Finally, to test the possibility that Scrib module localization is influenced by regulated turnover and degradation, we overexpressed Hrs, an ESCRT-0 protein that mediates recognition of ubiquitinylated cargo for internalization into multivesicular bodies (MVBs)(Grant and Donaldson, 2009). However, we did not observe altered Scrib or Dlg localization in Hrs overexpressing cells (**Fig. 5.1E**). Together, these results indicate that Scrib module cortical localization is independent of endocytic trafficking and suggests the possibility that the Scrib module functions upstream or in parallel to endocytosis to regulate apicobasal polarity.

Apicobasal polarity antagonism retains function in endocytic mutants

As the Scrib module proteins localized normally in endocytic mutants, we wondered if they were also functioning properly. The Scrib module functions to block spread of the apical Par complex into the basolateral domain (Elsum et al., 2012). Lgl is the primary actor, as it is both a substrate and a competitive inhibitor of the apical kinase, aPKC (Betschinger et al., 2003; Lee et al., 2006; Wirtz-Peitz et al., 2008). In contrast, Scrib and Dlg participate indirectly, by protecting Lgl from aPKC phosphorylation at the basolateral side (See Chapter 2, (Khoury and Bilder, 2020; Ventura et al., 2020)). To assess the status of apicobasal antagonism, we analyzed the localizations of aPKC and Lgl in *ap2σ*^{KG0245} mutant follicle cell clones. As expected, these cells exhibit phenotypes of polarity loss, such as multilayering and aPKC and Lgl mislocalization in multilayered areas of the epithelium (**Fig. 5.2A)**. Unlike Scrib module mutants, aPKC mislocalization was incompletely penetrant in *ap2σ*^{KG0245} mutant cells (**Fig. 5.2A**). Interestingly,

we note that even though lateral aPKC spread is observed, mutual exclusion between apical and basolateral identities can still maintained in some cases (**Fig. 5.2B,C**).

These results suggest that some amount of Scrib module function is maintained in the absence of endocytosis. Consistent with this idea, when we co-depleted *dlg* and the endocytic adaptor *ap2α* by RNAi, we observed enhanced aPKC spread to the lateral membrane, compared to cells depleted for *ap2α* alone (**Fig. 5.2F,G**). In contrast, cells expressing *ap2α* RNAi alone maintain cortical Lgl levels, although its basolateral distribution may be altered (**Fig. 5.2D,H**). Interestingly, we noticed that although greatly enhanced in *ap2α dlg* double depleted cells (**Fig 5.2I**), *ap2α* depleted cells nevertheless exhibited a significant degree of aPKC mislocalization compared to WT cells (**Fig. 5.2I)**. Together, these results support the idea that endocytic traffic and the Scrib module regulate polarity via incompletely overlapping mechanisms.

Endocytosis and the Scrib module exhibit additive interactions

To further probe the functional relationship between the Scrib module and endocytic trafficking pathways, we examined the localization of the apically localized Notch receptor (NECD), as a readout of endocytic traffic. In *ap2α* depleted follicle cells, NECD accumulated in enlarged puncta associated with the cell cortex, presumably representing failed endocytic events, as observed previously (**Fig. 5.3A,B**)(Windler and Bilder, 2010). In contrast, in *dlg* depleted cells, NECD was weakly mislocalized to the lateral membrane, but did not strongly accumulate intracellularly (**Fig. 5.3C,D**). When we combined *ap2α* and *dlg* loss of function, we observed a novel phenotype in which there was accumulation of NECD puncta as in *ap2α* alone, but also a greatly enhanced basolateral cortical trapping compared *dlg* alone (**Fig. 5.3E,F**). We interpret this to be an additive phenotype in the *ap2α dlg* double depleted cells that arises because failure to internalize NECD due to *ap2α* loss reveals the mislocalization resulting from *dlg* knockdown. This genetic interaction provides further support for a model where endocytosis and the Scrib module function in separate, parallel pathways.

The balance of Par-Scrib antagonism regulates retromer

Previous work has shown that the Scrib module regulates cargo trafficking via the retromer pathway, but how this contributes to polarity establishment or maintenance is not known (de Vreede et al., 2014; Lohia et al., 2012). One hypothesis is that the Scrib module could control the levels of specific polarity-relevant proteins at the membrane by controlling their recycling via retromer. Crb has been proposed to be one such protein, since it is a retromer cargo (Pocha et al., 2011; Zhou et al., 2011). Crb localization to the apical membrane is also known to be aPKC dependent, and its lateral mislocalization in *scrib* mutants is rescued upon co-depletion of aPKC (Khoury and Bilder, 2020; Morais-de-Sá et al., 2010; Sotillos et al., 2004). Therefore, we wondered if Par-Scrib antagonism played a role in setting the balance of retromer-dependent trafficking. Using Vps26 as a marker of the core retromer complex, we observed localization in concentrated apical puncta in WT follicle cells (**Fig. 5.4A'**). Upon knockdown of *dlg*, we observed a depletion of this concentrated apical localization, similar to what has been described previously in imaginal discs (**Fig. 5.4A'**)(de Vreede et al., 2014). When we co-depleted *apkc* within *dlg* knockdown cells, we observed largely restored apical Vps26 localization (**Fig. 5.4B'**). We also noticed that NECD mislocalization to the lateral membrane was partially rescued in *dlg apkc* double knockdown cells (**Fig. 5.4A,B**). Together, these data suggest that the balance of Par-Scrib antagonism regulates retromer trafficking. Furthermore, our data using NECD localization suggest that apical cargo sorting is independent of mutual antagonism between the apical and basolateral

domains, as laterally mislocalized NECD in *scrib* mutants is rescued to its normal apical position in the absence of both the Par complex and Scrib module.

aPKC maintains apical identity in part by limiting internalization of apical proteins

The ability of NECD to be properly trafficked to the apical membrane in the absence of a functional polarity circuit is puzzling because previous work has argued for a model in which polarity regulators directly influence endocytic trafficking to achieve a steady state polarized distribution of transmembrane cargoes, such as Crb (Fletcher et al., 2012). These studies have suggested that the Par complex stabilizes the apical localization of such proteins by inhibiting their endocytosis (Georgiou et al., 2008; Harris and Tepass, 2008; Leibfried et al., 2008), whereas the Scrib module may promote their recycling back to the apical surface (de Vreede et al., 2014; Fletcher et al., 2012). Therefore, we wondered if the apical expansion phenotype seen in *scrib* module mutants could be alleviated by removal of apical determinants through increased endocytic internalization. To test this, we overexpressed constitutively active Rab5 ($Rab5^{Q88L}$) in follicle cells depleted of *dlg* by RNAi and assessed apical spread by examining aPKC localization. Compared to *dlg* RNAi alone, cells co-expressing $Rab5^{Q88L}$ had reduced levels of aPKC mislocalization to the lateral membrane (**Fig. 5.5A-C**). However, this was a partial rescue as *dlg* cells expressing $Rab5^{Q88L}$ still exhibited significantly increased lateral aPKC spread compared to WT (**Fig 5.5C**). Together, these results support a model where the Par complex maintains apical identity in part by limiting endocytosis of apical proteins.

Defective Grnd trafficking does not contribute to neoplasia in *scrib* mutants

In the imaginal disc, mutation in genes encoding Scrib module proteins or endocytic regulators results in formation of neoplastic tumors (Vaccari and Bilder, 2009). It is known that tumorigenic overgrowth in *scrib* mutants requires c-Jun N-terminal Kinase (JNK) signaling activity (Igaki et al., 2006; Richardson and Portela, 2018). JNK is a mitogen activated protein kinase (MAPK) pathway that is activated under a number of pathological and stress conditions in *Drosophila*. In the context of tumorigenesis, it has been shown that in many cases, the *Drosophila* Tumor Necrosis Factor Receptor (TNFR) homolog, Grindelwald (Grnd) is upstream of JNK activation and is required for overgrowth and polarity loss phenotypes (Andersen et al., 2015; de Vreede et al., 2018). Because mis-trafficking of mitogenic receptors has been previously shown to be causative of tumorous overgrowth in certain neoplastic tumor suppressor mutants (Vaccari and Bilder, 2005; Vaccari et al., 2009), we hypothesized that dysfunctional Grnd trafficking might be a mechanism for neoplasia in *scrib* mutants. When we examined Grnd in *dlg* mutant wing imaginal discs, we noticed mislocalization compared to WT, as noted previously (**Fig. 5.6A,B**)(de Vreede et al., 2022). This is not due to increased *grnd* transcription (Bunker et al., 2015). The punctate localization was reminiscent of endocytic compartments, thus we performed colocalization studies of Grnd with a panel of markers for various vesicular compartments in the endocytic and biosynthetic trafficking pathways. However, we noted no significant difference in colocalization of Grnd with any of these markers or in the morphology of these compartments themselves in *dlg* mutants compared to WT (**Fig. 5.6C-T**)(de Vreede et al., 2014). Treatment with lysosomal degradation inhibitors also revealed no difference in Grnd accumulation in Arl8+ lysosomes in *dlg* mutants compared to WT (**Fig. 5.6U,V**). Together, these data fail to find evidence for a specific mis-trafficking of Grnd in *scrib* module mutants.

To assess whether there exists a general defect in endocytosis in *scrib* module mutants, we used a pulse-chase assay where the extracellular domain of NECD is labeled with specific

antibodies in live tissue *ex vivo* and then its internalization and trafficking along the endolysosomal pathway can be followed (Le Borgne and Schweisguth, 2003). When we performed this assay in *dlg* mutant wing disc tumors, we did not observe any obvious differences compared to WT at any time point examined (**Fig. 5.7A,B**); NECD was internalized and degraded within 5 hours, as previously described for WT cells (Lu and Bilder, 2005). We also repeated this experiment in clones of cells knocked down for *dlg*, as it has been proposed that increased rates of endocytosis facilitate elimination of *dlg* mutant cells in the context of cell competition (Igaki et al., 2009). However, we failed to find any difference in NECD trafficking in *dlg* clones compared to surrounding WT tissue (**Fig. 5.7C**), suggesting that *scrib* module mutants have no defects in general endocytic trafficking, consistent with previous studies (de Vreede et al., 2014).

Grnd signaling in the absence of endocytosis

Given the lack of evidence for an endocytic defect in *scrib* mutants and for a Grnd-specific trafficking defect, we wondered if JNK signaling downstream of Grnd reflected a conserved, endocytosis-independent mechanism of tumor formation. *grnd* knockdown suppresses the neoplastic tumor phenotype of early endocytic *avl* RNAi (**Fig. 5.8A-C**), consistent with previous observation (Andersen et al., 2015). *grnd* knockdown and downstream JNK inhibition via expression of dominant negative JNK (Bsk^{DN}) are equally effective at suppressing the *avl* phenotype, suggesting that Grnd is the main input to JNK signaling that drives neoplasia in this context (**Fig. 5.8C,D**). Importantly, although blocking JNK signaling rescues the tumor phenotype in *avl* mutants, endocytosis is not restored, as we do not observe intracellular NECD puncta as seen in WT (**Fig. 5.8E-G**)(Vaccari et al., 2008; Windler and Bilder, 2010). In many cases, mammalian TNFRs are internalized in multimeric complexes to large, specialized endosomes called signalosomes where they are active in signaling (Schneider-Brachert et al., 2013; Schütze et al., 2008). Since the *avl* phenotype is Grnd-dependent, we wondered whether this reflected an ability of Grnd to signal from the plasma membrane. To test this we took advantage of a previously established conditional cell ablation system that relies on expression of the TNF Eiger (Egr)(Smith-Bolton et al., 2009) in combination with a temperature sensitive mutant of the early endocytic regulator, Shibire (*Drosophila* dynamin, Shi^{ts}). This allowed us to induce Egr/Grnd-dependent cell ablation while blocking endocytosis (**Fig. 5.8K**). When we induced ablation at the restrictive temperature for Shi^{ts}, we observed identical extents of cell death in both the control and Shi^{ts}-endocytosis inhibited cases and robust induction of MMP1, an Egr-JNK target gene (**Fig. 5.8H-J**). Similarly, we observed that overexpression of transgenic Egr in *avl* depleted wing discs was also able to cause cell death (**Fig. 5.8L,M**). These results suggest that Egr-Grnd signaling can occur from the plasma membrane and does not require endocytosis.

DISCUSSION

Polarity proteins and endocytic regulators can be viewed as different evolutionary solutions to an identical biological problem: asymmetric localization of proteins and other molecules within the cell. Despite this, a detailed understanding of crosstalk between the cell polarity and vesicle trafficking machineries is lacking. Work in mammalian tissue culture supports the idea that membrane traffic is crucial to build a polarized cell (Jewett and Prekeris, 2018; Rodriguez-Boulan et al., 2005; Román-Fernández and Bryant, 2016; Weisz and Rodriguez-Boulan, 2009). However, the conservation of these findings to *in vivo* systems is unclear (Shivas et al., 2010; Vaccari and Bilder, 2009). Similarly, the demonstration that endocytosis affects epithelial polarity in *Drosophila* was surprising, both because exocytosis was thought to be the major contributor to

polarity in vertebrate cells and because endocytosis is an essential process; thus the survival (and polarity loss) of endocytic mutant cells was puzzling (Vaccari and Bilder, 2009). Here, we sought to explore the relationship between the endocytic and basolateral polarity pathways. Our results support a model where endocytosis and the Scrib module operate in distinct, parallel pathways to polarize epithelial cells. We propose that both pathways function to limit the size and spread of the apical domain, but may operate on different targets.

Localization of several apical polarity regulators has been previously shown to depend on endocytic traffic (Stoops and Caplan, 2014). Specifically, Crb, the sole transmembrane protein among polarity regulators, requires a combination of AP2-dependent endocytosis, retromer-mediated recycling and Rab11 trafficking for its proper localization (DeBruhl et al., 2015; Fletcher et al., 2012; Pocha et al., 2011; Roeth et al., 2009; Zhou et al., 2011). Intriguingly, it was recently shown that, although not a transmembrane protein, aPKC also requires the Rab11 pathway for its localization (Calero-Cuenca and Sotillos, 2018; Calero-Cuenca et al., 2016). As Crb localization is also dependent on aPKC kinase activity (Morais-de-Sá et al., 2010; Sotillos et al., 2004), it will be interesting to determine whether aPKC also regulates the endocytic itinerary of Crb. In contrast, the dependence of Scrib module localization on intracellular traffic was not known. It has been noted previously that both Scrib and Lgl often exhibit punctate staining patterns reminiscent of vesicles (Bilder and Perrimon, 2000; Legouis et al., 2003; Liu et al., 2017; Parsons et al., 2014). However, we find that localization of all three Scrib module proteins is unaffected by inhibiting AP2-dependent endocytosis. This suggests that if Scrib module proteins do associate with vesicles, it is not to regulate their own localization, but potentially an unknown effector function. We note that while Scrib module localization is AP2-independent, other endocytic pathways could contribute, as cells have multiple, non-equivalent endocytic pathways (Doherty and McMahon, 2009; Windler and Bilder, 2010).

For most polarity regulators, including the Scrib module, cortical localization is required for function (Johnston, 2018; Martin-Belmonte and Mostov, 2008; Rodriguez-Boulan and Macara, 2014; St Johnston and Ahringer, 2010). The normal localization of Scriba bd Dlg in *ap2* mutants suggests that these proteins are still functional. The incomplete mislocalization of Lgl in *ap2* mutants in particular, suggests that Scrib and Dlg are still able to protect basolateral Lgl from aPKC to some extent, in the absence of AP2-dependent endocytosis. Furthermore, the ectopic lateral aPKC spread in *ap2* mutants suggests that while endocytosis is dispensable for basolateral polarity, it may be required to maintain apical polarity and/or limit apical domain spread. The mechanisms and key apical molecules subject to this regulation will be important to determine. Two possibilities are Crb and aPKC, as both have already been shown to be regulated by endocytosis, as mentioned above. Consistent with the idea that endocytosis specifically regulates the apical domain, we observe partial rescue of lateral aPKC spread in *dlg* mutants with increased endocytic activity via activated Rab5 expression. This type of mechanism has been previously proposed as a type of feedback in the polarity circuit (Fletcher et al., 2012).

Our findings suggest that both endocytosis and the Scrib module regulate or antagonize apical polarity in parallel. Our genetic interaction experiments reveal a novel mislocalization phenotype of the apical transmembrane cargo, Notch, suggesting that both the Scrib module and endocytic pathways regulate its localization but in distinct manners. Our data suggest that the Scrib module acts to block lateral spread of Notch, whereas endocytosis may promote recycling of inappropriately localized Notch back to the apical membrane, perhaps via a transcytosis route. Indeed, such a model is consistent with both the canonical function ascribed to the Scrib module in preventing lateral spread of the Par and Crb complexes and with previously described recycling

pathways for other transmembrane cargos, such as E-cadherin and FasIII (Desclozeaux et al., 2008; Laiouar et al., 2020; Lock and Stow, 2005; Roeth et al., 2009; Woichansky et al., 2016). Additionally, mislocalization of Notch in polarity mutants has been attributed to the neoplastic overgrowth phenotypes (Vaccari and Bilder, 2005; Vaccari et al., 2008; Windler and Bilder, 2010).

There is ample evidence for crosstalk between the Scrib module and various steps of the intracellular trafficking route. In *Drosophila* Lgl associates with multiple vesicular compartments and is suggested to regulate Notch trafficking and signaling (Parsons et al., 2014; Portela et al., 2018). Lgl has also been implicated in N-cadherin trafficking in the developing mammalian nervous system and polarized trafficking in neurons (Jossin et al., 2017; Wang et al., 2011). Scrib also regulates basolateral cargo sorting in *C. elegans* epithelia, acting as a Rab5 effector, facilitating Rab10 activity during cargo recycling (Liu et al., 2017). Both the Scrib module and Par complex are also involved in cargo sorting through the retromer, an atypical Golgi-to-endosomal recycling pathway (de Vreede et al., 2014; Gallon and Cullen, 2015; Lohia et al., 2012). In spite of these appealing links, the mechanistic basis for their contribution to polarity is murky, although several hypotheses have been proposed (Jewett and Prekeris, 2018; Román-Fernández and Bryant, 2016; Shivas et al., 2010). Previous studies have suggested that Crb is a likely candidate to mediate crosstalk between polarity and trafficking, as it is the only transmembrane polarity regulator (de Vreede et al., 2014; Fletcher et al., 2012; Lu and Bilder, 2005). However, *crb* and endocytic double mutants do not rescue cell polarity (de Vreede et al., 2014). Thus, it is unlikely that there is a single "polarity-regulating cargo" involved in the crosstalk between polarity and trafficking machinery and the functional relationship is certain to be complex.

A second complicating factor arises when considering the second major branch of intracellular traffic: exocytosis. This mode of vesicle transport has received much less attention in the study of cell polarity in *Drosophila*, although some studies suggest that the exocyst complex, required for vesicle fusion with the plasma membrane, participates in epithelial polarity by regulating apical and junctional cargoes (Beronja et al., 2005; Blankenship et al., 2007; Langevin et al., 2005; Li et al., 2007; Murthy and Schwarz, 2003). Interestingly, work in mammalian cell culture originally proposed that exocytic traffic was the primary route for localization of basolateral membrane proteins (Mostov et al., 2003; Stoops and Caplan, 2014). Indeed, mammalian Lgl and its yeast homologs Sro7p and Sro77p interact with secretory machinery, including Rab4 and SNARE proteins (Gangar et al., 2005; Grosshans et al., 2006; Hattendorf et al., 2007; Rossi and Brennwald, 2011; Watson et al., 2015; Zhang et al., 2005). Dlg also associates with myosin and kinesin motors to direct post-Golgi vesicles and the t-SNARE, syntaxin-18 (Asaba et al., 2003; Gorczyca et al., 2007). In addition, we have identified potential interactions of Dlg with several members of the COPII coat complex, Vps13 and Rab1; all involved in secretory traffic (Sharp et al., 2021). One model supported by these observations is that basolateral polarity proteins, like the Scrib module, direct secretory traffic to the basolateral membrane and then apically-destined cargoes are selectively internalized by endocytosis and recycled to the apical membrane (Rodriguez-Boulan et al., 2004; Rodriguez-Boulan et al., 2005; Shivas et al., 2010). This, together with our suggestion of the parallel activities of endocytosis and the Scrib module would give rise to a plausible, integrated view of how polarity and membrane traffic cooperate to polarize epithelial cells.

In addition to polarity itself, previous work has argued for involvement of endocytosis in the JNK-dependent tumorigenesis and cell competition phenotypes of Scrib module mutant cells (Igaki et al., 2009). Our data fail to find support for this, as Scrib module mutants have no apparent defects in endocytosis or Grnd-specific trafficking, and neoplastic Grnd signaling can occur in the

absence of endocytosis. What could be triggering Grnd-JNK signaling during neoplastic transformation? Our data suggest that the receptor-ligand complex would not require internalization to signal. Alternatively, internalization may only be required in the case of competitive elimination (a scenario we did not examine), as mammalian TNFR signalosomes often induce apoptosis (Schütze et al., 2008). Therefore, by signaling from the surface in the tumor context, the signal may be converted to pro-proliferative, rather than pro-apoptotic. The mechanisms that would underlie this speculative sign inversion are unclear. Another possibility is that signaling may be activated at the intracellular side of the receptor in a ligand-independent manner; JNK activation at multiple downstream steps is sufficient to cause neoplastic transformation in cooperation with oncogenic Ras (data not shown) (La Marca and Richardson, 2020). Finally, involvement of the second known *Drosophila* TNFR, Wengen (Wgn) is also possible, although previous work failed to find evidence for involvement in endocytic mutant phenotypes (Andersen et al., 2015; Kanda et al., 2002; Kauppila et al., 2003).

Overall, we propose a model in which the Scrib module and endocytosis regulate polarity in parallel: the Scrib module prevents the spread of the apical domain by as yet unknown mechanisms, perhaps by inhibiting aPKC activity via Lgl, while endocytosis maintains localization of proteins at the apical domain by internalization from the basolateral domain and recycling. We also demonstrate this separation of function in the physiological context of neoplastic tumor formation. Our work provides an important advance in the understanding of the cell polarity network by more clearly defining the functional relationship with the vesicle trafficking pathway and illustrates the complexity in these interactions. Future studies of these relationships will be a challenging but rewarding avenue to understand the mechanisms underlying the spatial organization of cell biology.

MATERIALS AND METHODS

Fly stocks and genetics

Drosophila stocks were raised on cornmeal molasses food at 25°C. *yw* or OreR was used as the WT control. All follicles shown are stages 5-8. Mutant alleles and transgenic lines used are listed in **Table 1**. Mutant follicle cell clones were generated using *hsFLP*. For clonal GAL4 expression using *hsFLP*, larvae were heat shocked once for 13 minutes 120 hours after egg deposition (AED). For all clones, adult females were fed with yeast and dissected 3 days after eclosion. Pan-follicle cell expression was induced in adults using *traffic jam-GAL4 (tj-GAL4)* and temperature-sensitive *GAL80*; these were fed yeast for 2 days before shifting to 29°C for 4 days. Overexpression in imaginal discs used *MS1096-GAL4*. Larvae were dissected between 6 and 9 days AED, depending on the genotype. To induce wing disc ablation with the rn^{ts}>egr system, crosses were kept at 18°C; larvae were upshifted to 29°C for 40 hours to induce egr expression 7dAED then returned to 18°C and dissected 48 hours later.

Immunofluorescence and microscopy

Follicles were dissected in Schneider's medium containing 15% FBS and fixed with 4% PFA in PBS for 20 minutes. Follicles were stained in PBS containing 0.1% Triton X-100, 1% BSA and 4% NGS overnight at 4°C. Primary antibodies and dilutions are listed in **Table 1**. Following secondary antibody incubation at 1:400 for 2 hours at room temperature, tissue was mounted in glycerol-based antifade (Invitrogen). Imaginal discs were dissected from larvae in PBS, fixed with 4% PFA for 20 minutes and stained following the same protocol described above.

Images were acquired using an inverted Zeiss LSM700 laser scanning confocal microscope with LD C-Apochromat 40x/NA 1.1 W or Plan apochromat 63x/NA 1.4 oil objectives at 1024x1024 pixel resolution with 2 line averages. For each experiment, greater than 6 imaginal discs or tissue from at least 5 females was analyzed and at least 10 ovarioles and 20 individual follicles were examined.

Image analysis and quantification

Image processing and quantification was performed using Fiji software (Schindelin et al., 2012). To quantify aPKC localization, intensity was measured by drawing a line along the lateral and apical membranes of a single cell in medial section using the measure function in Fiji. A ratio of lateral:apical intensities was then calculated per cell and used to compute an average ratio per cell per genotype. Lgl cortical intensity measurements were obtained by drawing a line along the membrane of interest of single cells and calculating averages per condition. Scrib and Dlg localization was measured by drawing a line of consistent length perpendicular to the basolateral membrane of single cells and using the plot profile function in Fiji. Apicolateral aPKC and Lgl localization was analyzed similarly, except that lines were drawn along the lateral membrane. The resulting data were then analyzed using Microsoft Excel and Graphpad Prism 6. For significance in statistical tests: n.s.=$p>0.05$, *=$p<0.05$, **=$p<0.01$, ***=$p<0.001$ and ****=$p<0.0001$. The results of all statistical tests are found in **Table 3**. Figures were assembled using Adobe Illustrator.

Endocytosis assays

The Notch pulse-chase experiments were performed as previously described, with modifications (Le Borgne and Schweisguth, 2003; Lu and Bilder, 2005). Briefly, wing imaginal discs were first dissected in Schneider's medium supplemented with 10% FBS and 1% Penicillin/Streptomycin (Pen/Strep) then pulsed with 1:25 anti-NECD antibody for 2 hours at 4°C. Following several washes in ice cold Schneider's media at 4°C, discs were fixed either immediately (t=0) or after 1 to 5 hours in warm Schneider's media at room temperature.

Lysosomal inhibitor experiments were performed as previously described (de Vreede et al., 2014). Wing imaginal discs were dissected in Schneider's media containing 10% FBS and 1% Pen/Strep and cultured for 4 hours in media containing 200μM leupeptin and 50mM NH_4Cl to inhibit lysosomal degradation. Media was replenished after 2 hours. Discs were then fixed and stained as described above.

FIGURES

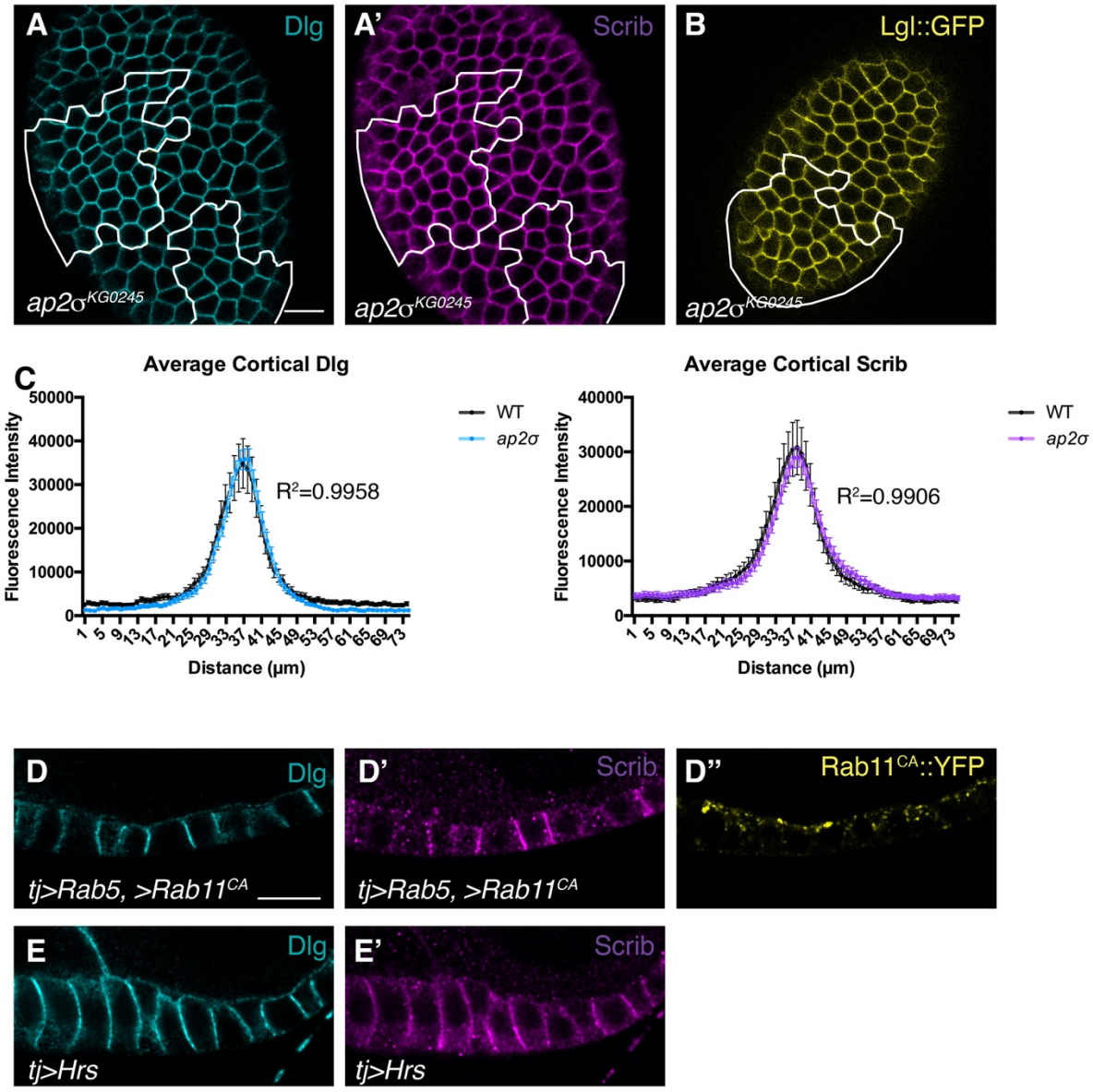

Figure 5.1. Scrib and Dlg localization is independent of endocytosis
(A,B) Dlg (A), Scrib (A') and Lgl (B) localization is unchanged in *ap2σ* mutant follicle cell clones (white lines) compared to control twin spots. (C) Line scan quantification of cortical Dlg and Scrib intensities from (A) across the basolateral membrane of single cells. (D) Ectopic activation of the Rab5-Rab11 pathway does not alter Dlg (D) or Scrib (D') localization in follicle cells. (E) Overexpression of the ESCRT-0 cargo adaptor, Hrs, does not alter Dlg (E) or Scrib (E') localization. Scale bars 10μm. White lines indicate mutant or GAL4 expressing clones in this and all subsequent figures. Error bars in (C) represent S.D. Pearson's correlation, $p<0.0001$ in both cases.

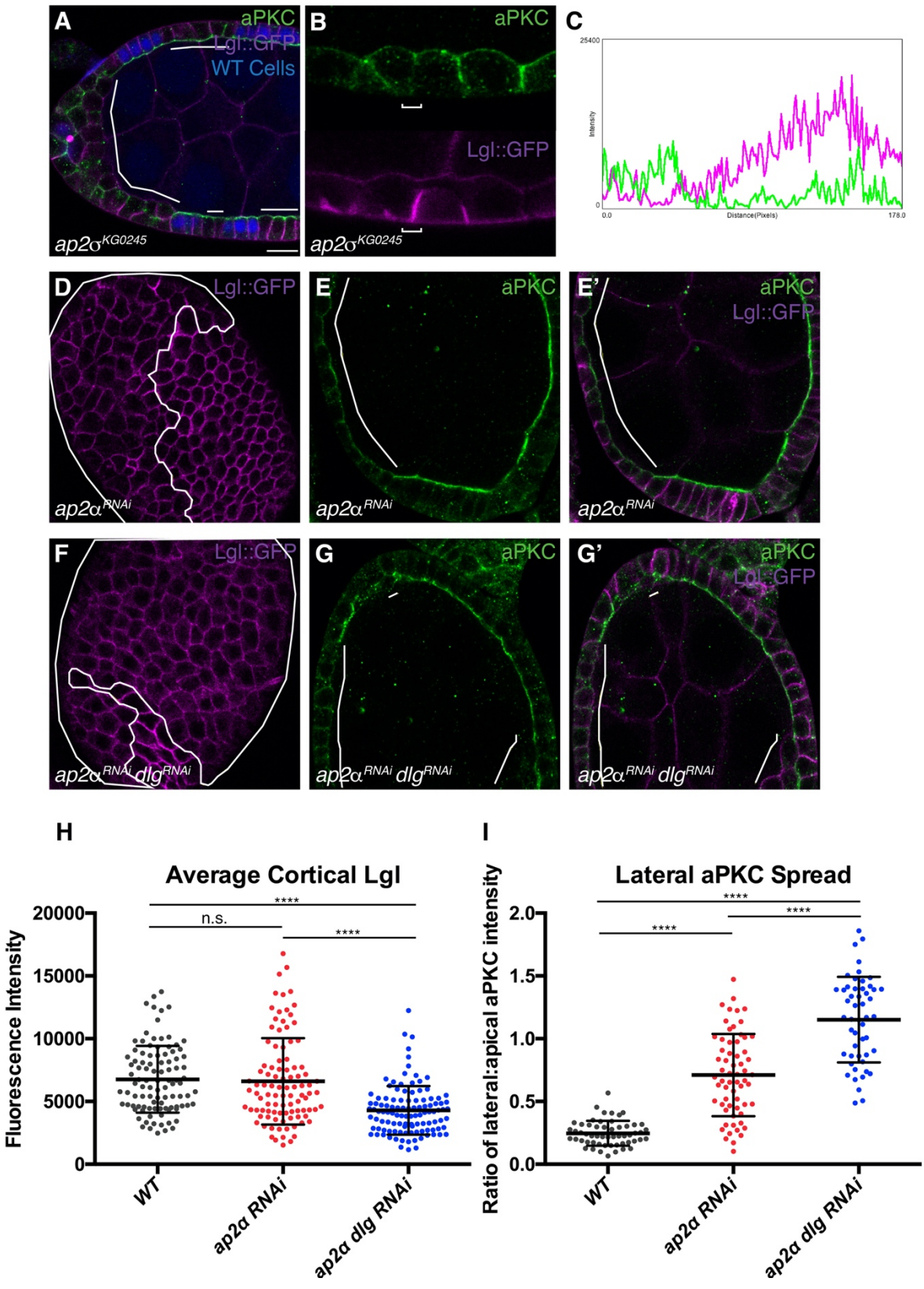
A
aPKC
Lgl::GFP
WT Cells
ap2σKG0245
B
aPKC
Lgl::GFP
ap2σKG0245
C
25400
Intensity
0
0.0
Distance(Pixels)
178.0
D
Lgl::GFP
ap2αRNAi
E
aPKC
ap2αRNAi
E'
aPKC
Lgl::GFP
ap2αRNAi
F
Lgl::GFP
ap2αRNAi dlgRNAi
G
aPKC
ap2αRNAi dlgRNAi
G'
aPKC
Lgl::GFP
ap2αRNAi dlgRNAi
H
Average Cortical Lgl
Fluorescence Intensity
20000
15000
10000
5000
0
n.s.
****
****
WT
ap2α RNAi
ap2α dlg RNAi
I
Lateral aPKC Spread
Ratio of lateral:apical aPKC intensity
2.0
1.5
1.0
0.5
0.0
****
****
****
WT
ap2α RNAi
ap2α dlg RNAi

Figure 5.2. Lgl-aPKC antagonism does not require endocytosis
(A) *ap2σ* mutant follicle cells lose polarity and multilayer at the egg chamber poles. (B) High magnification view of *ap2σ* mutant cells: in some instances, aPKC and Lgl maintain mutually exclusive localization even though aPKC mislocalizes. (C) Line scan of the basolateral membrane bracketed in (B) showing an example of partially maintained exclusivity between Lgl and aPKC localizations. (D-G) loss of *dlg* enhances polarity phenotypes of *ap2α* depleted cells. Lgl (D) and aPKC (E) are mildy affected in *ap2α* depleted cells. Additional loss of *dlg* strongly enhances loss of cortical Lgl (F) and aPKC lateral spread phenotypes (G). (H) Quantification of cortical Lgl levels in *ap2α* compared to *ap2α dlg* double depleted cells as a measure of membrane intensity in single cells. (I) Quantification of aPKC mislocalization in *ap2α* compared to *ap2α dlg* double depleted cells, represented as a ratio of lateral:apical membrane intensity in single cells. Scale bars, 10μm. Error bars represent S.D. One way ANOVA with Tukey's multiple comparisons test.

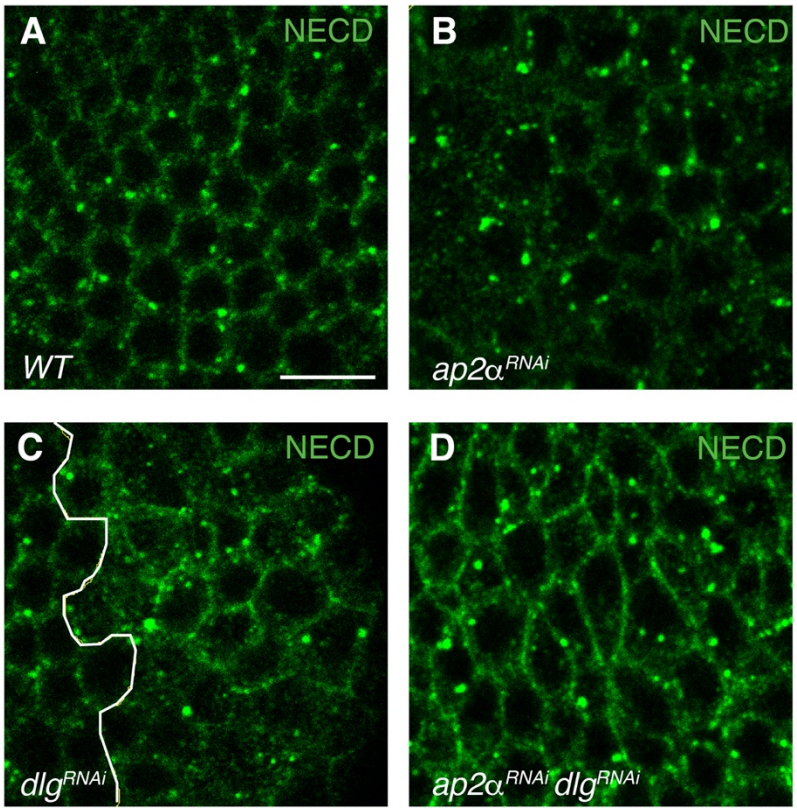

Figure 5.3. Additive phenotypes of Scrib module and endocytic mutants
(A-B) In *ap2α* depleted cells (B), Notch (NECD) is mislocalized and accumulates in intracellular puncta. (C) In *dlg* depleted cells, Notch exhibits weak membrane retention. (D) In *ap2α dlg* double depleted cells, Notch mislocalizes to intracellular puncta as in cells depleted of *ap2α* alone, but cortical retention is strongly enhanced compared to *dlg* depleted cells. Scale bars, 10μm.

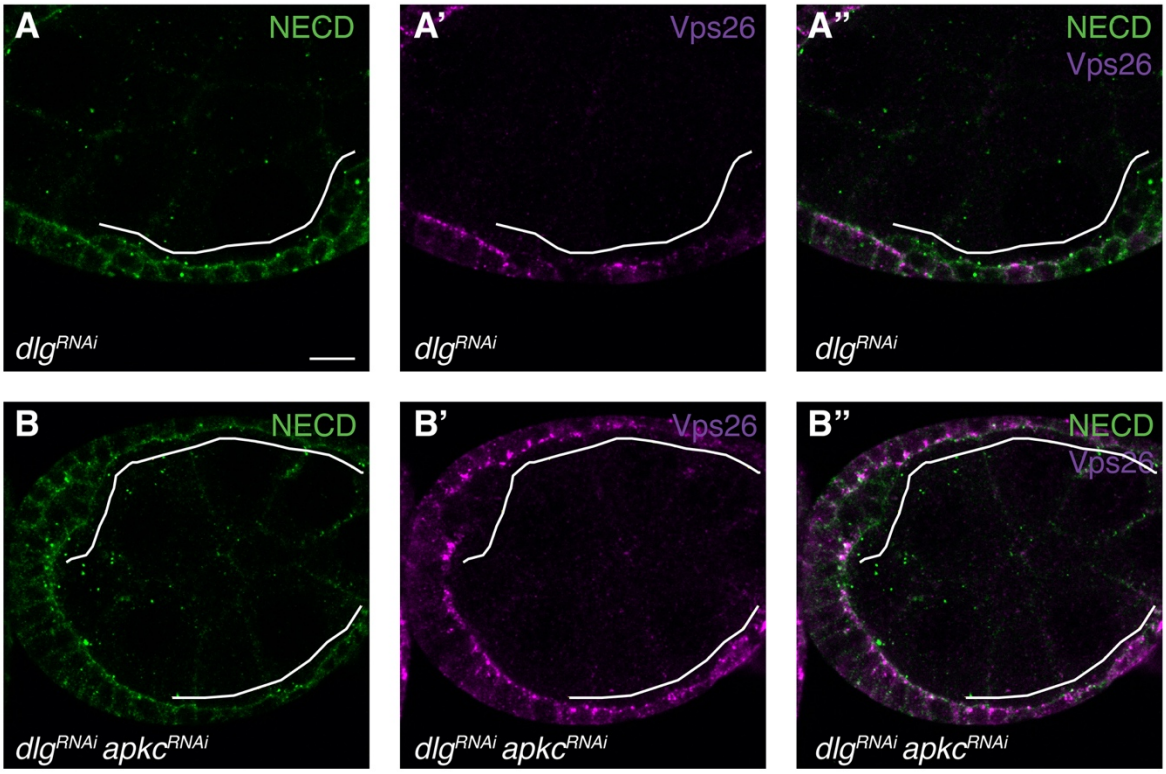

Figure 5.4. Apicobasal antagonism regulates trafficking and retromer
(A) *dlg* depleted cells weakly mislocalize Notch to the lateral membrane and have reduced apical levels of Vps26 (A'). (B) Co-depletion of *apkc* prevents the lateral Notch mislocalization in *dlg* depleted cells and also restores apical Vps26 (B'). Scale bars, 10µm.

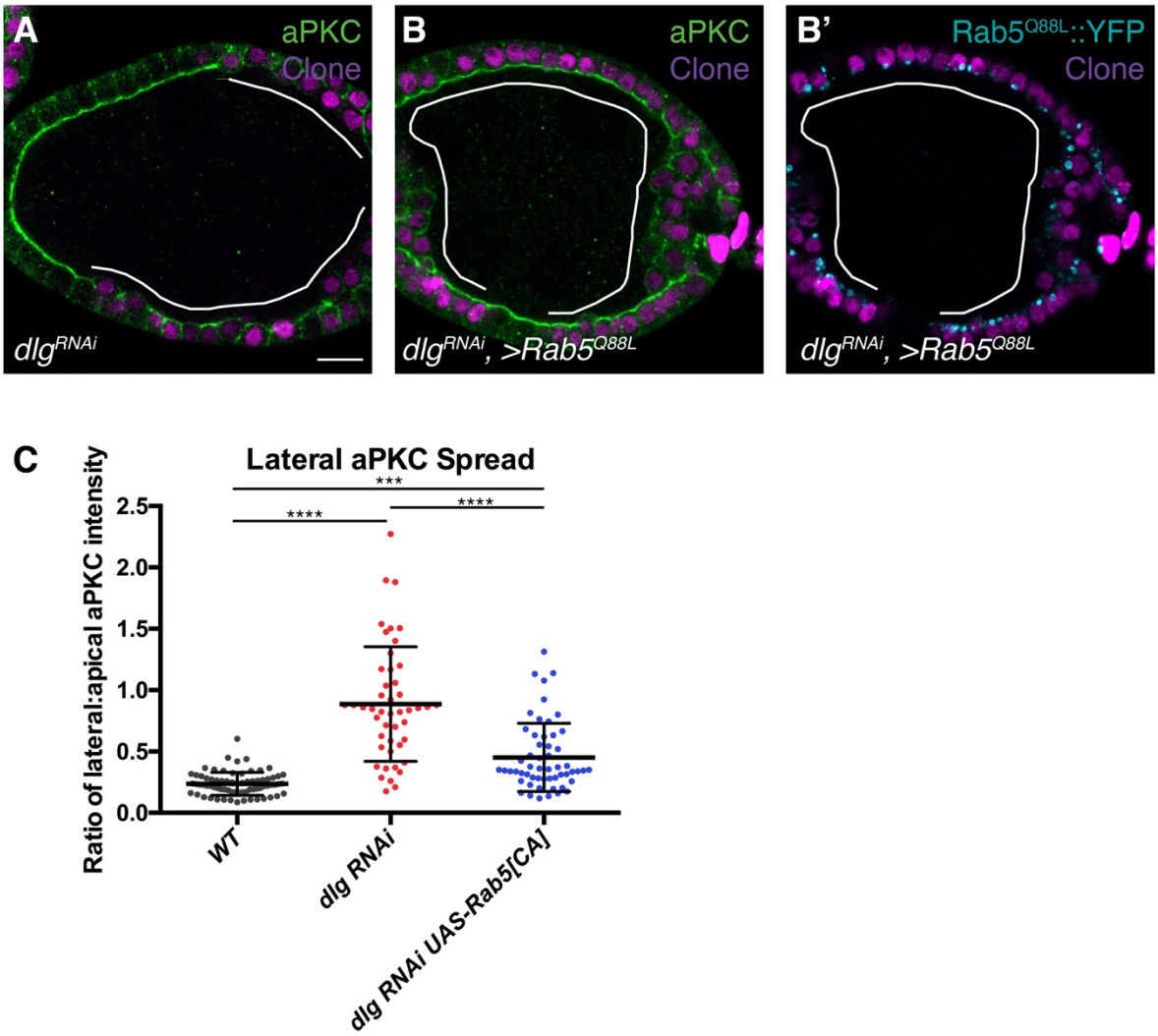

Figure 5.5. Endocytosis can regulate apical domain size independently of the Scrib module
(A) In *dlg* depleted cells, aPKC mislocalizes and spreads through the lateral cortex. (B) Overexpression of constitutively active Rab5 in *dlg* depleted cells partially rescues aPKC mislocalization in *dlg* depleted cells. (C) Quantification of lateral aPKC spread in *dlg* depleted cells with or with out $Rab5^{Q88L}$ expression compared to WT, represented as a ratio of lateral:apical aPKC membrane intensity in single cells. Scale bars, 10µm. Error bars represent S.D. One way ANOVA with Tukey's multiple comparisons test.

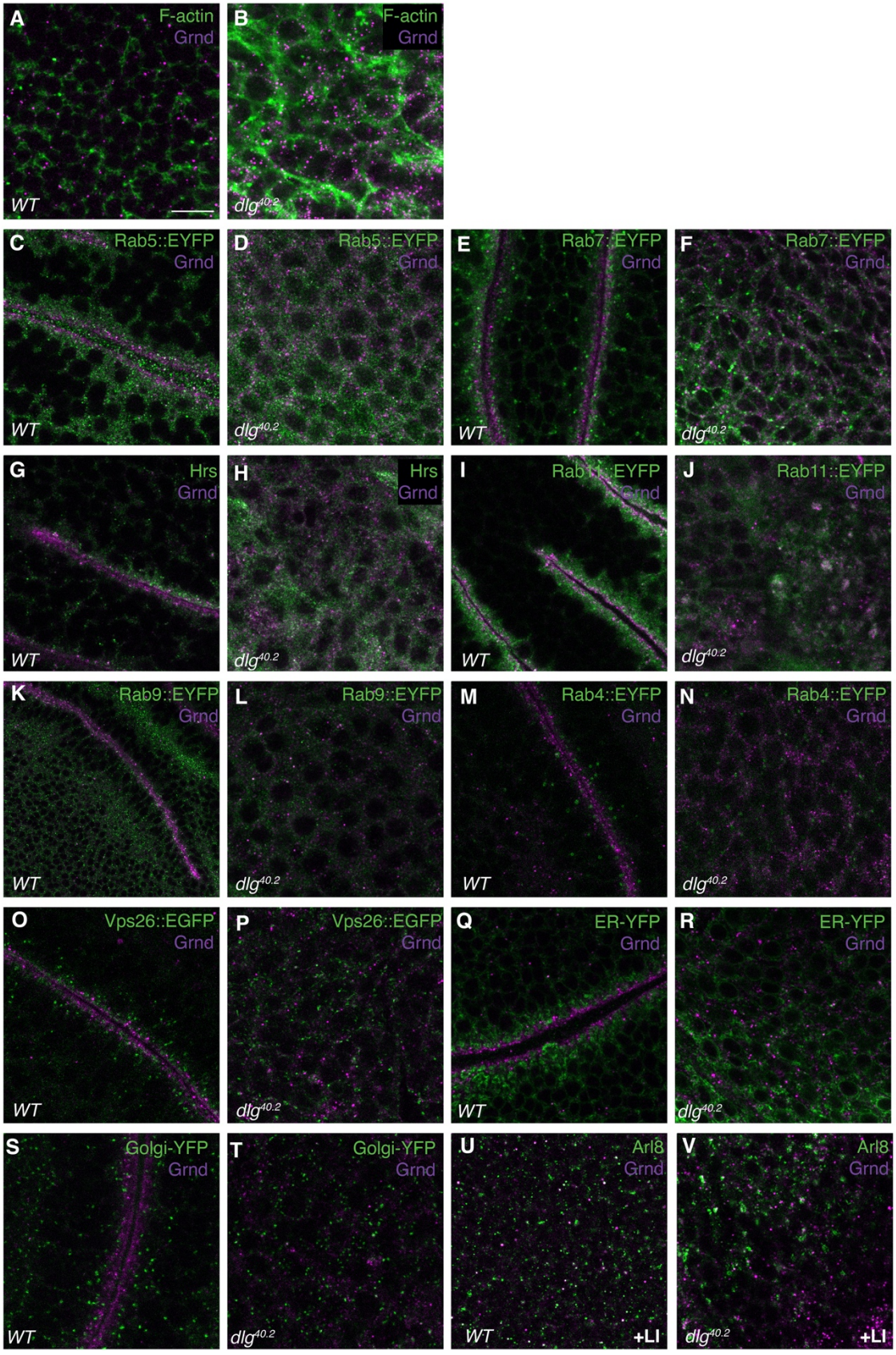
A
F-actin
Grnd
WT
B
F-actin
Grnd
dlg40.2
C
Rab5::EYFP
Grnd
WT
D
Rab5::EYFP
Grnd
dlg40.2
E
Rab7::EYFP
Grnd
WT
F
Rab7::EYFP
Grnd
dlg40.2
G
Hrs
Grnd
WT
H
Hrs
Grnd
dlg40.2
I
Rab11::EYFP
Grnd
WT
J
Rab11::EYFP
Grnd
dlg40.2
K
Rab9::EYFP
Grnd
WT
L
Rab9::EYFP
Grnd
dlg40.2
M
Rab4::EYFP
Grnd
WT
N
Rab4::EYFP
Grnd
dlg40.2
O
Vps26::EGFP
Grnd
WT
P
Vps26::EGFP
Grnd
dlg40.2
Q
ER-YFP
Grnd
WT
R
ER-YFP
Grnd
dlg40.2
S
Golgi-YFP
Grnd
WT
T
Golgi-YFP
Grnd
dlg40.2
U
Arl8
Grnd
WT
+LI
V
Arl8
Grnd
dlg40.2
+LI

Figure 5.6. Grnd trafficking is not altered in *dlg* mutants
(A,B) Compared to WT (A), punctate Grnd levels are increased in *dlg* mutant wing imaginal disc cells (B). *dlg* mutant cells do not show altered Grnd trafficking compared to WT at the level of the early endosome (C,D), late endosome (E,F), MVB (G,H), recycling endosome (I,J), retromer (K,L, O,P), rapid recycling pathway (M,N) or biosynthetic pathway (Q-T). Grnd lysosomal flux is normal in *dlg* mutant cells, revealed by treatment with lysosomal degradation inhibitors (U,V). Scale bars, 10μm.

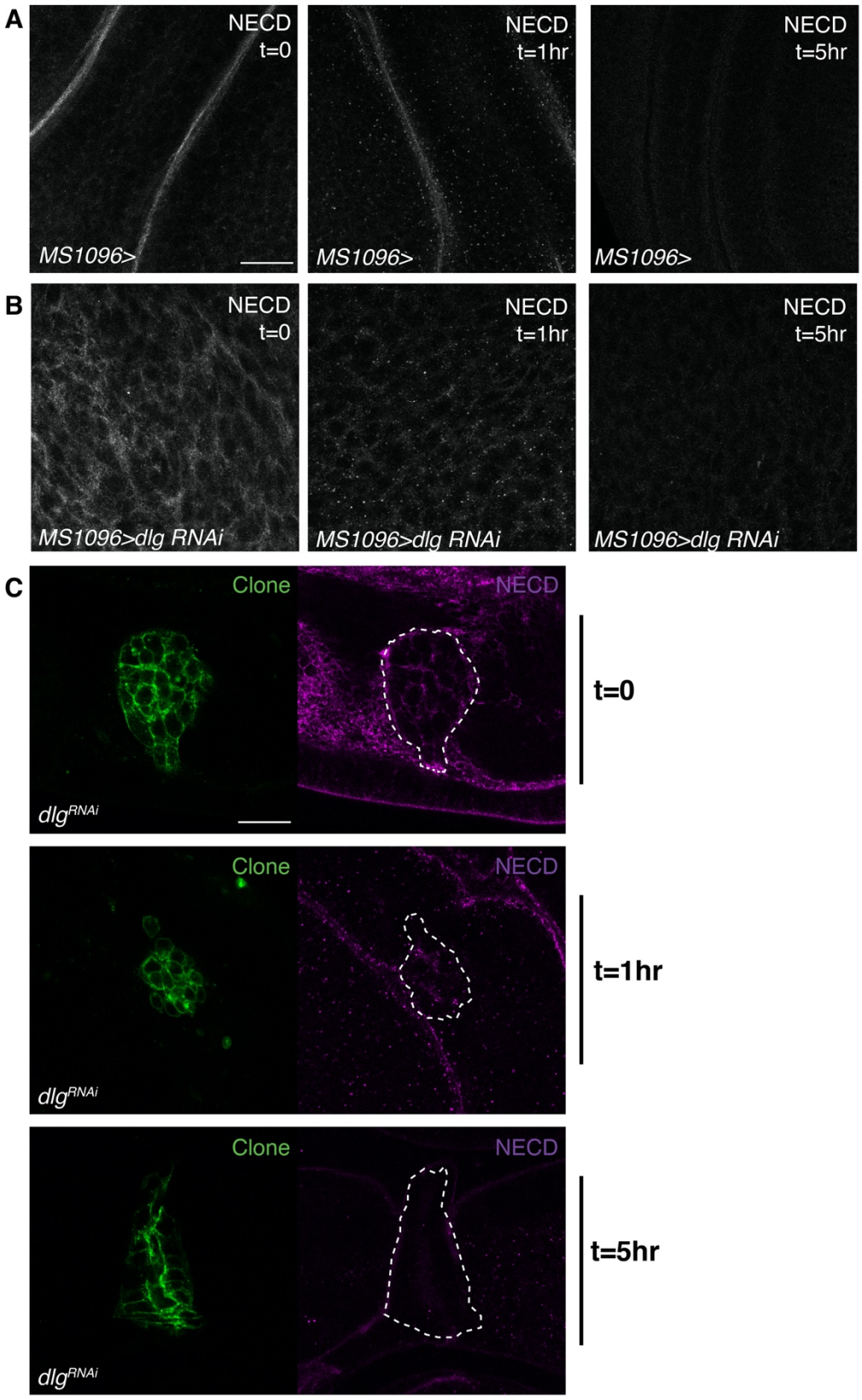
A
NECD
t=0
MS1096>
NECD
t=1hr
MS1096>
NECD
t=5hr
MS1096>
B
NECD
t=0
MS1096>dlg RNAi
NECD
t=1hr
MS1096>dlg RNAi
NECD
t=5hr
MS1096>dlg RNAi
C
Clone
NECD
dlgRNAi
t=0
Clone
NECD
dlgRNAi
t=1hr
Clone
NECD
dlgRNAi
t=5hr

Figure 5.7. Scrib module mutants do not have general endocytic defects
(A-C) Wing imaginal discs were surface labeled *ex vivo* with anti-NECD antibody at 4°C and then chased at RT for the indicated times. (A,B) Compared to WT cells (A), *dlg* mutant cells do not have defects in internalization, sorting and degradation kinetics of Notch. (C) Compared to surrounding WT cells, *dlg* depleted clones (white dotted lines) do not have defects in normal internalization and degradation of Notch.

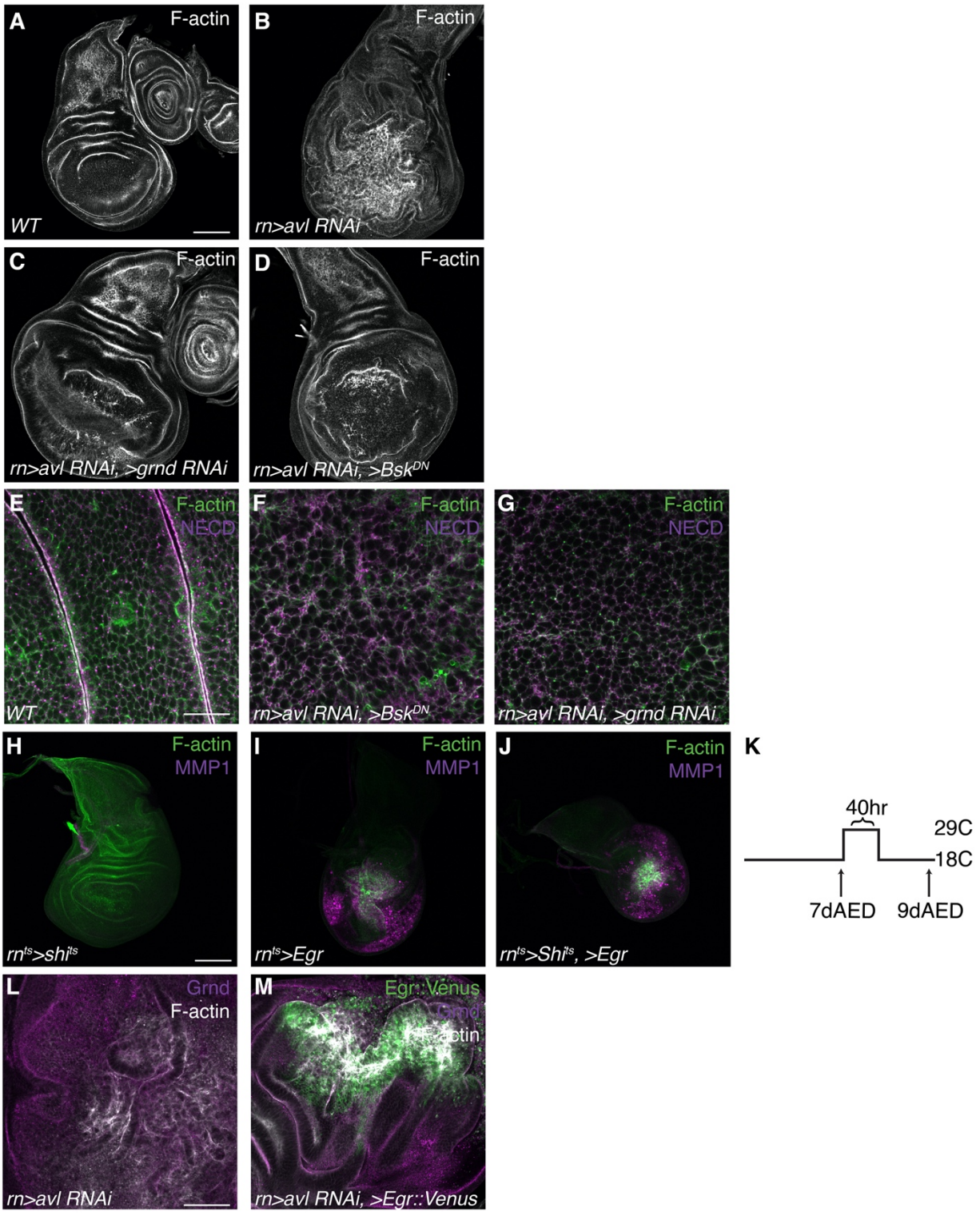

Figure 5.8. Grnd does not require endocytosis to signal
(A-D) Knockdown of the early endosome regulator *avl* causes neoplastic tumors in wing imaginal discs (B). Blocking JNK signaling by depleting *grnd* (C) or inhibiting Bsk (D) rescues *avl* tumors.

(E-G) Rescued *avl* tumors with Bsk inhibition (F) or *grnd* depletion (G) do not have restored endocytosis, as intracellular NECD puncta are not seen as in WT (E). (H-J) Egr expression activates JNK signaling and causes cell death in wing imaginal discs (I). JNK activation and ablation by Egr still occurs when endocytosis is blocked by Shi^{ts} expression (J). Shi^{ts} expression alone does not cause cell death (H). (K) Schematic of the ablation paradigm. Larvae are grown at the permissive temperature of 18°C until 7dAED. Shifting to the restrictive temperature (29°C) for 40hr induces ablation by Egr overexpression and endocytic blockade by Shi^{ts} expression. After ablation larvae are returned to 18°C and dissected 1-2 days later. (L-M) Overexpression of Egr in *avl* knockdown wing discs induces cell death (M) compared to *avl* depletion alone (L). Scale bars, 200µm in A-D and H-J and 10µm in E-G and L,M. Conditional ablation system described in (Smith-Bolton et al., 2009).

Table 1. Key Resources

Reagent	Reference and Source
Fly Stocks	
ap2σ^{K02457}	BDSC: 65750
dlg$^{40.2}$	(Mendoza-Topaz et al., 2008)
Lgl::GFP	(Dong et al., 2015)
tj-GAL4	Kyoto Stock Center: 104055
UAS-Rab5, UAS-Rab11^{CA}	BDSC: 24616 & 9791
UAS-Hrs	BDSC: 42692
UAS-ap2α RNAi	BDSC: 32866
UAS-dlg RNAi	BDSC: 39035
UAS-aPKC RNAi	BDSC: 25946
UAS-Rab5^{Q88L}	BDSC: 9773
Rab4, Rab5, Rab7, Rab9, Rab11 EYFP lines	BDSC & (Dunst et al., 2015)
Vps26::EGFP	BDSC: 67153
Golgi-YFP	BDSC: 7193
ER-YFP	BDSC: 7195
MS1096-GAL4	BDSC: 8860
UAS-avl RNAi	(Andersen et al., 2015)
UAS-grnd RNAi	(de Vreede et al., 2018)
UAS-Bsk^{DN}	BDSC: 6409
rn-GAL4	BDSC: 7405
rn-GAL4, tub-GAL80^{ts}; UAS-Egr	(Smith-Bolton et al., 2009)
act>y+>GAL4 UAS-his::RFP	BDSC: 30558
UAS-Egr::Venus	(de Vreede et al., 2018)
Antibodies	
1:100 mouse anti-Dlg (IHC)	Developmental Studies Hybridoma Bank (DSHB): 4F3
1:500 guinea pig anti-Scrib (IHC)	(Bilder and Perrimon, 2000)
1:200 rabbit anti-aPKC (IHC)	Santa Cruz Biotechnology: sc-216
1:25 mouse anti-Notch ECD	DSHB: C458.2H
1:500 guinea pig anti-Vps26	Generously provided by H. Bellen
1:500 mouse anti-Grnd	(de Vreede et al., 2018)
1:250 anti-Hrs	(Vaccari and Bilder, 2005)
1:200 anti-Arl8	DSHB: Arl8
1:100 mouse anti-MMP1	DSHB: 5H7B11, 3B8D12, 3A6B4

References

Aguilar-Aragon, M., Elbediwy, A., Foglizzo, V., Fletcher, G. C., Li, V. S. W. and Thompson, B. J. (2018). Pak1 Kinase Maintains Apical Membrane Identity in Epithelia. *Cell Rep.* **22**, 1639–1646.

Al-Bassam, S., Xu, M., Wandless, T. J. and Arnold, D. B. (2012). Differential trafficking of transport vesicles contributes to the localization of dendritic proteins. *Cell Rep.* **2**, 89–100.

Albertson, R. and Doe, C. Q. (2003). Dlg, Scrib and Lgl regulate neuroblast cell size and mitotic spindle asymmetry. *Nat. Cell Biol.* **5**, 166–170.

Albertson, R., Chabu, C., Sheehan, A. and Doe, C. Q. (2004). Scribble protein domain mapping reveals a multistep localization mechanism and domains necessary for establishing cortical polarity. *J. Cell Sci.* **117**, 6061–70.

Alkhatib, S. G. and Landry, J. W. (2011). The Nucleosome Remodeling Factor. *FEBS Lett.* **585**, 3197–3207.

Almagor, L., Ufimtsev, I. S., Ayer, A., Li, J. and Weis, W. I. (2019). Structural insights into the aPKC regulatory switch mechanism of the human cell polarity protein lethal giant larvae 2. *Proc. Natl. Acad. Sci.* 201821514.

Amacher, J. F., Brooks, L., Hampton, T. H. and Madden, D. R. (2020). Specificity in PDZ-peptide interaction networks: Computational analysis and review. *J. Struct. Biol. X* **4**, 100022.

Anastas, J. N., Biechele, T. L., Robitaille, M., Muster, J., Allison, K. H., Angers, S. and Moon, R. T. (2012). A protein complex of SCRIB, NOS1AP and VANGL1 regulates cell polarity and migration, and is associated with breast cancer progression. *Oncogene* **31**, 3696–3708.

Andersen, D. S., Colombani, J., Palmerini, V., Chakrabandhu, K., Boone, E., Röthlisberger, M., Toggweiler, J., Basler, K., Mapelli, M., Hueber, A.-O., et al. (2015). The Drosophila TNF receptor Grindelwald couples loss of cell polarity and neoplastic growth. *Nature* **522**, 482–6.

Arora, P., Dongre, S., Raman, R. and Sonawane, M. (2020). Stepwise polarisation of developing bilayered epidermis is mediated by aPKC and E-cadherin in zebrafish. *Elife* **9**, 1–25.

Asaba, N., Hanada, T., Takeuchi, A. and Chishti, A. H. (2003). Direct interaction with a kinesin-related motor mediates transport of mammalian discs large tumor suppressor homologue in epithelial cells. *J. Biol. Chem.* **278**, 8395–8400.

Ashburner, M., Ball, C. A., Blake, J. A., Botstein, D., Butler, H., Cherry, J. M., Davis, A. P., Dolinski, K., Dwight, S. S., Eppig, J. T., et al. (2000). Gene ontology: tool for the unification of biology. The Gene Ontology Consortium. *Nat. Genet.* **25**, 25–29.

Atkins, M., Potier, D., Romanelli, L., Jacobs, J., Mach, J., Hamaratoglu, F., Aerts, S. and Halder, G. (2016). An Ectopic Network of Transcription Factors Regulated by Hippo Signaling Drives Growth and Invasion of a Malignant Tumor Model. *Curr. Biol.* **26**, 714–723.

Atwood, S. X., Chabu, C., Penkert, R. R., Doe, C. Q. and Prehoda, K. E. (2007). Cdc42 acts downstream of Bazooka to regulate neuroblast polarity through Par-6 aPKC. *J. Cell Sci.* **120**, 3200–3206.

Audebert, S., Navarro, C., Nourry, C., Chasserot-Golaz, S., Lécine, P., Bellaiche, Y., Dupont, J. L., Premont, R. T., Sempéré, C., Strub, J. M., et al. (2004). Mammalian scribble forms a tight complex with the βPIX exchange factor. *Curr. Biol.* **14**, 987–995.

Awadia, S., Huq, F., Arnold, T. R., Goicoechea, S. M., Sun, Y. J., Hou, T., Kreider-Letterman, G., Massimi, P., Banks, L., Fuentes, E. J., et al. (2019). SGEF forms a complex with Scribble and Dlg1 and regulates epithelial junctions and contractility. *J. Cell Biol.* **218**, jcb.201811114.

Bachmann, A., Timmer, M., Sierralta, J., Pietrini, G., Gundelfinger, E. D., Knust, E. and Thomas, U. (2004). Cell type-specific recruitment of Drosophila Lin-7 to distinct MAGUK-based protein complexes defines novel roles for Sdt and Dlg-S97. *J. Cell Sci.* **117**, 1899–1909.

Badenhorst, P., Voas, M., Rebay, I. and Wu, C. (2002). Biological functions of the ISWI chromatin remodeling complex NURF. *Genes Dev.* **16**, 3186–98.

Bagci, H., Sriskandarajah, N., Robert, A., Boulais, J., Elkholi, I. E., Tran, V., Lin, Z. Y., Thibault, M. P., Dubé, N., Faubert, D., et al. (2020). Mapping the proximity interaction network of the Rho-family GTPases reveals signalling pathways and regulatory mechanisms. *Nat. Cell Biol.* **22**, 120–134.

Bailey, M. J. and Prehoda, K. E. (2015). Establishment of Par-Polarized Cortical Domains via Phosphoregulated Membrane Motifs. *Dev. Cell* **35**, 199–210.

Baker, N. E. (2020). Emerging mechanisms of cell competition. *Nat. Rev. Genet.* **21**, 683–697.

Bartles, J. R., Feracci, H. M., Stieger, B. and Hubbard, A. L. (1987). Biogenesis of the rat hepatocyte plasma membrane in vivo: Comparison of the pathways taken by apical and basolateral proteins using subcellular fractionation. *J. Cell Biol.* **105**, 1241–1251.

Baumgartner, R., Stocker, H. and Hafen, E. (2013). The RNA-binding Proteins FMR1, Rasputin and Caprin Act Together with the UBA Protein Lingerer to Restrict Tissue Growth in Drosophila melanogaster. *PLoS Genet.* **9**, e1003598.

Beatty, A., Morton, D. and Kemphues, K. (2010). The C. elegans homolog of Drosophila Lethal giant larvae functions redundantly with PAR-2 to maintain polarity in the early embryo. *Development* **137**, 3995–4004.

Bell, G. P., Fletcher, G. C., Brain, R. and Thompson, B. J. (2015). Aurora kinases phosphorylate Lgl to induce mitotic spindle orientation in drosophila epithelia. *Curr. Biol.* **25**, 61–68.

Bellaïche, Y., Radovic, A., Woods, D. F., Hough, C. D., Parmentier, M.-L., O'Kane, C. J., Bryant, P. J. and Schweisguth, F. (2001). The Partner of Inscuteable/Discs-Large Complex Is Required to Establish Planar Polarity during Asymmetric Cell Division in Drosophila. *Cell* **106**, 355–366.

Belotti, E., Polanowska, J., Daulat, A. M., Audebert, S., Thomé, V., Lissitzky, J.-C., Lembo, F., Blibek, K., Omi, S., Lenfant, N., et al. (2013). The Human PDZome: A Gateway to PSD95-Disc Large-Zonula Occludens (PDZ)-mediated Functions. *Mol. Cell. Proteomics* **12**, 2587–2603.

Benton, R. and St Johnston, D. (2003). Drosophila PAR-1 and 14-3-3 inhibit Bazooka/PAR-3 to establish complementary cortical domains in polarized cells. *Cell* **115**, 691–704.

Bergstralh, D. T., Lovegrove, H. E. and St Johnston, D. (2013). Discs large links spindle orientation to apical-basal polarity in drosophila epithelia. *Curr. Biol.* **23**, 1707–1712.

Bergstralh, D. T., Lovegrove, H. E., Kujawiak, I., Dawney, N. S., Zhu, J., Cooper, S., Zhang, R. and St Johnston, D. (2016). Pins is not required for spindle orientation in the *Drosophila* wing disc. *Development* dev.135475.

Beronja, S., Laprise, P., Papoulas, O., Pellikka, M., Sisson, J. and Tepass, U. (2005). Essential function of Drosophila Sec6 in apical exocytosis of epithelial photoreceptor cells.

J. Cell Biol. **169**, 635–646.

Betanzos, A., Huerta, M., Lopez-Bayghen, E., Azuara, E., Amerena, J. and González-Mariscal, L. (2004). The tight junction protein ZO-2 associates with Jun, Fos and C/EBP transcription factors in epithelial cells. *Exp. Cell Res.* **292**, 51–66.

Betschinger, J., Mechtler, K. and Knoblich, J. J. A. (2003). The Par complex directs asymmetric cell division by phosphorylating the cytoskeletal protein Lgl. *Nature* **422**, 326–30.

Betschinger, J., Eisenhaber, F. and Knoblich, J. A. (2005). Phosphorylation-induced autoinhibition regulates the cytoskeletal protein Lethal (2) giant larvae. *Curr. Biol.* **15**, 276–282.

Bhat, M. A., Izaddoost, S., Lu, Y., Cho, K.-O. O., Choi, K.-W. W. and Bellen, H. J. (1999). Discs Lost, a Novel Multi-PDZ Domain Protein, Establishes and Maintains Epithelial Polarity. *Cell* **115**, 765–766.

Biehler, C., Wang, L., Sévigny, M., Jetté, A., Gamblin, C. L., Catterall, R., Houssin, E., McCaffrey, L. and Laprise, P. (2020). Girdin is a component of the lateral polarity protein network restricting cell dissemination. *PLOS Genet.* **16**, e1008674.

Bilder, D. (2004). Epithelial polarity and proliferation control: Links from the Drosophila neoplastic tumor suppressors. *Genes Dev.* **18**, 1909–1925.

Bilder, D. and Perrimon, N. (2000). Localization of apical epithelial determinants by the basolateral PDZ protein Scribble. *Nature* **403**, 676–680.

Bilder, D., Birnbaum, D., Borg, J.-P., Bryant, P., Huigbretse, J., Jansen, E., Kennedy, M. B., Labouesse, M., Legouis, R., Mechler, B., et al. (2000a). Collective nomenclature for LAP proteins. *Nat. Cell Biol.* **2**, E114–E114.

Bilder, D., Li, M. and Perrimon, N. (2000b). Cooperative Regulation of Cell Polarity and Growth by Drosophila Tumor Suppressors. *Science (80-.).* **289**, 113–116.

Bilder, D., Li, M. and Perrimon, N. (2000c). Cooperative regulation of cell polarity and growth by Drosophila tumor suppressors. *Science* **289**, 113–116.

Bilder, D., Schober, M. and Perrimon, N. (2003). Integrated activity of PDZ protein complexes regulates epithelial polarity. *Nat Cell Biol* **5**, 53–58.

Bilder, D., Ong, K., Hsi, T. C., Adiga, K. and Kim, J. (2021). Tumour–host interactions through the lens of Drosophila. *Nat. Rev. Cancer* **0123456789**,.

Bit-Avragim, N., Rohr, S., Rudolph, F., Van Der Ven, P., Fürst, D., Eichhorst, J., Wiesner, B. and Abdelilah-Seyfried, S. (2008). Nuclear localization of the zebrafish tight junction protein nagie oko. *Dev. Dyn.* **237**, 83–90.

Blankenship, J. T., Fuller, M. T. and Zallen, J. A. (2007). The Drosophila homolog of the Exo84 exocyst subunit promotes apical epithelial identity. *J. Cell Sci.* **120**, 3099–3110.

Bo Zhai, J. V., Beausoleil, S. A., Mintseris, J. and Gygi, S. P. (2008). Phosphoproteome analysis of drosophila melanogaster embryos. *J. Proteome Res.* **7**, 1675–1682.

Bonello, T. T. and Peifer, M. (2018). Scribble: A master scaffold in polarity, adhesion, synaptogenesis, and proliferation. *J. Cell Biol.* jcb.201810103.

Bonello, T. T., Choi, W. and Peifer, M. (2019). Scribble and discs-large direct initial assembly and positioning of adherens junctions during establishment of apical-basal polarity. *Development* dev.180976.

Bossinger, O., Klebes, A., Segbert, C., Theres, C. and Knust, E. (2001). Zonula adherens formation in Caenorhabditis elegans requires dlg-1, the homologue of the Drosophila gene discs large. *Dev. Biol.* **230**, 29–42.

Bouazoune, K. and Brehm, A. (2006). ATP-dependent chromatin remodeling complexes in Drosophila. *Chromosom. Res.* **14**, 433–449.

Britton, J. S., Lockwood, W. K., Li, L., Cohen, S. M. and Edgar, B. A. (2002). Drosophila's insulin/PI3-kinase pathway coordinates cellular metabolism with nutritional conditions. *Dev. Cell* **2**, 239–249.

Brumby, A. M. and Richardson, H. E. (2003). scribble mutants cooperate with oncogenic Ras or Notch to cause neoplastic overgrowth in Drosophila. *EMBO J.* **22**, 5769–5779.

Brumby, A., Secombe, J., Horsfield, J., Coombe, M., Amin, N., Coates, D., Saint, R. and Richardson, H. (2004). A genetic screen for dominant modifiers of a cyclin E hypomorphic mutation identifies novel regulators of S-phase entry in drosophila. *Genetics* **168**, 227–251.

Bryant, D. M., Datta, A., Rodríguez-Fraticelli, A. E., PeräCurrency Signnen, J., Martín-Belmonte, F. and Mostov, K. E. (2010). A molecular network for de novo generation of the apical surface and lumen. *Nat. Cell Biol.* **12**, 1035–1045.

Bryant, D. M., Roignot, J., Datta, A., Overeem, A. W., Kim, M., Yu, W., Peng, X., Eastburn, D. J., Ewald, A. J., Werb, Z., et al. (2014). A molecular switch for the orientation of epithelial cell polarization. *Dev. Cell* **31**, 171–187.

Buckley, C. E. and St Johnston, D. (2022). Apical–basal polarity and the control of epithelial form and function. *Nat. Rev. Mol. Cell Biol.* **0123456789**,.

Bunker, B. D., Nellimoottil, T. T., Boileau, R. M., Classen, A. K. and Bilder, D. (2015). The transcriptional response to tumorigenic polarity loss in Drosophila. *Elife* **2015**,.

Buszczak, M., Paterno, S., Lighthouse, D., Bachman, J., Planck, J., Owen, S., Skora, A. D., Nystul, T. G., Ohlstein, B., Allen, A., et al. (2007). The carnegie protein trap library: A versatile tool for drosophila developmental studies. *Genetics* **175**, 1505–1531.

Calero-Cuenca, F. J. and Sotillos, S. (2018). Nuf and Rip11 requirement for polarity determinant recycling during Drosophila development. *Small GTPases* **9**, 352–359.

Calero-Cuenca, F. J., Espinosa-Vázquez, J. M., Reina-Campos, M., Díaz-Meco, M. T., Moscat, J. and Sotillos, S. (2016). Nuclear fallout provides a new link between aPKC and polarized cell trafficking. *BMC Biol.* **14**, 32.

Campanale, J. P., Sun, T. Y. and Montell, D. J. (2017). Development and dynamics of cell polarity at a glance. *J. Cell Sci.* **130**,.

Carbon, S., Douglass, E., Good, B. M., Unni, D. R., Harris, N. L., Mungall, C. J., Basu, S., Chisholm, R. L., Dodson, R. J., Hartline, E., et al. (2021). The Gene Ontology resource: enriching a GOld mine. *Nucleic Acids Res.* **49**, D325–D334.

Caria, S., Magtoto, C. M., Samiei, T., Portela, M., Lim, K. Y. B., How, J. Y., Stewart, B. Z., Humbert, P. O., Richardson, H. E. and Kvansakul, M. (2018). Drosophila melanogaster guk-holder interacts with the scribbled PDZ1 domain and regulates epithelial development with scribbled and discs large. *J. Biol. Chem.* **293**, 4519–4531.

Caruana, G. and Bernstein, A. (2001). Craniofacial Dysmorphogenesis Including Cleft Palate in Mice with an Insertional Mutation in the discs large Gene. *Mol. Cell. Biol.* **21**, 1475.

Carvalho, C. A., Moreira, S., Ventura, G., Sunkel, C. E. and Morais-De-Sá, E. (2015). Aurora a triggers Lgl cortical release during symmetric division to control planar spindle orientation. *Curr. Biol.* **25**, 53–60.

Cereijido, M., Contreras, R. G. and Shoshani, L. (2004). Cell adhesion, polarity, and epithelia in the dawn of metazoans. *Physiol. Rev.* **84**, 1229–1262.

Ceulemans, H., Vulsteke, V., De Maeyer, M., Tatchell, K., Stalmans, W. and Bollen, M. (2002). Binding of the concave surface of the Sds22 superhelix to the α4/α5/α6-triangle of

protein phosphatase-1. *J. Biol. Chem.* **277**, 47331–47337.
Chen, C.-L., Hu, Y., Udeshi, N. D., Lau, T. Y., Wirtz-Peitz, F., He, L., Ting, A. Y., Carr, S. A. and Perrimon, N. (2015). Proteomic mapping in live Drosophila tissues using an engineered ascorbate peroxidase. *Proc. Natl. Acad. Sci. U. S. A.* **112**, 12093–8.
Chen, B., Zheng, B., Deran, M., Jarugumilli, G. K., Fu, J., Brooks, Y. S. and Wu, X. (2016a). ZDHHC7-mediated S-palmitoylation of Scribble regulates cell polarity. *Nat. Chem. Biol.* **12**, 686–693.
Chen, D. Y., Lipari, K. R., Dehghan, Y., Streichan, S. J. and Bilder, D. (2016b). Symmetry Breaking in an Edgeless Epithelium by Fat2-Regulated Microtubule Polarity. *Cell Rep.* **15**, 1125–1133.
Chen, J., Sayadian, A.-C., Lowe, N., Lovegrove, H. E. and St Johnston, D. (2018). An alternative mode of epithelial polarity in the Drosophila midgut. *PLOS Biol.* **16**, e3000041.
Chen, D.-Y., Crest, J., Streichan, S. J. and Bilder, D. (2019). Extracellular matrix stiffness cues junctional remodeling for 3D tissue elongation. *Nat. Commun.* **10**, 3339.
Chetkovich, D. M., Bunn, R. C., Kuo, S. H., Kawasaki, Y., Kohwi, M. and Bredt, D. S. (2002). Postsynaptic targeting of alternative postsynaptic density-95 isoforms by distinct mechanisms. *J. Neurosci.* **22**, 6415–6425.
Choi, J., Troyanovsky, R. B., Indra, I., Mitchell, B. J. and Troyanovsky, S. M. (2019). Scribble, Erbin, and Lano redundantly regulate epithelial polarity and apical adhesion complex. *J. Cell Biol.* **218**, 2277–2293.
Chou, T. Bin and Perrimon, N. (1996). The autosomal FLP-DFS technique for generating germline mosaics in Drosophila melanogaster. *Genetics* **144**, 1673–1679.
Claret, S., Jouette, J., Benoit, B., Legent, K. and Guichet, A. (2014). PI(4,5)P2 produced by the PI4P5K SKTL controls apical size by tethering PAR-3 in drosophila epithelial cells. *Curr. Biol.* **24**, 1071–1079.
Clark, B. S., Cui, S., Miesfeld, J. B., Klezovitch, O., Vasioukhin, V. and Link, B. A. (2012). Loss of Llgl1 in retinal neuroepithelia reveals links between apical domain size, Notch activity and neurogenesis. *Development* **139**, 1599–1610.
Dash, B. P., Schnöder, T. M., Kathner, C., Mohr, J., Weinert, S., Herzog, C., Godavarthy, P. S., Zanetti, C., Perner, F., Braun-Dullaeus, R., et al. (2018). Diverging impact of cell fate determinants Scrib and Llgl1 on adhesion and migration of hematopoietic stem cells. *J. Cancer Res. Clin. Oncol.* **144**, 1933–1944.
David, D. J. V, Tishkina, A. and Harris, T. J. C. (2010). The PAR complex regulates pulsed actomyosin contractions during amnioserosa apical constriction in Drosophila. *Development* **137**, 1645–1655.
Daynac, M., Chouchane, M., Collins, H. Y., Murphy, N. E., Andor, N., Niu, J., Fancy, S. P. J., Stallcup, W. B. and Petritsch, C. K. (2018). Lgl1 controls NG2 endocytic pathway to regulate oligodendrocyte differentiation and asymmetric cell division and gliomagenesis. *Nat. Commun.* **9**, 2862.
de Vreede, G., Schoenfeld, J. D., Windler, S. L., Morrison, H., Lu, H. and Bilder, D. (2014). The Scribble module regulates retromer-dependent endocytic trafficking during epithelial polarization. *Development* **141**, 2796–802.
de Vreede, G., Morrison, H. A., Houser, A. M., Boileau, R. M., Andersen, D., Colombani, J. and Bilder, D. (2018). A Drosophila Tumor Suppressor Gene Prevents Tonic TNF Signaling through Receptor N-Glycosylation. *Dev. Cell* **45**, 595-605.e4.
de Vreede, G., Gerlach, S. U. and Bilder, D. (2022). Epithelial integrity monitoring via ligand-

receptor segregation ensures malignant cell elimination. *Science (80-.).* **in press**, 297–301.

Deborde, S., Perret, E., Gravotta, D., Deora, A., Salvarezza, S., Schreiner, R. and Rodriguez-Boulan, E. (2008). Clathrin is a key regulator of basolateral polarity. *Nature* **452**, 719–23.

DeBruhl, H., Albertson, R., Swider, Z. and Sullivan, W. (2015). AP-2 complex-mediated endocytosis of Drosophila Crumbs regulates polarity via antagonizing Stardust. *J. Cell Sci.* **44**, 4–8.

Desclozeaux, M., Venturato, J., Wylie, F. G., Kay, J. G., Joseph, S. R., Le, H. T. and Stow, J. L. (2008). Active Rab11 and functional recycling endosome are required for E-cadherin trafficking and lumen formation during epithelial morphogenesis. *AJP Cell Physiol.* **295**, C545–C556.

Dobrosotskaya, I., Guy, R. K. and James, G. L. (1997). MAGI-1, a Membrane-associated Guanylate Kinase with a Unique Arrangement of Protein-Protein Interaction Domains. *J. Biol. Chem.* **272**, 31589–31597.

Doggett, K., Grusche, F. A., Richardson, H. E. and Brumby, A. M. (2011). Loss of the Drosophila cell polarity regulator Scribbled promotes epithelial tissue overgrowth and cooperation with oncogenic Ras-Raf through impaired Hippo pathway signaling. *BMC Dev. Biol.* **11**, 57.

Doherty, G. J. and McMahon, H. T. (2009). Mechanisms of endocytosis. *Annu. Rev. Biochem.* **78**, 857–902.

Dong, W., Zhang, X., Liu, W., Chen, Y. jiun, Huang, J., Austin, E., Celotto, A. M., Jiang, W. Z., Palladino, M. J., Jiang, Y., et al. (2015). A conserved polybasic domain mediates plasma membrane targeting of Lgl and its regulation by hypoxia. *J. Cell Biol.* **211**, 273–286.

Dong, W., Lu, J., Zhang, X., Wu, Y., Letteri, K. and Hammond, G. R. (2019). A Polybasic Domain in aPKC Mediates Par-6-Dependent Control of Plasma Membrane Targeting and Kinase Activity. *bioRxiv* 588624.

Dong, W., Lu, J., Zhang, X., Wu, Y., Lettieri, K., Hammond, G. R. and Hong, Y. (2020). A polybasic domain in aPKC mediates Par6-dependent control of membrane targeting and kinase activity. *J. Cell Biol.* **219**, 588624.

Dow, L. E., Brumby, A. M., Muratore, R., Coombe, M. L., Sedelies, K. A., Trapani, J. A., Russell, S. M., Richardson, H. E. and Humbert, P. O. (2003). hScrib is a functional homologue of the Drosophila tumour suppressor Scribble. *Oncogene* **22**, 9225–9230.

Drew, K., Lee, C., Huizar, R. L., Tu, F., Borgeson, B., McWhite, C. D., Ma, Y., Wallingford, J. B. and Marcotte, E. M. (2017). Integration of over 9,000 mass spectrometry experiments builds a global map of human protein complexes. *Mol. Syst. Biol.* **13**, 932.

Drummond, M. L. and Prehoda, K. E. (2016). Molecular Control of Atypical Protein Kinase C: Tipping the Balance between Self-Renewal and Differentiation. *J. Mol. Biol.* **428**, 1455–1464.

Dunst, S., Kazimiers, T., von Zadow, F., Jambor, H., Sagner, A., Brankatschk, B., Mahmoud, A., Spannl, S., Tomancak, P., Eaton, S., et al. (2015). Endogenously Tagged Rab Proteins: A Resource to Study Membrane Trafficking in Drosophila. *Dev. Cell* **33**, 351–365.

Elsum, I., Yates, L., Humbert, P. O. and Richardson, H. E. (2012). The Scribble-Dlg-Lgl polarity module in development and cancer: From flies to man. *Essays Biochem.* **53**, 141–

168.
Enomoto, M. and Igaki, T. (2011). Deciphering tumor-suppressor signaling in flies: Genetic link between Scribble/Dlg/Lgl and the Hippo pathways. *J. Genet. Genomics* **38**, 461–470.
Farías, G. G., Cuitino, L., Guo, X., Ren, X., Jarnik, M., Mattera, R. and Bonifacino, J. S. (2012). Signal-Mediated, AP-1/Clathrin-Dependent Sorting of Transmembrane Receptors to the Somatodendritic Domain of Hippocampal Neurons. *Neuron* **75**, 810–823.
Fehon, R. G., Oren, T., LaJeunesse, D. R., Melby, T. E. and McCartney, B. M. (1997). Isolation of mutations in the Drosophila homologues of the human Neurofibromatosis 2 and yeast CDC42 genes using a simple and efficient reverse-genetic method. *Genetics* **146**, 245–252.
Figueroa-Clarevega, A. and Bilder, D. (2015). Malignant drosophila tumors interrupt insulin signaling to induce cachexia-like wasting. *Dev. Cell* **33**, 47–56.
Firestein, B. L. and Rongo, C. (2001). DLG-1 is a MAGUK similar to SAP97 and is required for adherens junction formation. *Mol. Biol. Cell* **12**, 3465–3475.
Fletcher, G. C., Lucas, E. P., Brain, R., Tournier, A. and Thompson, B. J. (2012). Positive feedback and mutual antagonism combine to polarize crumbs in the drosophila follicle cell epithelium. *Curr. Biol.* **22**, 1116–1122.
Flinn, M. A., Otten, C., Brandt, Z. J., Bostrom, J. R., Kenarsary, A., Wan, T. C., Auchampach, J. A., Abdelilah-Seyfried, S., O'Meara, C. C. and Link, B. A. (2020). Llgl1 regulates zebrafish cardiac development by mediating Yap stability in cardiomyocytes. *Development* **147**, dev193581.
Flores-Benitez, D. and Knust, E. (2016). Dynamics of epithelial cell polarity in Drosophila: how to regulate the regulators? *Curr. Opin. Cell Biol.* **42**, 13–21.
Fölsch, H., Mattila, P. E. and Weisz, O. A. (2009). Taking the Scenic Route: Biosynthetic Traffic to the Plasma Membrane in Polarized Epithelial Cells. *Traffic* **10**, 972.
Franz, A. and Riechmann, V. (2010). Stepwise polarisation of the Drosophila follicular epithelium. *Dev. Biol.* **338**, 136–147.
Funke, L., Dakoji, S. and Bredt, D. S. (2005). Membrane-associated guanylate kinases regulate adhesion and plasticity at cell junctions. *Annu. Rev. Biochem.* **74**, 219–245.
Gallego-Gutiérrez, H., González-González, L., Ramírez-Martínez, L., López-Bayghen, E. and González-Mariscal, L. (2021). Tight junction protein ZO-2 modulates the nuclear accumulation of transcription factor TEAD. *Mol. Biol. Cell* **32**, mbc.E20-07-0470.
Gallon, M. and Cullen, P. J. (2015). Retromer and sorting nexins in endosomal sorting. *Biochem. Soc. Trans.* **43**, 33–47.
Gamblin, C. L., Hardy, É. J. L., Chartier, F. J. M., Bisson, N. and Laprise, P. (2014). A bidirectional antagonism between aPKC and Yurt regulates epithelial cell polarity. *J. Cell Biol.* **204**, 487–495.
Gangar, A., Rossi, G., Andreeva, A., Hales, R. and Brennwald, P. (2005). Structurally conserved interaction of Lgl family with SNAREs is critical to their cellular function. *Curr. Biol.* **15**, 1136–1142.
Garcia, J. D., Dewey, E. B. and Johnston, C. A. (2014). Dishevelled binds the Discs large "Hook" domain to activate GukHolder-dependent spindle positioning in Drosophila. *PLoS One* **9**, 1–17.
Gateff, E. (1978). The genetics and epigenetics of neoplasms in Drosophila. *Biol. Rev. Camb. Philos. Soc.* **53**, 123–68.
Gateff, E. and Schneiderman, H. A. (1969). Neoplasms in mutant and cultured wild-tupe

tissues of Drosophila. *Natl. Cancer Inst. Monogr.* **31**, 365–397.
Gateff, E. and Schneiderman, H. A. (1974). Developmental capacities of benign and malignant neoplasms of Drosophila. *Wilhelm Roux Arch. für Entwicklungsmechanik der Org.* **176**, 23–65.
Georgiou, M., Marinari, E., Burden, J. and Baum, B. (2008). Cdc42, Par6, and aPKC Regulate Arp2/3-Mediated Endocytosis to Control Local Adherens Junction Stability. *Curr. Biol.* **18**, 1631–1638.
Gervais, L., Claret, S., Januschke, J., Roth, S. and Guichet, A. (2008). PIP5K-dependent production of PIP2 sustains microtubule organization to establish polarized transport in the Drosophila oocyte. *Development* **135**, 3829–3838.
Gingras, A.-C., Abe, K. T. and Raught, B. (2019). Getting to know the neighborhood: using proximity-dependent biotinylation to characterize protein complexes and map organelles. *Curr. Opin. Chem. Biol.* **48**, 44–54.
Goentoro, L. A., Yakoby, N., Goodhouse, J., Schüpbach, T. and Shvartsman, S. Y. (2006). Quantitative analysis of the GAL4/UAS system in Drosophila oogenesis. *Genesis* **44**, 66–74.
Goldstein, B. and Macara, I. G. (2007). The PAR Proteins: Fundamental Players in Animal Cell Polarization. *Dev. Cell* **13**, 609–622.
Golub, O., Wee, B., Newman, R. A., Paterson, N. M. and Prehoda, K. E. (2017). Activation of Discs large by aPKC aligns the mitotic spindle to the polarity axis during asymmetric cell division. *Elife* **6**, 1–17.
González-Mariscal, L., Islas, S., Contreras, R. G., García-Villegas, M. R., Betanzos, A., Vega, J., Diaz-Quiñónez, A., Martín-Orozco, N., Ortiz-Navarrete, V., Cereijido, M., et al. (1999). Molecular Characterization of the Tight Junction Protein ZO-1 in MDCK Cells. *Exp. Cell Res.* **248**, 97–109.
González-Mariscal, L., Ponce, A., Alarcón, L. and Jaramillo, B. E. (2006). The tight junction protein ZO-2 has several functional nuclear export signals. *Exp. Cell Res.* **312**, 3323–3335.
Gorczyca, D., Ashley, J., Speese, S., Gherbesi, N., Thomas, U., Gundelfinger, E., Gramates, L. S. and Budnik, V. (2007). Postsynaptic membrane addition depends on the discs-large-interacting t-SNARE Gtaxin. *J. Neurosci.* **27**, 1033–1044.
Gottardi, C. J., Arpin, M., Fanning, A. S. and Louvard, D. (1996). The junction-associated protein, zonula occludens-1, localizes to the nucleus before the maturation and during the remodeling of cell-cell contacts. *Proc. Natl. Acad. Sci. U. S. A.* **93**, 10779–84.
Grant, B. D. and Donaldson, J. G. (2009). Pathways and mechanisms of endocytic recycling. *Nat. Rev. Mol. Cell Biol.* **10**, 597–608.
Graybill, C. and Prehoda, K. E. (2014). Ordered multisite phosphorylation of lethal giant larvae by atypical protein kinase C. *Biochemistry* **53**, 4931–4937.
Graybill, C., Wee, B., Atwood, S. X. and Prehoda, K. E. (2012). Partitioning-defective protein 6 (Par-6) activates atypical protein kinase C (aPKC) by pseudosubstrate displacement. *J. Biol. Chem.* **287**, 21003–21011.
Grifoni, D., Garoia, F., Bellosta, P., Parisi, F., De Biase, D., Collina, G., Strand, D., Cavicchi, S. and Pession, A. (2007). aPKCζ cortical loading is associated with Lgl cytoplasmic release and tumor growth in Drosophila and human epithelia. *Oncogene* **26**, 5960–5965.
Grosshans, B. L., Andreeva, A., Gangar, A., Niessen, S., Yates, J. R., Brennwald, P. and Novick, P. (2006). The yeast lgl family member Sro7p is an effector of the secretory Rab

GTPase Sec4p. *J. Cell Biol.* **172**, 55–66.
Grzeschik, N. A., Parsons, L. M., Allott, M. L., Harvey, K. F. and Richardson, H. E. (2010). Lgl, aPKC, and Crumbs Regulate the Salvador/Warts/Hippo Pathway through Two Distinct Mechanisms. *Curr. Biol.* **20**, 573–581.
Gui, J., Huang, Y. and Shimmi, O. (2016). Scribbled Optimizes BMP Signaling through Its Receptor Internalization to the Rab5 Endosome and Promote Robust Epithelial Morphogenesis. *PLoS Genet.* **12**, e1006424.
Haigo, S. L. and Bilder, D. (2011). Global Tissue Revolutions in a Morphogenetic Movement Controlling Elongation. *Science (80-.).* **331**, 1071–1074.
Halaoui, R. and McCaffrey, L. (2015). Rewiring cell polarity signaling in cancer. *Oncogene* **34**, 939–50.
Hamaratoglu, F., Willecke, M., Kango-Singh, M., Nolo, R., Hyun, E., Tao, C., Jafar-Nejad, H. and Halder, G. (2006). The tumour-suppressor genes NF2/Merlin and Expanded act through Hippo signalling to regulate cell proliferation and apoptosis. *Nat. Cell Biol.* **8**, 27–36.
Hao, Y., Boyd, L. and Seydoux, G. (2006). Stabilization of cell polarity by the C. elegans RING protein PAR-2. *Dev. Cell* **10**, 199–208.
Hariharan, I. K. and Bilder, D. (2006). Regulation of imaginal disc growth by tumor-suppressor genes in Drosophila. *Annu. Rev. Genet.* **40**, 335–361.
Harmansa, S., Hamaratoglu, F., Affolter, M. and Caussinus, E. (2015). Dpp spreading is required for medial but not for lateral wing disc growth. *Nature* **527**, 317–322.
Harmansa, S., Alborelli, I., Caussinus, E. and Affolter, M. (2017). A nanobody-based toolset to investigate the role of protein localization and dispersal in Drosophila. *Elife* **6**, 668–675.
Harris, T. J. C. and Peifer, M. (2004). Adherens junction-dependent and -independent steps in the establishment of epithelial cell polarity in Drosophila. *J. Cell Biol.* **167**, 135–147.
Harris, T. J. C. and Peifer, M. (2005). The positioning and segregation of apical cues during epithelial polarity establishment in Drosophila. *J. Cell Biol.* **170**, 813–823.
Harris, K. P. and Tepass, U. (2008). Cdc42 and Par proteins stabilize dynamic adherens junctions in the Drosophila neuroectoderm through regulation of apical endocytosis. *J. Cell Biol.* **183**, 1129–1143.
Hattendorf, D. A., Andreeva, A., Gangar, A., Brennwald, P. J. and Weis, W. I. (2007). Structure of the yeast polarity protein Sro7 reveals a SNARE regulatory mechanism. *Nature* **446**, 567–571.
Hendrickx, A., Beullens, M., Ceulemans, H., Den Abt, T., Van Eynde, A., Nicolaescu, E., Lesage, B. and Bollen, M. (2009). Docking Motif-Guided Mapping of the Interactome of Protein Phosphatase-1. *Chem. Biol.* **16**, 365–371.
Heroes, E., Lesage, B., Görnemann, J., Beullens, M., Van Meervelt, L. and Bollen, M. (2013). The PP1 binding code: A molecular-lego strategy that governs specificity. *FEBS J.* **280**, 584–595.
Hoege, C., Constantinescu, A. T., Schwager, A., Goehring, N. W., Kumar, P. and Hyman, A. A. (2010). LGL can partition the cortex of one-cell caenorhabditis elegans embryos into two domains. *Curr. Biol.* **20**, 1296–1303.
Holly, R. W. and Prehoda, K. E. (2019). Phosphorylation of Par-3 by Atypical Protein Kinase C and Competition between Its Substrates. *Dev. Cell* **49**, 678–679.
Hong, Y. (2018). aPKC : the Kinase that Phosphorylates Cell Polarity [version 1 ; referees : 2 approved]. *F1000Research* **7**, 1–8.

Horne-Badovinac, S. and Bilder, D. (2005). Mass transit: Epithelial morphogenesis in the Drosophila egg chamber. *Dev. Dyn.* **232**, 559–574.

Horne-Badovinac, S., Lin, D., Waldron, S., Schwarz, M., Mbamalu, G., Pawson, T., Jan, Y. N., Stainier, D. Y. R. and Abdelilah-Seyfried, S. (2001). Positional cloning of heart and soul reveals multiple roles for PKCλ in zebrafish organogenesis. *Curr. Biol.* **11**, 1492–1502.

Hough, C. D., Woods, D. F., Park, S. and Bryant, P. J. (1997). Organizing a functional junctional complex requires specific domains of the Drosophila MAGUK Discs large. *Genes Dev.* **11**, 3242–3253.

Hsu, V. W., Bai, M. and Li, J. (2012). Getting active: protein sorting in endocytic recycling. *Nat. Rev. Mol. Cell Biol.*

Hsueh, Y.-P., Wang, T.-F., Yang, F.-C. and Sheng, M. (2000). Nuclear translocation and transcription regulation by the membrane-associated guanylate kinase CASK/LIN-2. *Nature* **404**, 298–302.

Huang, J., Zhou, W., Dong, W., Watson, A. M. and Hong, Y. (2009). Directed, efficient, and versatile modifications of the Drosophila genome by genomic engineering. *Proc. Natl. Acad. Sci. U. S. A.* **106**, 8284–9.

Huerta, M., Muñoz, R., Tapia, R., Soto-Reyes, E., Ramírez, L., Recillas-Targa, F., González-Mariscal, L. and López-Bayghen, E. (2007). Cyclin D1 is transcriptionally down-regulated by ZO-2 via an E box and the transcription factor c-Myc. *Mol. Biol. Cell* **18**, 4826–36.

Humbert, P. O., Grzeschik, N. A., Brumby, A. M., Galea, R., Elsum, I. and Richardson, H. E. (2008). Control of tumourigenesis by the Scribble/Dlg/Lgl polarity module. *Oncogene* **27**, 6888–6907.

Hung, V., Zou, P., Rhee, H.-W., Udeshi, N. D., Cracan, V., Svinkina, T., Carr, S. A., Mootha, V. K. and Ting, A. Y. (2014). Proteomic mapping of the human mitochondrial intermembrane space in live cells via ratiometric APEX tagging. *Mol. Cell* **55**, 332–41.

Hung, V., Udeshi, N. D., Lam, S. S., Loh, K. H., Cox, K. J., Pedram, K., Carr, S. A. and Ting, A. Y. (2016). Spatially resolved proteomic mapping in living cells with the engineered peroxidase APEX2. *Nat. Protoc.* **11**, 456–475.

Hunziker, W. and Fumey, C. (1994). A di-leucine motif mediates endocytosis and basolateral sorting of macrophage IgG Fc receptors in MDCK cells. *EMBO J.* **13**, 2963–2969.

Hutterer, A., Betschinger, J., Petronczki, M. and Knoblich, J. A. (2004). Sequential roles of Cdc42, Par-6, aPKC, and Lgl in the establishment of epithelial polarity during Drosophila embryogenesis. *Dev. Cell* **6**, 845–854.

Igaki, T., Pagliarini, R. A. and Xu, T. (2006). Loss of Cell Polarity Drives Tumor Growth and Invasion through JNK Activation in Drosophila. *Curr. Biol.* **16**, 1139–1146.

Igaki, T., Pastor-Pareja, J. C., Aonuma, H., Miura, M. and Xu, T. (2009). Intrinsic Tumor Suppression and Epithelial Maintenance by Endocytic Activation of Eiger/TNF Signaling in Drosophila. *Dev. Cell* **16**, 458–465.

Iizuka-Kogo, A., Ishidao, T., Akiyama, T. and Senda, T. (2007). Abnormal development of urogenital organs in Dlgh1-deficient mice. *Development* **134**, 1799–1807.

Islas, S., Vega, J., Ponce, L. and González-Mariscal, L. (2002). Nuclear Localization of the Tight Junction Protein ZO-2 in Epithelial Cells. *Exp. Cell Res.* **274**, 138–148.

Ivanov, A. I., Young, C., Beste, K. Den, Capaldo, C. T., Humbert, P. O., Brennwald, P., Parkos, C. A. and Nusrat, A. (2010). Tumor suppressor scribble regulates assembly of tight junctions in the intestinal epithelium. *Am. J. Pathol.* **176**, 134–145.

Ivarsson, Y., Arnold, R., McLaughlin, M., Nim, S., Joshi, R., Ray, D., Liu, B., Teyra, J., Pawson, T., Moffat, J., et al. (2014). Large-scale interaction profiling of PDZ domains through proteomic peptide-phage display using human and viral phage peptidomes. *Proc. Natl. Acad. Sci. U. S. A.* **111**, 2542–7.

Izumi, Y. and Furuse, M. (2014). Molecular organization and function of invertebrate occluding junctions. *Semin. Cell Dev. Biol.* **36**, 186–193.

Jacob, L., Opper, M., Metzroth, B., Phannavong, B. and Mechler, B. M. (1987). Structure of the I(2)gl gene of Drosophila and delimitation of its tumor suppressor domain. *Cell* **50**, 215–225.

Jaramillo, B. E., Ponce, A., Moreno, J., Betanzos, A., Huerta, M., Lopez-Bayghen, E. and Gonzalez-Mariscal, L. (2004). Characterization of the tight junction protein ZO-2 localized at the nucleus of epithelial cells. *Exp. Cell Res.* **297**, 247–258.

Jékely, G., Sung, H. H., Luque, C. M. and Rørth, P. (2005). Regulators of endocytosis maintain localized receptor tyrosine kinase signaling in guided migration. *Dev. Cell* **9**, 197–207.

Jewett, C. E. and Prekeris, R. (2018). Insane in the apical membrane: Trafficking events mediating apicobasal epithelial polarity during tube morphogenesis. *Traffic* **19**, 666–678.

Jiménez-Amilburu, V. and Stainier, D. Y. R. (2019). The transmembrane protein Crb2a regulates cardiomyocyte apicobasal polarity and adhesion in zebrafish. *Development* dev.171207.

Jiménez-Amilburu, V., Rasouli, S. J., Staudt, D. W., Nakajima, H., Chiba, A., Mochizuki, N. and Stainier, D. Y. R. (2016). In Vivo Visualization of Cardiomyocyte Apicobasal Polarity Reveals Epithelial to Mesenchymal-like Transition during Cardiac Trabeculation. *Cell Rep.* **17**, 2687–2699.

Johnston, D. S. (2018). Establishing and transducing cell polarity: common themes and variations. *Curr. Opin. Cell Biol.* **51**, 33–41.

Johnston, C. A. (2020). A Cell Adhesion-Based Reconstitution Method for Studying Cell Polarity. *Front. Cell Dev. Biol.* **8**, 1–11.

Johnston, C. A., Hirono, K., Prehoda, K. E. and Doe, C. Q. (2009). Identification of an Aurora-A/PinsLINKER/ Dlg Spindle Orientation Pathway using Induced Cell Polarity in S2 Cells. *Cell* **138**, 1150–1163.

Johnston, C. A., Whitneye, D. S., Volkmane, B. F., Doe, C. Q. and Prehoda, K. E. (2011). Conversion of the enzyme guanylate kinase into a mitotic-spindle orienting protein by a single mutation that inhibits GMP-induced closing. *Proc. Natl. Acad. Sci. U. S. A.* **108**, E973–E978.

Jossin, Y., Lee, M., Klezovitch, O., Kon, E., Cossard, A., Lien, W.-H., Fernandez, T. E., Cooper, J. A. and Vasioukhin, V. (2017). Llgl1 Connects Cell Polarity with Cell-Cell Adhesion in Embryonic Neural Stem Cells. *Dev. Cell* 1–15.

Kanda, H., Igaki, T., Kanuka, H., Yagi, T. and Miura, M. (2002). Wengen, a member of the Drosophila tumor necrosis factor receptor superfamily, is required for eiger signaling. *J. Biol. Chem.* **277**, 28372–28375.

Kauppila, S., Maaty, W. S. A., Chen, P., Tomar, R. S., Eby, M. T., Chapo, J., Chew, S., Rathore, N., Zachariah, S., Sinha, S. K., et al. (2003). Eiger and its receptor, Wengen, comprise a TNF-like system in Drosophila. *Oncogene* **22**, 4860–4867.

Kharfallah, F., Guyot, M. C., El Hassan, A. R., Allache, R., Merello, E., De Marco, P., Di Cristo, G., Capra, V. and Kibar, Z. (2017). Scribble1 plays an important role in the

pathogenesis of neural tube defects through its mediating effect of Par-3 and Vangl1/2 localization. *Hum. Mol. Genet.* **26**, 2307–2320.

Khoury, M. J. and Bilder, D. (2020). Distinct activities of Scrib module proteins organize epithelial polarity. *Proc. Natl. Acad. Sci.* **117**, 11531–11540.

Kim, S., Gailite, I., Moussian, B., Luschnig, S., Goette, M., Fricke, K., Honemann-Capito, M., Grubmüller, H. and Wodarz, A. (2009). Kinase-activity-independent functions of atypical protein kinase C in Drosophila. *J. Cell Sci.* **122**, 3759–71.

Klezovitch, O., Fernandez, T. E., Tapscott, S. J. and Vasioukhin, V. (2004). Loss of cell polarity causes severe brain dysplasia in Lgl1 knockout mice. *Genes Dev.* **18**, 559–571.

Koh, Y. H., Popova, E., Thomas, U., Griffith, L. C. and Budnik, V. (1999). Regulation of DLG localization at synapses by CaMKII-dependent phosphorylation. *Cell* **98**, 353–363.

Kohu, K., Ogawa, F. and Akiyama, T. (2002). The SH3, HOOK and guanylate kinase-like domains of hDLG are important for its cytoplasmic localization. *Genes to Cells* **7**, 707–715.

Köppen, M., Simske, J. S., Sims, P. A., Firestein, B. L., Hall, D. H., Radice, A. D., Rongo, C. and Hardin, J. D. (2001). Cooperative regulation of AJM-1 controls junctional integrity in Caenorhabditis elegans epithelia. *Nat. Cell Biol.* **3**, 983–991.

Krahn, M. P. and Wodarz, A. (2012). Phosphoinositide lipids and cell polarity: linking the plasma membrane to the cytocortex. *Essays Biochem.* **53**, 15–27.

Krahn, M. P., Bückers, J., Kastrup, L. and Wodarz, A. (2010). Formation of a Bazooka-Stardust complex is essential for plasma membrane polarity in epithelia. *J. Cell Biol.* **190**, 751–760.

Kriebel, P. W., Barr, V. A., Rericha, E. C., Zhang, G. and Parent, C. A. (2008). Collective cell migration requires vesicular trafficking for chemoattractant delivery at the trailing edge. *J. Cell Biol.* **183**, 949–961.

Kulshammer, E., Mundorf, J., Kilinc, M., Frommolt, P., Wagle, P. and Uhlirova, M. (2015). Interplay among Drosophila transcription factors Ets21c, Fos and Ftz-F1 drives JNK-mediated tumor malignancy. *DMM Dis. Model. Mech.* **8**, 1279–1293.

Kwon, S. Y., Grisan, V., Jang, B., Herbert, J. and Badenhorst, P. (2016). Genome-Wide Mapping Targets of the Metazoan Chromatin Remodeling Factor NURF Reveals Nucleosome Remodeling at Enhancers, Core Promoters and Gene Insulators. *PLOS Genet.* **12**, e1005969.

La Marca, J. E. and Richardson, H. E. (2020). Two-Faced: Roles of JNK Signalling During Tumourigenesis in the Drosophila Model. *Front. Cell Dev. Biol.* **8**, 1–20.

Laiouar, S., Berns, N., Brech, A. and Riechmann, V. (2020). RabX1 Organizes a Late Endosomal Compartment that Forms Tubular Connections to Lysosomes Consistent with a "Kiss and Run" Mechanism. *Curr. Biol.* **30**, 1177-1188.e5.

Lam, S. S., Martell, J. D., Kamer, K. J., Deerinck, T. J., Ellisman, M. H., Mootha, V. K. and Ting, A. Y. (2014). Directed evolution of APEX2 for electron microscopy and proximity labeling. *Nat. Methods* **12**, 51–54.

Lanahan, A. A., Hermans, K., Claes, F., Kerley-Hamilton, J. S., Zhuang, Z. W., Giordano, F. J., Carmeliet, P. and Simons, M. (2010). VEGF receptor 2 endocytic trafficking regulates arterial morphogenesis. *Dev. Cell* **18**, 713–724.

Lang, C. F. and Munro, E. (2017). The PAR proteins: from molecular circuits to dynamic self-stabilizing cell polarity. *Development* **144**, 3405–3416.

Langevin, J., Morgan, M. J., Rossé, C., Racine, V., Sibarita, J. B., Aresta, S., Murthy, M., Schwarz, T., Camonis, J. and Bellaïche, Y. (2005). Drosophila exocyst components sec5,

sec6, and Sec15 regulate DE-Cadherin trafficking from recycling endosomes to the plasma membrane. *Dev. Cell* **9**, 365–376.

Laprise, P., Viel, A. and Rivard, N. (2004). Human Homolog of Disc-large Is Required for Adherens Junction Assembly and Differentiation of Human Intestinal Epithelial Cells. *J. Biol. Chem.* **279**, 10157–10166.

Laprise, P., Lau, K. M., Harris, K. P., Silva-Gagliardi, N. F., Paul, S. M., Beronja, S., Beitel, G. J., McGlade, C. J. and Tepass, U. (2009). Yurt, Coracle, Neurexin IV and the Na+,K+-ATPase form a novel group of epithelial polarity proteins. *Nature* **459**, 1141–1145.

Le Borgne, R. and Schweisguth, F. (2003). Unequal segregation of neuralized biases Notch activation during asymmetric cell division. *Dev. Cell* **5**, 139–148.

Lee, J. Y. and Harland, R. M. (2010). Endocytosis Is Required for Efficient Apical Constriction during Xenopus Gastrulation. *Curr. Biol.* **20**, 253–258.

Lee, T. and Luo, L. (1999). Mosaic analysis with a repressible cell marker for studies of gene function in neuronal morphogenesis. *Neuron* **22**, 451–61.

Lee, C. Y., Robinson, K. J. and Doe, C. Q. (2006). Lgl, Pins and aPKC regulate neuroblast self-renewal versus differentiation. *Nature* **439**, 594–598.

Lee, K. H., Lee, J. S., Lee, D., Seog, D. H., Lytton, J., Ho, W. K. and Lee, S. H. (2012). KIF21A-mediated axonal transport and selective endocytosis underlie the polarized targeting of NCKX2. *J. Neurosci.* **32**, 4102–4117.

Lee, S. R., Hong, S. T. and Choi, K. W. (2020). Regulation of epithelial integrity and organ growth by Tctp and Coracle in Drosophila. *PLoS Genet.* **16**, e1008885.

Legouis, R., Gansmuller, A., Sookhareea, S., Bosher, J. M., Baillie, D. L. and Labouesse, M. (2000). LET-413 is a basolateral protein required for the assembly of adherens junctions in Caenorhabditis elegans. *Nat. Cell Biol.* **2**, 415–422.

Legouis, R., Jaulin-Bastard, F., Schott, S., Navarro, C., Borg, J. P. and Labouesse, M. (2003). Basolateral targeting by leucine-rich repeat domains in epithelial cells. *EMBO Rep.* **4**, 1096–1102.

Lehman, K., Rossi, G., Adamo, J. E. and Brennwald, P. (1999). Yeast Homologues of Tomosyn and lethal giant larvae Function in Exocytosis and Are Associated with the Plasma Membrane SNARE, Sec9. *J. Cell Biol.* **146**, 125–140.

Lei, Y., Zhu, H., Duhon, C., Yang, W., Ross, M. E., Shaw, G. M. and Finnell, R. H. (2013). Mutations in Planar Cell Polarity Gene SCRIB Are Associated with Spina Bifida. *PLoS One* **8**, 1–8.

Leibfried, A., Fricke, R., Morgan, M. J., Bogdan, S. and Bellaiche, Y. (2008). Drosophila Cip4 and WASp Define a Branch of the Cdc42-Par6-aPKC Pathway Regulating E-Cadherin Endocytosis. *Curr. Biol.* **18**, 1639–1648.

Li, B. X., Satoh, A. K. and Ready, D. F. (2007). Myosin V, Rab11, and dRip11 direct apical secretion and cellular morphogenesis in developing Drosophila photoreceptors. *J. Cell Biol.* **177**, 659–669.

Lin, D., Edwards, A. S., Fawcett, J. P., Mbamalu, G., Scott, J. D. and Pawson, T. (2000). A mammalian PAR-3-PAR-6 complex implicated in Cdc42/Rac1 and aPKC signalling and cell polarity. *Nat. Cell Biol.* **2**, 540–547.

Liu, H., Wang, S., Hang, W., Gao, J., Zhang, W., Cheng, Z., Yang, C., He, J., Zhou, J., Chen, J., et al. (2017). LET-413/Erbin acts as a RAB-5 effector to promote RAB-10 activation during endocytic recycling. *J. Cell Biol.* **217**, jcb.201705136.

Lizama, C. O. and Zovein, A. C. (2013). Polarizing pathways: Balancing endothelial polarity,

permeability, and lumen formation. *Exp. Cell Res.* **319**, 1247–1254.
Lock, J. G. and Stow, J. L. (2005). Rab11 in Recycling Endosomes Regulates the Sorting and Basolateral Transport of E-Cadherin. *Mol. Biol. Cell* **16**, 1744–1755.
Lohia, M., Qin, Y. and Macara, I. G. (2012). The Scribble Polarity Protein Stabilizes E-Cadherin/p120-Catenin Binding and Blocks Retrieval of E-Cadherin to the Golgi. *PLoS One* **7**,.
Lu, H. and Bilder, D. (2005). Endocytic control of epithelial polarity and proliferation in Drosophila. *Nat. Cell Biol.* **7**, 1232–1239.
Lu, J., Dong, W., Tao, Y. and Hong, Y. (2021). Electrostatic plasma membrane targeting contributes to Dlg function in cell polarity and tumorigenesis. *Development* dev.196956.
Ma, R., Gong, D., You, H., Xu, C., Lu, Y., Bergers, G., Werb, Z., Klein, O. D., Petritsch, C. K. and Lu, P. (2022). LGL1 binds to Integrin β1 and inhibits downstream signaling to promote epithelial branching in the mammary gland. *Cell Rep.* **38**, 110375.
Madeira, F., Park, Y. M., Lee, J., Buso, N., Gur, T., Madhusoodanan, N., Basutkar, P., Tivey, A. R. N., Potter, S. C., Finn, R. D., et al. (2019). The EMBL-EBI search and sequence analysis tools APIs in 2019. *Nucleic Acids Res.* **47**, W636–W641.
Mannix, K. M., Starble, R. M., Kaufman, R. S. and Cooley, L. (2019). Proximity labeling reveals novel interactomes in live Drosophila tissue. *Development* **146**, dev176644.
Mantovani, F. and Banks, L. (2003). Regulation of the Discs Large Tumor Suppressor by a Phosphorylation-dependent Interaction with the β-TrCP Ubiquitin Ligase Receptor. *J. Biol. Chem.* **278**, 42477–42486.
Marcette, J., Hood, I. V., Johnston, C. A., Doe, C. Q. and Prehoda, K. E. (2009). Allosteric control of regulated scaffolding in membrane-associated guanylate kinases. *Biochemistry* **48**, 10014–10019.
Martell, J. D., Deerinck, T. J., Sancak, Y., Poulos, T. L., Mootha, V. K., Sosinsky, G. E., Ellisman, M. H. and Ting, A. Y. (2012). Engineered ascorbate peroxidase as a genetically encoded reporter for electron microscopy. *Nat. Biotechnol.* **30**, 1143–8.
Martin-Belmonte, F. and Mostov, K. (2008). Regulation of cell polarity during epithelial morphogenesis. *Curr. Opin. Cell Biol.* **20**, 227–234.
Martin-Belmonte, F. and Perez-Moreno, M. (2011). Epithelial cell polarity, stem cells and cancer. *Nat. Rev. Cancer* **12**, 23–38.
Martin-Belmonte, F., Gassama, A., Datta, A., Yu, W., Rescher, U., Gerke, V. and Mostov, K. (2007). PTEN-Mediated Apical Segregation of Phosphoinositides Controls Epithelial Morphogenesis through Cdc42. *Cell* **128**, 383–397.
Mathew, D., Gramates, L. S., Packard, M., Thomas, U., Bilder, D., Perrimon, N., Gorczyca, M. and Budnik, V. (2002). Recruitment of Scribble to the synaptic scaffolding complex requires GUK-holder, a novel DLG binding protein. *Curr. Biol.* **12**, 531–539.
McCann, J. J., Zheng, L., Rohrbeck, D., Felekyan, S., Kühnemuth, R., Sutton, R. B., Seidel, C. A. M. and Bowen, M. E. (2012). Supertertiary structure of the synaptic MAGuK scaffold proteins is conserved. *Proc. Natl. Acad. Sci. U. S. A.* **109**, 15775–15780.
McCartney, B. M., Kulikauskas, R. M., LaJeunesse, D. R. and Fehon, R. G. (2000). The neurofibromatosis-2 homologue, Merlin, and the tumor suppressor expanded function together in Drosophila to regulate cell proliferation and differentiation. *Development* **127**, 1315–24.
McGee, A. W. and Bredt, D. S. (1999). Identification of an intramolecular interaction between the SH3 and guanylate kinase domains of PSD-95. *J. Biol. Chem.* **274**, 17431–17436.

McGee, A. W., Dakoji, S. R., Olsen, O., Bredt, D. S., Lim, W. A. and Prehoda, K. E. (2001). Structure of the SH3-guanylate kinase module from PSD-95 suggests a mechanism for regulated assembly of MAGUK scaffolding proteins. *Mol. Cell* **8**, 1291–1301.

McMahon, L., Legouis, R., Vonesch, J. L. and Labouesse, M. (2001). Assembly of C. elegans apical junctions involves positioning and compaction by LET-413 and protein aggregation by the MAGUK protein DLG-1. *J Cell Sci* **114**, 2265–2277.

Mendoza-Topaz, C., Urra, F., Barría, R., Albornoz, V., Ugalde, D., Thomas, U., Gundelfinger, E. D., Delgado, R., Kukuljan, M., Sanxaridis, P. D., et al. (2008). DLGS97/SAP97 is developmentally upregulated and is required for complex adult behaviors and synapse morphology and function. *J. Neurosci.* **28**, 304–314.

Menut, L., Vaccari, T., Dionne, H., Hill, J., Wu, G. and Bilder, D. (2007). A mosaic genetic screen for Drosophila neoplastic tumor suppressor genes based on defective pupation. *Genetics* **177**, 1667–1677.

Mi, H., Muruganujan, A., Ebert, D., Huang, X. and Thomas, P. D. (2019). PANTHER version 14: more genomes, a new PANTHER GO-slim and improvements in enrichment analysis tools. *Nucleic Acids Res.* **47**, D419–D426.

Michaelis, U. R., Chavakis, E., Kruse, C., Jungblut, B., Kaluza, D., Wandzioch, K., Manavski, Y., Heide, H., Santoni, M. J., Potente, M., et al. (2013). The polarity protein scrib is essential for directed endothelial cell migration. *Circ. Res.* **112**, 924–934.

Moberg, K. H., Schelble, S., Burdick, S. K. and Hariharan, I. K. (2005). Mutations in erupted, the Drosophila ortholog of mammalian tumor susceptibility gene 101, elicit non-cell-autonomous overgrowth. *Dev. Cell* **9**, 699–710.

Montcouquiol, M., Rachel, R. A., Lanford, P. J., Copeland, N. G., Jenkins, N. A. and Kelley, M. W. (2003). Identification of Vangl2 and Scrb1 as planar polarity genes in mammals. *Nature* **423**, 173–177.

Morais-de-Sá, E., Mirouse, V. and St Johnston, D. (2010). aPKC Phosphorylation of Bazooka Defines the Apical/Lateral Border in Drosophila Epithelial Cells. *Cell* **141**, 509–523.

Moreira, S. and Morais-de-Sá, E. (2016). Spatiotemporal phosphoregulation of Lgl: Finding meaning in multiple on/off buttons. *Bioarchitecture* **6**, 29–38.

Moreira, S., Osswald, M., Ventura, G., Gonçalves, M., Sunkel, C. E. and Morais-de-Sá, E. (2019). PP1-Mediated Dephosphorylation of Lgl Controls Apical-basal Polarity. *Cell Rep.* **26**, 293–301.

Morrison, H. A., Dionne, H., Rusten, T. E., Brech, A., Fisher, W. W., Pfeiffer, B. D., Celniker, S. E., Stenmark, H. and Bilder, D. (2008). Regulation of early endosomal entry by the Drosophila tumor suppressors Rabenosyn and Vps45. *Mol. Biol. Cell* **19**, 4167–4176.

Mostov, K., Su, T. and ter Beest, M. (2003). Polarized epithelial membrane traffic: Conservation and plasticity. *Nat. Cell Biol.* **5**, 287–293.

Motegi, F., Zonies, S., Hao, Y., Cuenca, A. A., Griffin, E. and Seydoux, G. (2011). Microtubules induce self-organization of polarized PAR domains in Caenorhabditis elegans zygotes. *Nat. Cell Biol.* **13**, 1361–1367.

Murdoch, J. N., Henderson, D. J., Doudney, K., Gaston-Massuet, C., Phillips, H. M., Paternotte, C., Arkell, R., Stanier, P. and Copp, A. J. (2003). Disruption of scribble (Scrb1) causes severe neural tube defects in the circletail mouse. *Hum. Mol. Genet.* **12**, 87–98.

Murthy, M. and Schwarz, T. (2003). The exocyst component Sec5 is required for membrane traffic and polarity in the Drosophila ovary. *Development* **131**, 377–388.

Musch, A., Cohen, D., Yeaman, C., Nelson, W., Rodriguez-Boulan, E. and Brennwald, P. (2002). Mammalian Homolog of Drosophila Tumor Suppressor Lethal (2) Giant Larvae Interacts with Basolateral Exocytic Machinery in Madin-Darby Canine Kidney Cells. *Mol. Biol. Cell* **13**, 158–168.

Nagasaka, K., Seiki, T., Yamashita, A., Massimi, P., Subbaiah, V. K., Thomas, M., Kranjec, C., Kawana, K., Nakagawa, S., Yano, T., et al. (2013). A Novel Interaction between hScrib and PP1γ Downregulates ERK Signaling and Suppresses Oncogene-Induced Cell Transformation. *PLoS One* **8**, 1–10.

Naim, E., Bernstein, A., Bertram, J. F. and Caruana, G. (2005). Mutagenesis of the epithelial polarity gene, discs large 1, perturbs nephrogenesis in the developing mouse kidney. *Kidney Int.* **68**, 955–965.

Nakajima, Y. ichiro (2021). Scrib module proteins: Control of epithelial architecture and planar spindle orientation. *Int. J. Biochem. Cell Biol.* **136**, 106001.

Nakajima, Y., Lee, Z. T., McKinney, S. A., Swanson, S. K., Florens, L. and Gibson, M. C. (2019). Junctional tumor suppressors interact with 14-3-3 proteins to control planar spindle alignment. *J. Cell Biol.* jcb.201803116.

Nam, S. C., Mukhopadhyay, B. and Choi, K. W. (2007). Antagonistic functions of Par-1 kinase and protein phosphatase 2A are required for localization of Bazooka and photoreceptor morphogenesis in Drosophila. *Dev. Biol.* **306**, 624–635.

Narayan, N., Subbaiah, V. K. and Banks, L. (2009). The high-risk HPV E6 oncoprotein preferentially targets phosphorylated nuclear forms of hDlg. *Virology* **387**, 1–4.

Navarro, C., Nola, S., Audebert, S., Santoni, M. J., Arsanto, J. P., Ginestier, C., Marchetto, S., Jacquemier, J., Isnardon, D., Le Bivic, A., et al. (2005). Junctional recruitment of mammalian Scribble relies on E-cadherin engagement. *Oncogene* **24**, 4330–4339.

Nechiporuk, T., Fernandez, T. E. and Vasioukhin, V. (2007). Failure of Epithelial Tube Maintenance Causes Hydrocephalus and Renal Cysts in Dlg5-/- Mice. *Dev. Cell* **13**, 338–350.

Newman, R. A. and Prehoda, K. E. (2009). Intramolecular interactions between the Src homology 3 and guanylate kinase domains of discs large regulate its function in asymmetric cell division. *J. Biol. Chem.* **284**, 12924–12932.

Nishimura, T. and Kaibuchi, K. (2007). Numb Controls Integrin Endocytosis for Directional Cell Migration with aPKC and PAR-3. *Dev. Cell* **13**, 15–28.

Nix, S. L., Chishti, A. H., Anderson, J. M. and Walther, Z. (2000). hCASK and hDlg associate in epithelia, and their Src homology 3 and guanylate kinase domains participate in both intramolecular and intermolecular interactions. *J. Biol. Chem.* **275**, 41192–41200.

Nunes de Almeida, F., Walther, R. F., Pressé, M. T., Vlassaks, E. and Pichaud, F. (2019). Cdc42 defines apical identity and regulates epithelial morphogenesis by promoting apical recruitment of Par6-aPKC and Crumbs. *Development* **146**, dev175497.

Oh, H., Slattery, M., Ma, L., Crofts, A., White, K. P., Mann, R. S. and Irvine, K. D. (2013). Genome-wide Association of Yorkie with Chromatin and Chromatin-Remodeling Complexes. *Cell Rep.* **3**, 309–318.

Ohshiro, T., Yagami, T., Zhang, C. and Matsuzaki, F. (2000). Role of cortical tumour-suppressor proteins in asymmetric division of Drosophila neuroblast. *Nature* **408**, 593–596.

Oka, T., Remue, E., Meerschaert, K., Vanloo, B., Boucherie, C., Gfeller, D., Bader, G. D., Sidhu, S. S., Vandekerckhove, J., Gettemans, J., et al. (2010). Functional complexes between YAP2 and ZO-2 are PDZ domain-dependent, and regulate YAP2 nuclear

localization and signalling1. *Biochem. J.* **432**, 461–478.
Olsen, O. and Bredt, D. S. (2003). Functional Analysis of the Nucleotide Binding Domain of Membrane-associated Guanylate Kinases. *J. Biol. Chem.* **278**, 6873–6878.
Oshima, K. and Fehon, R. G. (2011). Analysis of protein dynamics within the septate junction reveals a highly stable core protein complex that does not include the basolateral polarity protein Discs large. *J. Cell Sci.* **124**, 2861–2871.
Osswald, M. and Morais-de-Sá, E. (2019). Dealing with apical–basal polarity and intercellular junctions: a multidimensional challenge for epithelial cell division. *Curr. Opin. Cell Biol.* **60**, 75–83.
Padash-Barmchi, M., Charish, K., Que, J. and Auld, V. J. (2013). Gliotactin and Discs large are co-regulated to maintain epithelial integrity. *J. Cell Sci.* **126**, 1134–1143.
Parisi, F., Stefanatos, R. K., Strathdee, K., Yu, Y. and Vidal, M. (2014). Transformed epithelia trigger non-tissue-autonomous tumor suppressor response by adipocytes via activation of toll and eiger/TNF signaling. *Cell Rep.* **6**, 855–867.
Parsons, L. M., Portela, M., Grzeschik, N. A. and Richardson, H. E. (2014). Lgl regulates notch signaling via endocytosis, independently of the apical aPKC-Par6-Baz polarity complex. *Curr. Biol.* **24**, 2073–2084.
Pearson, H. B., McGlinn, E., Phesse, T. J., Schlüter, H., Srikumar, A., Gödde, N. J., Woelwer, C. B., Ryan, A., Phillips, W. A., Ernst, M., et al. (2015). The polarity protein Scrib mediates epidermal development and exerts a tumor suppressive function during skin carcinogenesis. *Mol. Cancer* **14**, 169.
Pelissier, A., Chauvin, J. P. and Lecuit, T. (2003). Trafficking through Rab11 Endosomes Is Required for Cellularization during Drosophila Embryogenesis. *Curr. Biol.* **13**, 1848–1857.
Percher, A., Thinon, E. and Hang, H. (2017). Mass-Tag Labeling Using Acyl-PEG Exchange for the Determination of Endogenous Protein S-Fatty Acylation. *Curr. Protoc. protein Sci.* **89**, 14.17.1-14.17.11.
Perrimon, N. (1988). The maternal effect of lethal(1)discs-large-1: A recessive oncogene of Drosophila melanogaster. *Dev. Biol.* **127**, 392–407.
Petronczki, M. and Knoblich, J. A. (2001). DmPAR-6 directs epithelial polarity and asymmetric cell division of neuroblasts in Drosophila. *Nat. Cell Biol.* **3**, 43–49.
Pickett, M. A., Naturale, V. F. and Feldman, J. L. (2019). A polarizing issue: Diversity in the mechanisms underlying apico-basolateral polarization in Vivo. *Annu. Rev. Cell Dev. Biol.* **35**, 285–308.
Piguel, N. H., Fievre, S., Blanc, J. M., Carta, M., Moreau, M. M., Moutin, E., Pinheiro, V. L., Medina, C., Ezan, J., Lasvaux, L., et al. (2014). Scribble1/AP2 complex coordinates NMDA receptor endocytic recycling. *Cell Rep.* **9**, 712–727.
Plant, P. J., Fawcett, J. P., Lin, D. C. C., Holdorf, A. D., Binns, K., Kulkarni, S. and Pawson, T. (2003). A polarity complex of mPar-6 and atypical PKC binds, phosphorylates and regulates mammalian Lgl. *Nat. Cell Biol.* **5**, 301–308.
Pocha, S. M., Wassmer, T., Niehage, C., Hoflack, B. and Knust, E. (2011). Retromer controls epithelial cell polarity by trafficking the apical determinant crumbs. *Curr. Biol.* **21**, 1111–1117.
Portela, M., Parsons, L. M., Grzeschik, N. A. and Richardson, H. E. (2015). Regulation of Notch signaling and endocytosis by the Lgl neoplastic tumor suppressor. *Cell Cycle* **14**, 1496–1506.
Portela, M., Yang, L., Paul, S., Li, X., Veraksa, A., Parsons, L. M. and Richardson, H. E.

(2018). Lgl reduces endosomal vesicle acidification and Notch signaling by promoting the interaction between Vap33 and the V-ATPase complex. *Sci. Signal.* **11**, eaar1976.

Qian, Y. and Prehoda, K. E. (2006). Interdomain interactions in the tumor suppressor discs large regulate binding to the synaptic protein GukHolder. *J. Biol. Chem.* **281**, 35757–35763.

Qin, Y., Capaldo, C., Gumbiner, B. M. and Macara, I. G. (2005). The mammalian Scribble polarity protein regulates epithelial cell adhesion and migration through E-cadherin. *J. Cell Biol.* **171**, 1061–1071.

Rademacher, N., Kuropka, B., Kunde, S.-A., Wahl, M. C., Freund, C. and Shoichet, S. A. (2019). Intramolecular domain dynamics regulate synaptic MAGUK protein interactions. *Elife* **8**,.

Ragkousi, K., Marr, K., Mckinney, S., Ellington, L., Gibson, M. C., Ragkousi, K., Marr, K., Mckinney, S., Ellington, L. and Gibson, M. C. (2017). Cell-Cycle-Coupled Oscillations in Apical Polarity and Intercellular Contact Maintain Order in Embryonic Epithelia. *Curr. Biol.* 1–6.

Raman, R., Damle, I., Rote, R., Banerjee, S., Dingare, C. and Sonawane, M. (2016). APKC regulates apical localization of Lgl to restrict elongation of microridges in developing zebrafish epidermis. *Nat. Commun.* **7**, 1–16.

Ramanujam, R., Han, Z., Zhang, Z., Kanchanawong, P. and Motegi, F. (2018). Establishment of the PAR-1 cortical gradient by the aPKC-PRBH circuit. *Nat. Chem. Biol.* 1.

Rhee, H.-W., Zou, P., Udeshi, N. D., Martell, J. D., Mootha, V. K., Carr, S. A. and Ting, A. Y. (2013). Proteomic mapping of mitochondria in living cells via spatially restricted enzymatic tagging. *Science* **339**, 1328–31.

Richardson, H. E. and Portela, M. (2018). Modelling Cooperative Tumorigenesis in Drosophila a Model for Understanding Human Cancer. *Biomed Res. Int.* **2018**, 23–25.

Riga, A., Castiglioni, V. G. and Boxem, M. (2020). New insights into apical-basal polarization in epithelia. *Curr. Opin. Cell Biol.* **62**, 1–8.

Riggs, B., Rothwell, W., Mische, S., Hickson, G. R. X., Matheson, J., Hays, T. S., Gould, G. W. and Sullivan, W. (2003). Actin cytoskeleton remodeling during early Drosophila furrow formation requires recycling endosomal components Nuclear-fallout and Rab11. *J. Cell Biol.* **163**, 143–154.

Roberts, S., Calautti, E., Vanderweil, S., Nguyen, H. O., Foley, A., Baden, H. P. and Viel, A. (2007). Changes in localization of human discs large (hDlg) during keratinocyte differentiation is associated with expression of alternatively spliced hDlg variants. *Exp. Cell Res.* **313**, 2521–2530.

Roberts, S., Delury, C. and Marsh, E. (2012). The PDZ protein discs-large (DLG): The "Jekyll and Hyde" of the epithelial polarity proteins. *FEBS J.* **279**, 3549–3558.

Robinson, B. S. and Moberg, K. H. (2011). Drosophila endocytic neoplastic tumor suppressor genes regulate Sav/Wts/Hpo signaling and the c-Jun N-terminal kinase pathwa. *Cell Cycle* **10**, 4110–4118.

Robinson, A., Escuin, S., Vekemans, K. D., Stevenson, R. E., Greene, N. D. E., Copp, A. J. and Stanier, P. (2012). Mutations in the planar cell polarity genes CELSR1 and SCRIB are associated with the severe neural tube defect craniorachischisis. *Hum. Mutat.* **33**, 440–447.

Rodriguez-Boulan, E. and Macara, I. G. (2014). Organization and execution of the epithelial polarity programme. *Nat. Rev. Mol. Cell Biol.* **15**, 225–242.

Rodriguez-Boulan, E., Müsch, A. and Le Bivic, A. (2004). Epithelial trafficking: New routes

to familiar places. *Curr. Opin. Cell Biol.* **16**, 436–442.
Rodriguez-Boulan, E., Kreitzer, G. and Müsch, A. (2005). Organization of vesicular trafficking in epithelia. *Nat. Rev. Mol. Cell Biol.* **6**, 233–247.
Rodriguez, J., Peglion, F., Martin, J., Hubatsch, L., Reich, J., Hirani, N., Gubieda, A. G., Roffey, J., Fernandes, A. R., St Johnston, D., et al. (2017). aPKC Cycles between Functionally Distinct PAR Protein Assemblies to Drive Cell Polarity. *Dev. Cell* 1–16.
Roegiers, F., Jan, L. Y. and Jan, Y. N. (2005). Regulation of membrane localization of Sanpodo by lethal giant larvae and neuralized in asymmetrically dividing cells of Drosophila sensory organs. *Mol. Biol. Cell* **16**, 3480–7.
Roeth, J. F., Sawyer, J. K., Wilner, D. A. and Peifer, M. (2009). Rab11 helps maintain apical crumbs and adherens junctions in the drosophila embryonic ectoderm. *PLoS One* **4**, e7634.
Rohr, S., Bit-Avragim, N. and Abdelilah-Seyfried, S. (2006). Heart and soul/PRKCi and nagie oko/Mpp5 regulate myocardial coherence and remodeling during cardiac morphogenesis. *Development* **133**, 107–115.
Román-Fernández, A. and Bryant, D. M. (2016). Complex Polarity: Building Multicellular Tissues Through Apical Membrane Traffic. *Traffic* **17**, 1244–1261.
Rossi, G. and Brennwald, P. (2011). Yeast homologues of lethal giant larvae and type V myosin cooperate in the regulation of Rab-dependent vesicle clustering and polarized exocytosis. *Mol. Biol. Cell* **22**, 842–857.
Rui, M., Qian, J., Liu, L., Cai, Y., Lv, H., Han, J., Jia, Z. and Xie, W. (2017). The neuronal protein Neurexin directly interacts with the Scribble–Pix complex to stimulate F-actin assembly for synaptic vesicle clustering. *J. Biol. Chem.* **292**, 14334–14348.
Rust, K. and Wodarz, A. (2021). Transcriptional control of apical-basal polarity regulators. *Int. J. Mol. Sci.* **22**, 1–13.
Saito, Y., Desai, R. R. and Muthuswamy, S. K. (2018). Reinterpreting polarity and cancer: The changing landscape from tumor suppression to tumor promotion. *Biochim. Biophys. Acta - Rev. Cancer* **1869**, 103–116.
Salinas-Saavedra, M., Rock, A. Q. and Martindale, M. Q. (2018). Germ layer-specific regulation of cell polarity and adhesion gives insight into the evolution of mesoderm. *Elife* **7**,.
Sampo, B., Kaech, S., Kunz, S. and Banker, G. (2003). Two distinct mechanisms target membrane proteins to the axonal surface. *Neuron* **37**, 611–624.
Schindelin, J., Arganda-Carreras, I., Frise, E., Kaynig, V., Longair, M., Pietzsch, T., Preibisch, S., Rueden, C., Saalfeld, S., Schmid, B., et al. (2012). Fiji: An open-source platform for biological-image analysis. *Nat. Methods* **9**, 676–682.
Schlüter, M. A., Pfarr, C. S., Pieczynski, J., Whiteman, E. L., Hurd, T. W., Fan, S., Liu, C.-J. and Margolis, B. (2009). Trafficking of Crumbs3 during Cytokinesis Is Crucial for Lumen Formation. *Mol. Biol. Cell* **20**, 4652–4663.
Schneider-Brachert, W., Heigl, U. and Ehrenschwender, M. (2013). Membrane trafficking of death receptors: Implications on signalling. *Int. J. Mol. Sci.* **14**, 14475–14503.
Schulte, J., Charish, K., Que, J., Ravn, S., MacKinnon, C. and Auld, V. J. (2006). Gliotactin and Discs large form a protein complex at the tricellular junction of polarized epithelial cells in Drosophila. *J. Cell Sci.* **119**, 4391–4401.
Schürmann, C., Dienst, F. L., Pálfi, K., Vasconez, A. E., Oo, J. A., Wang, S. P., Buchmann, G. K., Offermanns, S., Van De Sluis, B., Leisegang, M. S., et al. (2019). The polarity protein Scrib limits atherosclerosis development in mice. *Cardiovasc. Res.* **115**, 1963–1974.

Schütze, S., Tchikov, V. and Schneider-Brachert, W. (2008). Regulation of TNFR1 and CD95 signalling by receptor compartmentalization. *Nat. Rev. Mol. Cell Biol.* **9**, 655–662.
Sflomos, G., Kostaras, E., Panopoulou, E., Pappas, N., Kyrkou, A., Politou, A. S., Fotsis, T. and Murphy, C. (2011). ERBIN is a new SARA-interacting protein: Competition between SARA and SMAD2 and SMAD3 for binding to ERBIN. *J. Cell Sci.* **124**, 3209–3222.
Shahab, J., Tiwari, M. D., Honemann-Capito, M., Krahn, M. P. and Wodarz, A. (2015). Bazooka/PAR3 is dispensable for polarity in Drosophila follicular epithelial cells. *Biol. Open* **4**, 528–541.
Sharifkhodaei, Z., Gilbert, M. M. and Auld, V. J. (2019). Scribble and Discs-large mediate tricellular junction formation. *Development* dev.174763.
Sharp, K. A., Khoury, M. J., Wirtz-Peitz, F. and Bilder, D. (2021). Evidence for a nuclear role for Drosophila Dlg as a regulator of the NURF complex. *Mol. Biol. Cell* **32**,.
Shivas, J. M., Morrison, H. A., Bilder, D. and Skop, A. R. (2010). Polarity and endocytosis: Reciprocal regulation. *Trends Cell Biol.* **20**, 445–452.
Siegrist, S. E. and Doe, C. Q. (2005). Microtubule-induced pins/Gαi cortical polarity in Drosophila neuroblasts. *Cell* **123**, 1323–1335.
Slaughter, B. D., Smith, S. E. and Li, R. (2009). Symmetry Breaking in the Life Cycle of the Budding Yeast. *Cold Spring Harb. Perspect. Biol.* **1**,.
Smith-Bolton, R. K., Worley, M. I., Kanda, H. and Hariharan, I. K. (2009). Regenerative Growth in Drosophila Imaginal Discs Is Regulated by Wingless and Myc. *Dev. Cell* **16**, 797–809.
Söderberg, O., Gullberg, M., Jarvius, M., Ridderstråle, K., Leuchowius, K. J., Jarvius, J., Wester, K., Hydbring, P., Bahram, F., Larsson, L. G., et al. (2006). Direct observation of individual endogenous protein complexes in situ by proximity ligation. *Nat. Methods* **3**, 995–1000.
Sokac, A. M. and Wieschaus, E. (2008). Local Actin-Dependent Endocytosis Is Zygotically Controlled to Initiate Drosophila Cellularization. *Dev. Cell* **14**, 775–786.
Sonawane, M., Carpio, Y., Geisler, R., Schwarz, H., Maischein, H. M. and Nuesslain-Volhard, C. (2005). Zebrafish penner/lethal giant larvae 2 functions in hemidesmosome formation, maintenance of cellular morphology and growth regulation in the developing basal epidermis. *Development* **132**, 3255–3265.
Song, S., Eckerle, S., Onichtchouk, D., Marrs, J. A., Nitschke, R. and Driever, W. (2013). Pou5f1-Dependent EGF Expression Controls E-Cadherin Endocytosis, Cell Adhesion, and Zebrafish Epiboly Movements. *Dev. Cell* **24**, 486–501.
Sotillos, S., Díaz-meco, M. T., Caminero, E., Moscat, J. and Campuzano, S. (2004). DaPKC-dependent phosphorylation of Crumbs is required for epithelial cell polarity in Drosophila. *J. Cell Biol.* **166**, 549–557.
Sripathy, S., Lee, M. and Vasioukhin, V. (2011). Mammalian Llgl2 Is Necessary for Proper Branching Morphogenesis during Placental Development. *Mol. Cell. Biol.* **31**, 2920–2933.
St Johnston, D. and Ahringer, J. (2010). Cell polarity in eggs and epithelia: Parallels and diversity. *Cell* **141**, 757–774.
Staller, M. V, Yan, D., Randklev, S., Bragdon, M. D., Wunderlich, Z. B., Tao, R., Perkins, L. A., De Pace, A. H. and Perrimon, N. (2013). Depleting gene activities in early drosophila embryos with the "maternal-Gal4-shRNA" system. *Genetics* **193**, 51–61.
Stephens, R., Lim, K., Portela, M., Kvansakul, M., Humbert, P. O. and Richardson, H. E. (2018). The Scribble Cell Polarity Module in the Regulation of Cell Signaling in Tissue

Development and Tumorigenesis. *J. Mol. Biol.* **430**, 3585–3612.
Stewart, M., Murphy, C. and Fristrom, J. W. (1972). The recovery and preliminary characterization of X chromosome mutants affecting imaginal discs ofDrosophila melanogaster. *Dev. Biol.* **27**, 71–83.
Stoops, E. H. and Caplan, M. J. (2014). Trafficking to the apical and basolateral membranes in polarized epithelial cells. *J. Am. Soc. Nephrol.* **25**, 1375–86.
Strand, D., Raska, I. and Mechler, B. M. (1994a). The Drosophila lethal(2)giant larvae tumor suppressor protein is a component of the cytoskeleton. *J. Cell Biol.* **127**, 1345–1360.
Strand, D., Jakobs, R., Merdes, G., Neumann, B., Kalmes, A., Heid, H. W., Husmann, I. and Mechler, B. M. (1994b). The Drosophila lethal(2)giant larvae tumor suppressor protein forms homo-oligomers and is associated with nonmuscle myosin II heavy chain. *J. Cell Biol.* **127**, 1361–73.
Strassburger, K., Kang, E. and Teleman, A. A. (2019). Drosophila ZDHHC8 palmitoylates scribble and Ras64B and controls growth and viability. *PLoS One* **14**, e0198149.
Stucke, V. M., Timmerman, E., Vandekerckhove, J., Gevaert, K. and Hall, A. (2007). The MAGUK protein MPP7 binds to the polarity protein hDlg1 and facilitates epithelial tight junction formation. *Mol. Biol. Cell* **18**, 1744–55.
Su, W.-H., Mruk, D. D., Wong, E. W. P., Lui, W.-Y. and Cheng, C. Y. (2012). Polarity protein complex Scribble/Lgl/Dlg and epithelial cell barriers. *Adv. Exp. Med. Biol.* **763**, 149–70.
Sun, G. and Irvine, K. D. (2011). Regulation of Hippo signaling by Jun kinase signaling during compensatory cell proliferation and regeneration, and in neoplastic tumors. *Dev. Biol.* **350**, 139–151.
Sun, S. D., Purdy, A. M. and Walsh, G. S. (2016). Planar cell polarity genes Frizzled3a, Vangl2, and Scribble are required for spinal commissural axon guidance. *BMC Neurosci.* **17**, 1–10.
Szczurkowska, J., Guo, A., Martin, J., Lee, S., Martinez, E., Chien, C. Te, Khan, T. A., Singh, R., Dadson, D., Tran, T. S., et al. (2022). Semaphorin3A/PlexinA3 association with the Scribble scaffold for cGMP increase is required for apical dendrite development. *Cell Rep.* **38**, 110483.
Tan, B., Yatim, S. M. J. M., Peng, S., Gunaratne, J., Hunziker, W. and Ludwig, A. (2020). The Mammalian Crumbs Complex Defines a Distinct Polarity Domain Apical of Epithelial Tight Junctions. *Curr. Biol.* 1–14.
Tanentzapf, G. and Tepass, U. (2003). Interactions between the crumbs, lethal giant larvae and bazooka pathways in epithelial polarization. *Nat. Cell Biol.* **5**, 46–52.
Tanimoto, H., Itoh, S., Ten Dijke, P. and Tabata, T. (2000). Hedgehog creates a gradient of DPP activity in Drosophila wing imaginal discs. *Mol. Cell* **5**, 59–71.
Tepass, U. (2012). The apical polarity protein network in Drosophila epithelial cells: regulation of polarity, junctions, morphogenesis, cell growth, and survival. *Annu. Rev. Cell Dev. Biol.* **28**, 655–685.
Tepass, U. and Tanentzapf, G. (2001). Epithelial cell polarity and cell junctions in Drosophila. *Annu. Rev. Genet.* **35**, 747–784.
Thomas, U., Ebitsch, S., Gorczyca, M., Koh, Y. H., Hough, C. D., Woods, D., Gundelfinger, E. D. and Budnik, V. (2000). Synaptic targeting and localization of Discs-large is a stepwise process controlled by different domains of the protein. *Curr. Biol.* **10**, 1108–1117.
Trinkle-Mulcahy, L. (2019). Recent advances in proximity-based labeling methods for

interactome mapping. *F1000Research* **8**, 135.
Troyanovsky, R. B., Indra, I., Kato, R., Mitchell, B. J. and Troyanovsky, S. M. (2021). Basolateral protein Scribble binds phosphatase PP1 to establish a signaling network maintaining apicobasal polarity. *J. Biol. Chem.* **297**, 101289.
Vaccari, T. and Bilder, D. (2005). The Drosophila tumor suppressor vps25 prevents nonautonomous overproliferation by regulating Notch trafficking. *Dev. Cell* **9**, 687–698.
Vaccari, T. and Bilder, D. (2009). At the crossroads of polarity, proliferation and apoptosis: The use of Drosophila to unravel the multifaceted role of endocytosis in tumor suppression. *Mol. Oncol.* **3**, 354–365.
Vaccari, T., Lu, H., Kanwar, R., Fortini, M. E. and Bilder, D. (2008). Endosomal entry regulates Notch receptor activation in Drosophila melanogaster. *J. Cell Biol.* **180**, 755–762.
Vaccari, T., Rusten, T. E., Menut, L., Nezis, I. P., Brech, A., Stenmark, H. and Bilder, D. (2009). Comparative analysis of ESCRT-I, ESCRT-II and ESCRT-III function in Drosophila by efficient isolation of ESCRT mutants. *J. Cell Sci.* **122**, 2413–2423.
Van Campenhout, C. A., Eitelhuber, A., Gloeckner, C. J., Giallonardo, P., Gegg, M., Oller, H., Grant, S. G. N., Krappmann, D., Ueffing, M. and Lickert, H. (2011). Dlg3 Trafficking and apical tight junction formation is regulated by Nedd4 and Nedd4-2 E3 Ubiquitin ligases. *Dev. Cell* **21**, 479–491.
Van Itallie, C. M., Aponte, A., Tietgens, A. J., Gucek, M., Fredriksson, K. and Anderson, J. M. (2013). The N and C termini of ZO-1 are surrounded by distinct proteins and functional protein networks. *J. Biol. Chem.* **288**, 13775–13788.
Vasioukhin, V. (2006). Lethal giant puzzle of Lgl. *Dev. Neurosci.* **28**, 13–24.
Ventura, G., Moreira, S., Barros-Carvalho, A., Osswald, M. and Morais-de-Sá, E. (2020). Lgl cortical dynamics are independent of binding to the Scrib-Dlg complex but require Dlg-dependent restriction of aPKC. *Development* dev.186593.
Visco, I., Hoege, C., Hyman, A. A. and Schwille, P. (2016). In vitro reconstitution of a membrane switch mechanism for the polarity protein LGL. *J. Mol. Biol.* **428**, 4828–4842.
Waaijers, S., Ramalho, J. J., Koorman, T., Kruse, E. and Boxem, M. (2015). The C. elegans Crumbs family contains a CRB3 homolog and is not essential for viability. *Biol. Open* **4**, 276–284.
Waaijers, S., Muñoz, J., Berends, C., Ramalho, J. J., Goerdayal, S. S., Low, T. Y., Zoumaro-Djayoon, A. D., Hoffmann, M., Koorman, T., Tas, R. P., et al. (2016). A tissue-specific protein purification approach in Caenorhabditis elegans identifies novel interaction partners of DLG-1/Discs large. *BMC Biol.* **14**, 66.
Wakula, P., Beullens, M., Ceulemans, H., Stalmans, W. and Bollen, M. (2003). Degeneracy and Function of the Ubiquitous RVXF Motif That Mediates Binding to Protein Phosphatase-1 *. *J. Biol. Chem.* **278**, 18817–18823.
Walch, L. (2013). Emerging role of the scaffolding protein Dlg1 in vesicle trafficking. *Traffic* **14**, 964–973.
Walther, R. F. and Pichaud, F. (2010). Crumbs/DaPKC-dependent apical exclusion of bazooka promotes photoreceptor polarity remodeling. *Curr. Biol.* **20**, 1065–1074.
Wan, J., Roth, A. F., Bailey, A. O. and Davis, N. G. (2007). Palmitoylated proteins: Purification and identification. *Nat. Protoc.* **2**, 1573–1584.
Wang, G.-S., Hong, C.-J., Yen, T.-Y., Huang, H.-Y., Ou, Y., Huang, T.-N., Jung, W.-G., Kuo, T.-Y., Sheng, M., Wang, T.-F., et al. (2004). Transcriptional Modification by a CASK-Interacting Nucleosome Assembly Protein. *Neuron* **42**, 113–128.

Wang, T., Liu, Y., Xu, X. H., Deng, C. Y., Wu, K. Y., Zhu, J., Fu, X. Q., He, M. and Luo, Z. G. (2011). Lgl1 activation of Rab10 Promotes axonal membrane trafficking underlying neuronal polarization. *Dev. Cell* **21**, 431–444.

Wang, S., Low, T. Y. F., Nishimura, Y., Gole, L., Yu, W. and Motegi, F. (2017). Cortical forces and CDC-42 control clustering of PAR proteins for Caenorhabditis elegans embryonic polarization. *Nat. Cell Biol.* **19**, 988–995.

Wang, X., Dong, B., Zhang, K., Ji, Z., Cheng, C., Zhao, H., Sheng, Y., Li, X., Fan, L., Xue, W., et al. (2018). E-cadherin bridges cell polarity and spindle orientation to ensure prostate epithelial integrity and prevent carcinogenesis in vivo. *PLOS Genet.* **14**, e1007609.

Watson, K., Rossi, G., Temple, B. and Brennwald, P. (2015). Structural basis for recognition of the Sec4 Rab GTPase by its effector, the Lgl/tomosyn homologue, Sro7. *Mol. Biol. Cell* **26**, 3289–300.

Weinkove, D., Neufeld, T. P., Twardzik, T., Waterfield, M. D. and Leevers, S. J. (1999). Regulation of imaginal disc cell size, cell number and organ size by Drosophila class I(A) phosphoinositide 3-kinase and its adaptor. *Curr. Biol.* **9**, 1019–1029.

Weisz, O. a and Rodriguez-Boulan, E. (2009). Apical trafficking in epithelial cells: signals, clusters and motors. *J. Cell Sci.* **122**, 4253–4266.

Windler, S. L. and Bilder, D. (2010). Endocytic Internalization Routes Required for Delta/Notch Signaling. *Curr. Biol.* **20**, 538–543.

Wirtz-Peitz, F., Nishimura, T. and Knoblich, J. A. (2008). Linking Cell Cycle to Asymmetric Division: Aurora-A Phosphorylates the Par Complex to Regulate Numb Localization. *Cell* **135**, 161–173.

Wodarz, A., Ramrath, A., Grimm, A. and Knust, E. (2000). Drosophila atypical protein kinase C associates with Bazooka and controls polarity of epithelia and neuroblasts. *J. Cell Biol.* **150**, 1361–1374.

Woichansky, I., Beretta, C. A., Berns, N. and Riechmann, V. (2016). Three mechanisms control E-cadherin localization to the zonula adherens. *Nat. Commun.* **7**, 10834.

Woods, D. F. and Bryant, P. J. (1989). Molecular cloning of the lethal(1)discs large-1 oncogene of Drosophila. *Dev. Biol.* **134**, 222–235.

Woods, D. F. and Bryant, P. J. (1993). ZO-1, DlgA and PSD-95/SAP90: homologous proteins in tight, septate and synaptic cell junctions. *Mech. Dev.* **44**, 85–89.

Woods, D. F., Hough, C., Peel, D., Callaini, G. and Bryant, P. J. (1996). Dlg protein is required for junction structure, cell polarity, and proliferation control in Drosophila epithelia. *J. Cell Biol.* **134**, 1469–1482.

Worzfeld, T. and Schwaninger, M. (2016). Apicobasal polarity of brain endothelial cells. *J. Cereb. Blood Flow Metab.* **36**, 340–362.

Xiao, H., Sandaltzopoulos, R., Wang, H.-M., Hamiche, A., Ranallo, R., Lee, K.-M., Fu, D. and Wu, C. (2001). Dual Functions of Largest NURF Subunit NURF301 in Nucleosome Sliding and Transcription Factor Interactions. *Mol. Cell* **8**, 531–543.

Yamanaka, T., Horikoshi, Y., Suzuki, A., Sugiyama, Y., Kitamura, K., Maniwa, R., Nagai, Y., Yamashita, A., Hirose, T., Ishikawa, H., et al. (2001). PAR-6 regulates aPKC activity in a novel way and mediates cell-cell contact-induces formation of the epithelial junctional complex. *Genes to Cells* **6**, 721–731.

Yamanaka, T., Horikoshi, Y., Sugiyama, Y., Ishiyama, C., Suzuki, A., Hirose, T., Iwamatsu, A., Shinohara, A. and Ohno, S. (2003). Mammalian Lgl forms a protein complex with PAR-6 and aPKC independently of PAR-3 to regulate epithelial cell polarity.

Curr. Biol. **13**, 734–743.
Yamanaka, T., Horikoshi, Y., Izumi, N., Suzuki, A., Mizuno, K. and Ohno, S. (2006). Lgl mediates apical domain disassembly by suppressing the PAR-3-aPKC-PAR-6 complex to orient apical membrane polarity. *J. Cell Sci.* **119**, 2107–2118.
Yan, Y., Denef, N., Tang, C. and Schupbach, T. (2011). Drosophila PI4KIIIalpha is required in follicle cells for oocyte polarization and Hippo signaling. *Development* **138**, 1697–1703.
Yates, L. L., Schnatwinkel, C., Hazelwood, L., Chessum, L., Paudyal, A., Hilton, H., Romero, M. R., Wilde, J., Bogani, D., Sanderson, J., et al. (2013). Scribble is required for normal epithelial cell-cell contacts and lumen morphogenesis in the mammalian lung. *Dev. Biol.* **373**, 267–280.
Yoshihara, K., Ikenouchi, J., Izumi, Y., Akashi, M., Tsukita, S. and Furuse, M. (2011). Phosphorylation state regulates the localization of Scribble at adherens junctions and its association with E-cadherin-catenin complexes. *Exp. Cell Res.* **317**, 413–422.
Young, L. C., Hartig, N., Muñoz-Alegre, M., Oses-Prieto, J. A., Durdu, S., Bender, S., Vijayakumar, V., VietriRudan, M., Gewinner, C., Henderson, S., et al. (2013). An MRAS, SHOC2, and SCRIB complex coordinates erk pathway activation with polarity and tumorigenic growth. *Mol. Cell* **52**, 679–692.
Zarnescu, D. C., Jin, P., Betschinger, J., Nakamoto, M., Wang, Y., Dockendorff, T. C., Feng, Y., Jongens, T. A., Sisson, J. C., Knoblich, J. A., et al. (2005). Fragile X protein functions with Lgl and the PAR complex in flies and mice. *Dev. Cell* **8**, 43–52.
Zeitler, J., Hsu, C. P., Dionne, H. and Bilder, D. (2004). Domains controlling cell polarity and proliferation in the Drosophila tumor suppressor scribble. *J. Cell Biol.* **167**, 1137–1146.
Zeng, M., Ye, F., Xu, J. and Zhang, M. (2017). PDZ Ligand Binding-Induced Conformational Coupling of the PDZ-SH3-GK Tandems in PSD-95 Family MAGUKs. *J. Mol. Biol.* **430**, 69–86.
Zhang, X., Wang, P., Gangar, A., Zhang, J., Brennwald, P., TerBush, D. and Guo, W. (2005). Lethal giant larvae proteins interact with the exocyst complex and are involved in polarized exocytosis. *J. Cell Biol.* **170**, 273–283.
Zhang, J., Lewis, S. M., Kuhlman, B. and Lee, A. L. (2013). Supertertiary structure of the MAGUK core from PSD-95. *Structure* **21**, 402–413.
Zhang, H., Neimanis, S., Lopez-Garcia, L. A., Arencibia, J. M., Amon, S., Stroba, A., Zeuzem, S., Proschak, E., Stark, H., Bauer, A. F., et al. (2014). Molecular mechanism of regulation of the atypical protein kinase C by N-terminal domains and an allosteric small compound. *Chem. Biol.* **21**, 754–765.
Zhou, B., Wu, Y. and Lin, X. (2011). Retromer regulates apical-basal polarity through recycling crumbs. *Dev. Biol.* **360**, 87–95.
Zhu, M., Xin, T., Weng, S., Gao, Y., Zhang, Y., Li, Q. and Li, M. (2010). Activation of JNK signaling links lgl mutations to disruption of the cell polarity and epithelial organization in Drosophila imaginal discs. *Cell Res.* **20**, 242–5.
Zhu, J., Shang, Y., Chen, J. and Zhang, M. (2012). Structure and function of the guanylate kinase-like domain of the MAGUK family scaffold proteins. *Front. Biol. (Beijing).* **7**, 379–396.
Zhu, J., Shang, Y., Wan, Q., Xia, Y., Chen, J., Du, Q. and Zhang, M. (2014). Phosphorylation-dependent interaction between tumor suppressors Dlg and Lgl. *Cell Res.* **24**, 451–463.
Žigman, M., Trinh, L. A., Fraser, S. E. and Moens, C. B. (2011). Zebrafish neural tube

morphogenesis requires scribble-dependent oriented cell divisions. *Curr. Biol.* **21**, 79–86.

Appendix 1: A preliminary Lgl proximity proteome

To discover functionally relevant protein Lgl binding partners, we took an APEX2-based approach, wherein the promiscuous biotin ligase, APEX2, is fused to a bait protein of interest and can biotinylate any nearby proteins within a 20nm radius. Biotinylated prey proteins are then purified and submitted for mass spectrometry. Importantly, the APEX2 technique can be performed in situ, in intact cells, and can identify low affinity, transient and low abundance interactions that may be missed by traditional biochemical assays for protein-protein interaction (Gingras et al., 2019; Hung et al., 2016). We had previously adapted this method to successfully identify proteins in close proximity to the polarity regulator, Dlg, in intact epithelia (Sharp et al., 2021).

To identify Lgl-proximal proteins, we expressed a functional UAS-Lgl::APEX2 construct in in larval epithelial cells using d174-GAL4 in an *lgl* null mutant background. We then dissected the thoracic imaginal discs (wing, haltere and leg discs) from wandering third instar (L3) larvae. These tissues were biotin labeled in vivo, and the purified biotinylated protein sample prepared for mass spec as previously described (Sharp et al., 2021).

The top 50 mass spec hits are given in **Table 1.** The full dataset can be downloaded at http://www.ocf.berkeley.edu/~bilder/wp-content/uploads/2022/03/Lgl_APEX2_data_extended.xlsx
(note that fold change is reversed such that enriched proteins have a lower fold change, due to the way the data were analyzed)

We identified expected proteins, such as Dlg and Scrib, as well as basolateral and junctional proteins such as Kune, Cora and Nrg. Interestingly, Scrib and Dlg were not among the most highly enriched in our dataset, supporting the idea that Scrib, Dlg and Lgl do not exist in a stable complex, although functionally they are mutually dependent (Ventura et al., 2020). We performed Gene Ontology (GO) term analysis (Ashburner et al., 2000; Carbon et al., 2021; Mi et al., 2019) and along with expected terms such as "protein binding," "kinase binding," and "cytoskeletal protein binding," we were surprised to see significant overrepresentation of what appear to be RNA binding proteins, with terms such as "mRNA 3'UTR binding" and "Poly(U) binding" (**Table 2**). Indeed, the top enriched term in the dataset was "Poly(G) binding," suggesting that a large number of Lgl proximal proteins and/or Lgl binding partners are themselves RNA binding proteins. Examples of these in the dataset include Fmr1, Yps, Vig and Caprin. This is interesting, given that a well-known Lgl binding partner is Fmr1 (aka FMRP), a highly studied mRNA binding protein that is involved in promoting translation of specific mRNAs in neurons (Zarnescu et al., 2005). The function of this putative Lgl activity is unclear.

Other GO terms of interest include "GTPase activity," with Rho1, RhoGEF2 and Cdc42 in the dataset, all of which have known polarity or epithelial morphogenesis roles. Interestingly, we identified several secretory proteins including Sec24AB, Sec24CD, Sec23 and Syx1A, which is consistent with early hypotheses that Lgl could be involved in exocytosis, based on the fact that the putative yeast Lgl homolog, Sro7/77 regulates the exocyst and polarized vesicle secretion (Lehman et al., 1999; Zhang et al., 2005).

However, we were surprised that we did not identify certain known Lgl binding partners in our dataset. For example, aPKC, arguably the most important Lgl regulator, was not present in the data. This may reflect the fact that kinase-substrate interactions are very transient, and once phosphorylated, Lgl would be ejected from aPKC's active site, resulting in low-level labeling in our experiment. Additionally, the majority of Lgl in the cell is at the basolateral cortex, meaning that proximity to aPKC would be limited to a very small pool of Lgl protein. We also failed to detect Pp1-87B in our dataset, a recently identified negative regulator of Lgl phosphorylation (Moreira et al., 2019).

In summary, this dataset will be a valuable resource to our lab and to the community for future studies of the enigmatic nature of Lgl function.

Table 1. Top 50 enriched Lgl-APEX2 hits

NAME	SYMBOL	p-value	q-value	fold change	Wilcoxon p-value	t-test p-value	resampled p-value
-	CG1648	3.155E-06	1.361E-06	0.1732	0.05	0.0009133	0.0156
lethal (2) giant larvae	l(2)gl	0.0000637	0.00002249	0.1758	0.05	0.001451	0.0171
scramblase 2	scramb2	1.971E-06	8.63E-07	0.1919	0.05	0.001204	0.0168
Aldolase 1	Ald1	0.00002449	9.271E-06	0.2034	0.05	0.001141	0.0168
-	CG8461	9.73E-07	4.40E-07	0.2044	0.05	0.004622	0.0185
Vesicle trafficking 1	Vta1	1.749E-06	7.68E-07	0.2158	0.05	0.001777	0.0141
Ran GTPase activating protein	RanGAP	0.0001139	0.00003866	0.223	0.05	0.001336	0.0156
kune-kune	kune	2.714E-06	1.177E-06	0.2231	0.05	0.001583	0.0129
vig2	vig2	0.00001563	0.00000612	0.2241	0.05	0.001237	0.0152
Ribosomal protein S10b	RpS10b	0.00000367	1.572E-06	0.2344	0.05	0.001162	0.0162
Caprin	Capr	0.00003198	0.00001187	0.2398	0.05	0.001605	0.0156
windpipe	wdp	0.00000238	1.035E-06	0.2472	0.05	0.001136	0.0171
eukaryotic translation initiation factor 4H1	eIF4H1	2.067E-06	9.03E-07	0.2503	0.05	0.001599	0.0144
Eb1	Eb1	6.421E-06	2.671E-06	0.2505	0.05	0.002413	0.0137

vasa intronic gene	vig	0.0000043	1.815E-06	0.2581	0.05	0.0008515	0.0169
epithelial membrane protein	emp	6.886E-06	2.844E-06	0.2583	0.05	0.006112	0.0169
lingerer	lig	0.00007169	0.00002506	0.2612	0.05	0.001249	0.0159
pasiflora 2	pasi2	0.00001166	4.682E-06	0.2622	0.05	0.0277	0.032
-	CG3760	3.196E-06	1.375E-06	0.2667	0.05	0.002906	0.0176
failed axon connections	fax	0.00002321	8.824E-06	0.2669	0.05	0.002413	0.0155
squid	sqd	0.00002119	8.146E-06	0.2674	0.05	0.001318	0.0168
eukaryotic translation elongation factor 1 delta	eEF1delta	6.694E-06	2.771E-06	0.2704	0.05	0.00122	0.0158
Pendulin	Pen	0.0001807	0.00005832	0.2714	0.05	0.0009284	0.0153
rasputin	rin	8.012E-06	3.277E-06	0.2722	0.05	0.0009835	0.0155
ubiquitin like	ubl	6.535E-06	2.711E-06	0.2734	0.05	0.001185	0.016
-	CG5174	0.00001347	5.347E-06	0.275	0.05	0.001089	0.0155
Innexin 2	Inx2	6.136E-06	2.564E-06	0.2754	0.05	0.003032	0.0164
-	CG10939	9.195E-06	3.752E-06	0.2764	0.05	0.002175	0.0151
coracle	cora	0.0003338	0.0001026	0.2772	0.05	0.001042	0.0146
beta1,3-galactosyltransferase 1	GalT1	7.129E-06	2.937E-06	0.2775	0.05	0.002868	0.0159
Fasciclin 3	Fas3	4.553E-06	1.912E-06	0.2832	0.05	0.003276	0.0157
Crk oncogene	Crk	0.00001077	4.365E-06	0.2838	0.05	0.001203	0.0145
Src oncogene at 42A	Src42A	0.00001047	4.251E-06	0.2846	0.05	0.002868	0.0137
Neuroglian	Nrg	0.00001186	0.00000475	0.2851	0.05	0.001184	0.0167
Annexin B9	AnxB9	0.0001102	0.00003747	0.2859	0.05	0.005511	0.0142

-	CG40045	0.00001432	5.642E-06	0.2894	0.05	0.004053	0.0157
Innexin 3	Inx3	0.00001542	0.00000605	0.2904	0.05	0.005853	0.0172
Aldehyde dehydrogenase type III	Aldh-III	0.0001429	0.00004753	0.2939	0.05	0.007075	0.0176
Lasp	Lasp	0.00001385	5.485E-06	0.2972	0.05	0.001259	0.0159
multiprotein bridging factor 1	mbf1	6.371E-06	2.656E-06	0.2979	0.05	0.001529	0.0153
Rho1	Rho1	0.00002274	8.686E-06	0.2991	0.05	0.001986	0.017
A kinase anchor protein 200	Akap200	0.00008308	0.00002881	0.2991	0.05	0.00178	0.0158
-	CG17765	9.456E-06	0.00000385	0.2992	0.05	0.001508	0.0167
belle	bel	0.00008808	0.00003036	0.3012	0.05	0.001041	0.0162
Cdc42	Cdc42	4.039E-06	1.713E-06	0.3028	0.05	0.001695	0.0161
Secretory 24CD	Sec24CD	0.0002024	0.00006498	0.3037	0.05	0.00164	0.014
Cdc37	Cdc37	0.00001238	4.937E-06	0.3047	0.05	0.001552	0.014
Chd64	Chd64	0.00003059	0.00001141	0.3053	0.05	0.002245	0.0167
Tetraspanin 42El	Tsp42El	0.00001614	6.305E-06	0.3056	0.05	0.005091	0.0149
stathmin	stai	0.00005285	0.00001897	0.3103	0.05	0.001859	0.0146

Table 2. GO term analysis of Lgl-APEX2 data

GO molecular function complete	**upload_1 (fold Enrichment)**	**upload_1 (raw P-value)**	**upload_1 (FDR)**
poly(G) binding (GO:0034046)	75.11	4.33E-05	2.90E-03
poly(U) RNA binding (GO:0008266)	27.31	3.51E-05	2.47E-03
poly-purine tract binding (GO:0070717)	25.04	4.64E-05	3.04E-03
poly-pyrimidine tract binding (GO:0008187)	20.03	9.58E-05	6.00E-03

protein tag (GO:0031386)	18.78	9.04E-04	4.73E-02
mRNA 3'-UTR binding (GO:0003730)	13.97	3.00E-07	6.64E-05
translation initiation factor activity (GO:0003743)	13.26	7.96E-08	1.91E-05
translation factor activity, RNA binding (GO:0008135)	12.35	1.05E-09	3.04E-07
translation initiation factor binding (GO:0031369)	12.02	5.30E-04	3.05E-02
single-stranded RNA binding (GO:0003727)	10.99	3.25E-05	2.40E-03
translation regulator activity, nucleic acid binding (GO:0090079)	10.73	9.80E-10	3.14E-07
translation regulator activity (GO:0045182)	10.41	3.11E-10	1.28E-07
actin filament binding (GO:0051015)	7.8	1.55E-05	1.44E-03
GTPase activator activity (GO:0005096)	7.61	1.84E-05	1.66E-03
SNARE binding (GO:0000149)	7.36	8.23E-04	4.47E-02
ribonucleoprotein complex binding (GO:0043021)	7.27	2.64E-04	1.58E-02
myosin binding (GO:0017022)	7.22	8.93E-04	4.76E-02
mRNA binding (GO:0003729)	7.22	1.83E-12	1.32E-09
actin binding (GO:0003779)	6.61	1.75E-06	2.96E-04
kinase binding (GO:0019900)	6.32	2.19E-05	1.85E-03
cell adhesion molecule binding (GO:0050839)	6.09	6.37E-04	3.60E-02
protein kinase binding (GO:0019901)	5.91	2.68E-04	1.58E-02
enzyme activator activity (GO:0008047)	5.66	7.08E-06	8.15E-04
cytoskeletal protein binding (GO:0008092)	5.45	4.35E-11	2.51E-08
GTP binding (GO:0005525)	5.33	1.20E-05	1.20E-03
guanyl ribonucleotide binding (GO:0032561)	5.2	1.51E-05	1.45E-03
GTPase activity (GO:0003924)	5.11	4.24E-05	2.91E-03

protein-containing complex binding (GO:0044877)	5.09	5.98E-09	1.57E-06
guanyl nucleotide binding (GO:0019001)	5.04	1.98E-05	1.73E-03
nucleoside-triphosphatase regulator activity (GO:0060589)	4.98	2.20E-05	1.81E-03
GTPase regulator activity (GO:0030695)	4.98	2.20E-05	1.76E-03
tubulin binding (GO:0015631)	4.48	2.63E-04	1.62E-02
RNA binding (GO:0003723)	4.2	1.03E-13	9.93E-11
nucleoside-triphosphatase activity (GO:0017111)	3.74	9.62E-06	1.07E-03
pyrophosphatase activity (GO:0016462)	3.47	2.33E-05	1.81E-03
hydrolase activity, acting on acid anhydrides, in phosphorus-containing anhydrides (GO:0016818)	3.39	3.14E-05	2.38E-03
hydrolase activity, acting on acid anhydrides (GO:0016817)	3.37	3.35E-05	2.41E-03
enzyme regulator activity (GO:0030234)	2.98	8.05E-05	5.16E-03
protein binding (GO:0005515)	2.92	1.05E-23	3.04E-20
purine ribonucleoside triphosphate binding (GO:0035639)	2.79	7.81E-07	1.50E-04
purine ribonucleotide binding (GO:0032555)	2.71	1.38E-06	2.48E-04
ATP-dependent activity (GO:0140657)	2.7	9.10E-04	4.68E-02
ribonucleotide binding (GO:0032553)	2.67	1.79E-06	2.87E-04
purine nucleotide binding (GO:0017076)	2.67	1.79E-06	2.72E-04
enzyme binding (GO:0019899)	2.66	6.91E-04	3.83E-02
nucleotide binding (GO:0000166)	2.44	5.85E-06	7.33E-04
nucleoside phosphate binding (GO:1901265)	2.44	5.85E-06	7.02E-04
carbohydrate derivative binding (GO:0097367)	2.4	5.20E-06	7.49E-04
anion binding (GO:0043168)	2.34	1.12E-05	1.19E-03
small molecule binding (GO:0036094)	2.29	1.15E-05	1.18E-03

nucleic acid binding (GO:0003676)	2.12	4.24E-07	8.72E-05
heterocyclic compound binding (GO:1901363)	2.05	1.62E-10	7.79E-08
organic cyclic compound binding (GO:0097159)	2.04	3.15E-10	1.13E-07
binding (GO:0005488)	1.87	1.13E-20	1.63E-17
molecular_function (GO:0003674)	1.16	5.47E-06	7.16E-04
Unclassified (UNCLASSIFIED)	0.39	5.47E-06	7.50E-04

Appendix 2: Other experiments related to Scrib module function

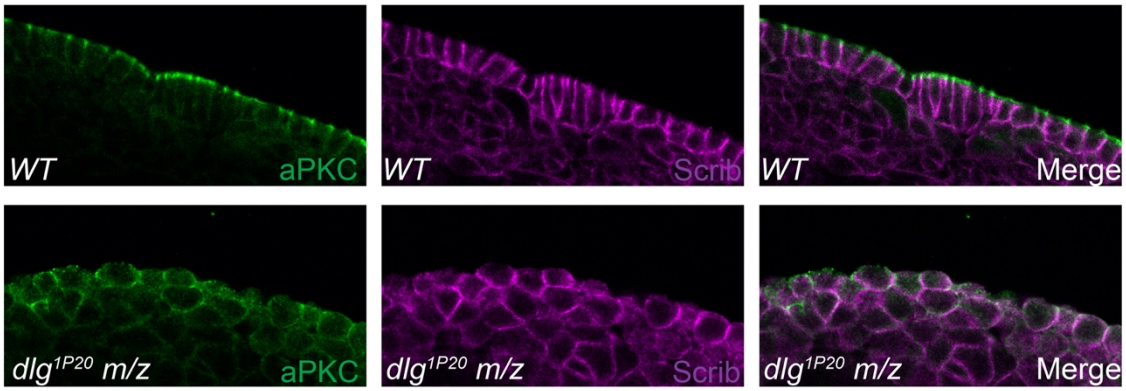

Context-dependent requirement of the Dlg GUK domain

Different cell and tissue types may exhibit differences in their requirements for polarity proteins (Pickett et al., 2019). In the wing imaginal disc and follicle epithelia, the Dlg GUK domain is dispensable for polarity (Hough et al., 1997; Khoury and Bilder, 2020; Lu et al., 2021). To explore whether this is universally true, we generated embryos that are maternal and zygotic mutant for *dlg*^{1P20}, a GUK-truncating *dlg* allele. Surprisingly, in contrast to imaginal disc and follicle cells, embryonic epidermis in *dlg*^{1P20} m/z mutants exhibited highly penetrant multilayering and aPKC mislocalization. Thus, the Dlg GUK domain is differentially required depending on the cell type context.

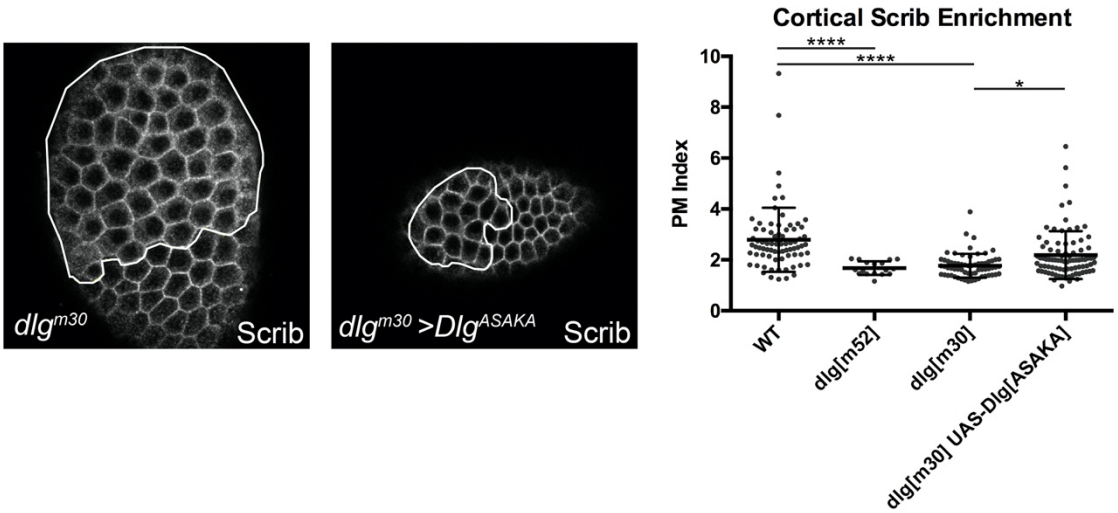

Testing Dlg SH3-HOOK function in trans assemblies

We found that the Dlg SH3 and HOOK domains comprise the minimal functional unit of the protein that is required and sufficient to regulate Scrib localization (see Chapter 3). In addition to intramolecular interactions, MAGUK SH3-HOOK-GUK domains can participate in intermolecular assembly to generate 'domain-swapped' oligomers (McGee et al., 2001). To test whether the Dlg SH3-HOOK module functions in both inter- and intramolecular modes to regulate Scrib recruitment, we expressed the HOOK domain mutant, *Dlg*^{ASAKA} in an SH3 mutant background (*dlg*^{m30}). We found that compared to a *dlg* null mutant (*dlg*^{m52}), *dlg*^{m30} mislocalized

Scrib. Expression of Dlg^{ASAKA} in dlg^{m30} mutant cells slightly, but significantly improved Scrib cortical localization, suggesting that SH3-HOOK activity may partly involve intermolecular domain swapping.

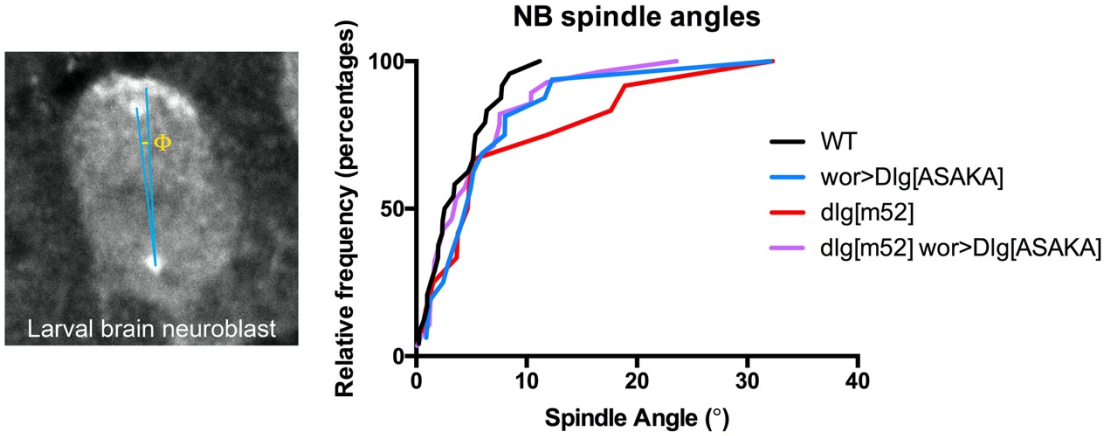

The Dlg HOOK domain may be dispensable for spindle orientation

Neuroblasts are asymmetrically dividing neural stem cells in the embryonic and larval *Drosophila* brain that divide to produce one differentiating daughter cell (Ganglion Mother Cell) and one stem cell (neuroblast). To ensure division asymmetry, neuroblasts must orient their spindles along their apical-basal axis. Dlg is known to be involved in this process (Golub et al., 2017; Siegrist and Doe, 2005); thus, we wondered if our recently characterized HOOK domain mutant construct, Dlg^{ASAKA}, which has complete loss of function phenotypes in epithelial cells, would be able to rescue neuroblast spindle orientation. We found that while WT cells had little variation in spindle angle and most were between 0-10°, *dlg* mutant neuroblasts had more widely varying spindle angles, consistent with previous studies. Dlg^{ASAKA} expression partially rescued spindle angle variance in *dlg* mutants, suggesting the HOOK domain is partly dispensable for spindle orientation.

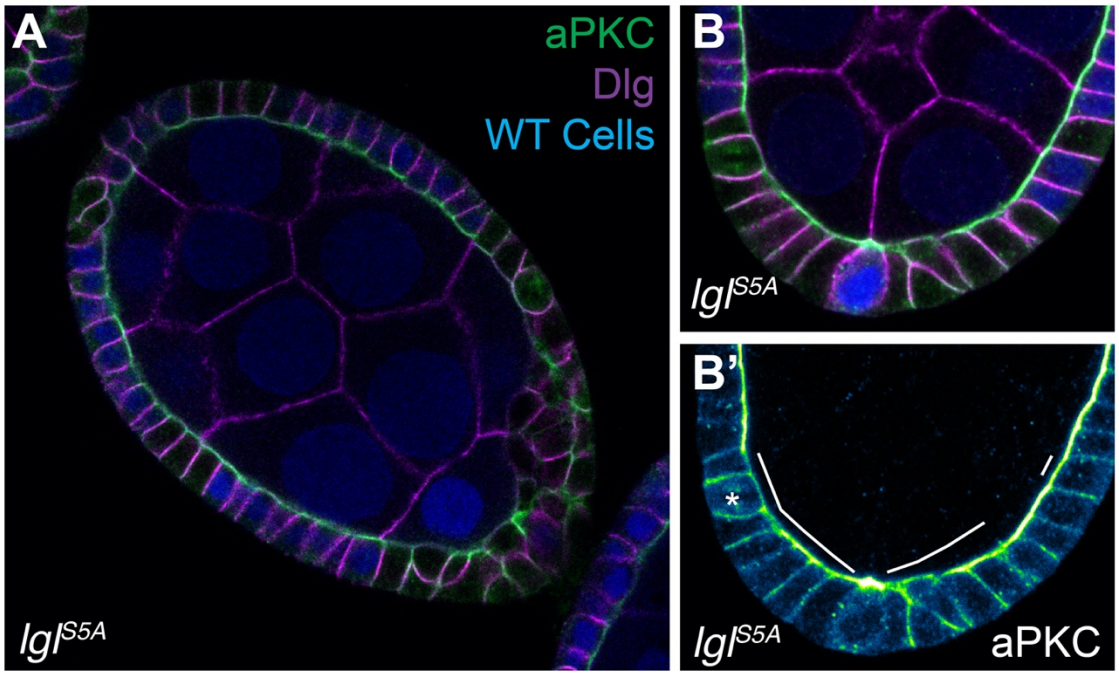

Lgl phosphorylation is required for function

We previously proposed a model where Scrib and Dlg are required to 'protect' basolateral Lgl from aPKC phosphorylation, where site-specific regulation of Lgl phosphorylation by Scrib and Dlg enables Lgl's aPKC-inhibiting activity via a competitive inhibition mechanism (Khoury and Bilder, 2020). An important assumption of this model is that basolateral Lgl must be in a partially phosphorylated state to act as a competitive aPKC inhibitor. Consistent with this idea, follicle cell clones homozygous for a non-phosphorylatable Lgl allele (Lgl^{S5A}) show phenotypes similar to *lgl* loss of function, including lateral aPKC spread (Dong et al., 2015). This suggests that in order to be functional, Lgl must be an aPKC substrate, supporting the idea of competitive inhibition, a phenomenon that has been demonstrated for other aPKC substrates (Graybill and Prehoda, 2014; Holly and Prehoda, 2019; Lin et al., 2000).

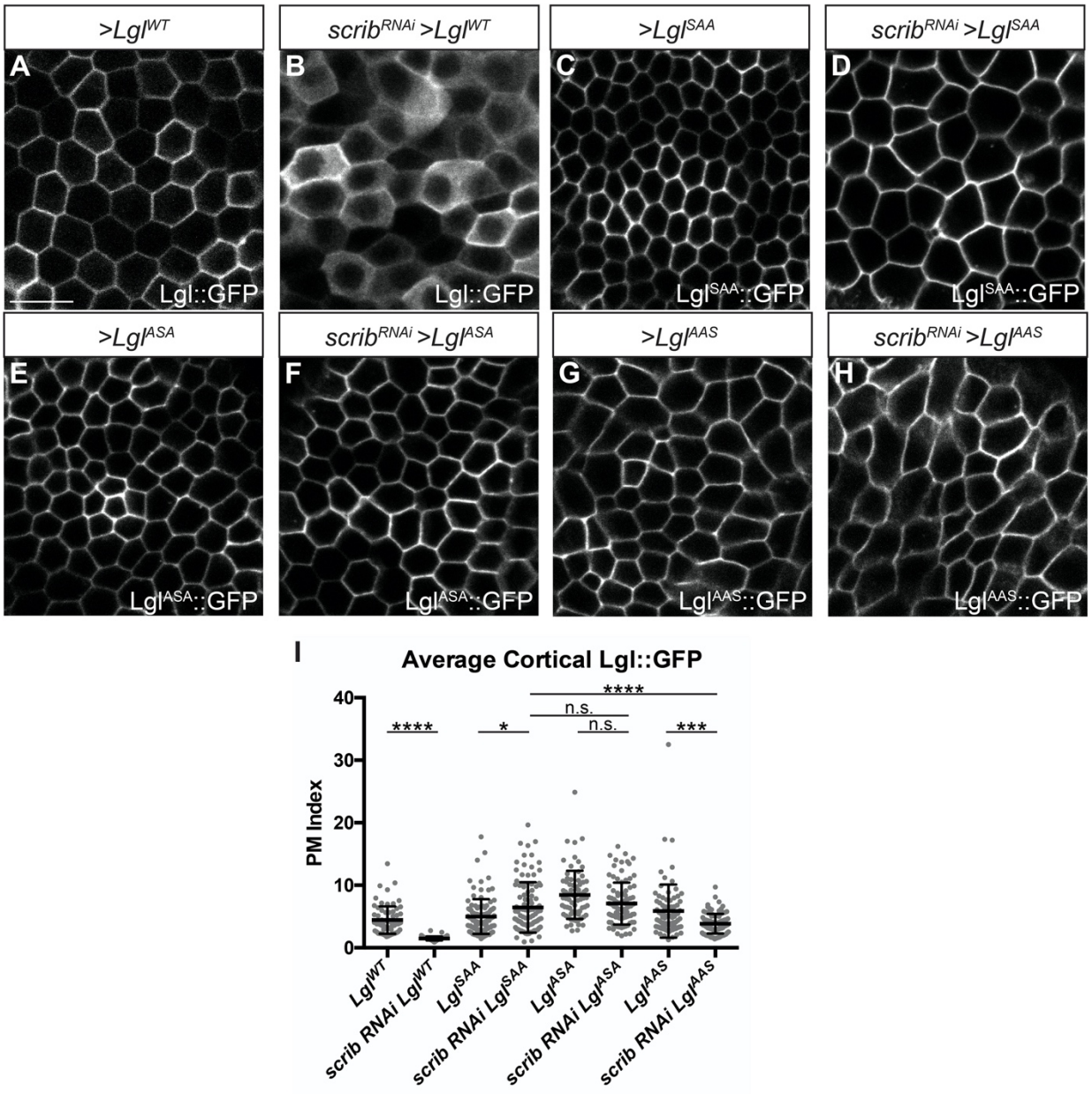

Functional differentiation of Lgl phosphorylation sites

We previously proposed a model where Scrib and Dlg negatively regulate Lgl phosphorylation through 'protection', limiting aPKC activity to specific residues that allow competitive inhibition of aPKC. To explore evidence for this *in vivo*, we measured the cortical localization of transgenic Lgl constructs in which only a single phosphorylation site is available, in WT versus *scrib*-depleted backgrounds. We hypothesized that the degree of mislocalization of each construct in *scrib*-depleted cells would allow us to infer the 'protectedness' of each phosphorylation site. Interestingly, we found that only Lgl^{AAS}, in which the S664 residue is the only available phosphorylation site, exhibited significantly reduced cortical localization in *scrib*-depleted cells These data are consistent with previous biochemical findings demonstrating that S664 has the fastest phosphorylation kinetics of the three sites, suggesting that it is the most rapidly phosphorylated upon loss of protection and supporting a competitive inhibition mechanism for the

observed dominant effects of Lgl^{AAS} expression (Carvalho et al., 2015; Graybill and Prehoda, 2014; Khoury and Bilder, 2020). These data also support the functional non-equivalence of Lgl phosphorylation sites observed *in vivo*, and suggest that contrary to cell culture experiments, Lgl phosphorylation does not simply act additively to displace Lgl from the membrane (Graybill and Prehoda, 2014; Moreira and Morais-de-Sá, 2016).

Egg chambers bearing polarity mutant follicle cells rotate

Egg chambers in the *Drosophila* ovary elongate from an initial spherical shape to an oblong shape in a process requiring a novel morphogenetic movement where the entire tissue rotates along its short axis (Haigo and Bilder, 2011). This rotation process involves PCP signaling to set the rotation direction (Chen et al., 2016b). Therefore, we wondered if this process was disrupted in apicobasal polarity mutants. To our surprise, live imaging egg chambers composed of *lgl* mutant follicle cells revealed that rotation can still occur in the absence of apicobasal polarity (data not shown). This raises questions about the ability of polarity mutant tissue to properly assemble a planar polarized basement membrane, and if other aspects of this morphogenetic process are disrupted when polarity is lost.